Etude de la stabilité des surfaces vicinales des métaux de transition à partir de leur structure électronique et vibrationnelle.

Faical Raouafi

UFR SCIENTIFIQUE D'ORSAY

THESE DE DOCTORAT

Présentée par

Fayçal RAOUAFI

pour obtenir le grade de

DOCTEUR EN SCIENCES
DE L'UNIVERSITE PARIS XI ORSAY

TITRE DE LA THESE

Etude de la stabilité des surfaces vicinales des métaux de transition à partir de leurs structures électronique et vibrationnelle.

Soutenue le 11 Octobre 2002 devant la Commission d'examen

Président:	A. FUCHS
Rapporteurs:	M. HANBUCKEN C. RAMSEYER
Examinateurs:	M. C. DESJONQUERES M. GUPTA D. SPANJAARD

A mes parents

REMERCIEMENTS

Cette thèse a été effectuée au sein du Commissariat à l'Energie Atomique, CEA Saclay dans le Service de Physique et Chimie des Surfaces et Interfaces dirigé par Elisabeth BOUCHAUD. Je tiens d'abord à la remercier pour m'avoir accueilli dans son service.

Mes plus vifs remerciements s'adressent à Marie Catherine DESJONQUERES, Daniel SPANJAARD et Cyrille BARRETEAU qui on fait beaucoup plus que d'encadrer ma thèse au jour le jour par le soutien et la patience au cours de ces années passées ensemble. Ils m'ont initié aux techniques théoriques nécessaires à l'accomplissement de cette étude. J'ai beaucoup apprécié leur façon de travailler. Je les remercie pour leur disponibilité. Qu'ils trouvent ici toute ma reconnaissance pour ces conseils qui m'ont été d'un très grand profit tout au long de ce travail.

J'adresse mes plus sincères remerciements à Margrit HANBUCKEN ainsi qu'à Cristophe RAMSEYER pour avoir accepté d'être rapporteurs de ma thèse et de trouver le temps de rédiger chacun des deux rapports.

Je remercie également vivement Alain FUCHS de m'avoir m'accepté au DEA de physico-chimie moléculaire de Paris-Sud et de présider le jury de cette thèse.

Je remercie vivement Michelle GUPTA d'avoir accepté de participer au jury et pour tout l'intérêt et l'enthousiasme qu'elle a manifesté pour cette thèse.

Je tiens à remercier Hervé NESS pour les nombreuses discussions scientifiques qui m'ont été d'un grand bénéfice pour ma thèse.

Ma gratitude s'adresse à Benoit SOEP pour les aides et les conseils qu'il m'a donné tout au long de mes études en FRANCE.

J'aimerais remercier tous les membres permanents, les thésards et les post-docs du service SPCSI.

Enfin, mes derniers remerciements iront à mes parents et mon grand frère Sahbi, qui, par leur aide, m'ont donné la possibilité de continuer mes études.....

Table des matières

Introduction.

L'étude des surfaces est d'un très grand intérêt tant du point de vue fondamental que de celui des applications. En effet, tout solide est limité par des surfaces qui sont en contact avec le vide ou un autre matériau. L'existence de ces surfaces modifie les propriétés du cristal. Ainsi beaucoup d'applications pratiques des cristaux dépendent de l'état de leurs surfaces et des propriétés de celles-ci. L'étude de la morphologie des surfaces permet de mettre en évidence l'existence de phénomènes aussi importants que la transition rugueuse, la croissance cristalline, l'épitaxie ou les réactions catalytiques, ou encore de comprendre la forme d'équilibre des cristaux. En effet, les propriétés physiques d'une surface sont sensibles à la structure atomique et, en particulier, à l'existence de défauts tels que marches, crans, adatomes ou adlacunes.

L'objet de cette thèse est l'étude théorique des propriétés électroniques et vibrationnelles et de la stabilité de surfaces vicinales idéales. Une telle surface est obtenue en taillant un cristal selon un plan cristallographique faisant un petit angle par rapport à un plan dense. Elle se présente donc sous la forme d'une succession périodique de marches de hauteur monoatomique séparées par des terrasses dont l'orientation est identique à celle du plan dense (Fig1). Les marches constituent des défauts essentiels dans la description des surfaces et, plus particulièrement, leurs évolutions avec la température et, lors d'un dépôt d'atomes, avec le temps. Elles sont connues pour jouer un rôle important dans le domaine de la croissance cristalline et de la catalyse où leur présence peut faciliter certaines réactions chimiques. Les surfaces vicinales sont donc un modèle très utile puisqu'elles présentent des marches bien régulières ce qui facilite leur étude théorique. De plus on sait les préparer expérimentalement et diverses techniques permettent de caractériser leurs propriétés, permettant ainsi une confrontation entre modèles et observations

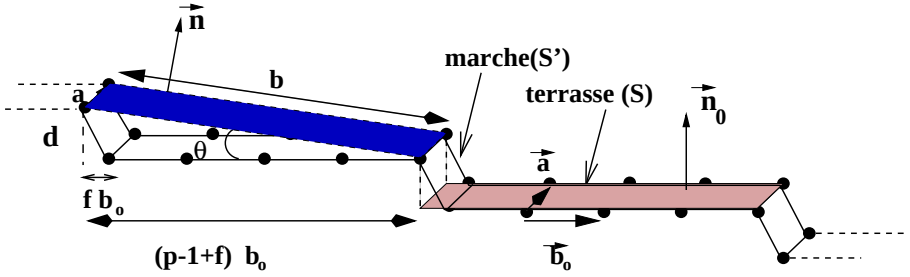

FIG. 1 – *Surface vicinale : b est la distance entre deux bords de marches consécutifs, b_o est la distance entre deux rangées atomiques dans la terrasse, Θ est l'angle de désorientation, p le nombre de rangées atomiques dans la terrasse, f est un facteur géométrique dépendant de la surface vicinale et d est la distance entre deux plans consécutifs parallèles à la terrasse.*

A l'inverse des surfaces plates qui sont aujourd'hui très bien comprises, les surfaces vicinales constituent actuellement un des domaines importants de la physique des surfaces.

Les surfaces vicinales des métaux ont ainsi suscité de nombreux travaux théoriques et expérimentaux. En effet depuis l'avènement des technologies d'ultra-vide, les expériences de diffraction (diffraction d'électrons lents, diffraction d'Hélium) [1, 2, 3] ont longtemps constitué les éléments clé de l'étude des surfaces à l'échelle atomique. Depuis une vingtaine d'années le développement des techniques de microscopies à effet tunnel (Scanning Tunneling Microscopy, STM) [4] a rendu possible l'observation dans l'espace direct de la morphologie des surfaces vicinales. En particulier l'analyse statistique de la distribution des marches permet de mesurer des paramètres énergétiques fondamentaux tels que l'énergie de formation des crans ou les interactions entre marches, qui commencent à être accessibles au calcul [5, 6, 7]. De plus l'observation de la forme d'équilibre des îlots de grande taille en homoépitaxie sur une surface plate donne accès à l'énergie de formation d'une marche isolée.

Ces progrès enregistrés dans les techniques expérimentales ont donc suscité un certain nombre de travaux théoriques. Ainsi pendant ces dernières années, beaucoup de modèles, ainsi que des méthodes pour les résoudre, ont été proposées pour calculer ces diverses énergies. Ces méthodes sont de deux types : celles utilisant des potentiels interatomiques plus ou moins empiriques et celles basées sur la détermination de la

structure électronique, c'est à dire où l'équation de Schrödinger est résolue explicitement pour les électrons. Les potentiels de paires ont été souvent utilisés pour l'étude des systèmes de grande taille, mais ils ne sont pas adaptés pour décrire l'énergie totale des systèmes métalliques. Depuis une vingtaine d'années, on s'est efforcé d'introduire des effets à N-corps dans les potentiels pour mieux décrire les propriétés physiques des métaux. Par exemple Norskov [8] est parti de l'idée que chaque atome d'un système métallique peut être considéré comme immergé dans un jellium dû à ses voisins. Ce problème peut être résolu exactement dans le cadre de la théorie de la fonctionnelle de la densité. L'introduction de termes correctifs lui a permis de proposer un potentiel analytique connu dans la littérature sous le nom de EMT (Effective Medium Theory). Daw et Baskes [9] ont développé une méthode assez voisine appelée EAM (Embedded Atom Method). D'autre part plusieurs potentiels derivés de la méthode des liaisons fortes dans l'approximation du second moment [10, 11] ont aussi été proposés dans la littérature. Tous ces potentiels appartiennent en fait à une même classe : ils ne dépendent que des distances interatomiques et sont la somme d'un terme de paire et d'un terme à N-corps. Ces potentiels ont été largement utilisés dans de nombreux problèmes liés aux grandeurs énergétiques. Les méthodes ab-initio basées sur la théorie de la fonctionnelle de la densité (TFD) [12, 13] cherchent à prédire le comportement énergétique des matériaux en se basant sur la résolution des équations de la mécanique quantique. Toutefois, en raison de la lourdeur de leur mise en oeuvre numérique (temps de calcul, mémoire informatique), la taille des systèmes qui peuvent être étudiés est restreinte à quelques dizaines d'atomes. L'approximation des liaisons fortes [14, 15], qui utilise un hamiltonien paramétrisé et une méthode approchée pour tenir compte des problèmes d'autocohérence, permet de calculer la structure électronique et d'en déduire l'énergie totale avec des temps de calculs beaucoup plus courts. Elle est très voisine des méthodes de Hückel en chimie et s'applique particulièrement bien à l'étude des bandes de valence (3d, 4d, 5d) des métaux de transition qui sont étroites.

Un problème particulièrement intéressant qui se pose dans l'étude des surfaces vicinales est celui de leur stabilité par rapport à un facettage. En effet ces surfaces ont une grande énergie de surface par unité de surface et on peut se demander s'il n'est pas énergétiquement favorable qu'elles adoptent spontanément un profil en "toit d'usine", tout en conservant leur orientation moyenne, en exposant au vide des facettes d'énergie de surface plus petites même si cette transformation augmente la surface totale. Ce phénomène, appelé facettage, est connu depuis une centaine d'années [16] et sa condition d'existence a été formulée par Herring [17] dans les années cinquante. Les progrès récents dans la détermination des énergies de surface en fonction de l'orientation cristallographique ont suscité un regain d'intérêt sur ce phénomène dont l'étude

est l'objet ultime de cette thèse.

Pour cela nous commencerons par une étude de la structure électronique à l'aide de la méthode des liaisons fortes qui nous fournira les grandeurs énergétiques nécessaires à 0K. Puis nous déterminerons, en utilisant un potentiel semi-empirique, les spectres de vibration de ces surfaces afin d'en déduire la contribution des phonons à l'énergie libre de surface. Enfin nous combinerons ces deux études pour en tirer des conclusions sur le phénomène de facettage.

Le manuscrit est organisé en quatre chapitres :

Dans le chapitre 1, nous donnons d'abord, une présentation générale du modèle des liaisons fortes *spd*. Nous expliquons la paramétrisation de l'hamiltonien dans une base orthonormée et son extension dans une base non-orthogonale. Puis nous introduisons la notion de densité d'états électronique locale et de densité spectrale locale d'états. Enfin nous discutons des problèmes d'autocohérence qui interviennent lorsque tous les atomes du système ne sont pas équivalents

Dans le chapitre 2, nous nous intéressons aux calculs de l'énergie de surface par unité de surface $\gamma(\theta)$ et de la structure électronique. Le calcul de $\gamma(\theta)$ nous permet d'extraire des quantités intéressantes telles que les énergies de marches isolées, nécessaires à la détermination de la forme des îlots en homoépitaxie sur les surfaces de bas indices, et les interactions électroniques entre marches. Nous calculons aussi les énergies de crans qui jouent un rôle important dans les fluctuations thermiques des bords de marche.

Le chapitre 3 est consacré à l'étude de la structure vibrationnelle des surfaces vicinales de Cuivre. Nous développons un potentiel semi-empirique qui permet de calculer le spectre de vibrations avec une grande précision en tout point de la zone de Brillouin. Nous comparons nos résultats avec les données expérimentales et les calculs ab-initio existants. Nous étudions en particulier les structures de bandes projetées phononiques des surfaces plates et des surfaces vicinales du Cuivre. Ceci nous conduit à discuter les états localisés et les résonances de surface. Enfin nous déterminons des quantités thermodynamiques vibrationnelles, telles que le déplacement carré moyen et l'énergie libre de vibration.

Enfin, dans le chapitre 4 nous présentons l'étude de la stabilité des surfaces vicinales des métaux de transition Rh, Pd et Cu par rapport à un facettage à partir des résultats obtenus aux chapitres 2 et 3. Nous montrons en particulier que les potentiels semi-empiriques sont trop simples pour décrire la variété des comportements possibles

Les chapitres 2 à 4 sont constitués des articles (publiés, à paraître ou soumis) précédés par un résumé des principaux résultats obtenus (les numéros de référence cités dans ces résumés se rapportent à la liste bibliographique de l'article correspondant).

´ ´

Chapitre 1

Structure électronique des métaux de transition dans le modèle des liaisons fortes.

1.1 Introduction

Le calcul de la structure électronique et de l'énergie totale d'un système quantique nécessite de résoudre l'équation de Schrödinger. On sait que dans les métaux de transition, les électrons de valence sont relativement localisés autour des noyaux. Leurs fonctions d'onde ressemblent donc aux fonctions d'onde des niveaux atomiques de valence. L'approximation des liaisons fortes est une excellente méthode pour simplifier le problème du calcul de l'énergie totale et de la structure électronique de ces éléments. Elle consiste à décrire les fonctions d'onde des électrons dans le solide comme une combinaison linéaire des orbitales atomiques centrées sur chaque site. Cette théorie est très voisine des méthodes de Hückel largement développées pour l'étude des molécules. Elle s'applique bien lorsque la distance inter-atomique dans le solide est grande par rapport à l'extension spatiale des fonctions d'onde atomiques. Elle est utile dans l'étude de la structure électronique des liaisons hybrides sp^3, sp^2 ou sp (par exemple de certains solides covalents tel que Si, Ge, C) et des bandes étroites ($3d$, $4d$, $5d$) des métaux de transition. De plus il a été montré récemment [14] que les électrons s et p de valence, bien que délocalisés, et leur hybridation avec les électrons d pouvaient être traités par cette méthode.

Dans ce chapitre, pour les métaux de transition, Rhodium et Palladium, nous développerons d'abord un modèle de liaisons fortes dans une base spd orthonormée [14] ;

ensuite nous passerons à son extension dans une base non-orthogonale [15] pour traiter le cas du Cuivre. Nous montrerons comment ces modèles peuvent s'appliquer à l'étude des surfaces vicinales qui font l'objet de ce travail. Nous terminerons enfin par la présentation des détails pratiques du calcul.

1.2 Modèle des liaisons fortes dans une base spd orthonormée

L'approximation des liaisons fortes est basée sur l'idée que le potentiel effectif ressenti par les électrons est très proche de la superposition des potentiels des atomes neutres [18] :

$$V_{eff} = \sum_i V_i \tag{1.1}$$

où V_i est le potentiel de l'atome centré au site i.
L'hamiltonien à un électron s'écrit donc :

$$H = T + \sum_i V_i \tag{1.2}$$

où T est le terme d'énergie cinétique.

1.2.1 Description de la base

L'hypothèse de base des liaisons fortes consiste à exprimer toutes les fonctions d'ondes propres du système, $|\Psi_n>$ d'énergie E_n, comme des combinaisons linéaires d'orbitales atomiques, $\Phi_\lambda(\overrightarrow{r} - \overrightarrow{R_i})$, où i est l'indice du site atomique ($i = 1, \ldots, N$)et λ numérote les diverses orbitales atomiques centrées sur le même site (λ =1, ...,ℓ où ℓ est le nombre total d'orbitales atomiques par site). Pour les métaux de transition, les électrons *s* et *p* délocalisés jouent un rôle non négligeable dans l'énergie de cohésion des métaux situés à la fin des séries. Nous verrons plus loin que l'introduction des orbitales *sp* de valence dans la base c'est à dire l'utilisation d'une base d'orbitales *s*, *p* et *d* permet de décrire correctement le spectre des niveaux d'énergie jusqu'à quelques eV au dessus du niveau de Fermi E_f. Dans cette base, les fonctions d'onde s'écrivent [19] :

$$\Psi_n(\overrightarrow{r}) = \sum_i \sum_\lambda C_{i,\lambda}^{(n)} \Phi_\lambda(\overrightarrow{r} - \overrightarrow{R_i}) \tag{1.3}$$

ou, en désignant $\Phi_\lambda(\overrightarrow{r} - \overrightarrow{R_i})$ par $|i\lambda>$:

$$|\Psi_n> = \sum_{i,\lambda} C_{i,\lambda}^{(n)} |i\lambda> \tag{1.4}$$

La bande *s* est non dégénérée, la bande *p* est dégénérée trois fois et la bande *d* est dégénérée cinq fois. Chaque état orbital peut être occupé par deux électrons de spins opposés si le système n'est pas magnétique. Les parties angulaires des fonctions d'onde, $|i\lambda>$, ont pour symétries respectives, *s*, p_x, p_y, p_z, d_{xy}, d_{yz}, d_{zx}, $d_{x^2-y^2}$ et $d_{3z^2-r^2}$ [19].

On suppose que cette base est orthonormée, c'est à dire :

$$\int d^3\overrightarrow{r} \Phi_\lambda^*(\overrightarrow{r} - \overrightarrow{R_i}) \Phi_\mu(\overrightarrow{r} - \overrightarrow{R_j}) = < i\lambda | j\mu > = \delta_{ij}\delta_{\lambda\mu} \tag{1.5}$$

1.2.2 Eléments de matrice de l'hamiltonien

Dans la base des orbitales atomiques orthonormée et supposée complète, les éléments de matrice de l'hamiltonien peuvent s'écrire :

$$H_{ij}^{\lambda\mu} = < i\lambda | T + \sum_k V_k | j\mu > = < i\lambda | T + V_j | j\mu > + < i\lambda | \sum_{k \neq j} V_k | j\mu > \tag{1.6}$$

Chaque orbitale atomique obéit à l'équation de Schrödinger pour un atome isolé. Dans la mesure où V_j est assimilable au potentiel d'un atome libre, on a :

$$(T + V_j) | j\mu > = \varepsilon_{j\mu}^o | j\mu > \tag{1.7}$$

où $\varepsilon_{j\mu}^o$ est le niveau atomique correspondant à l'orbitale $|j\mu>$. Dans un cristal volumique tous les sites sont équivalents donc $\varepsilon_{j\mu}^o = \varepsilon_\mu^o$, nous verrons par la suite que cela ne s'applique pas aux sites proches des défauts et, en particulier, des surfaces. Pour plus de généralité, nous conserverons la notation $\varepsilon_{j\mu}^o$. Ceci permet d'écrire (1.6) sous la forme :

$$H_{ij}^{\lambda\mu} = \varepsilon_{i\lambda}^{o}\delta_{ij}\delta_{\lambda\mu} + \sum_{k\neq j} < i\lambda|V_k|\,j\mu > \tag{1.8}$$

On peut écrire aussi $H_{ij}^{\lambda\mu}$ sous la forme suivante :

$$H_{ij}^{\lambda\mu} = \varepsilon_{i\lambda}^{o}\delta_{ij}\delta_{\lambda\mu} + < i\lambda|\sum_{k\neq i} V_k|i\mu > \delta_{ij} + < i\lambda|\sum_{k\neq j} V_k|\,j\mu > (1-\delta_{ij}) \tag{1.9}$$

On remarque que l'hamiltonien des liaisons fortes contient des termes intra -atomiques et des termes inter-atomiques.

a) Eléments intra-atomiques : niveaux s, p et d

Partant de l'équation (1.9), on remarque que les deux premiers termes à droite représentent les éléments de matrice intra-atomiques, ils s'écrivent :

$$H_{ii}^{\lambda\mu} = \varepsilon_{i\lambda}^{o}\delta_{\lambda\mu} + < i\lambda|\sum_{k\neq i} V_k|i\mu > \tag{1.10}$$

Le second terme à droite de l'équation (1.10) est connu sous le nom d'intégrales de champ cristallin. Elles dépendent de l'environnement local de l'atome i et modifient la position moyenne des niveaux. Les termes $\lambda = \mu$ ont pour effet d'abaisser légèrement le niveau atomique. Ces intégrales de champ cristallin sont habituellement négligées. Le modèle des liaisons fortes *spd* fait intervenir trois types d'orbitales atomiques pour décrire un système. De ce fait, on a trois types de niveaux atomiques $\varepsilon_{i\lambda}^{o}$ de l'atome i pour l'orbitale λ : ε_{is}^{o}, ε_{ip}^{o} et ε_{id}^{o}. Ces paramètres dépendent de l'environnement atomique.

b)Eléments de matrice inter-atomiques : intégrales de saut de Slater- Koster

Dans l'expression de l'hamiltonien de liaisons fortes apparaissent des éléments de matrice $< i\lambda|V_k|\,j\mu >$ ($k \neq j$ et $i \neq j$). Ces termes comprennent des intégrales à deux centres ($k = i$) et des intégrales à trois centres ($i \neq k \neq j$). Les intégrales à trois centres sont faibles à cause de la décroissance rapide du potentiel et des fonctions d'onde, donc elles sont généralement négligées. Ainsi parmi les éléments $< i\lambda|V_k|\,j\mu >$, on ne conserve que ceux où $k = i \neq j$. Ils sont appelés les intégrales de saut ou de transfert :

$$H_{ij}^{\lambda\mu} =< i\lambda|V_i|\,j\mu >= \beta_{ij}^{\lambda\mu} \tag{1.11}$$

Les intégrales de saut représentent l'interaction énergétique entre deux orbitales centrées sur les sites i et j. Elles sont responsables de la formation d'une bande d'énergie à partir des niveaux atomiques discrets, et permettent aux électrons de sauter de site en site dans le solide. Elles sont fonction des cosinus directeurs (l,m,n) du vecteur $\overrightarrow{R_{ij}}$ et de son module R_{ij} et sont définies pour un couple ij donné comme les éléments d'une matrice de dimension (9×9) :

$$[\mathbb{B}]^{\lambda\mu}(R_{ij}, l, m, n) = \beta^{\lambda\mu}(\overrightarrow{R_{ij}}) = \beta_{ij}^{\lambda\mu} \tag{1.12}$$

Quand la liaison ij est dirigée selon l'axe Oz, les intégrales de saut prennent une forme simple, dépendant d'un nombre restreint de paramètres, appelés les paramètres de Slater-Koster [20], qui ne sont fonction que de la distance inter-atomique R_{ij}. Dans le modèle *spd*, ces paramètres sont au nombre de dix : ssσ, spσ, sdσ, ppσ, ppπ, pdσ, pdπ, ddσ, ddπ et ddδ. Ils sont représentés sur la figure (1.1).

On tenant compte de la symétrie des orbitales et du potentiel, on montre facilement que $\mathbb{B}(R_{ij}, 0, 0, 1)$ s'écrit :

$$\begin{pmatrix}
ss\sigma & 0 & 0 & sp\sigma & 0 & 0 & 0 & 0 & sd\sigma \\
0 & pp\pi & 0 & 0 & 0 & 0 & pd\pi & 0 & 0 \\
0 & 0 & pp\pi & 0 & 0 & pd\pi & 0 & 0 & 0 \\
-sp\sigma & 0 & 0 & pp\sigma & 0 & 0 & 0 & 0 & pd\sigma \\
0 & 0 & 0 & 0 & dd\delta & 0 & 0 & 0 & 0 \\
0 & 0 & -pd\pi & 0 & 0 & dd\pi & 0 & 0 & 0 \\
0 & -pd\pi & 0 & 0 & 0 & 0 & dd\pi & 0 & 0 \\
0 & 0 & 0 & 0 & 0 & 0 & 0 & dd\delta & 0 \\
sd\sigma & 0 & 0 & -pd\sigma & 0 & 0 & 0 & 0 & dd\sigma
\end{pmatrix} \tag{1.13}$$

Pour une direction de liaison $\overrightarrow{R_{ij}}$ quelconque, les intégrales de saut sont obtenues par rotation des axes de quantification locaux. Cette rotation est caractérisée par une matrice unitaire $\mathbb{P}$ dans l'espace des orbitales atomiques. En d'autres termes, cette matrice est fonction des cosinus directeurs, (l,m,n) du vecteur $\overrightarrow{R_{ij}}$.

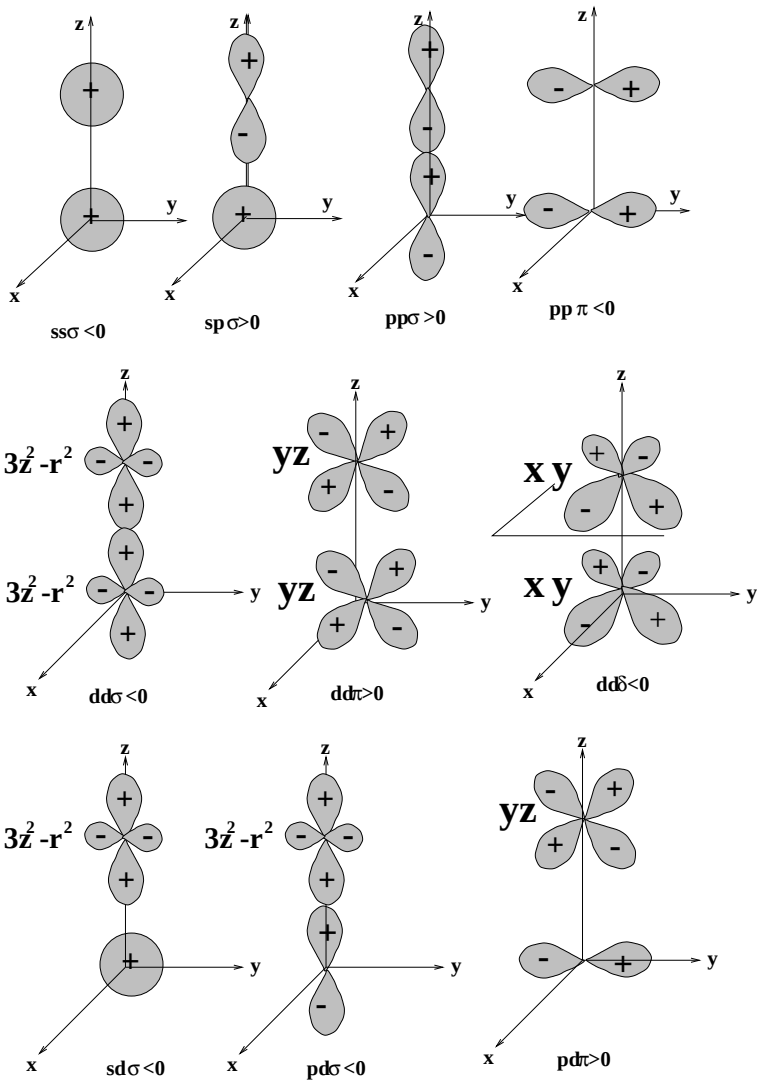

FIG. 1.1 – *Intégrales de sauts de Slater-Koster*

On obtient les intégrales de saut $\beta^{\lambda\mu}(\overrightarrow{R_{ij}})$ dans une direction quelconque, en fonction des paramètres de Slater et Koster définis ci-dessus pour les bandes *s*, *p* et *d* et des cosinus directeurs (*l*,*m*,*n*) du vecteur $\overrightarrow{R_{ij}}$ par la transformation :

$$\mathbb{B}(R_{ij},l,m,n) = \mathbb{P}^{-1}(l,m,n)\mathbb{B}(R_{ij},0,0,1)\mathbb{P}(l,m,n) \tag{1.14}$$

Les résultats ont été tabulés par Slater et Koster [20]

1.2.3 Résolution de l'équation de Schrödinger dans le volume.

La résolution de l'équation de Schrödinger permet d'accéder aux états propres et aux énergies propres du système :

$$H|\Psi_n>=E_n|\Psi_n> \tag{1.15}$$

Nous avons vu précédemment que $|\Psi_n>$ s'écrit sous la forme :

$$|\Psi_n>=\sum_{i\lambda} C_{i\lambda}^{(n)}|i\lambda> \qquad \begin{cases} i=1,...,N \\ \\ \lambda=1,...,\ell \end{cases} \tag{1.16}$$

Dans la base des orbitales atomiques $|i\lambda>$, l'équation (1.15) s'écrit :

$$(\varepsilon_{i\lambda}^{o}-E_n)C_{i\lambda}^{(n)}+\sum_{\substack{j\mu \\ j\neq i}}\beta_{ij}^{\lambda\mu}C_{j\mu}^{(n)}=0 \tag{1.17}$$

Dans une structure périodique, le théorème de Bloch établit que les solutions de l'équation de Schrödinger pour un potentiel périodique s'écrivent comme le produit d'une onde plane $e^{i\overrightarrow{k}.\overrightarrow{r}}$ par une fonction $u_{\overrightarrow{k}}(\overrightarrow{r})$:

$$\Psi_{\overrightarrow{k}}(\overrightarrow{r})=u_{\overrightarrow{k}}(\overrightarrow{r})e^{i\overrightarrow{k}.\overrightarrow{r}} \tag{1.18}$$

où $\overrightarrow{k}$ est le vecteur d'onde et $u_{\overrightarrow{k}}(\overrightarrow{r})$ une fonction qui a les mêmes périodicités que le réseau cristallin :

$$u_{\overrightarrow{k}}(\overrightarrow{r}+\overrightarrow{R})=u_{\overrightarrow{k}}(\overrightarrow{r}) \tag{1.19}$$

si le cristal est invariant par la translation $\overrightarrow{R}$.
Donc :

$$\Psi_{\overrightarrow{k}}(\overrightarrow{r}+\overrightarrow{R})=\Psi_{\overrightarrow{k}}(\overrightarrow{r})e^{i\overrightarrow{k}.\overrightarrow{R}} \tag{1.20}$$

On impose cette condition à la solution (1.16), on trouve par identification que les coefficients correspondant à l'onde de Bloch $\Psi_n(\overrightarrow{k})$ sont de la forme :

$$C_{i\lambda}^{(n)} = \frac{1}{\sqrt{N}} e^{i\vec{k}.\vec{R_i}} C_{\lambda}^{(n)}(\vec{k}) \tag{1.21}$$

La fonction d'onde correspondant au vecteur $\vec{k}$ s'écrira finalement :

$$|\Psi_n(\vec{k})> = \frac{1}{\sqrt{N}} \sum_{i\lambda} e^{i\vec{k}.\vec{R_i}} C_{\lambda}^{(n)}(\vec{k}) |i\lambda> = \sum_{\lambda} C_{\lambda}^{(n)}(\vec{k}) |\vec{k}\lambda> \tag{1.22}$$

avec

$$|\vec{k}\lambda> = \frac{1}{\sqrt{N}} \sum_{i} e^{i\vec{k}.\vec{R_i}} |i\lambda> \tag{1.23}$$

Enfin l'équation (1.17) devient :

$$(\varepsilon_{i\lambda}^{o} - E_n(\vec{k})) C_{\lambda}^{(n)}(\vec{k}) \delta_{ij}\delta_{\lambda\mu} + \sum_{\substack{j\neq i \\ \mu}} \beta_{ij}^{\lambda\mu} e^{i\vec{k}.\vec{R_{ij}}} C_{\mu}^{(n)}(\vec{k}) = 0 \tag{1.24}$$

Ceci conduit à résoudre un problème de valeurs propres et de vecteurs propres qui s'écrit sous forme matricielle :

$$\mathbb{H}\mathbb{C}^{(n)} = E_n \mathbb{C}^{(n)} \tag{1.25}$$

où $\mathbb{H}$ est une matrice de taille (9×9), qui tient compte des hybridations entre les différentes orbitales atomiques, *s*, *p* et *d*.

Les solutions de l'équation (1.24) en tout point $\vec{k}$ de la première zone de Brillouin donnent les courbes de dispersion $E_n(\vec{k})$ et permettent de calculer la densité d'états.

1.2.4 Détermination des paramètres

a) Energie totale

La méthode des liaisons fortes constitue le formalisme le plus simple pour décrire le comportement des électrons dans le cadre de la mécanique quantique. Dans la théorie de la fonctionnelle de la densité (TFD), l'énergie totale est donnée par [12, 13] :

$$E[n(\overrightarrow{r})] = \sum_n E_n + F[n(\overrightarrow{r})] \tag{1.26}$$

où $E[n(\overrightarrow{r})]$ est l'énergie totale et E_n les niveaux d'énergie occupés du système, $n(\overrightarrow{r})$ la densité électronique et la fonctionnelle $F[n(\overrightarrow{r})]$ est donnée par :

$$\begin{aligned} F[n(\overrightarrow{r})] &= -\frac{1}{2}\int \frac{n(\overrightarrow{r})n(\overrightarrow{r'})}{|\overrightarrow{r}-\overrightarrow{r'}|} d^3\overrightarrow{r} d^3\overrightarrow{r'} - \int n(\overrightarrow{r}) V_{xc}[n(\overrightarrow{r})] d^3\overrightarrow{r} \\ &\quad + E_{xc}[n(\overrightarrow{r})] + E_{ion-ion} \end{aligned} \tag{1.27}$$

Cette fonctionnelle $F[n(\overrightarrow{r})]$ contient les contributions à l'énergie qui proviennent de l'interaction de Coulomb électron-électron, des interactions d'échange et corrélation à travers l'énergie $E_{xc}[n(\overrightarrow{r})]$ et le potentiel $V_{xc}[n(\overrightarrow{r})] = \frac{\delta E_{xc}[n(\overrightarrow{r})]}{\delta n(\overrightarrow{r})}$ et enfin de l'interaction ion-ion, $E_{ion-ion}$.

La fonctionnelle $E[n(\overrightarrow{r})]$ est indépendante du choix du zéro pour le potentiel effectif.

Dans la TFD, les niveaux E_n sont obtenus par la résolution auto-cohérente des équations de Kohn-Sham :

$$[T + V_{eff}[\overrightarrow{r}, n(\overrightarrow{r})]]\Psi_n(\overrightarrow{r}) = E_n \Psi_n(\overrightarrow{r}) \tag{1.28}$$

$$n(\overrightarrow{r}) = 2e\sum_n |\Psi_n(\overrightarrow{r})|^2 \tag{1.29}$$

où e est la charge de l'électron.
Le potentiel effectif s'écrit :

$$V_{eff}[\overrightarrow{r}, n(\overrightarrow{r})] = V_{ion}(\overrightarrow{r}) + V_{Hartree}(n(\overrightarrow{r})) + V_{xc}[n(\overrightarrow{r})] \tag{1.30}$$

où V_{ion} est le potentiel dû aux ions et $V_{Hartree}(\overrightarrow{r}) = \int \frac{n(\overrightarrow{r'})}{|\overrightarrow{r}-\overrightarrow{r'}|} d^3\overrightarrow{r'}$.

Les méthodes de liaisons fortes permettent de déterminer uniquement le premier terme de (1.26) et le deuxième terme doit être traité par un autre moyen. La procédure proposée par Cohen et al. [21] et qui a été adoptée par Barreteau et al.[14] consiste à déplacer tous les niveaux de façon que l'énergie totale soit égale à la somme des niveaux occupés :

$$E[n(\overrightarrow{r})] = \sum_n E_n^{'} \tag{1.31}$$

où $E_n^{'} = E_n + \frac{F[n(\overrightarrow{r})]}{N_e}$ est le niveau qui a été déplacé et N_e est le nombre d'électrons du système.

La résolution de l'hamiltonien conduit au spectre énergétique $E_n^{'}$ des électrons de valence du cristal et détermine l'énergie totale. La contribution de ces énergies électroniques constitue à la fois la partie attractive et la partie répulsive de l'énergie totale du système. En d'autres termes, la contribution répulsive est comptée à l'intérieur de la contribution de bande. Ceci est dû aux paramètres intra-atomiques qui dépendent de l'environnement atomique. Le calcul de ces derniers termes fera l'objet du prochain paragraphe.

b) Les termes intra-atomiques

Le modèle de liaisons fortes *spd* que nous utilisons, fait intervenir trois types d'orbitales atomiques pour décrire un système. Les paramètres intra-atomiques sont donc au nombre de trois : ε_s^o, ε_p^o et ε_d^o. Les orbitales atomiques *d* se recouvrent faiblement, elles donnent naissance à une bande très étroite, contenant 10 électrons par atome dans laquelle se trouve le niveau de Fermi E_f, ainsi la densité des états correspondante est très élevée. Les électrons *d* localisés, ont une contribution attractive à l'énergie totale si l'on choisit le centre de gravité de la bande *d* pour origine des énergies. Lorsque l'on fait varier la distance interatomique autour de l'équilibre, le niveau atomique *d* se déplace faiblement. Par contre les orbitales atomiques *s* et *p* se recouvrent fortement, ceci donne naissance à une bande très large contenant 8 électrons par atome et une densité d'états faible par comparaison à celle de la bande *d*, (Fig (1.2)). Lorsque l'on comprime le cristal, les niveaux atomiques *sp* remontent fortement. Ce phénomène reflète le fait que les nuages électroniques ne peuvent s'interpénétrer. En conséquence, les éléments de matrice intra-atomiques $\varepsilon_{i\lambda}^o$ de l'hamiltonien doivent être considérés

maintenant comme fonctions de l'environnement atomique local. Cette dépendance de l'environnement est déterminée par l'introduction d'une "densité" associée à l'atome i [14, 15] :

$$\rho_i = \sum_{j \neq i} \exp[-p(\frac{R_{ij}}{R_o} - 1)] f_c(R_{ij}) \tag{1.32}$$

où R_o est la distance entre premiers voisins dans le volume à l'équilibre et $f_c(R_{ij})$ est donnée par :

$$f_c(R_{ij}) = [1 + \exp(\frac{R_{ij} - R_c}{\triangle})]^{-1} \tag{1.33}$$

R_c et $\triangle$ déterminent respectivement la distance de coupure et sa raideur et on pose :

$$\varepsilon^o_{i\lambda} = a_\lambda + b_\lambda \rho_i^{\frac{2}{3}} + c_\lambda \rho_i^{\frac{4}{3}} + d_\lambda \rho_i^2 \tag{1.34}$$

avec $\lambda = s, p, d$.

On voit donc dans cette approche, que $\varepsilon^o_{i\lambda}$ dépend de la coordinance du site i et des distances inter-atomiques correspondantes.

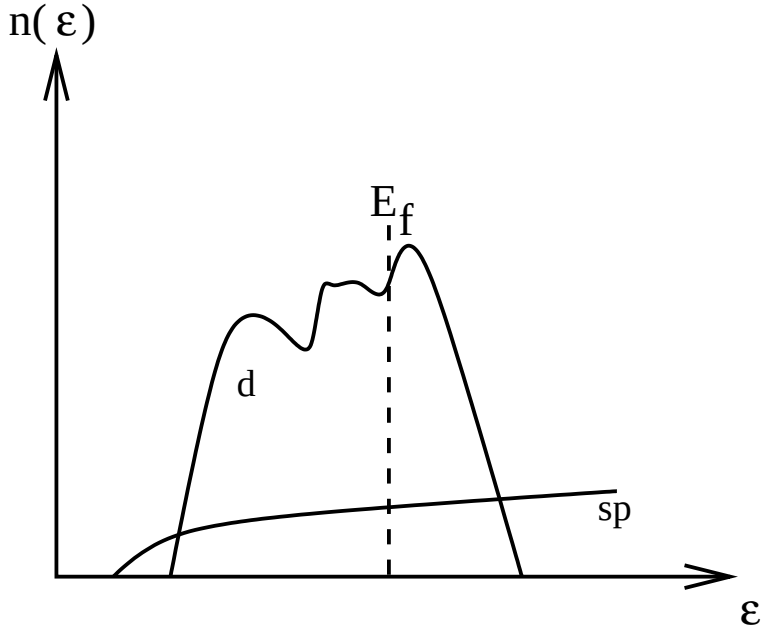

FIG. 1.2 – *Densités d'états des électrons s, p et d de valence dans un métal de transition.*

c) Choix de la loi de variation des intégrales de saut.

Rappelons que les intégrales de saut $\beta_{ij}^{\lambda\mu}$ s'expriment en fonction des cosinus directeurs (l, m, n) du vecteur $\overrightarrow{R_{ij}}$ et des paramètres de Slater-Koster qui décroissent rapidement quand la distance inter-atomique R_{ij} croît (Fig (1.3)).

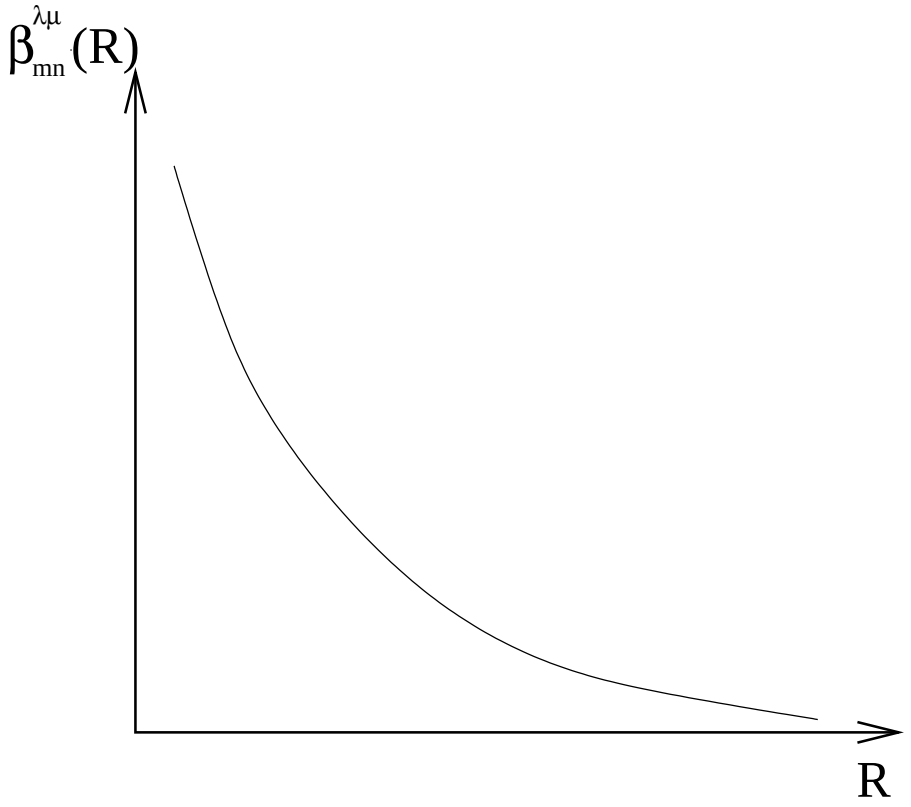

FIG. 1.3 – *Variation des intégrales de saut en fonction de la distance inter-atomique.*

Différentes formes analytiques ont été considérées pour ces paramètres. Les formes analytiques les plus employées sont les lois en exponentielle et en puissance [19, 22] :

$$\beta(R_{ij}) = \beta_o \exp(-q_\beta(\frac{R_{ij}}{R_o} - 1)) \tag{1.35}$$

et

$$\beta(R_{ij}) = \beta_o \left(\frac{R_o}{R_{ij}} \right)^{q_\beta} \tag{1.36}$$

où β_o est la valeur numérique de l'intégrale de saut β à la distance d'équilibre du solide R_o. Le paramètre q_β ne dépend que des moments angulaires des orbitales concernées. Il y a donc six paramètres : q_{ss}, q_{sp}, q_{sd}, q_{pp}, q_{pd} et q_{dd} [14].

Il faut noter que les deux lois de variation des paramètres $\beta(R_{ij})$ sont équivalentes au premier ordre dans un développement autour de la distance d'équilibre R_o. Dans ce travail, nous avons adopté des lois exponentielles et introduit la fonction de coupure $f_c(R_{ij})$ (1.33) soit :

$$\beta(R_{ij}) = \beta_o \exp(-q_\beta(\frac{R_{ij}}{R_o} - 1))\, f_c(R_{ij}) \tag{1.37}$$

d) Détermination des paramètres.

Le modèle des liaisons fortes *spd* possède vingt neuf paramètres (dix intégrales de saut, six paramètres $q_{\lambda\mu}$, et treize paramètres pour fixer les termes intra-atomiques) qui sont déterminés à l'aide d'une méthode de moindres carrés. Pour ce faire on ajuste les structures de bande et les variations de l'énergie totale en fonction de la distance inter-atomique obtenues à l'aide de méthodes basées sur la TFD pour deux structures périodiques (cfc et cc). Le code utilisé est un code ASW utilisant une base d'ondes sphériques augmentées (ASW = Augmented Spherical Waves)

Les paramètres obtenus par Barreteau et al. [14] pour Rh et Pd sont donnés dans les tableaux (1.1) et (1.2) et permettent de retrouver avec une excellente précision la structure de bande jusqu'à quelques eV au dessus du niveau de Fermi [Fig (1.4)] ainsi que les courbes donnant l'énergie de cohésion en fonction du rayon de Wigner-Seitz [Fig (1.5)].

élément	orbitale	a_λ	b_λ	c_λ	d_λ
Rh	**s**	1.3329	3.0637	-0.1788	0.0069
	p	6.1674	2.9454	-0.2247	0.0094
	d	0.1259	-0.0370	0.0233	-0.0009
Pd	**s**	1.4263	2.6678	-0.2389	0.0113
	p	6.0623	2.7530	-0.2000	0.0085
	d	-0.0167	-0.0756	0.0203	-0.0007

TAB. 1.1 – *Les paramètres (eV) qui déterminent les éléments de matrice intra-atomiques s, p et d pour Rh et Pd. La valeur de p dans l'équation (1.32) est :* $p = 9.527$ *pour Rh et* $p = 9.100$ *pour Pd. Le paramètre* a_λ *a été fixé de manière que l'énergie totale soit égale, en valeur absolue, à l'énergie de cohésion expérimentale.*

élément		β_o	q_β
Rh	ssσ	-0.9755	2.2556
	spσ	1.9945	2.9709
	sdσ	-0.9488	2.6455
	ppσ	3.3313	3.1266
	ppπ	-0.1218	3.1266
	pdσ	-1.3096	3.7810
	pdπ	0.1561	3.7810
	ddσ	-0.9132	4.8526
	ddπ	0.5176	4.8526
	ddδ	-0.0806	4.8526
Pd	ssσ	-0.7396	1.9904
	spσ	1.7554	2.7568
	sdσ	-0.7354	2.5920
	ppσ	3.2554	3.3543
	ppπ	-0.0862	3.3543
	pdσ	-1.0231	3.9167
	pdπ	0.1343	3.9167
	ddσ	-0.7077	4.9402
	ddπ	0.4172	4.9402
	ddδ	-0.0728	4.9402

TAB. 1.2 – *Les paramètres de Slater-Koster (eV) à la distance d'équilibre entre premiers voisins de Rh et Pd dans la phase cfc et les paramètres q_β qui déterminent leur variation avec la distance (Eq. 1.37)*

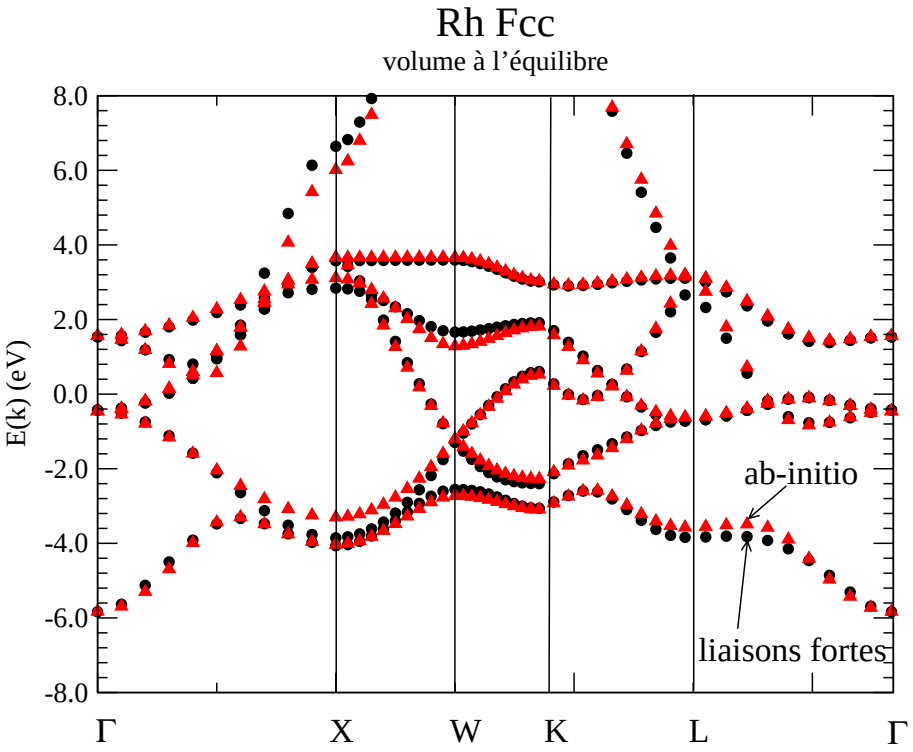

FIG. 1.4 – *La structure de bandes de Rh cfc à la distance d'équilibre entre premiers voisins calculée avec la méthode ASW, comparée à celle obtenue avec la méthode des liaisons fortes.*

1.2.5 Cas d'une surface

Une surface est limitée par un plan cristallographique d'indices de Miller donnés. En principe il faudrait résoudre le cas d'un cristal semi-infini. Dans la pratique, nous considérons un nombre limité de plans (méthodes des couches).

a) Géométrie des couches.

Les systèmes que nous allons étudier sont donc des cristaux limités par deux plans et constitués de P plans atomiques. Le nombre de plans atomiques doit être suffisament grand pour que les atomes dans les plans centraux aient des propriétés proches de celles du volume et pour que l'interaction entre les deux surfaces soit négligeable, (Fig (1.6)). Notons que la méthode des liaisons fortes permet de satisfaire à ces conditions de façon beaucoup plus stricte que les méthodes basées sur la TFD car le nombre P peut être choisi beaucoup plus grand. Il s'agit donc d'un système présentant une périodicité à deux dimensions (2D) déterminée par la géométrie du plan cristallographique choisi pour la surface et possédant P atomes par maille, en l'absence de reconstruction.

RHODIUM

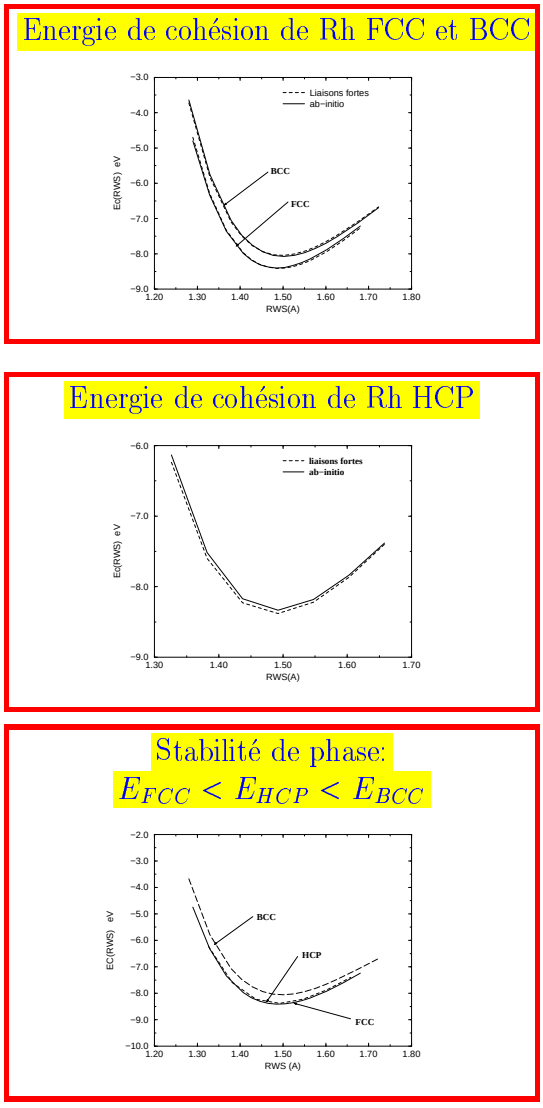

FIG. 1.5 – *L'énergie totale en fonction du rayon de Wigner-Seitz (R_{ws}) de Rh dans l'état massif dans les structures cc et cfc, obtenue avec la méthode des liaisons fortes comparée aux calculs de premiers principes (ASW). La figure du bas montre que la structure d'équilibre cfc est correctement prévue.*

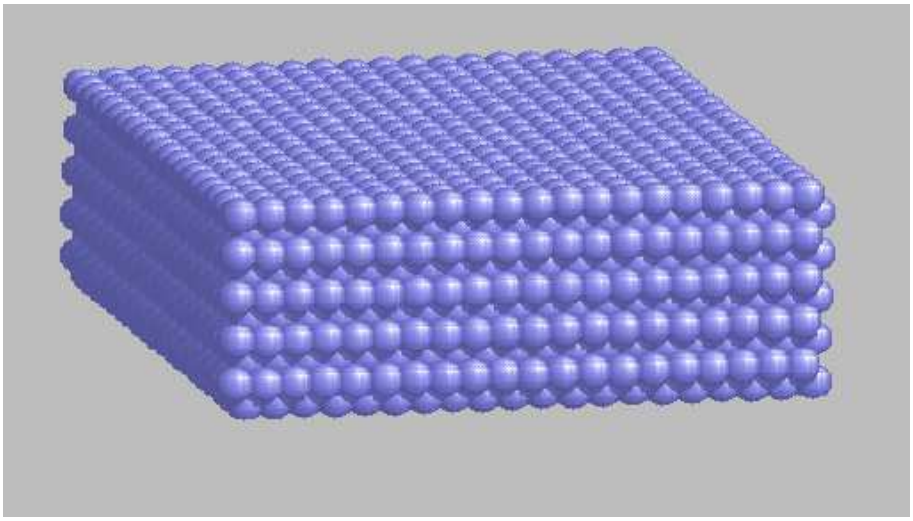

FIG. 1.6 – *Exemple de géométrie de couche.*

b) Les points $\vec{k}_{\|}$.

Le théorème de Bloch s'applique toujours dans une structure périodique à deux dimensions, de même que les conditions de Born von Karman, et les fonctions d'onde électroniques sont de la forme :

$$\Psi_{\overrightarrow{k_{\|}}}(\overrightarrow{r_{\|}},z) = e^{i\overrightarrow{k_{\|}}.\overrightarrow{r_{\|}}} u_{\overrightarrow{k_{\|}}}(\overrightarrow{r_{\|}},z) \tag{1.38}$$

où $\overrightarrow{k_{\|}}$, composante du vecteur d'onde parallèle à la surface, est réelle et $\overrightarrow{r}$ =($\overrightarrow{r_{\|}}$,z) sont les coordonnées. La fonction $u_{\overrightarrow{k_{\|}}}$ possède la périodicité de translation du réseau bidimensionnel.

Pour trouver les valeurs propres de l'hamiltonien on choisit des vecteurs d'onde $\overrightarrow{k_{\|}}$ dans la partie irréductible de la première zone de Brillouin correspondant au réseau bidimensionnel.

Les grandeurs calculées, l'énergie totale par exemple, nécessitent d'effectuer une sommation sur toutes les valeurs de $\overrightarrow{k_{\|}}$, la diagonalisation de l'hamiltonien est réalisée pour un ensemble fini de points $\overrightarrow{k_{\|}}$ choisis dans la partie irréductible de la première zone de Brillouin à deux dimensions. Cunningham [23] a montré comment on pouvait choisir ces points, appelés points $\overrightarrow{k_{\|}}$ spéciaux, de manière à accélérer la convergence de cette sommation. Nous avons donc adopté ces points.

c) Calcul des éléments de matrice de l'hamiltonien $H_{pq}^{\lambda\mu}(\overrightarrow{k_{\|}})$ dans la méthode des couches.

Les systèmes que nous étudierons comportent P atomes par maille. Chaque atome appartient à un plan différent de la couche qui est repéré par un vecteur $\overrightarrow{\tau_p}$ (un atome est placé à $\overrightarrow{\tau_p} = \overrightarrow{0}$) dans la maille choisie pour origine. A partir de cette maille on obtient tout le système par les vecteurs de translations élémentaires $\overrightarrow{R_{i\|}}$ du plan cristallographique déterminant l'orientation de la couche. Dans ces conditions une direction de liaison qui joint un atome du plan p dans la maille i à un atome du plan q dans la maille j est :

$$\overrightarrow{U_{ij}^{pq}} = \overrightarrow{R_{j\|}} + \overrightarrow{\tau_q} - \overrightarrow{R_{i\|}} - \overrightarrow{\tau_p} \tag{1.39}$$

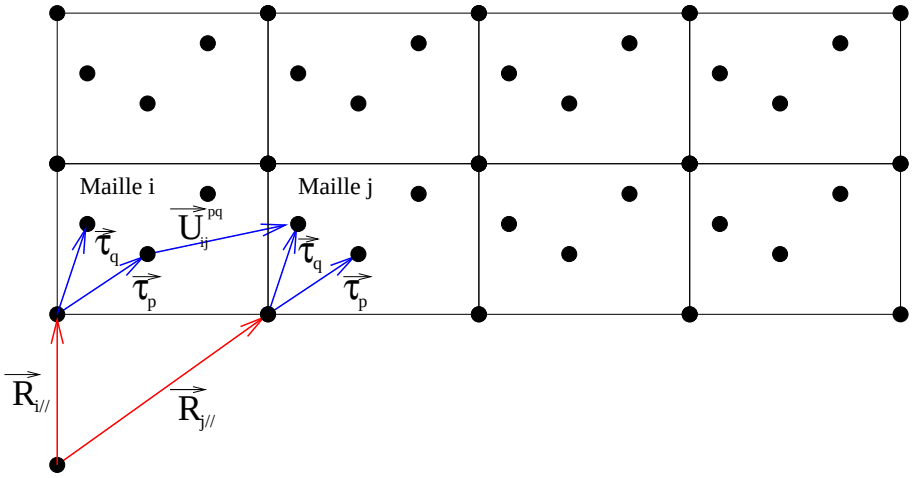

FIG. 1.7 – *Réseau periodique à 2D à 4 atomes par maille*

où p est le numéro du plan atomique, $\overrightarrow{R_{i\|}}$ le vecteur position d'un atome origine dans la maille i du cristal, $\overrightarrow{\tau_p}$ le vecteur position de l'atome dans la maille et $\overrightarrow{U_{ij}^{pq}}$ est un vecteur entre deux atomes du cristal.

Pour des surfaces infinies, la solution de l'équation de Schrödinger se décompose sur une base d'ondes de Bloch $|\overrightarrow{k_{\|}}, p, \lambda>$ localisées sur chacun des plans p :

$$|\overrightarrow{k_{\|}}, p, \lambda> = \frac{1}{\sqrt{N}} e^{i\overrightarrow{k_{\|}}.\overrightarrow{\tau_p}} \sum_i e^{i\overrightarrow{k_{\|}}.\overrightarrow{R_{i\|}}} |i, p, \lambda> \tag{1.40}$$

où $|i,p,\lambda>$ est l'orbitale λ de l'atome p de la maille i.

Dans le modèle des liaisons fortes à plusieurs atomes par maille, la fonction d'onde s'écrit comme une combinaison linéaire des orbitales atomiques sous la forme suivante :

$$\Psi_{\overrightarrow{k_\parallel},n}(\overrightarrow{r}) = \sum_{i,p,\lambda} C^{(n)}_{i,p,\lambda}(\overrightarrow{k_\parallel})|i,p,\lambda> \tag{1.41}$$

La condition pour que $\Psi_{\overrightarrow{k_\parallel},n}(\overrightarrow{r})$ soit une fonction de Bloch s'écrit alors :

$$C^{(n)}_{i,p,\lambda} = \frac{1}{\sqrt{N}} e^{i\overrightarrow{k_\parallel}.\overrightarrow{R_i}_\parallel} e^{i\overrightarrow{k_\parallel}.\overrightarrow{\tau_p}} C^{(n)}_{p\lambda}(\overrightarrow{k_\parallel}) \tag{1.42}$$

Les solutions de l'équation de Schrödinger sont donc de la forme :

$$\Psi_{\overrightarrow{k_\parallel},n}(\overrightarrow{r}) = \sum_{p\lambda} C^{(n)}_{p,\lambda}(\overrightarrow{k_\parallel})|\overrightarrow{k_\parallel},p,\lambda> \tag{1.43}$$

Les éléments de la matrice de l'hamiltonien sont donnés dans la base des ondes de Bloch par l'expression :

$$<\overrightarrow{k_\parallel},p,\lambda|H|\overrightarrow{k_\parallel},q,\mu> = \frac{1}{N}\sum_{j,i} e^{i\overrightarrow{k_\parallel}.(\overrightarrow{R_j}_\parallel+\overrightarrow{\tau_q}-\overrightarrow{\tau_p})} e^{-i\overrightarrow{k_\parallel}.\overrightarrow{R_i}_\parallel} <i,p,\lambda|H|j,q,\mu> \tag{1.44}$$

Puisqu'on utilise des conditions périodiques de Born Von Karman on peut toujours poser $\overrightarrow{R_i}_\parallel = \overrightarrow{0}$. L'équation (1.44) devient alors

$$H^{\lambda\mu}_{pq}(\overrightarrow{k_\parallel}) = <\overrightarrow{k_\parallel},p,\lambda|H|\overrightarrow{k_\parallel},q,\mu> = \sum_j e^{i\overrightarrow{k_\parallel}.(\overrightarrow{R_j}_\parallel+\overrightarrow{\tau_q}-\overrightarrow{\tau_p})} H^{\lambda\mu}(\overrightarrow{R_j}_\parallel + \overrightarrow{\tau_q} - \overrightarrow{\tau_p}) \tag{1.45}$$

Ceci conduit à un système linéaire de dimension $P\ell \times P\ell$ et l'équation aux valeurs propres s'écrit :

$$\mathbb{H}(\overrightarrow{k_\parallel})\mathbb{C}^{(n)}(\overrightarrow{k_\parallel}) = E_n(\overrightarrow{k_\parallel})\mathbb{C}^{(n)}(\overrightarrow{k_\parallel}) \tag{1.46}$$

tel que $\mathbb{H}(\overrightarrow{k_\parallel})$ est un Hamiltonien qui comprend $P \times P$ blocs de taille $\ell \times \ell$ et le vecteur $\mathbb{C}^{(n)}(\overrightarrow{k_\parallel})$ contient P sous vecteurs $(C^{(n)}_i)$ de taille ℓ

$$\begin{pmatrix} (H_{11}) & . & . & . & . & . & . & . & (H_{1P}) \\ . & . & . & . & . & . & . & . & . \\ . & . & . & . & . & . & . & . & . \\ . & . & . & . & . & . & . & . & . \\ . & . & . & . & (H_{ii}) & . & . & . & . \\ . & . & . & . & . & . & . & . & . \\ . & . & . & . & . & . & . & . & . \\ . & . & . & . & . & . & . & . & . \\ (H_{P1}) & . & . & . & . & . & . & . & (H_{PP}) \end{pmatrix} \begin{pmatrix} (C_1^{(n)}) \\ . \\ . \\ . \\ (C_i^{(n)}) \\ . \\ . \\ . \\ (C_P^{(n)}) \end{pmatrix} = E_n(\overrightarrow{k_\parallel}) \begin{pmatrix} (C_1^{(n)}) \\ . \\ . \\ . \\ (C_i^{(n)}) \\ . \\ . \\ . \\ (C_P^{(n)}) \end{pmatrix}$$

où

$$\begin{cases} C_p^{(n)}(\overrightarrow{k_\parallel}) = [C_{p\lambda}^{(n)}(\overrightarrow{k_\parallel})]_{(\lambda=1,\ell)} = < \overrightarrow{k_\parallel}, p, \lambda | \Psi_{\overrightarrow{k_\parallel},n}(\overrightarrow{r}) > \\ \\ H_{pq}(\overrightarrow{k_\parallel}) = [H_{pq}^{\lambda\mu}(\overrightarrow{k_\parallel})]_{(\lambda=1,\ell,\mu=1,\ell)} \end{cases} \tag{1.47}$$

d) La condition de neutralité locale.

Lorsque l'on veut appliquer la méthode des liaisons fortes à des systèmes dont les atomes ne sont pas tous équivalents, une difficulté supplémentaire doit être résolue car la fonction qui détermine les éléments de matrice intra-atomiques $\varepsilon_{i\lambda}^{o}$ a été ajustée sur des systèmes dans lesquels tous les atomes sont équivalents. Bien que dépendant de l'environnement ces éléments de matrice ne décrivent pas correctement l'effet des transferts de charge qui sont attendus dans les systèmes inhomogènes comme les surfaces où les états électroniques subissent localement des perturbations. En effet, si l'on définit le nombre d'électrons sur un atome appartenant au plan p comme la somme des carrés des modules des projections des états occupés sur toutes les orbitales atomiques d'un atome du plan p, l'origine par exemple, ce nombre N_p vaut :

$$N_p = 2 \sum_{\substack{\lambda \\ \overrightarrow{k_\parallel}(E_n(\overrightarrow{k_\parallel})<E_f)}} | < i=0, p, \lambda | \Psi_{\overrightarrow{k_\parallel},n}(\overrightarrow{r}) > |^2 = 2 \sum_{\substack{\lambda \\ \overrightarrow{k_\parallel}(E_n(\overrightarrow{k_\parallel})<E_f)}} |C_{p\lambda}^{(n)}(\overrightarrow{k_\parallel})|^2 \tag{1.48}$$

Si les paramètres $\varepsilon_{i\lambda}^{o}$ (1.34) sont utilisés sans modification on trouve que N_p n'est pas égal au nombre d'électrons de valence N_a par atome de l'élément mais il existe un

transfert de charge $|N_p - N_a|$ qui peut atteindre quelques dixièmes d'électrons sur les atomes des plans dont le nombre de premiers voisins n'est pas celui du volume.

Dans les calculs de premiers principes, l'hamiltonien est résolu de façon auto-cohérente et les transferts de charge sont très faibles ($\leq 0.1e$) comme on peut s'y attendre dans les métaux. Dans la méthode des liaisons fortes, la densité de charge n'étant pas connue, on ne peut pas résoudre les équations de façon auto-cohérente. Une manière de s'approcher de cette solution est d'imposer la neutralité locale de charge. Pour cela et pour garder la méthode au niveau le plus simple, on introduit généralement [19] dans les systèmes ayant des sites inéquivalents, un déplacement additionnel δV_i des éléments de matrice intra-atomiques $\varepsilon^o_{i\lambda}$ au site i,

$$\varepsilon_{i\lambda} = \varepsilon^o_{i\lambda} + \delta V_i \tag{1.49}$$

Ce déplacement est le même pour toutes les orbitales considérées et sa valeur est déterminée de façon auto-cohérente pour assurer la neutralité locale de la charge [14].

Enfin, puisque les déplacements δV_i sont dus à des modifications des interactions électron-électron, il faut soustraire de l'équation (1.31) qui donne l'énergie totale un terme évitant de compter deux fois ces modifications. L'expression de ce terme est dérivée dans la Ref. [14, 19] et l'énergie totale s'écrit

$$E_{tot} = \sum_{nocc} E_n^{'} - N_a \sum_i \delta V_i \tag{1.50}$$

où N_a est le nombre total d'électrons *spd* par atome du métal considéré.

e) Expression de l'énergie de surface.

L'énergie de surface est l'une des quantités de base dans la physique des surfaces. Elle est définie comme l'énergie nécessaire par unité de surface (ou par atome de surface) pour séparer un cristal infini en deux cristaux semi-infinis. Elle est calculée en adoptant la géométrie des couches avec P plans atomiques et en utilisant un nombre important de points spéciaux $\overrightarrow{k_{\|}}$ pour avoir une bonne convergence. Elle est donnée par l'équation :

$$E_s = \frac{E_{couche} - PE_{volume}}{2} \tag{1.51}$$

où E_s est l'énergie de surface par atome de surface, E_{couche} l'énergie totale par maille unité de la couche de P plans considérée et E_{volume} est l'énergie d'un atome

de volume. Pour simplifier les calculs nous n'avons pas pris en compte la relaxation atomique des surfaces.

1.2.6 Description de la structure électronique

a) Structure de bandes projetée.

Pour calculer la structure de bande projetée, on détermine les valeurs propres de l'énergie pour une série de vecteurs d'onde $\overrightarrow{k_{\parallel}}$ le long des directions de haute symétrie de la zone de Brillouin à 2D. Pour un $\overrightarrow{k_{\parallel}}$ donné, les spectres des énergies propres se composent d'une partie quasi-continue pouvant présenter des bandes interdites à l'intérieur desquelles on trouve souvent des états discrets. La partie quasi-continue du spectre est appelée la structure de bande projetée de volume alors que les états discrets sont des états localisés à la surface appelés états de surface. Pour certaines énergies permises dans le volume on peut également trouver des états, appelés états résonants, pour lesquels la probabilité de présence de l'électron est fortement augmentée à la surface.

b) Densité d'états locale.

La diagonalisation de l'hamiltonien des liaisons fortes permet de déterminer les états propres du système. A partir de ces états, on calcule la densité d'états locale $n_{p\lambda}(E)$ sur un site du plan p pour l'orbitale λ [24]. Elle est donnée par :

$$n_{p\lambda}(E) = \sum_{\substack{n \\ k_{\parallel}}} C_{p\lambda}^{(n)*}(\overrightarrow{k_{\parallel}}) C_{p\lambda}^{(n)}(\overrightarrow{k_{\parallel}}) \delta(E - E_n(\overrightarrow{k_{\parallel}})) \tag{1.52}$$

La sommation sur toutes les orbitales atomiques donne la densité d'états locale (LDOS) sur ce site, $n_p(E)$:

$$n_p(E) = 2 \sum_{\lambda=1}^{\ell} n_{p\lambda}(E) \tag{1.53}$$

où ℓ est le nombre d'orbitales atomiques par site. Notons qu'en intégrant $n_p(E)$ jusqu'au niveau de Fermi, on retrouve le nombre N_p d'électrons sur un atome du plan p défini plus haut (1.48).

Les coefficients des fonctions d'onde électroniques vérifient la relation suivante :

$$\sum_{p\lambda} C_{p\lambda}^{(n)*}(\overrightarrow{k_{\|}}) C_{p\lambda}^{(n)}(\overrightarrow{k_{\|}}) = \sum_{\substack{n \\ k_{\|}}} C_{p\lambda}^{(n)*}(\overrightarrow{k_{\|}}) C_{p\lambda}^{(n)}(\overrightarrow{k_{\|}}) = 1 \tag{1.54}$$

et, avec la condition de normalisation introduite, la quantité $n_{p\lambda}(E)$ est normalisée à l'unité. La densité d'états locale $n_p(E)$ est donc normalisée à 2ℓ c'est à dire

$$\int_{-\infty}^{+\infty} n_p(E)dE = 2\ell \tag{1.55}$$

Finalement la densité d'états totale par atome (normalisée à 2ℓ) est :

$$n(E) = \frac{2}{P} \sum_{p\lambda} \sum_{\substack{n \\ \overrightarrow{k_{\|}}}} C_{p\lambda}^{(n)*}(\overrightarrow{k_{\|}}) C_{p\lambda}^{(n)}(\overrightarrow{k_{\|}}) \delta(E - E_n(\overrightarrow{k_{\|}})) \tag{1.56}$$

c) Densité spectrale à $\vec{k}_{\|}$ donné.

La densité d'états spectrale est le nombre d'états d'énergie comprise entre E et E + dE ayant un vecteur d'onde $\overrightarrow{k_{\|}}$ donné :

$$n(E, \overrightarrow{k_{\|}}) = \sum_{n} \delta(E - E_n(\overrightarrow{k_{\|}})) \tag{1.57}$$

où $E_n(\overrightarrow{k_{\|}})$ sont les valeurs propres.

On peut généraliser cette notion de façon à lui donner un caractère local, en faisant intervenir les vecteurs propres de l'hamiltonien. La densité spectrale d'un atome du plan p pour l'orbitale λ et pour une valeur donnée de $\overrightarrow{k_{\|}}$ est définie par :

$$n_{p\lambda}(E, \overrightarrow{k_{\|}}) = \sum_{n} C_{p\lambda}^{(n)*}(\overrightarrow{k_{\|}}) C_{p\lambda}^{(n)}(\overrightarrow{k_{\|}}) \delta(E - E_n(\overrightarrow{k_{\|}})) \tag{1.58}$$

La comparison des densités spectrales au voisinage de la surface avec la densité d'états spectrale du volume permet de mettre en évidence la portée de la perturbation due à la surface et l'existence d'états localisés à la surface. Ainsi, si un pic apparaît dans la densité spectrale, de vecteur d'onde $\overrightarrow{k_{\|}}$ donné à une énergie donnée située dans une bande interdite du volume, cela signale l'existence d'états localisés à la surface.

1.3 Extension à une base non-orthogonale

Nous rappelons que pour les métaux de transition appartenant à la fin des séries, les électrons *sp*, qui ont un caractère fortement délocalisé, contribuent de façon significative à l'énergie totale. Pour les métaux nobles (Cu, Ag, Au) dont la bande *d* est quasi pleine, cette contribution devient largement dominante. Il convient d'améliorer la description des électrons *sp* en tenant compte du recouvrement de ces orbitales. L'objet de ce paragraphe est de décrire l'extension du modèle de liaisons fortes précédemment exposé au cas où est la base est non orthogonale. Dans les chapitres suivants ce modèle sera appliqué au Cuivre.

1.3.1 Définition des intégrales de recouvrement.

Dans une base non-orthogonale l'intégrale de recouvrement des orbitales atomiques $|i\lambda>$ et $|j\mu>$ est définie par :

$$S_{ij}^{\lambda\mu} = \int d^3\overrightarrow{r}\Phi_{\lambda}^{*}(\overrightarrow{r}-\overrightarrow{R_i})\Phi_{\mu}(\overrightarrow{r}-\overrightarrow{R_j}) =< i\lambda|j\mu >\neq \delta_{ij}\delta_{\lambda\mu} \qquad (1.59)$$

La matrice S est symétrique et la valeur des éléments diagonaux ($i = j$, $\lambda = \mu$), est égale à 1, les orbitales atomiques étant orthonormées sur le même site ($S_{ii}^{\lambda\mu} = 0$ si $\lambda \neq \mu$). Il est facile de montrer que, comme les intégrales de saut, les intégrales de recouvrement sont déterminées pour une liaison suivant Oz par une matrice similaire à (1.13) en remplaçant les paramètres de Slater-Koster (ssσ,....) par les intégrales de recouvrement correspondantes (ssσ$'$,...). Pour une liaison d'orientation quelconque la loi (1.14) s'applique en remplaçant $\mathbb{B}$ par $\mathbb{S}$.

1.3.2 Equation aux valeurs propres généralisée.

La résolution de l'équation de Schrödinger dans un base non orthogonale, permet d'écrire :

$$\sum_{j\mu} H_{ij}^{\lambda\mu} C_{j\mu}^{(n)} = E_n \sum_{j\mu} S_{ij}^{\lambda\mu} C_{j\mu}^{(n)} \qquad (1.60)$$

avec $H_{ij}^{\lambda\mu} =< i\lambda|H|j\mu >$

On obtient un problème de valeurs propres et de vecteurs propres généralisé, qui nous permet d'écrire l'équation (1.60) en notation matricielle,

$$\mathbb{HC}^{(n)} = E_n \mathbb{SC}^{(n)} \tag{1.61}$$

Il y a plusieurs méthodes mathématiques pour résoudre ce problème. On adopte la décomposition de Cholesky qui consiste à écrire la matrice de recouvrement d'une manière unique :

$$\mathbb{S} = \mathbb{T}^{+}\mathbb{T} \tag{1.62}$$

où $\mathbb{T}$ est une matrice triangulaire supérieure avec des éléments diagonaux réels et positifs et $\mathbb{T}^{+}$ est la matrice transposée et conjuguée de $\mathbb{T}$. L'idée consiste à définir le vecteur $\mathbb{C}^{'} = \mathbb{TC}$ et la matrice $\mathbb{H}^{'} = (\mathbb{T}^{+})^{-1}\mathbb{HT}^{-1}$ qui transforment le problème des valeurs propres généralisé initial en un problème de valeurs propres simple :

$$\mathbb{H}^{'}\mathbb{C}^{'(n)} = E_n \mathbb{C}^{'(n)} \tag{1.63}$$

Les vecteurs propres de l'équation généralisée (1.61) sont obtenues par la relation linéaire $\mathbb{C}^{(n)} = \mathbb{T}^{-1}\mathbb{C}^{'}$.

1.3.3 Les paramètres et leurs lois de variation.

Pour le cas du Cuivre, nous avons utilisé les paramètres de Papaconstantopoulos dans une base non-orthogonale. Les paramètres intra-atomiques restent donnés par les équations analogues à (1.32) et (1.34).

Aux 10 intégrales de saut s'ajoutent 10 intégrales de recouvrement. Ces 20 paramètres sont supposés varier avec la distance selon la loi suivante [15, 25]

$$P_\gamma(R) = (e_\gamma + f_\gamma R)e^{-g_\gamma^2 R^2} f_c(R) \tag{1.64}$$

où γ est le type d'interaction (ssσ,..., ss$\sigma^{'}$, ..), R est la distance entre les atomes et $f_c(R)$ la fonction de coupure donnée par (1.33). Il faut donc ajuster trois paramètres e_γ, f_γ, g_γ qui sont différents pour chaque type d'interactions.

Le modèle des liaisons fortes dans une base non-orthogonale comporte 73 paramètres qui sont déterminés par un ajustement, à l'aide de la méthode de moindres carrés, à des calculs de structure de bande et d'énergie totale de premier principe pour plusieurs structures périodiques avec divers paramètres de réseau.

1.3.4 Théorème de Bloch.

Dans le cas d'une base non-orthogonale et pour un cristal volumique, le théorème de Bloch établit que l'équation (1.60) en tenant compte de (1.21) s'écrit sous la forme :

$$\sum_{\mu} C_{\mu}^{(n)}(\overrightarrow{k}) \sum_{j} e^{i\overrightarrow{k}.\overrightarrow{R_j}} H_{ij}^{\lambda\mu} = E_n(\overrightarrow{k}) \sum_{\mu} C_{\mu}^{(n)}(\overrightarrow{k}) \sum_{j} e^{i\overrightarrow{k}.\overrightarrow{R_j}} S_{ij}^{\lambda\mu} \tag{1.65}$$

Ceci conduit à un problème de valeurs propres et de vecteurs propres généralisé :

$$\mathbb{H}(\overrightarrow{k})\mathbb{C}^{(n)}(\overrightarrow{k}) = E_n(\overrightarrow{k})\mathbb{S}(\overrightarrow{k})\mathbb{C}^{(n)}(\overrightarrow{k}) \tag{1.66}$$

Pour le cas d'un système comportant P atomes par maille et présentant une périodicité à 2 dimensions, la résolution de l'équation de Schrödinger, telle que $\Psi_{\overrightarrow{k_{\|}}}(\overrightarrow{r}) = \sum_{p\lambda} C_{p\lambda}^{(n)}(\overrightarrow{k_{\|}}) |\overrightarrow{k_{\|}}, p, \lambda >$, permet d'écrire :

$$\sum_{q\mu} H_{pq}^{\lambda\mu}(\overrightarrow{k_{\|}}) C_{q\mu}^{(n)}(\overrightarrow{k_{\|}}) = E_n(\overrightarrow{k}) \sum_{q\mu} S_{pq}^{\lambda\mu}(\overrightarrow{k_{\|}}) C_{q\mu}^{(n)}(\overrightarrow{k_{\|}}) \tag{1.67}$$

Les éléments de la matrice de l'hamiltonien sont toujours donnés par l'équation (1.45) et les intégrales de recouvrement s'écrivent :

$$S_{pq}^{\lambda\mu}(\overrightarrow{k_{\|}}) = \sum_{j} e^{i\overrightarrow{k_{\|}}.(\overrightarrow{R_{j\|}} + \overrightarrow{\tau_q} - \overrightarrow{\tau p})} S^{\lambda\mu}(\overrightarrow{R_{j\|}} + \overrightarrow{\tau_q} - \overrightarrow{\tau p}) \tag{1.68}$$

Nous obtenons un système linéaire de dimension $P\ell \times P\ell$ et une équation aux valeurs propres généralisée :

$$\mathbb{H}(\overrightarrow{k_{\|}})\mathbb{C}^{(n)}(\overrightarrow{k_{\|}}) = E_n(\overrightarrow{k_{\|}})\mathbb{S}(\overrightarrow{k_{\|}})\mathbb{C}^{(n)}(\overrightarrow{k_{\|}}) \tag{1.69}$$

1.3.5 La neutralité locale et l'expression de l'énergie totale.

La charge locale s'identifie à la population de Mulliken dont nous allons rappeler la définition. La charge totale est donnée par une intégration du système sur tout l'espace de la somme des probabilités de présence de tous les l'électrons :

$$NN_a = 2\sum_{n_{occ}} \int |\Psi_n|^2 d^3\overrightarrow{r} = 2\sum_{n_{occ}} \int [\sum_{i\lambda}\sum_{j\mu} C_{i\lambda}^{*(n)} C_{j\mu}^{(n)} \Phi_{i\lambda}^{*} \Phi_{j\mu}] d^3\overrightarrow{r} \tag{1.70}$$

donc

$$NN_a = 2\sum_{i\lambda}\sum_{n_{occ}}[\sum_{j\mu} C_{i\lambda}^{*(n)} C_{j\mu}^{(n)} S_{ij}^{\lambda\mu}] = 2\sum_{i\lambda} N_{i\lambda} \tag{1.71}$$

où $N_{i\lambda}$ est la charge locale de l'orbitale λ centrée sur le site i.
Enfin la charge locale sur le site i, ou population de Mulliken, est donnée par :

$$N_i = 2\sum_{n_{occ}}\sum_{\lambda}[\sum_{j\mu} C_{i\lambda}^{*(n)} C_{j\mu}^{(n)} S_{ij}^{\lambda\mu}] = 2\sum_{\lambda} N_{i\lambda} \tag{1.72}$$

Dans le cas d'une base orthogonale et d'un système homogène, un déplacement uniforme δV_o de tous les éléments diagonaux de l'hamiltonien déplace tous les niveaux de δV_o sans modifier les fonctions d'onde et donc les populations locales. En effet cela revient à changer l'origine des énergies. Dans le cas d'une base non orthogonale, si l'on veut déplacer tous les niveaux de δV_o il faut ajouter à l'hamiltonien la perturbation suivante [26]

$$\delta V_{ij}^{\lambda\mu} = < i\lambda|\delta V|j\mu > = \delta V_o S_{ij}^{\lambda\mu} \tag{1.73}$$

La généralisation de cette formule dans le cas d'un système inhomogène est [26] :

$$\delta V_{ij}^{\lambda\mu} = < i\lambda|\delta V|j\mu > = \frac{1}{2}(\delta V_i + \delta V_j) S_{ij}^{\lambda\mu} \tag{1.74}$$

Pour assurer la neutralité de charge on modifie δV_i de façon autocohérente, c'est à dire jusqu'à ce que la charge N_i soit égale à la charge de valence N_a par atome. Enfin, pour calculer l'énergie totale du système, il faut soustraire les termes de double comptage dus aux modifications des interactions entre les électrons [19].

On montre facilement que l'énergie totale reste donnée par l'équation (1.50).

1.3.6 Généralisation des grandeurs locales.

Il est, toujours utile de représenter les variations de la densité d'états locale, dans le cas d'une base non-orthogonale.

D'une manière générale on définit la densité d'états locale au point $\overrightarrow{r}$ par l'expression suivante :

$$n(E,\overrightarrow{r}) = 2\sum_n |\Psi_n(\overrightarrow{r})|^2 \delta(E-E_n) \tag{1.75}$$

Cette définition qui ne fait intervenir que les états propres est indépendante de la base. Dans une base d'orbitales atomiques réelles, orthonormée ou non :

$$n(E,\overrightarrow{r}) = 2\sum_n \sum_{i\lambda,\,j\mu} C_{i\lambda}^{(n)} C_{j\mu}^{(n)} \Phi_{i\lambda}(\overrightarrow{r}) \Phi_{j\mu}(\overrightarrow{r}) \delta(E-E_n) \tag{1.76}$$

La densité d'états totale s'obtient en intégrant sur tout l'espace.

$$n(E) = 2\int_{-\infty}^{\infty} n(E,\overrightarrow{r}) d^3\overrightarrow{r} = 2\sum_n \sum_{i\lambda,\,j\mu} C_{i\lambda}^{(n)} C_{j\mu}^{(n)} S_{ij}^{\lambda\mu} \delta(E-E_n) \tag{1.77}$$

On peut donc définir une densité d'états locale $n_i(E)$ telle que :

$$n(E) = 2\sum_{i\lambda} n_{i\lambda}(E) = \sum_i n_i(E) \tag{1.78}$$

avec

$$n_{i\lambda}(E) = \sum_n \sum_{j\mu} C_{i\lambda}^{(n)} C_{j\mu}^{(n)} S_{ij}^{\lambda\mu} \delta(E-E_n) \tag{1.79}$$

En intégrant $n_i(E)$ jusqu'au niveau de Fermi on obtient la charge locale au site i, N_i, qui n'est autre que la charge de Mulliken définie par l'équation (1.72)

Pour la géométrie des couches que nous avons adoptée et qui présente une périodicité à 2 dimensions à P atomes par maille, chaque atome engendrant un plan p, la densité d'états locale sur un atome de ce plan s'écrit en utilisant le théorème de Bloch :

$$n_p(E) = 2\sum_\lambda n_{p\lambda}(E) = 2\sum_{\substack{n,q \\ \lambda\mu}} C_{p\lambda}^{(n)}(\overrightarrow{k_\parallel}) C_{q\mu}^{(n)}(\overrightarrow{k_\parallel}) S_{pq}^{\lambda\mu}(\overrightarrow{k_\parallel}) \delta(E-E_n(\overrightarrow{k_\parallel})) \tag{1.80}$$

et la charge locale sur le plan p est :

$$N_p = \int_{-\infty}^{E_f} n_p(E) dE \tag{1.81}$$

1.4 Détails pratiques du calcul.

Dans ce travail, l'hamiltonien est de taille finie et il est diagonalisé en un nombre fini de point $\overrightarrow{k}$ (ou $\overrightarrow{k_{\|}}$) [23, 27]. On obtient un nombre fini de niveaux d'énergie. Jusqu'à présent nous avons considéré que tous les niveaux étaient occupés jusqu'au niveau de Fermi et inoccupés au dessus. Pour accélérer la convergence du calcul de l'énergie totale et des charges locales, chaque niveau E_n est élargi selon la loi :

$$f_n = f(E_n) = \frac{1}{[1+exp(\frac{E_n-E_f}{\omega_f})]} \tag{1.82}$$

où $\omega_f = 0.2$ eV. Cela revient à effectuer le calcul à une température électronique $T_e = \frac{\omega_f}{k_B}$ où k_B est la constante de Boltzmann. Toutes les équations précédentes donnant l'énergie totale et les charges locales restent valables à condition d'effectuer les sommes sur tous les niveaux n, en pondérant chaque niveau par le facteur f_n. Pour obtenir l'énergie totale à température nulle, on utilise la formule d'extrapolation proposée par Weinert et al. [28] :

$$E_{tot}(T=0) \approx E_{tot}(T_e) - \frac{1}{2}T_e S_e + O(T^2) \tag{1.83}$$

où S_e est l'entropie électronique donnée par :

$$S_e = -k_B \sum_n [f_n Ln f_n + (1-f_n)Ln(1-f_n)] \tag{1.84}$$

La condition de neutralité locale consiste à ajuster les paramètres δV_p par un processus d'itérations jusqu'à ce que la différence de charge entre deux itérations consécutives soit inférieure à 10^{-2} e^- par atome et la différence d'énergie inférieure à 10^{-4}eV. Pour réduire le nombre d'itérations il faut partir de valeurs approchées de δV_p. Nous verrons plus loin qu'une bonne approximation consiste à écrire :

$$\delta V_p \approx \alpha(Z_{volume} - Z_p) \tag{1.85}$$

où Z_p et Z_{volume} sont les nombres de premiers proches voisins d'un atome du plan p et d'un atome de volume. Dans le cas d'un cfc ($Z_{volume} = 12$) et α est une constante

qui peut être estimée à partir de la valeur des variations de potentiel sur les surfaces de bas indices (001), (111) et (011).

Finalement mentionnons que le temps de calcul de la charge varie comme N^2, où N est la taille de la matrice de l'hamiltonien, dans notre cas $N = 9 \times P$. Dans le cas d'un modèle de liaisons fortes avec une base non-orthogonale, le calcul des charges de Mulliken est fortement ralenti par la nécessité d'effectuer une sommation sur tous les voisins de l'atome considéré.

Chapitre 2

Energétique des surfaces vicinales de Rh, Pd et Cu dans l'approximation des liaisons fortes.

2.1 Introduction

Dans l'article présenté dans ce chapitre nous nous intéressons au calcul de la structure électronique des surfaces vicinales à partir duquel on peut déduire l'énergie totale et en extraire les énergies de marche, leurs variations en fonction de la largeur des terrasses [2] qui révèlent l'existence d'interactions oscillantes d'origine électronique ainsi que les énergies de cran [3,4]. Ces quantités sont en effet très utiles car elles déterminent la forme des îlots en homoépitaxie sur une surface [1], interviennent dans la transition rugueuse et jouent un rôle dans la stabilité des surfaces vicinales par rapport à un facettage [47] comme nous le montrerons au chapitre 4. Nous utilisons une méthode de liaisons fortes où les fonctions d'onde électroniques sont décomposées sur une base d'orbitales *s*, *p*, et *d* de valence (chapitre 1) [16,17]. Cette méthode est actuellement la seule, basée sur la mécanique quantique, permettant ce type de calculs. En effet les méthodes ab-initio qui sont fondées sur la fonctionnelle de la densité électronique ne permettent pas d'atteindre des mailles élémentaires suffisamment grandes pour de telles études. D'autre part, si les potentiels semi-empiriques [9,10,11,12] peuvent donner accès aux interactions élastiques, comme on le verra au chapitre suivant, ils sont trop rudimentaires pour rendre compte de façon assez précise des effets quantiques. Résumons maintenant les principaux résultats obtenus.

2.2 Energie de marche

Nous présentons ci-dessous le travail que nous avons effectué à partir du modèle des liaisons fortes en base *spd* [16,17]. Ce modèle a été exposé au chapitre 1.

Ce travail est consacré aux métaux de transition appartenant à la fin des séries : Rhodium, Palladium et Cuivre. Il a porté sur le calcul des énergies de surface de surfaces vicinales pour diverses orientations avec des largeurs de terrasse variables. A partir de ces résultats, nous calculons les énergies d'une marche isolée et les interactions entre les marches d'origine électronique.

L'énergie de marche d'une surface vicinale de p rangées atomiques (voir Figure 5) dans la terrasse est définie par [13] :

$$E_{marche}(p) = E_{surf}(p) - (p - 1 + f)E_{surf}(\infty) \tag{2.1}$$

où $E_{marche}(p)$ est l'énergie de marche (par atome de marche) pour la surface vicinale considérée, $E_{surf}(p)$ l'énergie par atome de surface de cette surface et $E_{surf}(\infty)$ l'énergie par atome de surface d'un plan infini parallèle aux terrasses. Le facteur géométrique f est défini sur la figure 1 et donné dans le Tableau 1 pour les surfaces étudiées.

L'énergie d'une marche isolée est la valeur asymptotique de l'énergie de marche dans le cas où le nombre de rangées atomiques p dans la terrasse tend vers l'infini. En pratique pour une largeur de terrasse d'environ 7 rangées atomiques, nous obtenons une convergence de l'énergie de marche.

L'expression de l'énergie de marche est toujours valable pour des marches crantées périodiques. Il existe une formule similaire à celle de l'énergie de marche pour calculer l'énergie de cran, mais qui est difficile à utiliser numériquement car, afin d'éviter les interactions entre crans, il faudrait faire tendre vers l'infini à la fois la distance entre marches et la distance entre crans, ce qui conduirait à des tailles de mailles élémentaires inaccessibles au calcul. Pour calculer l'énergie de cran nous avons donc utilisé la géométrie de supercellules adoptée par Feibelman [7]. Cette géométrie est décrite dans la figure (2) et l'énergie de cran est donnée par l'équation (10).

2.3 Energétique et structure électronique des surfaces vicinales

2.3.1 Energétique

Nous avons étudié cinq géométries de surfaces vicinales de terrasses d'orientation (111), (100) et (110) de Rhodium, Palladium et Cuivre [22]. Pour une surface vicinale donnée, il existe souvent deux types de maille élémentaire (rectangulaire primitive et rectangulaire centrée) dépendant de la largeur de terrasse (p pair ou impair). Dans toutes les surfaces vicinales considérées, les atomes le long des bords de marche sont premiers voisins sauf pour la surface p(100)×(010) qui sont seconds voisins. Nous résumons les caractéristiques géométriques des surfaces étudiées dans le Tableau (1) de l'article.

Nous avons calculé les énergies de marche en fonction du nombre de rangées atomiques p dans la terrasse (Fig 5-7). Nous montrons que les interactions entre marches présentent un profil oscillant et amorti mettant en évidence que les interactions peuvent être attractives pour certaines distances et répulsives pour d'autres [2,37,38,40]. Nous montrerons par la suite (chapitre 4) le rôle joué par ces interactions dans la stabilité des surfaces vicinales. Le comportement est très différent selon les types de marche et de surface si bien qu'il est difficile de définir un comportement général. Le calcul a été effectué sur réseau fixe à 0K, donc sans prendre en compte les effets de la relaxation atomique. Dans ce cas les interactions élastiques [9,33-35] dues au champ de déformation autour de chaque marche sont nulles. De même les interactions entropiques [36] dues aux fluctuations des bords de marches et les interactions dipolaires dues au transfert de charge sont aussi nulles car on a imposé la neutralité de charge sur chaque atome (voir paragraphe 1.3.5 du chapitre 1). Les interactions mises en évidence sont donc des interactions purement électroniques. Elles sont dues aux oscillations de densité de charge autour des marches [41,42].

Il est intéressant de comparer nos résultats obtenus à l'aide du modèle de liaisons fortes *spd* avec les résultats d'un modèle de potentiel de paire effectif proposé par Vitos et al. [13]. Ce modèle est basé sur les énergies des surfaces denses (111), (100) et (110) calculées avec différentes méthodes ab-initio. A partir des énergies de ces surfaces, on détermine les potentiels d'interaction de paires entre plus proches voisins. La portée du potentiel de paire effectif est limitée aux troisièmes voisins. L'accord entre tous les résultats est très raisonnable pour les surfaces de terrasse (111).

Les énergies de marches des surfaces vicinales de terrasse (100) dépendent du potentiel d'interaction entre seconds voisins V_2. Toutefois ce potentiel dépend fortement des énergies de surface utilisées, c'est pourquoi on obtient une grande différence entre les résultats des différents calculs. Les énergies de marches des surfaces de terrasse (110) sont dans tous les cas très faibles et positives. En effet, ces surfaces ne sont pas loin d'être instables par rapport à une reconstruction en rangées manquantes qui peut d'ailleurs être induite par des adsorbats.

Nous utilisons aussi nos résultats pour vérifier la validité de l'approche de Vitos et al. [13]. A partir des énergies de surfaces denses calculées avec le modèle de liaisons fortes spd, nous déterminons les potentiels d'interaction entre plus proches voisins V_1, V_2 et V_3. Les valeurs des énergies des marches correspondantes sont en bon accord avec le calcul complet utilisant le modèle de liaisons fortes spd. Les résultats sont présentés dans le Tableau (2) de l'article.

Cependant la méthode de potentiel de paire effectif [13] ne permet pas de faire la différence entre une marche de type A (surface vicinale de terrasses (111) et de contre-marches (100)) et une marche de type B (surface vicinale de terrasses (111) et de contre-marches ($\overline{1}11$)) et ne permet pas non plus de déterminer les interactions entre marches. Toutefois nos calculs montrent que le modèle de potentiel de paire effectif proposé par Vitos est justifié à condition de calculer les énergies de surface et les énergies de marche avec la même approche.

Les méthodes expérimentales déterminent l'énergie de marche en se basant sur la forme d'équilibre d'un îlot à deux dimensions sur une surface [27-30]. Les énergies de coin sont négligeables pour un îlot de grande taille. A partir du théorème de Wulff, en se basant sur les énergies de marches, nous pouvons tirer des informations sur la forme d'un îlot en homoépitaxie sur une surface. En effet un îlot sur la surface (111) a une symétrie d'ordre trois. Il a trois bords de marche de type A et trois bords de marche de type B. Il a donc une forme hexagonale. Quand l'énergie de la marche de type A est égale à l'énergie de la marche de type B, la forme de l'îlot est un hexagone régulier. Elle serait un triangle équilatéral avec des bords de type B dans le cas où l'énergie de la marche A est supérieure à deux fois l'énergie de la marche B. Toutefois ce cas n'est pas réaliste car la différence entre les énergies des marches A et B est de l'ordre de 1%.

De même un îlot sur une surface (100) est de symétrie d'ordre quatre. Il peut avoir une forme carrée avec des microfacettes de type (111) ou une forme carrée à coins cassés avec des microfacettes de type (111) et (010) [31]. Le deuxième cas se produit

lorsque l'énergie par atome de marche de microfacettes (010) est inférieure au double de celle des marches de microfacettes (111).

Pour le Rhodium et le Palladium, il n'existe pas à notre connaissance de résultats expérimentaux. Par contre plusieurs études ont été effectuées sur le Cuivre [27,28,29]. Les résultats du modèle de liaisons fortes *spd* sont en bon accord avec l'expérience : les ilôts sur la surface (111) sont des hexagones légèrement irréguliers avec une prédominance de bords de type B. Les îlots sur la surface (100) présentent des coins cassés et le rapport des longueurs des deux types de marche, qui est déterminé par le rapport des énergies de marches correspondantes, est bien prévu par le calcul.

Nous présentons également des calculs d'énergie de cran sur les surfaces vicinales de terrasses (111) et (100) de Rhodium, Palladium et Cuivre (Tableau 4). Dans le modèle de potentiel de paire effectif toutes les énergies de cran sont égales à la valeur de V_1. Les énergies de cran avec le modèle des liaisons fortes *spd* sont très proches de cette valeur. Elles sont en bon accord avec d'autres calculs et les résultats expérimentaux existants sur le cuivre [4,29,44]

2.3.2 Etude de la structure électronique

Nous présentons ensuite les résultats concernant la structure électronique des surfaces vicinales. Elle est caractérisée par trois quantités intéressantes : la densité des états locale (LDOS), la structure de bande projetée et la densité spectrale locale des états (voir les équations 1.56 et 1.57).

Les densités d'états locales (LDOS) des atomes de terrasse, de bord de marche, de cran et de volume ont des formes différentes. La densité d'états locale des atomes de bord de marche et de cran est rétrécie notablement par rapport a la densité d'états locale des atomes de terrasse et de volume car la largeur moyenne de la densité d'états locale croît avec le nombre de coordination de l'atome considéré. D'autre part au niveau de Fermi, la densité d'états locale des atomes de cran et de bord de marche est parfois élevée par rapport à celle d'un atome de volume. D'après le critère de Stoner ceci peut conduire à l'existence d'un moment magnétique le long des bords de marche ou sur les crans [18].

La structure de bande projetée de la surface (111) présente des bandes interdites et des états de surface localisés pour certains domaines de $\overrightarrow{k_{\|}}$ [17]. Il est intéressant d'étudier l'évolution de ces bandes interdites et des états de surface en fonction de

la largeur de la terrasse. Nous présentons sur la figure 9 de l'article les structures de bande projetées pour les surfaces vicinales $3(111)\times(100)$ et $7(111)\times(100)$. Les bandes interdites de la surface (111) n'apparaissent pas sur ces surfaces vicinales. Cependant des résonances de surface persistent. En effet si l'on augmente le nombre des rangées atomiques p dans la terrasse, on diminue l'aire de la zone de Brillouin à deux dimensions et on augmente le domaine de k_z [31]. Ceci a pour effet de refermer les bandes interdites et de transformer les états de surface en résonances. On observe le même effet sur les densités spectrales locales d'états. Nous présentons la densité spectrale locale des états au point Γ sur un atome au milieu de la terrasse [45]. La figure 10 montre l'apparition progressive des bandes interdites lorsque le nombre de rangées atomiques p augmente.

2.4 Conclusion

Le modèle des liaisons fortes *spd*, nous a permis de calculer les énergies de marche et de cran et de mettre en évidence des interactions électroniques oscillantes entre marches. Nos résultats rendent bien compte des données expérimentales existantes. Le calcul des énergies de marche et de cran à partir de l'approche de Vitos, en utilisant les énergies des surfaces denses (111), (100) et (110) calculées avec le modèle des liaisons fortes *spd*, est en bon accord avec les résultats d'un calcul direct utilisant le même modèle. Ceci justifie l'approche de Vitos et al. [13]. Par contre cette approche ne permet pas de déterminer les interactions entre les marches. De même elle ne fait la distinction ni entre une marche de type A et une marche de type B sur les surfaces vicinales de terrasses (111), ni entre les énergies de crans. Cependant dans cette approche les énergies de marche et de cran sont sensibles aux énergies de surfaces de bas indices, qui diffèrent parfois de façon appréciable d'un calcul ab-initio à l'autre.

2.5 Articles :

- **Energetics of stepped and kinked surfaces of Rh, Pd and Cu from electronic structure calculations.**

- **Step energies and step-step interactions on vicinal surfaces of Rh and Pd.**

Après cette brève introduction, nous reproduisons tel quels, les articles qui ont été publié dans la revue "Surface Science"

ELSEVIER

Surface Science 505 (2002) 183–199

SURFACE SCIENCE

www.elsevier.com/locate/susc

Energetics of stepped and kinked surfaces of Rh, Pd and Cu from electronic structure calculations

F. Raouafi [a], C. Barreteau [a,*], M.C. Desjonquères [a], D. Spanjaard [b]

[a] *DSM/DRECAM/SPCSI, CEA Saclay, Bâtiment 462, F-91 191 Gif sur Yvette, France*
[b] *Laboratoire de Physique des Solides, Université Paris Sud, F-91 405 Orsay, France*

Received 1 November 2001; accepted for publication 7 January 2002

Abstract

We apply the *spd* tight-binding models, that have been recently developed, to the calculations of the surface energies of several vicinal surfaces of Rh, Pd and Cu with (1 1 1), (1 0 0) and (1 1 0) terraces of increasing widths. From these results we extract the isolated step energies and the step–step electronic interactions. These interactions are most often decaying oscillatory functions of the interstep distance which are strongly dependent of the step geometry. Kink energies are also computed. Our results are in complete agreement with the existing experimental data, in particular on the equilibrium shapes of adislands, which are only available in the literature for Cu. Finally the electronic structure of the vicinal surfaces is also discussed. © 2002 Published by Elsevier Science B.V.

Keywords: Semi-empirical models and model calculations; Surface energy; Epitaxy; Rhodium; Palladium; Copper; Vicinal single crystal surfaces; Surface defects

1. Introduction

The role of steps and kinks is fundamental for understanding the morphology of crystal surfaces and, in particular, its evolution with time and temperature as well as the equilibrium surface structure. Thanks to scanning tunneling microscopy (STM) a breakthrough in the real space observation of this morphology was achieved in recent years. Information on the energetics of surface defects can henceforth be derived from a statistical study of STM images and their evolution with temperature. For instance, the study of the equilibrium shape of large adislands grown by homoepitaxy on monocrystalline surfaces has been used to determine the anisotropy of step energies, and, more recently, the absolute values of step and kink energies [1]. Other interesting quantities have been derived from experimental investigations on vicinal surfaces. The interaction between steps, which are crucial for the roughening transition at surfaces and the stabilization of vicinals, can be drawn from the study of terrace width distributions [2]. Kink energies can also be obtained from the observation of the spatial equilibrium fluctuations of step edges [3,4]. However, these STM

* Corresponding author. Tel.: +33-1-69-08-29-51; fax: +33-1-69-08-84-46.
E-mail address: barreto@drecam.saclay.cea.fr (C. Barreteau).

0039-6028/02/$ - see front matter © 2002 Published by Elsevier Science B.V.
PII: S0039-6028(02)01156-1

investigations, which are complementary to usual diffraction experiments, have, up to now, only been carried out on a limited number of metals mainly Cu, Ag and Pt.

All these experiments have motivated a number of theoretical works. Due to the very low symmetry of these systems, first-principle calculations are scarce and limited to a very small number of geometries and metals, for instance Al [5,6], Cu [7], Pt [8]. On the contrary many theoretical works have been based on semi-empirical potentials like embedded atom model (EAM) [9,10], Sutton–Chen potential [11] or effective medium theory (EMT) [12]. In another approach Vitos et al. [13] have derived step and kink energies of most transition metals from effective pair potentials (EPP) deduced from a first-principle data base of surface energies. However, in all the above methods, electronic step–step interactions are disregarded. In ab initio methods all step–step interactions (except entropic ones) are actually present when the atomic structure is relaxed but, due to computation time, usually a single supercell is used and, consequently, nothing is learnt about their variation with distance. The elastic step–step interactions due to atomic relaxations around the steps are expected to be reasonably estimated with the help of semi-empirical potentials. However, these potentials are still not precise enough to describe in a correct way the variation of the total energy due to charge density oscillations around defects which are at the origin of electronic step–step interactions. Finally, in Vitos et al. model step–step interactions are completely neglected.

In the case of transition metals, tight-binding (TB) models for total energy seem to be the right compromise since they are able to describe correctly the quantum mechanical behavior and, the computational effort being much less than in ab initio methods, they allow to study complex systems with a large number of inequivalent atoms. They have already been used to calculate step energies and step–step interactions in FCC metals [14] and W [15]. However, in these works, the basis set was limited to *d* orbitals. Recently, TB models have been extended to include *s* and *p* orbitals [16,17] and an excellent agreement with ab initio methods has been achieved, not only for the details of the band structure but also for surface energies [17].

In this work we use these *spd* TB models, on the one hand, to calculate the surface energies of different vicinals of Rh, Pd and Cu for increasing terrace widths and, on the other hand, to calculate kink energies. We concentrate on electronic effects at 0 K. Thus no entropic term will be present and, since we study unrelaxed structures, no elastic deformation contribution will be present either. From our surface energies, we will extract the energy of isolated steps and step–step electronic interactions. The paper is organized as follows. In Section 2 the model is briefly summarized and made explicit for applications to steps on vicinal surfaces and kinks. In Section 3 we first present our numerical results for step energies and discuss their consequences on the equilibrium shapes of adislands. Then we comment on step–step electronic interactions. Finally the kink energies are presented. All along this section our results are compared with experimental data and other theoretical works. In Section 4, the electronic structure of stepped surfaces is briefly discussed. Conclusions are drawn in Section 5.

2. The model

2.1. The spd tight-binding model

In this section we describe the two rather similar *spd* TB models that are used in this work: the first one is based on an orthogonal scheme and proved to be very efficient in previous studies of transition metals [17], the second one is based on a non-orthogonal scheme [16]. This last scheme is a little more time consuming but it was found to be essential for a correct description of the *sp* electrons in a noble metal such as copper for which the *d* band is full.

2.1.1. Orthogonal basis set

The TB model used here has been described in details in a previous paper [17], thus we will only recall its main features. The Hamiltonian is defined by its matrix elements in an orthogonal basis set built from s, $p(x,y,z)$, $d(xy,yz,zx,x^2-y^2,3z^2-r^2)$

valence atomic orbitals $|i\lambda\rangle$ centered at each atomic site i. The intersite elements (hopping integrals) are determined from the ten Slater Koster hopping integrals ($ss\sigma, sp\sigma, sd\sigma, pp\sigma, pp\pi, pd\sigma, pd\pi, dd\sigma, dd\pi, dd\delta$). A simple exponential decay of these elements with distance is assumed and three-center integrals are neglected. Following Ref. [16] the on-site terms of the Hamiltonian are defined in such a way that the total energy is obtained by summing up the occupied energy levels. This means that the usual repulsive contribution is accounted for by a dependence on the atomic environment of the on-site terms that we write in the simple form [16] ($\lambda = s, p, d$):

$$\varepsilon^0_{i\lambda} = a_\lambda + b_\lambda \rho_i^{2/3} + c_\lambda \rho_i^{4/3} + d_\lambda \rho_i^2 \tag{1}$$

with

$$\rho_i = \sum_{j\neq i} \exp(-p_\rho(R_{ij}/R_0 - 1)) \tag{2}$$

where R_{ij} is the distance between atoms i and j and R_0 is a reference distance, usually the bulk interatomic spacing.

The parameters of the model are determined by a non-linear least mean square fit on ab initio band structure and total energy curves of two different crystallographic structures (FCC and BCC) at several interatomic distances and their values for palladium and rhodium have been given in our previous publications [17,18].

One should note that these parameters are obtained from systems in which all atoms are neutral since they are geometrically equivalent. When this is not the case we have added a shift δV_i to the on-site terms in order to ensure the local charge neutrality (LCN) which is almost strictly obeyed since screening is very efficient in metals. This potential arises from electron–electron interactions, thus one should not forget to subtract the corresponding double counting terms from the sum of occupied levels in the expression of the total energy which is then written as

$$E_{\text{tot}} = \sum_{n_{\text{occ}}} \epsilon_n - N_{\text{val}} \sum_i \delta V_i \tag{3}$$

where N_{val} is the total number of valence *spd* electrons per atom of the metal.

2.1.2. Non-orthogonal basis set

In the case of copper the non-orthogonal TB scheme was found to be more appropriate. This is due to the more delocalized character of the *sp* electrons which give an important contribution to the total energy since the *d* band is full. We therefore used the TB model developed by Mehl and Papaconstantopoulos [16] that we have extended by including the LCN condition. The charges N_i on site i are defined in the usual Mulliken manner. However the non-orthogonality leads to a generalized eigenvalue problem and makes things a little more tricky since it is well known that a rigid shift of the on-site levels of the Hamiltonian do not produce a rigid shift of the eigenvalues [19]. The potential that must be added to the Hamiltonian matrix $H_{ij}^{\lambda\mu}$ to produce a rigid shift δV_0 of the eigenvalues has the following expression in the atomic orbital basis:

$$\delta V_{ij}^{\lambda\mu} = \langle i\lambda|\delta V|j\mu\rangle = \delta V_0 S_{ij}^{\lambda\mu} \tag{4}$$

where $S_{ij}^{\lambda\mu}$ is the overlap integral between orbital $|i\lambda\rangle$ and orbital $|j\mu\rangle$. The generalization of this formula to the case of an inhomogeneous system is straightforward [19]:

$$\delta V_{ij}^{\lambda\mu} = \langle i\lambda|\delta V|j\mu\rangle = \tfrac{1}{2}(\delta V_i + \delta V_j) S_{ij}^{\lambda\mu} \tag{5}$$

The procedure to ensure LCN is to modify δV_i in a self-consistent way until the charge N_i of each site i is equal to the valence charge N_{val} per atom. Of course, as in the non-orthogonal model, one has also to subtract the double counting terms which have exactly the same expression as in (3).

2.2. Energetics of vicinal surfaces

2.2.1. Step energy

Let us consider a vicinal surface presenting a periodic succession of terraces with equal widths, separated by steps of monoatomic height, and define the step energy per unit step length in this surface. If we call $\mathbf{n}$ and $\mathbf{n}_0$ the directions normal to the vicinal crystallographic planes and to the terraces, respectively, the step energy (per unit length) $\beta(\theta)$ of the vicinal surface is defined by the equation:

$$\gamma(\mathbf{n}) = \gamma(\mathbf{n}_0)\cos(\theta) + \beta(\theta)\sin(\theta)/h \tag{6}$$

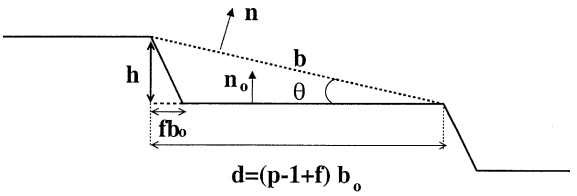

Fig. 1. Cut of a vicinal surface through a plane normal to the step edges: b is the distance between two consecutive steps, b_0 is the distance between two consecutive rows in a terrace, θ is the misorientation angle and p the number of atomic rows (including the inner edge) parallel to the step edge in a terrace, f is a geometrical factor depending on the vicinal surface and h is the interplanar spacing along the direction normal to the terraces.

where $\gamma(\mathbf{n})$ is the surface energy (per unit area) of the crystallographic plane normal to $\mathbf{n}$, θ is the misorientation angle, i.e., the angle between $\mathbf{n}$ and $\mathbf{n}_0$ and h is the interplanar distance in the $\mathbf{n}_0$ direction (Fig. 1). Note that due to the presence of the array of steps with a period depending on θ, $\beta(\theta)$ is expected to vary with θ as a result of step–step interactions. The value of the step energy for an isolated step is then obtained in the limit $\theta \to 0$. Consequently, the nature (oscillatory or monotonic) and the order of magnitude of step–step interactions can be inferred from the study of the quantity $\beta_{\text{int}} = \beta(\theta) - \beta(\theta \to 0)$ for vicinal surfaces with increasing terrace widths. Here we will focus on the electronic step–step interactions.

It is easy to show [13] that (6) can be transformed into the convenient form:

$$E_{\text{step}}(p) = E_{\text{S}}(p) - (p - 1 + f)E_{\text{S}}(\infty) \tag{7}$$

where $E_{\text{step}}(p)$ is now the step energy per step atom in a vicinal surface in which the terraces have p atomic rows parallel to the step edge (including the inner edge), $E_{\text{S}}(p)$ ($E_{\text{S}}(\infty)$) is the surface energy per surface atom of the vicinal (flat) surface. Finally, f is a geometrical factor depending on the vicinal surface which is defined in Fig. 1.

In the following the surface energies of the vicinal (flat) surfaces are calculated using a slab geometry with N_{slab} atomic layers normal to $\mathbf{n}$ ($\mathbf{n}_0$). The surface energy per surface atom is then given by

$$E_{\text{S}} = (E_{\text{slab}} - N_{\text{slab}} E_{\text{bulk}})/2 \tag{8}$$

where E_{slab} is the total energy per two-dimensional (2D) unit cell of the slab and E_{bulk} is the bulk energy per atom. Both quantities are calculated using our *spd* TB model, E_{slab} (E_{bulk}) being obtained from a summation over the 2D (3D) Brillouin zone at special points [20,21].

2.2.2. Kink energy

Finally let us define the kink energy. In the preceding section the step edge may be close-packed or not. Selected non-close-packed edges can be considered as close-packed edges showing a succession of equidistant kinks of monoatomic height. In this case and similarly to (7), the kink energy per kink can be defined as

$$E_{\text{kink}} = E_{\text{step},k}(p_k) - (p'_k - 1 + f'_k)E_{\text{step}}(p) \tag{9}$$

where $E_{\text{step},k}(p_k)$ and $E_{\text{step}}(p)$ are the step energies per step atom of a vicinal surface with kinked edges and close-packed edges, respectively, p'_k is the number of atoms between two consecutive kinks along the close-packed direction and f'_k is a geometrical factor defined as in Fig. 1 which obviously can also be considered as representing a kinked step edge. Like for steps, there are kink–kink interactions, on the one hand, between kinks of the same step edge and, on the other hand, between kinks of different edges. Thus the energy of an isolated kink should be obtained when p (and thus p_k) and p'_k tend to infinity. However, in spite of the large number of atoms which can be treated in a TB calculation, the highest values that p and p'_k can reach remain rather limited. Furthermore convergence on $\mathbf{k}_{//}$ summation, which was achieved for step energies, becomes now very cumbersome since the corresponding 2D Brillouin zone varies with p, p_k, p'_k. Consequently, it seems to be out of reach to study kink–kink interactions at the present time. However, these energies are expected to be at most of the same order of magnitude as step–step interactions. Thus the study of the kink energy using a supercell geometry should give its value to at most 10^{-2} eV as we will see in the following. Moreover, $\mathbf{k}_{//}$ summation errors can be minimized by using the same $\mathbf{k}_{//}$ sampling, i.e., the same 2D Brillouin zone. For this reason we have adopted the supercell geometry already proposed by Feibelman [7] which is

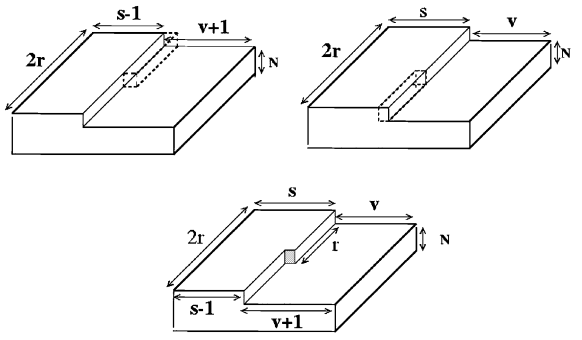

Fig. 2. Unit cells for calculating kink energies: a block of r atoms (dashed lines) is transferred from the second to the first one, leading to two cells identical to the one below.

described in Fig. 2 and leads to a kink formation energy given by

$$4E_{\text{kink}} = 2E_{\text{kinked}}(r,s,v) - [E(s,v) + E(s-1,v+1)] \quad (10)$$

where $E_{\text{kinked}}(r,s,v)$ is the energy per unit cell of the kinked systems and $E(s,v)$ is the energy per unit cell of a system showing perfect stripes with s rows in the stripes and v rows in the valleys where rows are $2r$ atoms long.

3. Results

3.1. Step energies

The calculation of step energies and especially of step–step interactions is a rather delicate task for several reasons: (i) the geometry of the system is more complex than that of low index surfaces leading to unusual unit cells, (ii) the energies considered are small (of the order of a few 10^{-1} eV for the step energies and a few 10^{-3} eV for the step–step interactions) and (iii) many parameters need to be checked carefully to be sure that the numerical results are meaningful. In the following we will first explain the procedure that we have developed to derive efficiently the step energies and step–step interactions. Then we will discuss the results of our calculations. Finally let us recall that no atomic relaxation has been allowed in order to extract purely electronic effects. Introducing these relaxations would slightly reduce the step energy.

3.1.1. Geometry of the vicinal surfaces

In this work we study five step geometries with (1 1 1), (1 0 0) and (1 1 0) terraces and, in each case, we calculate the step energy as a function of the terrace width. The geometrical features of the five types of vicinal surfaces, denoted using Lang et al. [22] notations, are given in Table 1. One can note that for a given step geometry there often exists two types of unit cell (primitive rectangular and centered rectangular) depending on the width of the terrace (p even or odd). In the five considered geometries, the atoms along the step are first neighbours and therefore the step edge is made of a close-packed row of atoms except for the $p(1\,0\,0)\times(0\,1\,0)$ surface for which the atoms are second neighbours and, consequently, the corresponding step edge has a zigzag shape that can be seen as a succession of kinks. Finally let us mention that in all our calculations the number of

Table 1
Geometrical features of the five types of vicinal surfaces

Somorjai notations [22]	Miller indices	f	Edge geometry	2D unit cell
$p(1\,1\,1)\times(1\,0\,0)$ step A	$(p+1,p-1,p-1)$	2/3	nn	p odd: PR p even: CR
$p(1\,1\,1)\times(\bar{1}\,1\,1)$ step B	$(p-2,p,p)$	1/3	nn	p odd: CR p even: PR
$p(1\,0\,0)\times(1\,1\,1)$	$(1,1,2p-1)$	1/2	nn	CR
$p(1\,0\,0)\times(0\,1\,0)$	$(0,1,p-1)$	0	nnn	p odd: CR p even: PR
$p(1\,1\,0)\times(1\,1\,1)$	$(2p-1,2p-1,1)$	1/2	nn	CR

The geometry of the step edge is indicated by the distance between two consecutive atoms: nearest neighbours (nn), next nearest neighbours (nnn). The nature of the 2D unit cell is rectangular, either primitive (PR) or centered (CR). Finally the usual notations, step A and step B, for the vicinals of (1 1 1) are indicated.

layers used in the slab geometry is equal to $N_{slab} = p \times n_{slab}$ where n_{slab} is at least equal to 10.

3.1.2. Computational details

We used a Fermi-level broadening $w_f = 0.2$ eV and 64 special $\mathbf{k}_{//}$ points [20], in the irreducible 2D Brillouin zone. The total energy is extrapolated at zero broadening using the usual approximation of Ref. [23]:

$$E_{tot}(T=0) \approx E_{tot}(T) - \tfrac{1}{2}TS_e + O(T^2) \qquad (11)$$

where S_e is the electronic entropy and T is the electronic temperature corresponding to the Fermi broadening. The energy convergence with respect to the thickness of the slabs, the number of $\mathbf{k}$ points and the Fermi-level broadening was checked carefully and found to be of the order of 1 meV.

Concerning the LCN self-consistent scheme, the iteration process is continued until the difference of charge between two consecutive iterations is $<0.01e^-$ per atom and the difference of energy $<10^{-4}$ eV. Furthermore, in order to reduce the number of iterations it is advisable to start from a good set of δV_i. Actually the potential shift δV_i is, to a good approximation, proportional to the number of first neighbour bonds of atom i broken by the surface. The adequacy of this approximation is clearly seen in Fig. 3 where we have represented the self-consistent potential shift on vicinal surfaces of rhodium as a function of the coordination number Z. These starting values for δV_i reduce drastically the number of iterations.

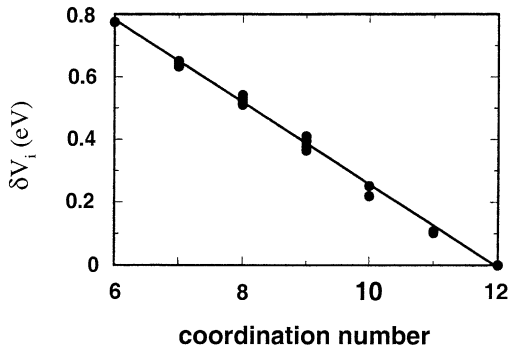

Fig. 3. Self-consistent potential δV_i (in eV) as a function of the coordination number for various sites on the vicinal surfaces of Rh.

3.1.3. Energies of isolated steps

The energy of an isolated step is the asymptotic value of $E_{step}(p)$ when p tends to infinity. Typically terraces with $p \geqslant 6$ are wide enough to get a convergence to about 1 meV, except for the steps with (1 1 0) terraces for which $p \simeq 9$ is needed. The results are given in Table 2 for Rh, Pd, and Cu. It is interesting to compare them with those deduced from the simple model recently proposed by Vitos et al. [13]. More precisely, these authors first determine EPP which are derived from the surface energies of low index surfaces calculated using an ab initio method and neglecting surface atomic relaxation. In the case of an FCC crystal the range of these EPP is limited to the third neighbours and their values V_1, V_2, V_3 are drawn from the (1 1 1), (1 0 0) and (1 1 0) surface energies. The step energy is then given by

$$E_{step}(p) = \sum_{s=1}^{3} n_{step,s}(p) V_s;$$
$$n_{step,s}(p) = n_s(p) - (p - 1 + f) n_s(\infty) \qquad (12)$$

The numbers $n_s(p)$ and $n_s(\infty)$ are the total number of bonds in the sth coordination sphere broken by the vicinal and flat surfaces, respectively. Due to the short range of the EPP, $n_{step,s}(p)$ becomes a constant as soon as p overcomes a value p_∞ which is actually very small, i.e., most often $p_\infty \leqslant 2$ [13]. As a consequence step interactions cannot be obtained within this model. The expressions of the isolated step energies as a function of V_1, V_2, V_3 are given in Table 2.

Our calculations allow to check the validity of this approach. The values of V_1, V_2, V_3 derived from the surface energies obtained from our TB model are given in Table 3. The corresponding values of the step energies are given in Table 2 (EPP-TB column). When comparing the results with our full TB calculations, it can be seen that the discrepancy is always smaller than 3×10^{-2} eV and very often as small as some meV. The agreement is thus surprisingly good so that we can conclude that when surface energies and step energies are calculated within the same approach, the method

Table 2
Step energies for various vicinal geometries

	Vicinal surface	Step energy E_{step} (eV/atom)						
	$p \to \infty$	TB	EPP					
				TB	Vitos	Methfessel	Eichler	Galanakis
Rh	$p(111)\times(100)$	0.638	$2V_1+4V_3$	0.657	0.583	0.520	0.650	0.670
	$p(111)\times(\bar{1}11)$	0.645	$2V_1+4V_3$	0.657	0.583	0.520	0.650	0.670
	$p(100)\times(111)$	0.393	V_1+2V_2	0.407	0.288	0.265	0.295	0.285
	$p(100)\times(010)$	0.747	$2V_1+2V_2$	0.738	0.550	0.480	0.580	0.596
	$p(110)\times(111)$	0.056	V_2+2V_3	0.035	0.043	0.070	0.045	0.011
Pd	$p(111)\times(100)$	0.425	$2V_1+4V_3$	0.429	0.460	0.423		0.500
	$p(111)\times(\bar{1}11)$	0.432	$2V_1+4V_3$	0.429	0.460	0.423		0.500
	$p(100)\times(111)$	0.289	V_1+2V_2	0.295	0.106	0.222		0.298
	$p(100)\times(010)$	0.536	$2V_1+2V_2$	0.533	0.265	0.427		0.548
	$p(110)\times(111)$	0.027	V_2+2V_3	0.006	0.045	0.015		0.024
Cu	$p(111)\times(100)$	0.348	$2V_1+4V_3$	0.347	0.380			0.426
	$p(111)\times(\bar{1}11)$	0.345	$2V_1+4V_3$	0.347	0.380			0.426
	$p(100)\times(111)$	0.191	V_1+2V_2	0.192	0.200			0.241
	$p(100)\times(010)$	0.352	$2V_1+2V_2$	0.359	0.363			0.456
	$p(110)\times(111)$	0.060	V_2+2V_3	0.020	0.046			0.011

Several types of results are presented: the full TB calculation and calculations based on EPPs V_1, V_2, V_3 (EPP) fitted on the (1 1 1), (1 0 0), and (1 1 0) surface energies obtained from various methods: TB, and ab initio methods (Vitos et al. [13], Methfessel et al. [24], Eichler et al. [25]) and Galanakis et al. [26]. Note that there is a misprint in the TB results for Rh and Pd $p(110)\times(111)$ in Table 2 of the preliminary account of this work published in Ref. [46].

Table 3
Surface energies in eV per atom of the low index surfaces of Rh, Pd and Cu

	Surface energies (eV/atom)			V_1	V_2	V_3	Reference	V_1^0
	(1 1 1)	(1 0 0)	(1 1 0)					
Rh	1.091	1.379	2.112	0.332	0.038	−0.001	This work	0.352
	1.002	1.310	1.919	0.262	0.013	0.015	Vitos et al. [13]	0.324
	0.99	1.27	1.84	0.215	0.025	0.023	Methfessel et al. [24]	0.313
	1.11	1.47	2.13	0.285	0.005	0.020	Eichler et al. [25]	0.360
	1.034	1.404	2.047	0.311	−0.013	0.012	Galanakis et al. [26]	0.344
Pd	0.665	0.828	1.317	0.238	0.029	−0.011	This work	0.217
	0.824	1.152	1.559	0.159	−0.027	0.036	Vitos et al. [13]	0.269
	0.68	0.89	1.33	0.205	0.008	0.003	Methfessel et al. [24]	0.223
	0.822	1.049	1.596	0.250	0.014	0.0	Galanakis et al. [26]	0.269
Cu	0.581	0.748	1.121	0.166	0.013	0.004	This work	0.188
	0.707	0.906	1.323	0.163	0.018	0.014	Vitos et al. [13]	0.224
	0.675	0.874	1.327	0.215	0.013	−0.001	Galanakis et al. [26]	0.221

V_n is the corresponding value of the EPP in eV between nth neighbours, V_1^0 is the value given by a least mean square fit of the three surface energies with an EPP limited to first nearest neighbours.

proposed by Vitos et al. [13] is quite valid if an estimation of step energies to $\simeq 10^{-2}$ eV is needed and step–step interactions as well as atomic relaxation are disregarded.

It is also interesting to compare our results with those obtained from the Vitos et al. method but using other data sets for the surface energies, for example those provided by Vitos et al. [13],

Methfessel et al. [24], Eichler et al. [25] and Galanakis et al. [26] (see Table 3 for the corresponding surface energies and numerical values of V_1, V_2, V_3). The results are given in Table 2. It is seen that the agreement between all results is reasonable for the stepped surfaces with (1 1 1) terraces. In addition, all calculations give a very small positive step energy on the vicinal of (1 1 0) for steps with (1 1 1) ledge orientation. This suggests that this surface is very close to an instability. Indeed, (1 1 0) FCC surfaces have a tendency to exhibit a (2×1) missing row reconstruction. In the EPP model it is easily shown that the reconstruction energy (per unit cell of the reconstructed surface) is equal to $2(V_2 + 2V_3)$, i.e., twice the formation energy of a step with a (1 1 1) ledge. This reconstruction does not occur for Rh, Pd and Cu when the surface is clean but it may be triggered by the presence of adsorbates when the gain in adsorption energy (due to an increased coordinence of the adatoms) is large enough. If we now consider the vicinals of (1 0 0) for which the value of V_2 plays an important role, large differences are found. From Table 3 it is indeed seen that the value of V_2 is strongly dependent on the surface energy data base. The largest discrepancy occurs between our results and those of Vitos et al., in the case of the (1 0 0) vicinal surfaces of Pd for which a factor of two, or even almost three, is found between the step energies. This is clearly due to the value of V_2 which is in both cases not negligible, but negative when using the surface energies of Vitos et al., and positive in our calculations. Nevertheless it should be noted that the EPP V_3 given by Vitos et al., is also not negligible and $V_3 > |V_2|$ so that we can suggest that, might be, in this particular case, the range of the EPP should be increased. On the contrary our results for the step energies of Pd with (1 0 0) terraces are very close to those that can be derived from the low index surface energies of Galanakis et al.

In addition, it has been noted by Galanakis et al., that the surface energies of metals scale quite accurately with the number of broken nearest neighbour bonds. For this reason and in view of the dispersion of the numerical results on V_2 and V_3, we have found interesting to compare the previous results with those obtained by limiting the pair potentials to first nearest neighbours. The corresponding parameter V_1^0 determined by a least mean square fit on the three low index surfaces, is equal to $[3E_S(1\,1\,1) + 4E_S(1\,0\,0) + 6E_S(1\,1\,0)]/61$.

The results are given in the last column of Table 3. It is seen that the dispersion of the numerical values of V_1^0, and thus of the step energies, is much smaller than previously but the agreement with the full TB calculations is less accurate.

However it must be noted that in the EPP approach the step energy of vicinals with (1 1 1) terraces is the same for both ledge orientations: (1 0 0) (i.e., type A step) and $(\bar{1}\,1\,1)$ (i.e., type B step). This is not the case in our full TB calculation in which the A step is slightly energetically favoured for Rh and Pd, the reverse being obtained for Cu.

Let us now compare our results with experimental data. Most of the experiments giving access to step energies are based on the observation of the equilibrium shape of 2D islands on surfaces as a function of temperature by means of STM [27–30]. For this purpose let us first comment on the implications of our results on the equilibrium shape at 0 K of large 2D islands built by homoepitaxy on the (1 1 1) and (1 0 0) surfaces.

On the (1 1 1) surface the island should, as the substrate, show three-fold symmetry. The edges of the island are thus made of three A steps and three B steps (Fig. 4). When the island is large enough, corner effects are negligible and the equilibrium shape, i.e., the ratio L_A/L_B of the lengths of steps A and steps B is derived from the Wulff theorem ($\beta_A/\beta_B = r_A/r_B$, $r_A(r_B)$ being the distance from

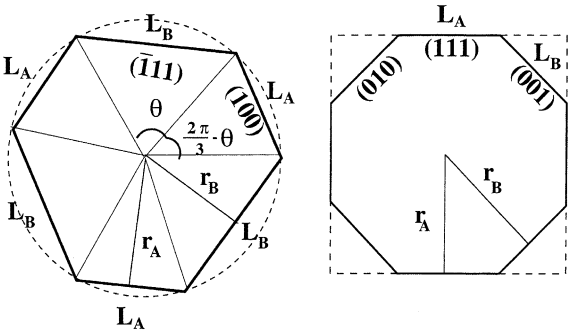

Fig. 4. The equilibrium shapes of islands on (1 1 1) (a) and (1 0 0) (b) FCC surfaces. The orientations of the microfacets are indicated.

the center of the island to the A (B) edges) which leads to:

$$\frac{L_A}{L_B} = \frac{2 - \beta_A/\beta_B}{2\beta_A/\beta_B - 1} \tag{13}$$

Note that for these steps $E^A_{step}/E^B_{step} = \beta_A/\beta_B$. As obvious, the equilibrium shape is a regular hexagon when $\beta_A/\beta_B = 1$. When the ratio of the two step energies is larger than 2, the shape is an equilateral triangle, the edges of which have the lowest step energy, but this ratio is quite unrealistic. From our present study $\beta_A/\beta_B = 1 \pm \epsilon$ where ϵ is small, this gives $L_A/L_B \simeq 1 \mp 3\epsilon$. For Rh, Pd and Cu the step energies differ by $\simeq$1% so that L_A and L_B should differ by $\simeq$3% (with $L_A > L_B$ for Rh, Pd and $L_A < L_B$ for Cu) and could be measured.

Let us consider an island on the (1 0 0) surface. The symmetry of the island should be four-fold. Using an EPP model extending to the next nearest neighbours, its equilibrium shape may be a square, or a square with broken corners [31] (Fig. 4). In view of the agreement between the full TB calculation and the EPP model, we can assume that both models predict the same equilibrium shape. The Wulff theorem yields:

$$\frac{L_A}{L_B} = \frac{\sqrt{2} - \beta_A/\beta_B}{\sqrt{2}\beta_A/\beta_B - 1} = \sqrt{2}\frac{1 - E^A_{step}/E^B_{step}}{2E^A_{step}/E^B_{step} - 1} \tag{14}$$

where A denotes the edges with (1 1 1) type microfacets, i.e., with nearest neighbour atomic spacing and B those with (0 1 0) type microfacets, i.e., with second nearest neighbour spacing. As a consequence the equilibrium shape is a perfect square when $E^A_{step}/E^B_{step} \leqslant 1/2$ and a square with broken corners in the opposite case. For rhodium our full TB calculations give a square with broken corners and $L_B/L_A \simeq 7\%$. In the EPP model it is easy to show that $E^A_{step}/E^B_{step} \leqslant 1/2$ when $V_2 \leqslant 0$ and $E^A_{step}/E^B_{step} > 1/2$ when $V_2 > 0$. The estimations based on EPP for which $V_2 > 0$ (Table 2) lead qualitatively to the same result as the full TB model whereas when using the surface energies of Galanakis et al. ($V_2 < 0$) a perfect square is predicted. For the same reason the results for Pd are also controversial since $L_B/L_A = 12\%$ in our full TB calculations, 14% for the Galanakis et al., data, 6% for the Methfessel et al., data, while from Vitos et al., result ($V_2 < 0$) a perfect square is expected. Finally, the equilibrium shape of islands of Cu on Cu(1 0 0) should be a square with broken corners, L_B/L_A being of the order of 15% both in our calculations and using Vitos et al., data, and 9% with Galanakis et al., data.

Unfortunately no data on step energies are available for Rh and Pd. The above results show that, in particular, it would be very interesting to have some experimental information on the equilibrium shapes of islands on Rh(1 0 0) and Pd-(1 0 0). On the contrary, several studies have been carried out on Cu yielding not only the ratio of step energies but also their average values. The most recent experiments by Giesen et al. [29] give an average step energy for the two kinds of steps on Cu(1 1 1) equal to 0.27 ± 0.03 eV per step atom, the energy of step A being measurably ($1.1 \pm 0.7\%$) larger than that of a B step. Note that previous experiments [27,28] concluded that step A was energetically favoured but it was argued by Giesen et al. [29] that in these experiments A edges may actually be B edges and vice-versa if the islands nucleate at HCP sites in the vicinity of steps. Other published results on the average step energy lie between 0.22 and 0.31 eV. Our full TB calculations lead to $E^A_{step} = 0.348$ eV and $E^B_{step} = 0.345$ eV. Consequently, our results agree with the most recent experiments concerning the relative stability of the two steps but seem to slightly overestimate the average step energy, which could be attributed, at least partly, to the neglect of atomic relaxation. Note that an ab initio calculation by Feibelman [7] which takes relaxation into account yields 0.27 eV for step A and 0.26 eV for step B in better agreement for the average step energy but with a slightly too large anisotropy ratio.

Giesen et al. [29] report also on similar experiments on Cu(1 0 0). Their extrapolation at 0 K of the observed aspect ratio yields $r_B/r_A = 1.24$ (see Fig. 4) which is in a quite satisfactory agreement with our full TB data: $r_B/r_A = E^B_{step}/(E^A_{step} \times \sqrt{2}) = 1.30$. The calculated energy of the straight step $(1\,0\,0) \times (1\,1\,1)$ (0.191 eV) is also in good agreement with the experiment (0.22 ± 0.02 eV). Finally we would like to emphasize that the presence of broken corners in the equilibrium shape cannot be explained in the framework of a first

nearest neighbour broken bond (or Ising) model which predicts a perfect square at 0 K ($L_B = 0$ thus $r_B/r_A = \sqrt{2}$).

3.1.4. Step–step interactions

Let us now discuss step–step interactions. There exists several types of interactions between steps. The most studied is the so-called elastic interaction due to the deformation fields around each step which interact repulsively. This elastic interaction gives rise in the continuum elasticity limit to an energy term varying at large interstep distance as $1/d^2$ where d is the distance between the two steps [32]. However, when trying to fit results derived from empirical potential on relaxed surfaces, it appears that for smaller d ($d \leqslant 6$ inter-row spacings) the behavior of $E_{step}(d)$ deviates significantly from this law [9,33–35].

An entropic interaction [36] coming from the fact that meandering steps cannot cross each other has also been taken into account also giving rise to a repulsive behavior varying as $1/d^2$ at large d. Charge transfers in the vicinity of the steps produce a dipole–dipole interaction (repulsive or attractive) varying also as $1/d^2$.

Finally oscillatory electronic interactions of the Friedel type should also be present similarly to those existing between chemisorbed atoms or defects [37,38] but they have attracted little attention, at least up to now. Such interactions have been invoked by Frohn et al. [39] to explain their STM observations on Cu(1 1 n). They have also been introduced theoretically by Redfield and Zangwill [40] and discussed in a phenomenogical manner by Pai et al. [2], who tried to fit their experimental distributions of terrace widths by means of Monte Carlo simulations using interacting potentials of the form:

$$U(d) = \frac{A}{d^n} + \frac{B\cos(\kappa d + \delta)}{d^m} \tag{15}$$

However their data sets are still too limited for a definitive conclusion concerning the values of the parameters of the model. Nowadays by STM imaging one can "visualize" charge density oscillations around adatoms and steps [41] that can create oscillatory interactions between these defects. This was shown, in particular of Cu adatoms on Cu(1 1 1) [42] and on the vicinity of steps on Au(1 1 1)($22 \times \sqrt{3}$) [43].

Up to now there exists no precise electronic structure calculations except one preliminary attempt with a simplified TB scheme, showing that these oscillatory interactions do exist [14,15]. In Ref. [14] general trends were put forward but the role played by *sp* electrons in the total energy, which is significant in FCC transition metals, was neglected. The *spd* TB model used in the present work enables us to avoid this approximation. In Figs. 5–7 we have represented the variation of the step energy as a function of p for the five step geometries on surfaces of Rh, Pd and Cu. Three main features can be extracted from these curves: (i) the step–step interaction has a damped behavior which is most often oscillatory, (ii) the amplitude of the oscillations can be as large as some 10^{-2} eV for small values of p and remains of the order of some 10^{-3} eV when $p \geqslant 5$ in the studied domain of p, (iii) the shape of the oscillations is quite stable for two neighbouring elements in the periodic table (rhodium and palladium) but it is strongly dependent on the orientation of the steps. It is also quite interesting to see that in some cases the oscillations are very weak ($p(1\,0\,0) \times (1\,1\,1)$) whereas in some other cases they can be rather large ($p(1\,0\,0) \times (0\,1\,0)$). Finally in the vicinal surfaces $p(1\,1\,0) \times (1\,1\,1)$, β_{int} is always attractive within the studied range of p for the three metals.

Let us now compare our results with related works. The electronic step–step interaction energies are of the same order of magnitude as the full step–step interactions derived from experiments using an analysis of terrace width distributions which most often assumes purely repulsive interactions varying as $1/d^2$. In view of the oscillatory character of electronic interactions this last assumption is questionable. The approach of Pai et al. [2] is a first attempt to get rid of this assumption but their potential (Eq. (15)) is likely too simple. Indeed it is difficult to fit the results by an analytical expression and extrapolate an asymptotic behavior which would be interesting to compare elastic and electronic interactions. In addition the damping factor may depend on the

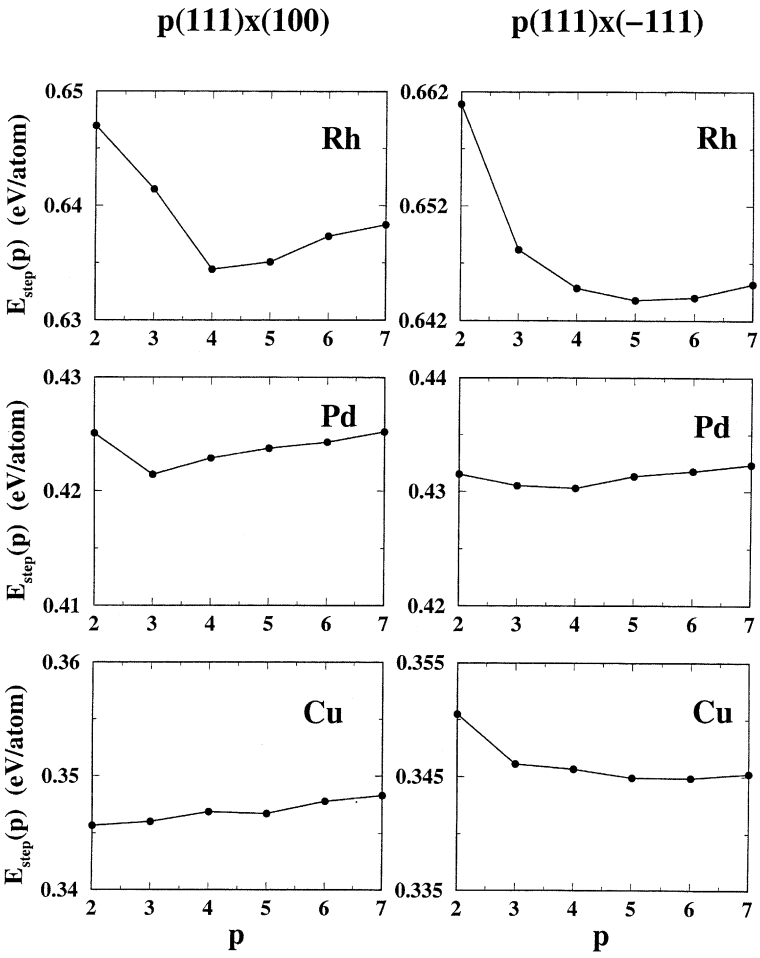

Fig. 5. The variation of the step energy (per step atom) as a function of the terrace width for the $p(111) \times (100)$ and $p(111) \times (\bar{1}11)$ vicinal surfaces of Rh, Pd and Cu.

possible existence of electronic states localized on terraces [2,40]. Note also that empirical potentials are too simple to describe properly electronic interactions and lead to monotonically decreasing repulsive interactions (for $p \geqslant 2$) [9].

Finally, there are very few experimental data on the domain of small terrace widths. However, an anomalous behavior of the terrace width distribution at low temperature for Cu $p(100) \times (111)$ has been observed by Frohn et al. [39]. They suggest that such a behavior may be interpreted by assuming repulsive interactions when $d \simeq 1$–2 (in units of the nearest neighbour distance) but attractive (or oscillatory) ones when $d \simeq 3$–5. This is quite consistent with our results as can be seen in Fig. 6.

3.2. Kink energy

We have calculated the kink energies on steps with close-packed edges and the most close-packed terraces ((111), (100)), i.e., the kink energies on the steps $(111) \times (100)$, $(111) \times (\bar{1}11)$ and $(100) \times (111)$. As explained above, it is presently out of reach to derive kink–kink interactions. Thus we used the geometry proposed by

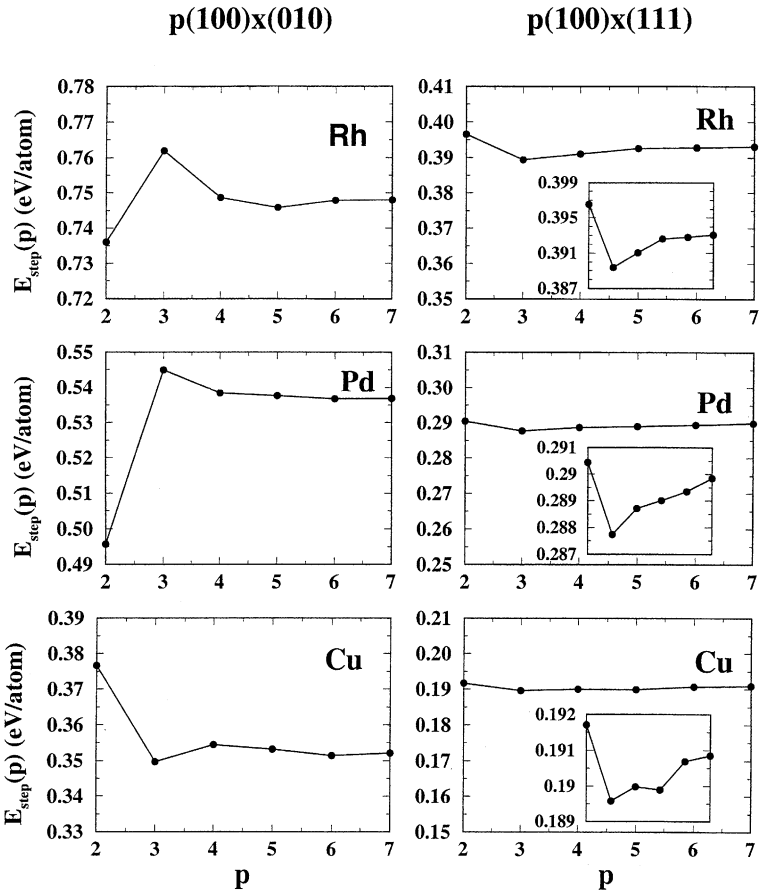

Fig. 6. The variation of the step energy (per step atom) as a function of the terrace width for the $p(100) \times (010)$ and $p(100) \times (111)$ (for which the energy scale has been enlarged in the insets to put forward clearly the sign of interactions) vicinal surfaces of Rh, Pd and Cu.

Feibelman [7] which yields kink energies to a few meV since it includes unavoidably kink–kink interactions. We have chosen the values ($s = 4$, $v = 4$, $r = 4$, $N = 7$) for the parameters defining the size of the unit cell (see Fig. 2). The number of atoms, N_{at}, in the unit cell needed to compute kink energies is thus $400 < N_{at} < 500$. Therefore, a single $\mathbf{k}_{//}$ point ($\mathbf{k}_{//} = 0$) was used. We have also checked that the numerical results are not changed by more than 0.01 eV when the parameters s, v, r and N are slightly increased or decreased. Finally, our calculations reveal that ensuring the LCN condition has a much smaller influence for Cu, in which the d band is full, than for Rh and Pd since the local charges are much larger for the latter metals than for Cu when the self-consistent potentials δV_i are neglected. In the latter case surface energies are decreased by $\simeq$15% for Rh, whereas for Cu the change is only $\simeq$2%. For this reason we have imposed the LCN condition in the calculations of kink energies for Rh and Pd, but not for Cu.

The results are given in Table 4. It is seen that the kink energy varies only slightly from one type of step to the other. In the EPP model the kink energy is the same for the three steps and equal to V_1 as long as the pair potentials are cutoff beyond third neighbours. It is indeed easily shown that in the process depicted in Fig. 2 the only bonds that have not been restored are the bonds between the kink atoms and their neighbours in the step edge. Actually, our kink energies calculated using the full TB model are always rather close to the cor-

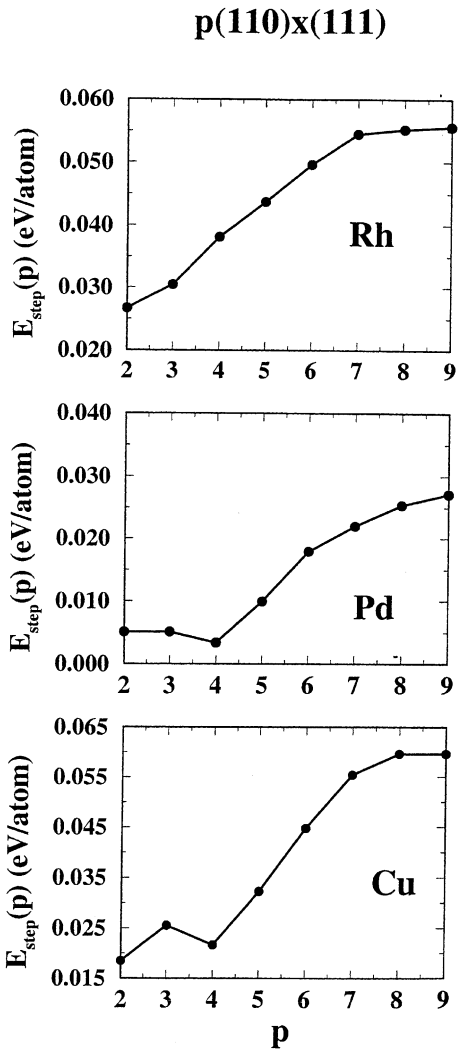

Fig. 7. The variation of the step energy (per step atom) as a function of the terrace width for the $p(110) \times (111)$ vicinal surfaces of Rh, Pd and Cu.

responding values of V_1. The small differences can be ascribed to the different local geometries, that come into play as soon as the interactions are not pairwise, or to different kink–kink interactions. Note that the latter effect is presumably smaller than the former in the difference between the kink energies on the two kinds of steps with (1 1 1) terraces since the kink–kink distances are the same in both cases.

Obviously, similarly to the case of step energies, the estimations based on EPP but using other surface energy data bases show a significant dispersion which is reduced when limiting the pair potentials to nearest neighbours. (see V_1^0 in Table 3).

Let us finally compare the results of our full TB model with calculations (other than with the EPP model) and experiments (Table 4). Like for steps, data are available only for Cu. For kinks on the $(100) \times (111)$ steps, our kink energy compares favourably with the EAM calculation of Liu et al. [44], and with the experimental result of Barbier et al. [4] and Giesen et al. [29]. In the case of the two types of steps with (1 1 1) terraces, we find a good agreement with experiments [29] not only for the average kink energy but also for the relative values, the kink energy on step A being slightly smaller than on step B. This effect was also found in the ab initio calculations by Feibelman [7]. However ab initio calculations predict a larger difference between the two steps and somewhat smaller kink energies.

Finally it is interesting to calculate the kink energy (per kink) in the 100% kinked step on (1 0 0) which is simply given by the difference of step energies per atom between $(100) \times (010)$ and $(100) \times (111)$. From our full TB calculations this gives: 0.354 eV (Rh), 0.247 eV (Pd) and 0.161 eV (Cu). These values are rather close to those reported in Table 4. This confirms that kink–kink interactions are very small.

Table 4
Kink energies for various steps with closed-packed edges in Rh, Pd and Cu (in eV)

(Terrace) × (ledge)	Rh	Pd	Cu		
			This work	Other calculations	Experiments
$(111) \times (100)$	0.339	0.249	0.143	0.092 [7]	0.113 ± 0.007 [29]
$(111) \times (\bar{1}11)$	0.329	0.242	0.148	0.117 [7]	0.121 ± 0.007 [29]
$(100) \times (111)$	0.349	0.247	0.146	0.139 [44]	0.123 [4] 0.129 ± 0.009 [29]
V_1	0.332	0.238	0.166		

4. Electronic structure

Let us now present our results concerning the electronic structure of the vicinal surfaces. Three interesting quantities can be used to characterize the electronic structure: the local density of states (LDOS) $n_i(E)$ at each site i, the projected band structure $E(\mathbf{k}_{//})$ and the spectral local densities of states $n_i(E,\mathbf{k}_{//})$. This will be illustrated in the case of rhodium.

Some typical examples of LDOS on atomic rows of the terrace parallel to the step edge and on kink atoms are shown in Fig. 8 and compared with bulk LDOS. As expected there is an overall narrowing of the LDOS on the less coordinated atoms and their shapes vary with the different sites. More surprisingly, the details of these LDOS are rather insensitive to the terrace width as soon as $p \geqslant 3$. In particular, the LDOS in the middle of the terraces tends very rapidly to the LDOS of the flat surface [17]. Note that the LDOS at the step edge is significantly enhanced compared to the bulk one in an energy range of $\simeq$2.5 eV below the Fermi level. Moreover the LDOS at the Fermi level is significantly increased at the outer edge atoms compared with that of bulk atoms and slightly larger than

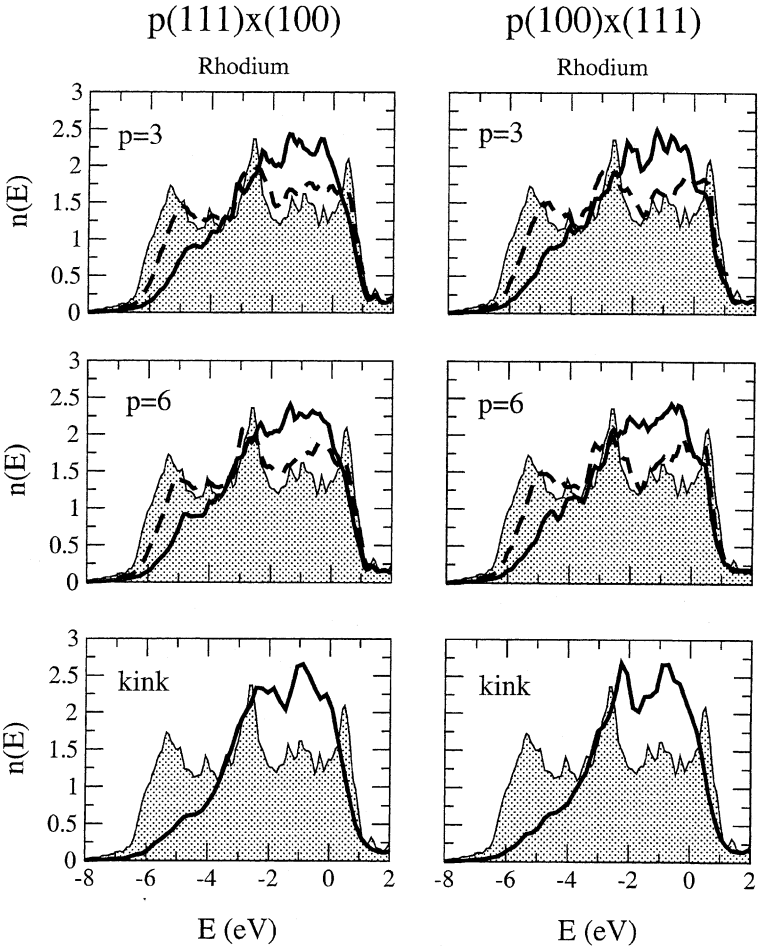

Fig. 8. The local densities of states on the outer (full lines) and inner (dashed lines) step edges and on kink sites (full lines) for the $p(111)\times(100)$ and $p(100)\times(111)$ vicinal surfaces of Rh compared to the bulk density of states (shaded). The Fermi level is the energy zero.

that of the flat surface. In a previous work [18], we showed that Rh(1 0 0) was close to the ferromagnetic instability, thus it would not be surprising that a magnetic moment appears at step edges or kinks on some vicinal surfaces of Rh.

Let us now comment on the surface projected band structure $E(\mathbf{k}_{//})$ for the $p(1\,1\,1)\times(1\,0\,0)$ surfaces. These surfaces have been chosen since the (1 1 1) surface exhibits well defined gaps and surface states [17]. Consequently it is interesting to study the evolution of these gaps and surface states with the terrace width. We show in Fig. 9 the results for $p = 3$ and 7. The most striking feature is the disappearance of almost all gaps, in particular near $\bar{\Gamma}$. Since as p increases the area of the 2D Brillouin zone decreases, the height of the surface adapted bulk Brillouin zone [31], i.e., the sampled domain of k_z increases accordingly. Therefore, for a given $\mathbf{k}_{//}$, more and more bulk states corresponding to lines with no symmetry in the 3D Brillouin zone are found. This explains the absence of gaps and of true surface states. However a number of surface resonances can be identified. In Fig. 9 states with more than 40% of the total intensity on the first p vicinal layers (i.e., on the terrace atoms) on both sides of the slab are marked as resonance states. Some of these states can be clearly associated to surface states of the (1 1 1) surface. In particular this latter surface has a surface state around 6 eV below the Fermi level which exists in a rather wide region of the 2D Brillouin zone around $\bar{\Gamma}$ and has a roughly parabolic dispersion along the $\bar{\Gamma}\bar{M}$ and $\bar{\Gamma}\bar{K}$ directions. This state becomes a resonance on the $p(1\,1\,1)\times(1\,0\,0)$ surface and can be clearly identified in the $\bar{\Gamma}\bar{X}$ direction, i.e., propagating along the steps. Its dispersion curve is still parabolic-like but, as p decreases, its energy increases due to the lateral confinement between two consecutive steps. This is also seen on the local spectral densities of states at the $\bar{\Gamma}$ point on the atomic row in the middle of the terrace (Fig. 10). In addition this figure shows the progressive appearance of gaps when p tends to infinity: when p increases the spectral LDOS becomes lower and lower in the energy domains corresponding to the (1 1 1) surface gaps. In the $\bar{\Gamma}\bar{Y}$ direction which corresponds to states propagating perpendicularly to the steps, the corresponding surface state of the (1 1 1) surface is expected to be strongly perturbed by the periodic lattice of steps as discussed by Davis et al. [45] in the particular case of the *sp* surface state of Au(1 1 1). Indeed in Fig. 9 this state is not seen except at the $\bar{\Gamma}$ point for the $3(1\,1\,1)\times(1\,0\,0)$ surface whereas it reappears

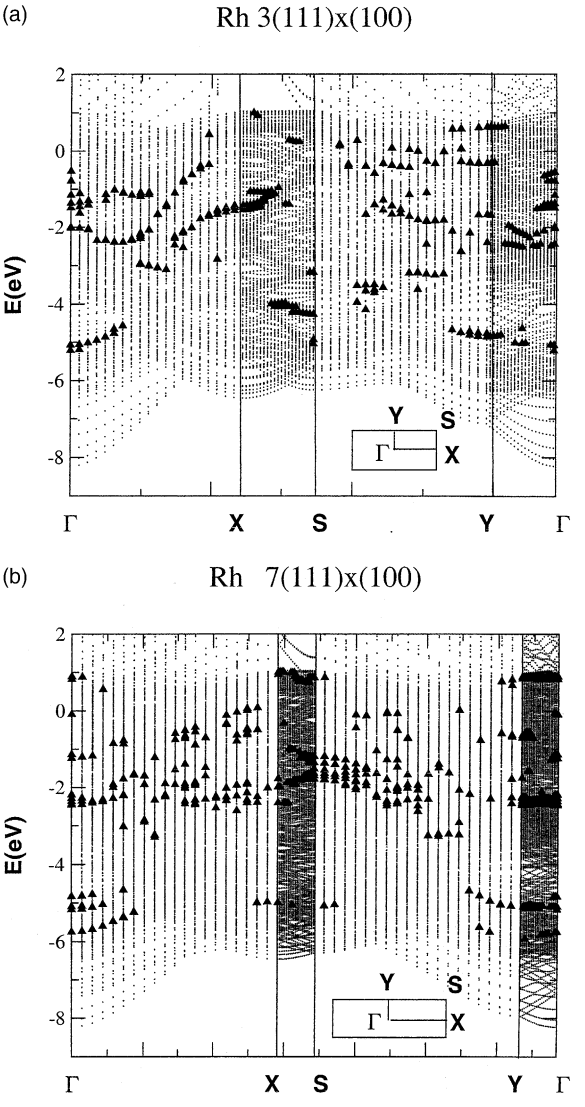

Fig. 9. The surface projected band structure of (a) Rh $3(1\,1\,1)\times(1\,0\,0)$-i.e., (2 1 1)- and (b) Rh $7(1\,1\,1)\times(1\,0\,0)$-i.e., (4 3 3)-vicinal surfaces along the symmetry lines of the 2D Brillouin zone shown in the inset. The Fermi level is the energy zero. The resonant states are marked as full triangles. The localization criterion is given in the main text.

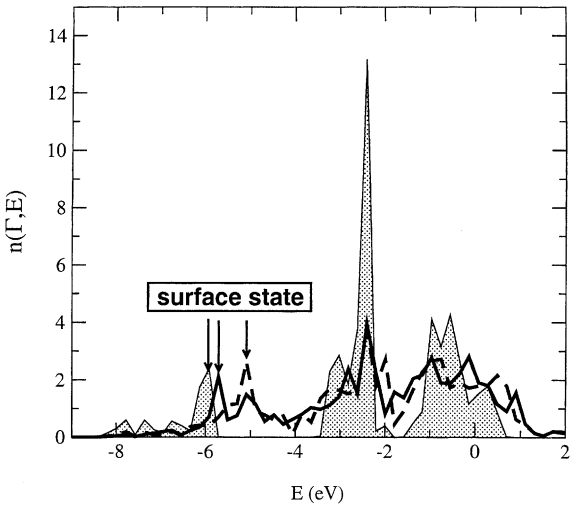

Fig. 10. The local spectral densities of states at $\bar{\Gamma}$ on the atomic row located in the middle of the terraces for the $3(1\,1\,1)\times(1\,0\,0)$ (dashed line), $7(1\,1\,1)\times(1\,0\,0)$ (full line) and $(1\,1\,1)$ (shaded) surfaces of Rh. The Fermi level is the energy zero. Each level has been broadened by 0.04 eV.

for the $7(1\,1\,1)\times(1\,0\,0)$ surface but with a quite different dispersion curve.

5. Conclusion

We have used the *spd* TB method to derive the formation energy of isolated steps on Rh, Pd and Cu surfaces for various geometries. A good agreement with existing experimental data has been obtained. In particular, for the shape of adislands of Cu on Cu(1 0 0), for the relative stability of the two types of steps on the vicinals of Cu(1 1 1), and for kink energies.

In addition we have shown that, from the knowledge of the surface energies of the three low index surfaces of an FCC crystal calculated from the *spd* TB Hamiltonian, one can deduce effective pair interactions giving step and kink energies in good agreement with those derived from the diagonalization of the *spd* TB Hamiltonian for vicinal surfaces. This fully justifies the approach of Vitos et al. [13]. However in the latter method step–step interactions are disregarded, no difference can be found neither between the energies of the two types of steps with (1 1 1) terraces nor between kink energies on steps with close-packed edges. Moreover the step and kink energies in the Vitos et al., model are sensitive to the surface energy data base.

Our study, based on the calculation of step energies on vicinal surfaces as a function of the terrace width, has enabled us to derive electronic step–step interactions for moderately wide terraces ($d \leqslant 20$ Å). These interactions are rapidly decaying and they may be attractive or repulsive depending on the terrace width. Moreover, in this range of widths, their order of magnitude is comparable to that of other interactions. Consequently, these interactions play a significant role in the stability of vicinal surfaces [47].

Finally, the investigation of the electronic structure suggests that, for some geometries, a magnetic moment may appear at step edges in Rh.

Acknowledgements

We are grateful to I. Galanakis for communicating his results prior to publication and to L. Barbier for stimulating discussions.

References

[1] M. Giesen, Prog. Surf. Sci. 68 (2001) 1, and references therein.
[2] W.W. Pai, J.S. Ozcomert, N.C. Bartelt, T.L. Einstein, J.E. Reutt-Robey, Surf. Sci. 307–309 (1994) 747.
[3] J. Villain, D.R. Grempel, J. Lapujoulade, J. Phys. F 15 (1985) 809.
[4] L. Barbier, L. Masson, J. Cousty, B. Salanon, Surf. Sci. 345 (1996) 197.
[5] J.S. Nelson, P.J. Feibelman, Phys. Rev. Lett. 68 (1992) 2188.
[6] R. Stumpf, M. Scheffler, Phys. Rev. B 53 (1996) 958.
[7] P.J. Feibelman, Phys. Rev. B 60 (1999) 11118.
[8] P.J. Feibelman, Surf. Sci. 463 (2000) L661.
[9] Z.T. Tian, T.S. Rahman, Phys. Rev. B 47 (1993) 9751.
[10] R.C. Nelson, T.L. Einstein, S.V. Khare, P.J. Rous, Surf. Sci. 295 (1993) 462.
[11] K.D. Hammonds, R.M. Lynden-Bell, Surf. Sci. 298 (1992) 437.
[12] J.W.M. Frenken, P. Stoltze, Phys. Rev. Lett. 82 (1999) 3500.
[13] L. Vitos, H.L. Skriver, J. Kollar, Surf. Sci. 425 (1999) 212.
[14] S. Papadia, M.C. Desjonquères, D. Spanjaard, Phys. Rev. B 53 (1996) 4083.

[15] Wei Xu, J.B. Adams, T.L. Einstein, Phys. Rev. B 54 (1996) 2910.
[16] M.J. Mehl, D.A. Papaconstantopoulos, Phys. Rev. B 54 (1996) 4519.
[17] C. Barreteau, D. Spanjaard, M.C. Desjonquères, Phys. Rev. B 58 (1998) 9721.
[18] C. Barreteau, R. Guirado-López, D. Spanjaard, M.C. Desjonquères, A.M. Oleś, Phys. Rev. B 61 (2000) 7781.
[19] P.O. Löwdin, J. Chem. Phys. 18 (1950) 365.
[20] S.L. Cunningham, Phys. Rev. B 10 (1974) 4988.
[21] D.J. Chadi, M.L. Cohen, Phys. Rev. B 8 (1973) 5747.
[22] B. Lang, R.W. Joyner, G.A. Somorjai, Surf. Sci. 30 (1972) 440.
[23] M. Weinert, J.W. Davenport, Phys. Rev. B 45 (1992) 13709.
[24] M. Methfessel, D. Henning, M. Scheffler, Phys. Rev. B 46 (1992) 4816.
[25] A. Eichler, J. Hafner, J. Furthmüller, G. Kresse, Surf. Sci. 346 (1996) 300.
[26] I. Galanakis, G. Bihlmayer, V. Bellini, N. Papanikolaou, R. Zeller, S. Blügel, P.H. Dederichs, Eur. Phys. Lett., submitted for publication;
I. Galanakis, V. Bellini, N. Papankolaou, R. Zeller, P.H. Dederichs, submitted to Surf. Sci.
[27] D.C. Schlösser, L.K. Verheij, G. Rosenfeld, G. Comsa, Phys. Rev. Lett. 82 (1999) 3843.
[28] G.S. Icking-Konert, M. Giesen, H. Ibach, Phys. Rev. Lett. 83 (1999) 3880.
[29] M. Giesen, C. Steimer, H. Ibach, Surf. Sci. 471 (2001) 80.
[30] C. Steimer, M. Geisen, L. Verheij, H. Ibach, Phys. Rev. B 64 (2001) 085416.
[31] M.C. Desjonquères, D. Spanjaard, in: Concepts in Surface Physics, second edition, Springer-Verlag, Berlin, 1996, p. 44.
[32] V.I. Marchenko, Y.A. Parshin, Sov. Phys. JETP 52 (1981) 129.
[33] D. Wolf, J. Jaszczaki, Surf. Sci. 277 (1992) 301.
[34] R. Najafabadi, D.J. Srolovitz, Surf. Sci. 317 (1994) 221.
[35] P. Hecquet, B. Salanon, Surf. Sci. 366 (1996) 415.
[36] C. Jayaprakash, C. Rottman, W.F. Saam, Phys. Rev. B 30 (1984) 6549.
[37] T.L. Einstein, J.R. Schrieffer, Phys. Rev. B 7 (1973) 3629.
[38] A. Yaniv, Phys. Rev. B 24 (1981) 7093.
[39] J. Frohn, M. Giesen, M. Poensgen, J.F. Wolf, H. Ibach, Phys. Rev. Lett. 67 (1991) 3543.
[40] A.C. Redfield, A. Zangwill, Phys. Rev. B 46 (1992) 4289.
[41] N. Knorr, H. Brune, M. Epple, A. Hirstein, M.A. Schneider, K. Kern, submitted for publication.
[42] J. Repp, F. Moresco, G. Meyer, K.H. Rieder, P. Hyldgaard, M. Persson, Phys. Rev. Lett. 85 (2000) 2981.
[43] Y. Hasegawa, Ph. Avouris, Phys. Rev. Lett. 71 (1993) 1071.
[44] C.L. Liu, J.B. Adams, Surf. Sci. 294 (1993) 211.
[45] L.C. Davis, M.P. Everson, R.C. Jaklevic, W. Shen, Phys. Rev. B 43 (1991) 3821.
[46] F. Raouafi, C. Barreteau, M.C. Desjonquères, D. Spanjaard, Surf. Sci. 482–485 (2001) 1413.
[47] M.C. Desjonquères, D. Spanjaard, C. Barreteau, F. Raouafi, Phys. Rev. Lett. 88 (2002) 056104.

ELSEVIER

Surface Science 482–485 (2001) 1413–1418

SURFACE SCIENCE

www.elsevier.nl/locate/susc

Step energies and step–step interactions on vicinal surfaces of Rh and Pd

F. Raouafi [a], C. Barreteau [a], M.C. Desjonquères [a,*], D. Spanjaard [b]

[a] *DSM/DRECAM/SPCSI, CEA Saclay, Bat. 462, F-91 191 Gif sur Yvette, France*
[b] *Laboratoire de Physique des Solides, Université Paris Sud, F-91 405 Orsay, France*

Abstract

The calculation of step energies and a fortiori of step–step interactions in transition metals remains up to now out of reach of ab initio methods. Using a tight-binding model in a s, p and d orbital basis set we have studied the energetics of several vicinal surfaces of Rh and Pd with (1 1 1), (1 0 0) and (1 1 0) terrace orientations. The energy per step atom exhibits a damped oscillatory behaviour as a function of the terrace width. This reveals the existence of oscillatory electronic step–step interactions that are strongly dependent on the geometry and on the element and are of the same order of magnitude as other interactions. The possible existence of a magnetic moment in the vicinity of the step edges is also discussed.

Keywords: Semi-empirical models and model calculations; Surface energy; Vicinal single crystal surfaces; Rhodium; Palladium

1. Introduction

It is well known that the energetic properties of steps govern the surface morphology and thus are fundamental in understanding epitaxial growth, surface roughening and equilibrium crystallite shapes. A handy structural model to compute step energies and their interactions is provided by vicinal surfaces which present a periodic array of steps.

There have been only a few systematic studies on step energies on transition and noble metal surfaces. Most of them have used empirical potentials such as embedded atom model (EAM) [1,2] and effective medium theory (EMT) [3]. In another approach Vitos et al. [4] have derived step energies from effective pair potentials deduced from a first principle database of surface energies. Ab initio calculations are in principle feasible but, due to the large number of atoms in the unit cell, they need a large amount of computer time and are rather scarce [5]. Moreover, in the above methods, the possibility of electronic step–step interactions is disregarded. Intermediate between the above types of calculations, the tight-binding (TB) scheme is very attractive since it is much less costly in computer time and still describes systems within the framework of quantum mechanics. It allows to investigate not only step energies but also their electronic interactions, as well as the step electronic structure and, in particular, the possible occurrence of states localized along the step edges. However, up to now, the TB basis set was limited

* Corresponding author. Tel.: +1-69-08-38-56; fax: +1-69-08-84-46.
E-mail address: mcdjs@drecam.saclay.cea.fr (M.C. Desjonquères).

0039-6028/01/$ - see front matter
PII: S0039-6028(01)00858-5

to d orbitals [6] and, even though general trends were derived, the numerical values of step energies were underestimated especially for elements at the end of the transition series. A major improvement is presented in this work by making use of the spd TB model [7] that we have recently set up and proved that it gives accurate surface energies. In this paper our results on step energies and step–step interactions in Rh and Pd are presented and discussed in connection with previous works. In addition we briefly comment on the step electronic structure, in particular on the possibility of occurrence of magnetism at step edges.

2. The model

The TB model used has been described in details in a previous paper [7], thus we will only recall its main features. The Hamiltonian is defined by its matrix elements in an orthogonal basis set built from s, p(x,y,z), d$(xy,yz,zx,x^2-y^2,3z^2-r^2)$ valence atomic orbitals $|i\lambda\rangle$ centered at each atomic site i. The intersite elements (hopping integrals) are determined from the ten Slater Koster hopping integrals (ssσ, spσ, sdσ, ppσ, ppπ, pdσ, pdπ, ddσ, ddπ, ddδ). A simple exponential decay with distance is assumed for these elements and three center integrals are neglected. Following Ref. [8] the on-site terms of the Hamiltonian are defined in such a way that the total energy is obtained by summing up the occupied energy levels. This means that the usual repulsive contribution is accounted for by a dependence on the atomic environment of the on-site terms that we write in the simple form [8] ($\lambda = \mathrm{s,p,d}$):

$$\varepsilon^0_{i\lambda} = a_\lambda + b_\lambda \rho_i^{2/3} + c_\lambda \rho_i^{4/3} + d_\lambda \rho_i^2 \tag{1}$$

with

$$\rho_i = \sum_{j\neq i} \exp(-p_\rho(R_{ij}/R_0 - 1)) \tag{2}$$

The parameters of the model are determined by a non-linear least mean square fitting on ab initio band structures and total energy curves of two different crystallographic structures (fcc and bcc) at several interatomic distances and their values for Palladium and Rhodium have been given in our previous publications [7,9].

One should note that these parameters are obtained from systems in which all atoms are neutral since they are geometrically equivalent. When this is not the case we have added a shift δV_i to the onsite terms in order to ensure the local charge neutrality which is almost strictly obeyed since screening is very efficient in metals. This potential arises from electron–electron interactions, thus one should not forget to subtract the corresponding double counting term in the expression of the total energy which is then written as [7]:

$$E_{\mathrm{tot}} = \sum_{\mathrm{nocc}} \epsilon_n - N_{\mathrm{val}} \sum_i \delta V_i \tag{3}$$

where N_{val} is the total number of valence spd electrons per atom of the metal.

Let us call $\mathbf{n}$ and $\mathbf{n_0}$ the directions normal to the vicinal crystallographic plane and to the terraces, respectively. The step energy, per unit step length, $\beta(\theta)$ is usually defined by the following equation:

$$\gamma(\mathbf{n}) = \gamma(\mathbf{n_0})\cos\theta + \beta(\theta)\frac{\sin\theta}{d} \tag{4}$$

where $\gamma(\mathbf{n})$ is the surface energy (per unit area) of the crystallographic plane normal to $\mathbf{n}$, θ is the angle between $\mathbf{n}$ and $\mathbf{n_0}$, d is the interplanar distance along the $\mathbf{n_0}$ direction.

Following Vitos et al. [4], this equation can be more conveniently transformed into:

$$E_{\mathrm{step}}(p) = E_{\mathrm{S}}(p) - (p - 1 + f)E_{\mathrm{S}}(\infty) \tag{5}$$

where $E_{\mathrm{step}}(p)$ is the step energy (per step atom), $E_{\mathrm{S}}(p)$ and $E_{\mathrm{S}}(\infty)$ are the surface energies (per surface atom) of the vicinal and flat surfaces, respectively, p is the number of atomic rows parallel to the step edges in the terrace (including the inner edge), finally f is defined in Fig. 1. The surface energies can be calculated using a slab geometry with N layers. They are given by the equation:

$$E_{\mathrm{S}} = (E_{\mathrm{slab}} - NE_{\mathrm{bulk}})/2 \tag{6}$$

where E_{slab} is the total energy per 2D unit cell of the slab and E_{bulk} is the bulk energy per atom. In all cases the summations over Brillouin zones are carried out using special points.

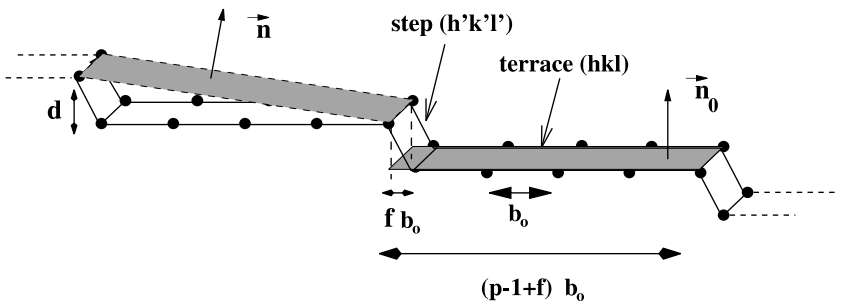

Fig. 1. Step geometry of a $p(h\,k\,l) \times (h'\,k'\,l')$ vicinal surface.

In the absence of step–step interactions $\beta(\theta)$ would be a constant. We will see below that, actually, $\beta(\theta)$ varies slightly with θ and tends to a limit β_0, which corresponds to the isolated step, when θ decreases (i.e., p increases). Therefore $(\beta - \beta_0)$ is a measure of step–step interactions.

3. Results

We have calculated the step energy as a function of the terrace width for five different step geometries with (1 1 1), (1 0 0) and (1 1 0) terrace orientations characterized in Table 1. The number of vicinal planes in the slab has been taken equal to $11p$ and the calculations have been carried out on a rigid lattice. We used a Fermi-level broadening of 0.2 eV and 64 special k points in the irreducible two dimensional Brillouin zone. The total energy at zero broadening is deduced using the method of Ref. [10]. The energy convergence was checked carefully and is of the order of 1 meV.

The energy of an isolated step is obtained for terraces wide enough for neglecting the interaction between steps. Typically terraces with $p \geqslant 6$ are sufficient to get a reasonable convergence. The results are presented in Table 2. It is interesting to compare them with those deduced from the simple model recently introduced by Vitos et al. [4]. Actually, these authors proposed to estimate step and kink energies by using effective pair potentials (EPP) up to the third neighbours (V_1, V_2, V_3) in fcc crystals, these potentials being determined from ab initio calculated surface energies of the three low-index surfaces (1 1 1), (1 0 0) and (1 1 0). In Table 2 we have also listed the results given by this model using our TB database of surface energies as well as ab initio ones from Vitos et al. [4], Eichler et al. [11] and Methfessel et al. [12]. When comparing the results of the full TB model with the EPP-TB ones, it can be seen that they are in a

Table 1
Geometrical features of the five types of vicinal surfaces

Somorjai notations	Miller indices	f	Edge geometry	2D unit cell
$p(1\,1\,1) \times (1\,0\,0)$ step A	$(p+1, p-1, p-1)$	2/3	nn	p odd: PR p even: CR
$p(1\,1\,1) \times (1\,1\,1)$ step B	$(p-2, p, p)$	1/3	nn	p odd: CR p even: PR
$p(1\,0\,0) \times (1\,1\,1)$	$(1, 1, 2p-1)$	1/2	nn	CR
$p(1\,0\,0) \times (0\,1\,0)$	$(0, 1, p-1)$	0	nnn	p odd: CR p even: PR
$p(1\,1\,0) \times (1\,1\,1)$	$(2p-1, 2p-1, 1)$	1/2	nn	CR

The geometry of the step edge is indicated by the distance between two consecutive atoms: nearest neighbours (nn), next nearest neighbours (nnn). The nature of the 2D unit cell is rectangular, either primitive (PR) or centered (CR). Finally the usual notations, step A and step B for the vicinals of (1 1 1) are indicated.

Table 2
Step energies for various vicinal geometries

Element	Vicinal surface	Step energy β_0					
		TB	EPP				
				TB	Vitos	Methfessel	Eichler
Rhodium	$p(1\,1\,1)\times(1\,0\,0)$	0.638	$2V_1+4V_3$	0.657	0.583	0.520	0.650
	$p(1\,1\,1)\times(\bar{1}\,1\,1)$	0.645	$2V_1+4V_3$	0.657	0.583	0.520	0.650
	$p(1\,0\,0)\times(1\,1\,1)$	0.393	V_1+2V_2	0.407	0.288	0.265	0.295
	$p(1\,0\,0)\times(0\,1\,0)$	0.747	$2V_1+2V_2$	0.738	0.550	0.480	0.580
	$p(1\,1\,0)\times(1\,1\,1)$	0.005	V_2+2V_3	0.035	0.043	0.070	0.045
Palladium	$p(1\,1\,1)\times(1\,0\,0)$	0.425	$2V_1+4V_3$	0.429	0.460	0.423	
	$p(1\,1\,1)\times(\bar{1}\,1\,1)$	0.432	$2V_1+4V_3$	0.429	0.460	0.423	
	$p(1\,0\,0)\times(1\,1\,1)$	0.289	V_1+2V_2	0.295	0.106	0.222	
	$p(1\,0\,0)\times(0\,1\,0)$	0.563	$2V_1+2V_2$	0.533	0.265	0.427	
	$p(1\,1\,0)\times(1\,1\,1)$	0.003	V_2+2V_3	0.006	0.045	0.015	

Several types of results are presented: a full TB calculation and a calculation based on EPP V_1, V_2, V_3 fitted on (1 0 0) (1 1 1) (1 1 0) surface energies obtained from various methods: TB, and ab initio methods [4,11,12].

surprisingly good agreement which justifies the approach of Vitos et al. Nevertheless some of the results obtained with the various EPP models differ significantly. Obviously the reason for this discrepancy comes from the surface energy database which, even in ab initio methods, can vary by 15–20%. However the step energy of the vicinals of (1 1 1) are in quite reasonable agreement and all calculations lead to positive step energies for the vicinal of (1 1 0) which are very small since the step energy does not depend on V_1. The largest difference occurs for the vicinals of (1 0 0) for which V_2 is important.

Thus our calculations prove that effective pair potentials are very valuable tools but, of course, there are some limitations: for example A and B steps on the (1 1 1) surface have the same energy in this model [4] whereas the full TB calculation shows that the A step is energetically favored.

Let us now discuss step–step interactions. There exists several types of interactions between steps. The most studied is the so-called elastic interaction due to the deformation fields around each step which interact repulsively. An entropic interaction coming from the fact that meandering steps cannot cross has also been taken into account. These interactions are repulsive and give rise to an energy term varying as $1/L^2$ where L is the distance between the two steps. Charge transfers in the vicinity of the steps give rise to a dipole–dipole interaction (repulsive or attractive) varying also as $1/L^2$. Finally there should also exist Friedel type oscillatory electronic interactions but which have attracted little attention, at least up to now. They are clearly seen on Fig. 2 on which we have represented the variation of the step energy as a function of p on the (1 0 0) surface of Rh and Pd for two step orientations. Three main features can be extracted from these curves: first the step–step interaction has a damped oscillatory behavior, second the amplitude of the oscillations can be as large as 10^{-2} eV, finally the shape of the oscillations is quite stable for two neighboring elements in the periodic table but it is strongly dependent on the orientation of the steps. This "electronic" interaction has the same order of magnitude as the other types of interactions, at least for small distances typically less than 10 atomic rows. However it is difficult to fit the result by an analytical expression. In addition the damping factor may depend on the possible existence of electronic states localized on terraces [13].

It must be emphasized that with our numerical accuracy ($\simeq$1 meV) we can be confident on our results, at least for the parameters used. However, in view of their very small amplitude, the detailed shape of the oscillations may somewhat depend on the set of TB parameters. In conclusion we have shown that oscillatory electronic step–step interactions exist and should be considered.

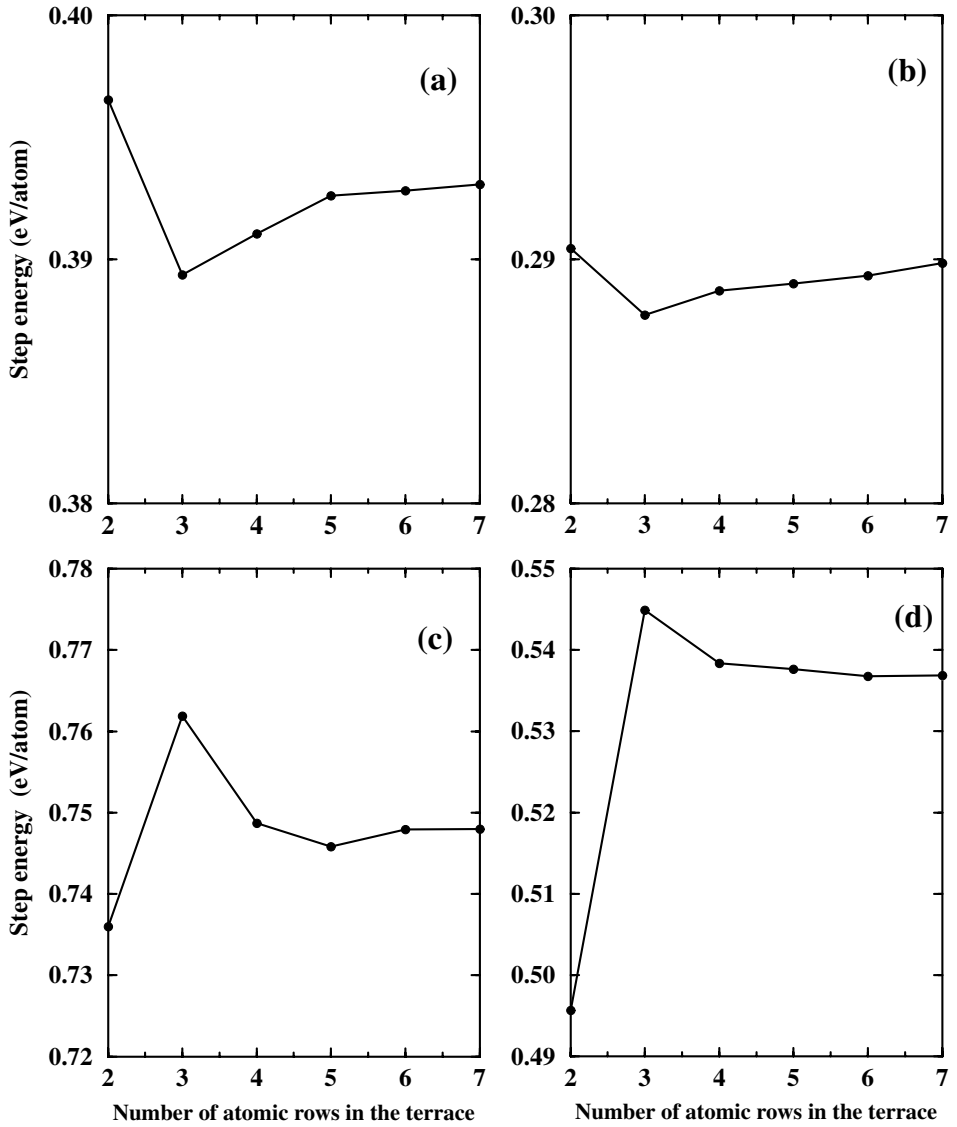

Fig. 2. The variation of the step energy (per step atom) as a function of the terrace width for the two vicinals of (100): (a) p(100) × (111) Rh, (b) p(100) × (111) Pd, (c) p(100) × (010) Rh, (d) p(100) × (010) Pd.

Finally let us comment on the electronic structure which is interesting for several reasons. The low coordination of surface steps could be a factor of enhancement of magnetism. In addition some electronic states strongly localized along the steps could appear depending on the step geometry, which may also be very sensitive to the lattice disorder along the step.

Recently it was shown experimentally [14] that the (100) surface bears a surface magnetic moment, however ab initio [15] as well as TB [9] calculations show that the non-magnetic state is the most stable but the energy variation as a function of the magnetic moment is extremely flat. Therefore, it can be inferred that magnetism could be stabilized by surface defects such as steps.

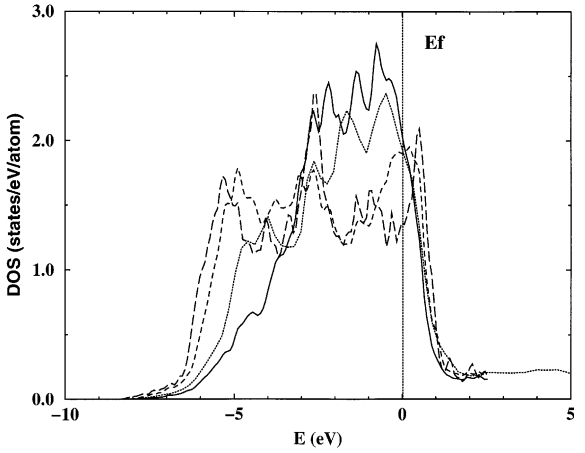

Fig. 3. The LDOS at the outer (solid line) and inner (short dashed line) edges of the $5(1\,0\,0) \times (0\,1\,0)$ vicinal surface of Rh compared with the flat surface LDOS (dotted line) and the bulk density of states (long dashed line).

We have performed calculations of local density of states (LDOS) for surface atoms in particular for atoms along the steps. On Fig. 3 we have shown the typical case of the $5(1\,0\,0) \times (0\,1\,0)$ Rh vicinal surface where four density of states are presented: the LDOS of atoms along the outer and inner edges, on the "flat" $(1\,0\,0)$ surface and the bulk LDOS. As expected there is an overall narrowing of the LDOS on the less coordinated atoms, but the details of their shape vary also with the different sites. One also notes that the density of states at the Fermi level is strongly enhanced for surface atoms and particularly for the outer edge atoms. Thus it would not be surprising that a magnetic moment localized along the steps appears.

It must also be emphasized that in some energy ranges the LDOS of the outer edge is strongly enhanced compared with the terrace and bulk LDOS. This suggest that 1D localized or resonant states may exist at the step edges. A detailed study of these states will be presented in a forthcoming paper.

4. Conclusion

Using an spd tight-binding model, we have shown that from the knowledge of the surface energies of the three low index surfaces of an fcc crystal one can deduce effective pair interactions giving step energies in a very good agreement with those derived from the diagonalization of the TB hamiltonian. This fully justifies the approach of Vitos et al. However the step energies in the Vitos et al. model are sensitive to the surface energy database. We have also shown that Friedel like electronic step–step interactions exist and are of the same order of magnitude as the other interactions. Finally the possibility of magnetism on step edges in Rh has been pointed out.

References

[1] K.D. Hammonds, R.M. Lynden-Bell, Surf. Sci. 278 (1992) 437.
[2] R.C. Nelson, T.L. Einstein, S.V. Khare, P.J. Rous, Surf. Sci. 295 (1993) 462.
[3] P. Stoltze, J. Phys.: Condens. Matter 6 (1994) 9495.
[4] L. Vitos, H.L. Skriver, J. Kollar, Surf. Sci. 425 (1999) 212.
[5] P.J. Feibelman, Phys. Rev. B 60 (1999) 11118.
[6] S. Papadia, M.C. Desjonquères, D. Spanjaard, Phys. Rev. B 53 (1996) 4083.
[7] C. Barreteau, D. Spanjaard, M.C. Desjonquères, Phys. Rev. B 58 (1998) 9721.
[8] M.J. Mehl, D.A. Papaconstantopoulos, Phys. Rev. B 54 (1996) 4519.
[9] C. Barreteau, R. Guirado-López, D. Spanjaard, M.C. Desjonquères, A.M. Oleś, Phys. Rev. B 61 (2000) 7781.
[10] M. Weinert, J.W. Davenport, Phys. Rev. B 45 (1992) 13709.
[11] A. Eichler, J. Hafner, J. Furthmüller, G. Kresse, Surf. Sci. 346 (1996) 300.
[12] M. Methfessel, D. Henning, M. Scheffler, Phys. Rev. B 46 (1992) 4816.
[13] W.W. Pai, J.S. Ozcomert, N.C. Bartelt, T.L. Einstein, J.E. Reutt-Robey, Surf. Sci. 307–309 (1994) 747.
[14] A. Goldoni, A. Baraldi, G. Comelli, S. Lizzit, G. Paolucci, Phys. Rev. Lett. 82 (1999) 3156.
[15] J.H. Cho, M. Scheffler, Phys. Rev. Lett. 78 (1997) 1299.

Chapitre 3

Propriétés vibrationnelles des surfaces vicinales du Cuivre.

3.1 Introduction

L'étude des vibrations des surfaces vicinales a connu un essor important ces vingt dernières années, période durant laquelle de nouvelles techniques expérimentales adaptées, comme par exemple la diffraction inélastique d'atomes d'hélium IHAS [5] et la spectroscopie d'électrons EELS [6] se sont développées. Ces techniques expérimentales ont permis de déterminer les courbes de dispersion de certains modes localisés ou résonants des surfaces. D'autre part, la connaissance de toutes les fréquences propres d'un système donne accès aux propriétés thermodynamiques vibrationnelles [7]. Pour cette raison nous nous sommes intéressés dans ce chapitre à la connaissance de ces propriétés. Il est apparu indispensable de développer des modèles de calcul qui apportent un aspect quantitatif pour interpréter les phénomènes observés par les expériences. Plusieurs types d'approches ont été adoptées pour étudier les vibrations des surfaces.

Les calculs ab-initio avec phonons gelés donnent de bons résultats en des points de haute symétrie de la zone de Brillouin [8], mais ces méthodes restent encore un peu limitées par la lourdeur de leur mise en oeuvre numérique. Elles permettent néanmoins de traiter des cellules de simulation d'une dizaine d'atomes dans des temps raisonnables. Toutefois, elles ne permettent pas la détermination des grandeurs thermodynamiques vibrationnelles dont le calcul nécessite d'effectuer des sommations sur tous les points de la zone de Brillouin.

Pour décrire l'ensemble des propriétés vibrationnelles d'une surface, les calculs sont donc effectués avec des potentiels semi-empiriques dans l'approximation har-

monique, sur des systèmes constitués d'un empilement de plans cristallographiques en nombre suffisant pour avoir le comportement de volume au centre de la couche (méthode des couches). Ces systèmes présentent une périodicité à deux dimensions (2D), on peut donc encore utiliser le théorème de Bloch. Ainsi, les calculs nous permettent de déterminer le spectre de vibration en tout point de la zone de Brillouin et les grandeurs thermodynamiques vibrationnelles. Par opposition aux potentiels de paires pour lesquels on n'introduit qu'une seule constante de force égale à la dérivée seconde du potentiel à l'équilibre par rapport à la distance interatomique, les potentiels semi-empiriques permettent d'avoir des constantes de force dépendant de l'environnement et qui sont donc modifiées par la relaxation.

Dans ce chapitre, nous développons un potentiel semi-empirique qui est utilisé pour l'étude des spectres de vibration. Nous présentons la structure de bande projetée et les densités spectrales à $\overrightarrow{k_{||}}$ donné pour un ensemble de surfaces vicinales en fonction de la largeur des terrasses et calculons des grandeurs thermodynamiques en nous limitant au déplacement carré moyen et à l'énergie libre dans le but d'étudier son influence sur la stabilité des surfaces vicinales par rapport au facettage.

3.2 Présentation du potentiel.

Le potentiel semi-empirique que nous avons développé, est obtenu à partir de l'addition d'un potentiel de paire et d'une contribution à N-corps. Ce potentiel a la forme :

$$V(R_1,...R_i,...) = A\sum_{\substack{i,j \\ i\neq j}}(\frac{R_o}{R_{ij}})^p f_c(R_{ij}) - \zeta\sum_i(\sum_{i\neq j} exp(-2q(\frac{R_{ij}}{R_o}-1))\, f_c(R_{ij}))^\alpha \quad (3.1)$$

où R_{ij} représente la distance entre les atomes i et j, R_o une distance de référence choisie habituellement égale à la distance entre premiers voisins à l'équilibre et f_c une fonction de coupure.

Dans ce potentiel, la détermination des paramètres A, p, q, ζ est réalisée en ajustant l'énergie de cohésion E_c et les constantes élastiques B (module de compressibilité) ainsi que C et $C^{'}$ (modules de cisaillement), sur les valeurs expérimentales du Cuivre cristallin. L'équation d'équilibre pour la distance entre premiers voisins $R_o = 2.5526A^o$ donne une relation entre les quatres paramètres. Nous avons effectué plusieurs ajustement des paramètres pour différentes valeurs de α et différents rayons de coupure R_c. On constate que ce potentiel reproduit bien les résultats expérimentaux avec une précision de 1 meV pour une portée du potentiel qui ne s'étend pas au delà des seconds

voisins $R_2 < R_c < R_3$ et une valeur de $\alpha = \frac{2}{3}$. Les valeurs de A, p, q, ζ ajustées sont alors les suivantes :

$$p = 7.206$$
$$q = 2.22$$
$$A = 0.206eV$$
$$\zeta = 1.102eV$$

Le potentiel semi-empirique que nous avons développé, s'inspire de l'approximation des liaisons fortes au second moment où $\alpha = \frac{1}{2}$ [9]. Cependant, le potentiel avec $\alpha = \frac{2}{3}$ donne de meilleures valeurs pour les énergies de surface et les relaxations de surface correspondantes sont très raisonnables. Notons que cet exposant avait déjà été proposé dans la littérature par Guevara et al. [10] pour prendre en compte l'effet des moments d'ordre supérieur et de la condition de neutralité locale.

Nous avons ainsi calculé les courbes de dispersion de volume dans l'approximation harmonique le long du chemin $\overline{\Gamma X W X \Gamma L}$, dans la zone de Brillouin (voir Figure 1). On peut noter que les résultats présentés sur cette figure sont en bon accord avec ceux mesurés par diffusion inélastique de neutrons [13].

3.3 Les surfaces de bas indices.

Pour les calculs de ce chapitre nous avons adopté la méthode des couches (voir chapitre 1) et pour les surfaces de bas indices nous avons fixé l'épaisseur à 75 plans cristallographiques.

Dans les Figures 3a, 3b et 3c, nous présentons les structures de bandes projetées des surfaces de bas indices (111), (100) et (110). Nous montrons la présence d'états localisés et de résonances de surface qui sont mis en évidence à l'aide d'un critère de localisation donné dans le texte de l'article. Nous identifions par exemple le phonon de Rayleigh localisé sur les atomes de surface. De même nous observons l'apparition d'autres modes de surface dans les bandes interdites.

Les limites des bandes de volume et les états localisés sont en bon accord avec les résultats expérimentaux pour les trois surfaces [17-23].

En conclusion le modèle de potentiel empirique que nous avons développé reproduit avec une bonne précision les résultats expérimentaux pour le cas du volume et des surfaces de bas indices. Par conséquent, nous utilisons ce potentiel pour étudier les surfaces vicinales de Cuivre.

3.4 Surfaces vicinales.

Le calcul concernant les surfaces vicinales est réalisé sur une couche “épaisse” comprenant 75×p plans où p est le nombre de rangées atomiques dans les terrasses. Nous présentons d’abord la relaxation des surfaces vicinales, puis analysons les courbes de dispersion des phonons. Finalement nous présentons des densités spectrales locales de phonons aux points $\overline{\Gamma}$ et $\overline{X}$ pour mieux analyser les phonons localisés ou résonants de surface.

Nous avons appliqué le potentiel semi-empirique (1) pour avoir accès à la configuration structurale stable des surfaces vicinales. Les atomes de terrasses, sauf l’atome de l’arête rentrante (CC) de la marche, relaxent vers l’intérieur du cristal comme dans le cas des surfaces de bas indices [25]. L’atome de l’arrête saillante (SC) de la marche a un fort déplacement vers l’intérieur du cristal. La distance atomique entre l’atome de l’arête saillante (SC) et l’atome BNN du (p+1) ième plan cristallographique (où p est le nombre des rangées atomiques dans les terrasses) est réduite par rapport à la distance d’équilibre dans le volume. Ceci a pour effet de durcir les constantes de forces.

Nous avons relaxé quatre surfaces vicinales (211), (511), (711) et (911). Nos résultats sont en bon accord avec les calculs ab-initio [26] pour les 10 premiers plans cristallographiques mais tendent à s’en écarter pour les autres plans (voir Figure 5). En effet les calculs ab-initio sont effectués sur des supercellules contenant un nombre de couches insuffisant pour assurer une région de volume entre les deux surfaces vicinales.

3.4.1 Structure de bandes projetées

Dans notre étude le critère de localisation des modes localisés ou résonants de surface est de 6%, plus précisément un mode est considéré comme un mode de surface si la somme de ses poids sur les $(p+1)$ premiers plans est supérieure à 6%.

Pour étudier l’évolution des structures de bandes projetées des surfaces vicinales en fonction de la largeur des terrasses, nous avons effectué des calculs sur les surfaces vicinales 2(100)×(111), 3(100)×(111), 4(100)×(111) et 9(100)×(111) de Cuivre pour lesquelles il existe des résultats expérimentaux (Figure 8) [5,6,29]. Une petite bande interdite apparait pour la surface (311) entre les points $\overline{X}$ et $\overline{S}$. Cette bande disparaît quand le nombre des rangées atomiques p dans les terrasses est supérieur à 2. En effet si l’on augmente le nombre des rangées atomiques p dans les terrasses, on diminue l’aire de la zone de Brillouin à deux dimensions [30] et on augmente le domaine correspon-

dant des valeurs de k_z puisque l'on échantillonne un volume de l'espace réciproque égal à celui de la première zone de Brillouin de volume. Ceci a pour effet de refermer les bandes interdites.

Pour toutes les surfaces vicinales étudiées nous identifions dans la direction $\overline{\Gamma X}$ (direction parallèle aux bords des marches), des modes localisés et résonants de surface [5,6] en particulier le mode de Rayleigh (R), un mode transverse et un mode de marche (E). Dans la direction $\overline{\Gamma Y}$ (direction perpendiculaire aux bords des marches) les structures obtenues peuvent se comprendre qualitativement par un repliement des courbes de dispersion du phonon de Rayleigh (R) [29] et du mode transverse (T). Ceci a pour effet de faire apparaître des modes optiques séparés par des bandes interdites, leur nombre augmentant avec la largeur de la terrasse.

D'autres surfaces vicinales sont étudiées, comme les surfaces vicinales (331) ou $2(110)\times(\overline{1}11)$ et (551) ou $3(110)\times(\overline{1}11)$. Nous présentons les résultats dans la Figure 9. Des petites bandes interdites apparaissent à hautes fréquences. Ces bandes se referment en fonction de la largeur des terrasses. De même, des modes accoustiques et optiques sont également présents.

Enfin nous avons aussi analysé la surface vicinale avec crans (532) (Figure 10). Cette surface présente des terrasses d'orientation (111), des contre-marches d'orientation (100) et des crans d'orientation $(11\overline{1})$. Nous identifions des modes localisés et des modes résonants sur les atomes de crans de cette surface vicinale.

La comparaison de nos résultats avec les données expérimentales existantes (IHAS et EELS) [5,6] montre un accord très satisfaisant. Notre potentiel devrait donc décrire correctement l'ensemble du spectre de phonons nécessaire pour le calcul des grandeurs thermodynamiques vibrationnelles.

Pour avoir des informations complémentaires sur la localisation des états, nous avons calculé les densités spectrales [31] aux points $\overline{\Gamma}$ et $\overline{X}$ sur différents sites des surfaces vicinales étudiées (l'atome de l'arête saillante de la marche SC, atome de terrasse TC, atome du plan numéro (p+1) BNN et un atome du volume). La Figure 5 montre l'apparition des bandes interdites.

3.4.2 Fonctions thermodynamiques vibrationnelles.

a) Déplacement carré moyen.

Dans la Figure 13 nous présentons le calcul du déplacement carré moyen d'un atome de volume en fonction de la température. Nous remarquons qu'autour de la

température ambiante nos résultats sont en bon accord avec les données expérimentales [31]. Par contre à température élevée, la courbe de déplacement carré moyen expérimentale est au-dessus de la courbe calculée. Ceci peut être attribué aux effets anharmoniques qui ne sont pas négligeables à ces températures.

Le déplacement carré moyen des atomes appartenant aux surfaces de bas indices est important dans la direction de faible densité atomique. La Figure 14 montre que les surfaces (100) et (111) présentent un déplacement carré moyen important dans la direction z (perpendiculaire à la surface). Par contre pour la surface (110), le plus grand déplacement carré moyen est obtenu dans la direction y (direction des seconds voisins). Dans la Figure 15 nous présentons des calculs de déplacement carré moyen de la surface vicinale (17,1,1). Nous montrons que le déplacement carré moyen est surtout déterminé par l'environnement local. Par exemple l'atome de l'arête saillante a le déplacement carré moyen le plus élevé par rapport aux autres atomes de la surface vicinale car il a la plus faible coordinance.

b) Energie libre vibrationnelle.

L'énergie de marche à 0K en fonction du nombre p de rangées atomiques dans les terrasses pour les surfaces vicinales p(100)×(111) et p(111)×(100), est présenté dans la Figure 6. Elle décroît monotonément en fonction de p. A l'inverse des calculs de structure électronique (chapitre 1) [1,2], l'énergie de marche, calculée à l'aide du potentiel semi-empirique (1) à 0K, n'a pas d'oscillations amorties en fonction de la largeur des terrasses. La variation de l'énergie de marche est due aux interactions élastiques répulsives entre marches. La valeur asymptotique de l'énergie de marche isolée est un peu plus faible que celle résultant des calculs de structure électronique.

Il est intéressant de calculer la contribution vibrationnelle à l'énergie de marche. La Figure 16 montre que l'énergie libre vibrationnelle de marche (par atome de marche) $F^{vib}_{marche}(T)$ décroit linéairement si la température est supérieure à 100K pour un nombre de rangées atomiques p donné. Par contre, elle décroit en valeur absolue en fonction de la largeur des terrasses pour une température donnée. Les phonons produisent donc des interactions attractives entre marches qui augmentent avec la température. Par la suite nous avons utilisé ces résultats pour étudier l'effet des phonons sur la stabilité des surfaces vicinales (chapitre 4).

3.5 Conclusion

Le potentiel semi-empirique à N-corps pour le Cuivre que nous avons mis au point donne de bons résultats pour la relaxation des surfaces de bas indices et des surfaces vi-

cinales. Il décrit correctement, dans l'approximation harmonique, la structure de bande projetée des phonons pour toutes les surfaces étudiées, car les courbes de dispersion des modes localisés ou résonants des surfaces sont en bon accord avec les données expérimentales existantes. Le même potentiel est utilisé avec succès pour calculer des grandeurs thermodynamiques vibrationnelles. Le calcul des énergies d'interaction entre marches pour les surfaces vicinales p(100)×(111) et p(111)×(100) montre que les phonons produisent des interactions attractives.

3.6 Articles :

- **The phonon spectra and vibrational thermodynamical properties of Cu vicinal surfaces.**

- **The phonon spectra of low and high index surfaces of copper.**

Nous reproduisons tel quels, les articles qui ont été soumis dans la revue "Surface science".

Available online at www.sciencedirect.com
SCIENCE DIRECT®
Surface Science 519 (2002) 15–32
SURFACE SCIENCE
www.elsevier.com/locate/susc

The phonon spectra and vibrational thermodynamical properties of Cu vicinal surfaces

C. Barreteau [a,*], F. Raouafi [a], M.C. Desjonquères [a], D. Spanjaard [b]

[a] DSM/DRECAM/SPCSI, CEA Saclay, Bâtiment 462, F-91 191 Gif sur Yvette, France
[b] Laboratoire de Physique des Solides, Bâtiment 510, Université Paris Sud, F-91 405 Orsay, France

Received 11 June 2002; accepted for publication 11 July 2002

Abstract

We present a many-body empirical potential giving the total energy in Cu crystals, the transferability of which is proven by comparing with experiments the phonon band structure for the bulk and the three low index surfaces. After the determination of the multilayer relaxation of a set of vicinal surfaces, we investigate their vibrational spectra by means of their projected phonon band structure and the local spectral densities of states corresponding to a given value of $\mathbf{k}_{//}$ which are discussed in relation with recent experiments. Finally, the root mean square displacement of specific atoms for low and high index surfaces are compared with the bulk one and the contribution of the vibrations to the free energy of steps is calculated as a function of temperature and of the terrace width for the $p(100)\times(111)$ and $p(111)\times(100)$ surfaces ($2\leqslant p\leqslant 7$). It is found that for these vicinal surfaces the step–step interactions mediated by phonons are attractive and may have the same order of magnitude as the other interactions.

Keywords: Copper; Vicinal single crystal surfaces; Semi-empirical models and model calculations; Phonons

1. Introduction

Vicinal surfaces are obtained by cutting a crystal by a crystallographic plane with high Miller indices and exhibit a periodic succession of terraces with low index orientation and steps of monoatomic height. They provide an handy tool in the quest of finding reliable models for various surface processes: diffusion at surfaces, roughening transition, surface growth and chemical reactions.

The presence of steps modifies the electronic and vibrational states compared to the flat surface with the same orientation as the terraces. In particular, the localized states propagating along the surface should be strongly perturbed especially when the direction of propagation is perpendicular to the step edges. In preceding papers we have studied the modification of the electronic structure, derived step energies and electronic step–step interactions [1,2] and discussed their influence on the stability of vicinal surfaces with respect to faceting [3,4]. In the present work we investigate the modifications of the vibrational states of copper and deduce the contribution to the free energy and the mean square displacements of specific

* Corresponding author. Tel.: +33-1-6908-2951; fax: +33-1-6908-8446.
E-mail address: cbarreteau@cea.fr (C. Barreteau).

0039-6028/02/$ - see front matter
PII: S0039-6028(02)02092-7

atoms as a function of temperature. Some inelastic helium atom scattering (IHAS) [5] and electron energy loss spectroscopy (EELS) [6] experiments have been carried out on a limited number of Cu vicinal surfaces. In IHAS the results were analysed in the harmonic approximation with a central pair potential and a rigid lattice using a single force constant. The agreement with experiments was qualitatively reasonable and was improved by changing some force constants in the vicinity of the surface, this change being related to local atomic relaxations. For EELS experiments an embedded atom model (EAM) potential which includes an N-body term was used, the system was fully relaxed and the results at the $\overline{\Gamma}$ point were interpreted using local spectral densities of states (LSDOS) at $\mathbf{k}_{//} = 0$. Note also that the vibrational thermodynamical properties of some Cu vicinal surfaces were also investigated by the same group [7]. An EAM potential has also been used for a study of the vibrational states on some metal vicinal surfaces, in particular of Cu [8]. Finally ab initio calculations have been carried out but were restricted to a few high symmetry points of the two-dimensional (2D) Brillouin zone [9].

In this paper we first derive (Section 2) an N-body semi-empirical potential for FCC Cu which has some similarity with the so-called tight-binding second moment potential. However it improves the numerical values of the surface energies and gives the best results when the interactions are cut-off between the second and third nearest neighbours. In particular this cut-off produces atomic relaxations at low index surfaces in good agreement with experiments. This has important consequences since any calculation of the phonon spectrum starts from the determination of the equilibrium atomic structure and the variation of the interatomic distances modifies the corresponding force constants. Its transferability is checked (Section 3) on a detailed study of the low index surfaces (1 1 1), (1 0 0) and (1 1 0). Then it is applied to the determination of the surface projected phonon dispersion curves (Section 4) of a set of vicinal surfaces with increasing terrace widths and the results are compared with existing experimental data. The localized and resonant vibrational states can be identified by using a localization criterion on the first layers and are discussed in more details by means of the local spectral densities with a given value of the component of the wave vector parallel to the surface, $\mathbf{k}_{//}$. In Section 5, the mean square displacements are derived on specific atoms. Finally, the vibrational free energy and its contribution to the free energy of the steps, as well as to step–step interactions due to phonons, are presented. In Section 6 conclusions are drawn.

2. The determination of the potential

We have developed a new empirical potential to describe the interatomic interactions of a set of atoms located at $\mathbf{R}_i$. Its analytical form is given by:

$$V(\mathbf{R_1},\ldots\mathbf{R_i},\ldots) = A\sum_{i,j,j\neq i}(R_0/R_{ij})^p f_c(R_{ij}) - \xi\sum_i\left(\sum_{j\neq i}\exp(-2q(R_{ij}/R_0-1))f_c(R_{ij})\right)^{\alpha} \quad (1)$$

where R_{ij} is the distance between atoms i and j, R_0 is a reference distance that we take equal to the bulk nearest neighbour spacing and $f_c(R) = 1/(1+\exp[(R-R_c)/\Delta])$ is a smooth cut-off function with a cut-off radius R_c ($\Delta = 0.05$ Å).

The parameters A, ξ, p and q are fitted to the experimental values of the cohesive energy E_c ($E_c = -3.5$ eV/at) and of the three elastic constants, i.e., the bulk modulus ($B = 10.470$ eV/at) and the two shear moduli C and C' ($C = 6.046$ eV/at, $C' = 1.917$ eV/at). The equilibrium equation at $R_0 = 2.5526$ Å gives a relation between the four parameters.

For a given value of α (1/2, 2/3, 4/5, 1) we determine by a least mean square fit four sets of parameters obtained with different radii R_c for which interactions are cut off beyond first, second, third and fourth neighbours. For each set of parameters we compare the fitted values of E_c, B, C, C', the surface relaxation of low index surfaces and the bulk phonon spectra to experiments. The best set of parameters is obtained for $\alpha = 2/3$ and a

cut-off radius $R_c = 4.02$ Å between second and third neighbours and the corresponding parameters are: $A = 0.206$ eV, $\xi = 1.102$ eV, $p = 7.206$, $q = 2.220$. Indeed with this potential the fit of E_c, B, C and C' is excellent (better than 1 meV per atom). When the potential includes only first nearest neighbours the shear moduli are not well reproduced and, in particular, C is about 25% smaller than the experimental value. The inclusion of third and fourth neighbours has a smaller influence. Note that the exponent $\alpha = 2/3$ was already proposed in the literature [10].

Moreover when $R_c = 4.02$ Å the surface relaxations of low index surfaces, calculated using a conjugate gradient algorithm, are predicted correctly. Note that large cut-offs systematically give too small inward surface relaxation and even a tendency to outward relaxation (see Table 1). We must emphasize that surface relaxation is important to get the local modifications of force constants.

The dispersion curves for bulk copper calculated in the harmonic approximation are presented in Fig. 1. The agreement with experiments [11] is excellent. Apart from the top of the spectrum at points X and L where the deviation between calculated and experimental frequencies is around 0.2 THz, everywhere else the deviation is less than 0.1 THz. Note also that the shallow minimum at W in the lowest frequency band along XWX is perfectly well reproduced only with a second neighbor potential.

Finally we must note that the surface energies of the three low index surfaces, eventhough not included in the fit, are significantly improved with respect to ab initio data [12] compared with the results of the conventional second moment potential in which $\alpha = 1/2$ (see Table 2). Moreover, the dimer bond length is in good agreement with ab initio calculations [13].

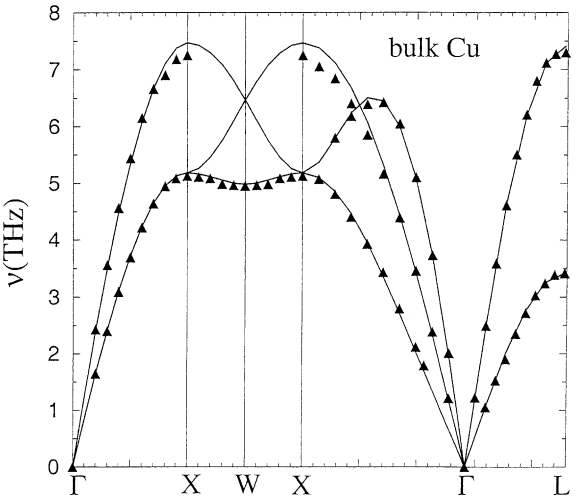

Fig. 1. Phonon dispersion curves of bulk copper. The full lines correspond to the calculated dispersion curves and the triangles to the phonon frequencies measured from neutron inelastic-scattering experiments (Ref. [11]). Each segment along the path $\Gamma(\Delta)X(Z)W(Z)X(\Sigma)\Gamma(\Lambda)L$ is proportional to its length in reciprocal space.

Table 2
Relaxed surface energies (in eV/atom) for the three low index surfaces using the empirical potential (1) with $\alpha = 1/2$ and $2/3$ compared to ab initio results [12]

Surface	$\alpha = 1/2$	$\alpha = 2/3$	Galanakis et al.
(1 1 1)	0.36	0.47	0.67
(1 0 0)	0.45	0.57	0.87
(1 1 0)	0.71	0.91	1.33

In conclusion, the potential that we have determined describes correctly all the bulk properties and seems to have a high degree of transferability

Table 1
Variation of the surface relaxation of low index surfaces as a function of the cut-off radius R_c

Surface	$R_1 < R_c < R_2$	$R_2 < R_c < R_3$	$R_3 < R_c < R_4$	$R_4 < R_c < R_5$	Experiment
(1 1 1)	−2.7%	−1.9%	−1.0%	−0.6%	[−0.7%, 0.7%]
(1 0 0)	−4.8%	−1.7%	−0.7%	0%	[−1.1%, −2.1%]
(1 1 0)	−11%	−5.3%	−3.2%	−1.9%	[−5.3%, −10%]

R_n is the radius of the nth coordination sphere. The potential is characterized by $\alpha = 0.666$, the four other parameters are chosen to satisfy the bulk equilibrium equation and to fit E_c, B, C and C' with a least mean square process. Lower and higher limits for the relaxation, derived from several experiments, are given in the last column.

which we are going to confirm by calculating the surface vibrations of low index surfaces. Then we will use it for the study of vicinal (high index) surfaces. In all cases we have used a slab geometry and the two-dimensional (2D) Bloch theorem. The different 2D Brillouin zones corresponding to the surfaces studied in this paper are shown in Fig. 2. They correspond to the five (2D) Bravais lattices: the square lattice ((1 0 0) surface), the rectangular lattice ((1 1 0), (2 1 1) surfaces), the hexagonal lattice ((1 1 1) surface), the centered rectangular lattice ((2p − 1,1,1), (5 5 1), (3 3 1) surfaces) and the oblique lattice ((5 3 2) surface). In Fig. 2 we have also indicated the different symmetry points defining the path along which the phonon spectrum is calculated and the irreducible part of the Brillouin zone defining the domain of the special $\mathbf{k}_{//}$ points [14] used for the calculation of thermodynamical quantities such as the vibrational free energy or the root mean square displacements.

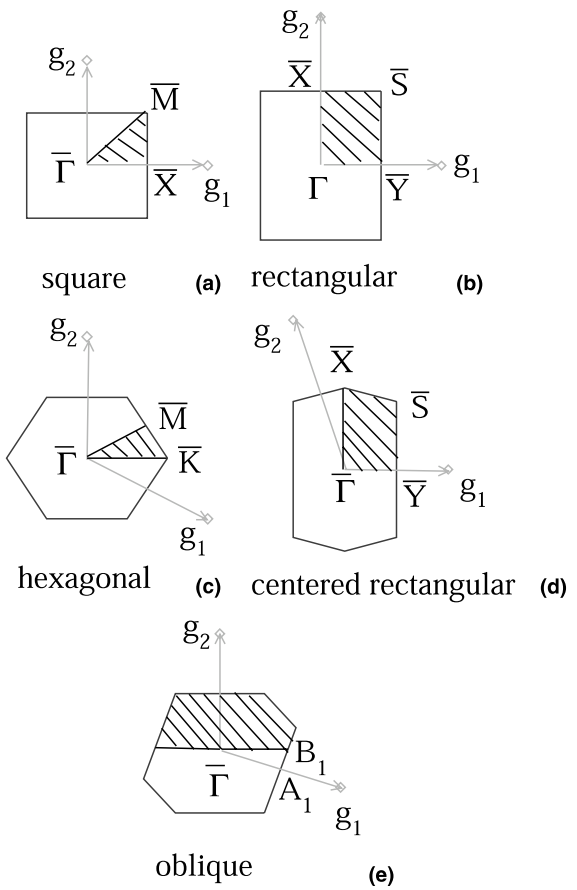

Fig. 2. The surface Brillouin zones built from the elementary vectors $\mathbf{g}_1$ and $\mathbf{g}_2$ defining the reciprocal lattice. The hatched area is the irreducible part. Particular points are labelled as usual. (a) Square lattice: (1 0 0) surface. (b) Rectangular lattice: (1 1 0), $p(1\,1\,1)\times(1\,0\,0)$ (p odd), $p(1\,1\,1)\times(\bar{1}\,1\,1)$ (p even) surfaces. (c) Hexagonal lattice: (1 1 1) surface. (d) Centered rectangular lattice: $p(1\,1\,1)\times(1\,0\,0)$ (p even), $p(1\,1\,1)\times(\bar{1}\,1\,1)$ (p odd), $p(1\,0\,0)\times(1\,1\,1)$ and $p(1\,1\,0)\times(1\,1\,1)$ surfaces. (e) Oblique lattice: (5 3 2) surface.

3. Vibrations at low index surfaces

In this section we present the surface projected band structure of phonons for the three low index surfaces (1 1 1), (1 0 0) and (1 1 0) (Fig. 3). The case of Cu(1 0 0) has been discussed in details in a preliminary account of this work [13]. For the sake of comparison with the other two surfaces, we just give here its projected band structure (Fig. 3b), calculated with a slab of 75 atomic layers, which shows an excellent agreement with EELS and IHAS experiments [15–17].

The surface projected dispersion relations of phonons for a slab with 75 layers of Cu(1 1 1) are shown in Fig. 3a and compared to experimental data [18–20]. It is seen that the Rayleigh wave (S_1) dispersion curve is very accurately reproduced. Note that, in particular, its frequency is higher at $\overline{K}$ than at $\overline{M}$ whereas calculations based on a single force constant give an almost flat band along $\overline{M}\,\overline{K}$ [20]. The surface phonon S_2 at $\overline{M}$ is found at 6.65 THz instead of 6.35 THz from experiments. The longitudinal resonances are clearly seen along $\overline{\Gamma}\,\overline{K}$ whereas with our localization criterion they are revealed by the calculation only partly along $\overline{\Gamma}\,\overline{M}$.

Finally Fig. 3c gives the surface projected dispersion relations of phonons for a slab of 75 layers of Cu(1 1 0). The surface features are compared with those observed and discussed in details in the work of Zeppenfeld et al. [21] using high resolution IHAS experiments. Along $\overline{\Gamma}\,\overline{Y}$ three localized (or resonant) surface dispersion curves are observed at low frequencies ($\nu < 4$ THz). The lowest one is the Rayleigh wave S_1 and its frequency is in perfect agreement with our calculations up to the middle

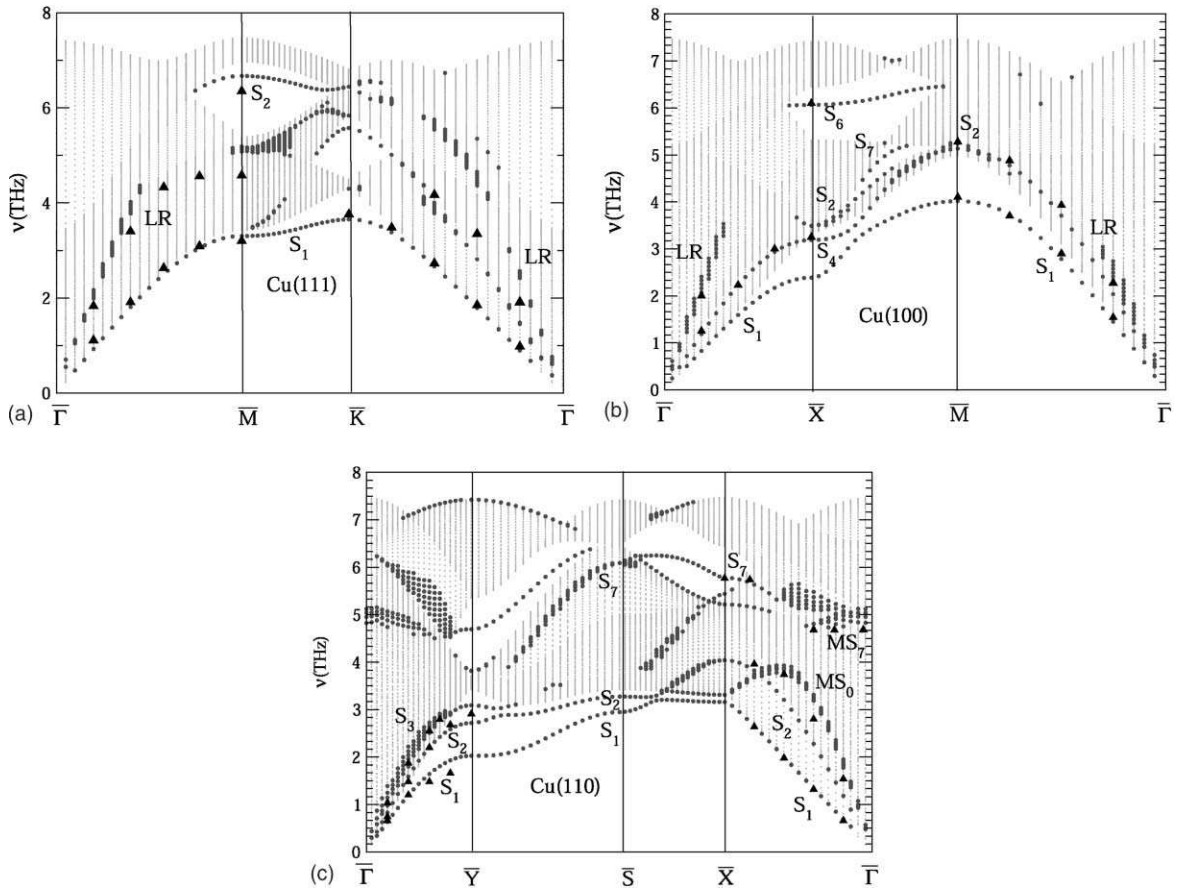

Fig. 3. Frequency spectrum of phonons for the low index surfaces of Cu as a function of $\mathbf{k}_{//}$ along a given path in the surface Brillouin zone. Each segment is proportional to its length in the reciprocal space. Bulk states are represented by small dots. Localized and resonant states are denoted by heavy dots and labelled with the usual notations. Only the modes with a weight larger than 6% of the total weight on the first two layers are shown. (a) (1 1 1) surface along $\overline{\Gamma}\,\overline{X}\,\overline{M}\,\overline{K}\,\overline{\Gamma}$ (see Fig. 2c). The slab is 75 layer thick. Experimental points (full triangles) are taken from Refs. [18–20]. (b) (1 0 0) surface along $\overline{\Gamma}\,\overline{X}\,\overline{M}\,\overline{\Gamma}$ (see Fig. 2a). The slab is 75 layer thick. Experimental points (full triangles) are taken from Refs. [15–17]. (c) (1 1 0) surface along $\overline{\Gamma}\,\overline{Y}\,\overline{S}\,\overline{X}\,\overline{\Gamma}$ (see Fig. 2b). The slab is 75 layer thick. Experimental points (full triangles) are taken from Ref. [21].

of $\overline{\Gamma}\,\overline{Y}$. One must note that at higher values of $\mathbf{k}_{//}$, S_1 appears as a very weak structure in the IHAS spectra. Consequently its frequency should be rather difficult to get accurately. Thus our calculated curve may be in the error bars of the experiments (which are not given in Ref. [21]). The other two curves, i.e., the transverse mode E (denoted as S_2 in Ref. [22]) which is a true surface phonon near $\overline{Y}$ and the surface transverse mode S_3 are almost perfectly reproduced. Along $\overline{\Gamma}\,\overline{X}$ the Rayleigh wave dispersion curve (S_1) coincides with experiment. The frequency of the MS_0 resonance is in good agreement with experiments, although not so perfect as for S_1. In addition, the gap mode S_7 around $\overline{X}$ and the resonance MS_7 around $\overline{\Gamma}$ are well obtained. Finally the horizontal shear mode S_2 is not detected by experiment. No experimental data are available at the $\overline{S}$ point. The only possible comparisons are with the frozen phonon ab initio method by Rodach et al. [22] and EAM calculations by Sklyadneva et al. [8]. Three surface phonons are clearly identified S_1, S_2 and S_7. Their

frequencies are 2.9, 3.2, 6.1 THz in our calculations to be compared with 2.8, 3.1, 5.7 THz in Ref. [22] and 2.7, 3.0, 6.2 THz in Ref. [8], respectively.

In conclusion, our potential gives the bulk and low index surface phonon spectra with a very good accuracy and thus we believe that it can be confidently used to study the vibrations of vicinal surfaces.

4. Vibrations at vicinal surfaces

Let us now present our results on vicinal surfaces. For all surfaces the coordinate system is chosen such that z is normal to the vicinal plane and $x(y)$ is perpendicular (parallel) to the step edges. We begin by discussing the multilayer relaxation of vicinal surfaces and extract its main characteristics. In the next section the phonon dispersion curves are analyzed, starting with a summary of the results obtained on the (2 1 1) and (5 1 1) surfaces that have already been presented in a previous paper [13]. We then discuss in more details the $p(1\,0\,0)\times(1\,1\,1)$ or $(2p-1,1,1)$ surfaces with increasing terrace widths ($p=2$, 3, 4 and $p=9$), and compare our results to existing IHAS [5] and EELS [6] experimental data, i.e., for $p=3$ ((5 1 1) surface) and $p=9$ ((17,1,1) surface). The case of three vicinal surfaces with the same terrace width $p=3$ but different terrace orientations: $3(1\,1\,1)\times(1\,0\,0)=(2\,1\,1)$, $3(1\,1\,0)\times(1\,1\,1)=(5\,5\,1)$ and $3(1\,1\,1)\times(1\,1\,\bar{1})=2(1\,1\,0)\times(1\,1\,1)=(3\,3\,1)$ is also presented. Finally the kinked vicinal surface (5 3 2) for which EELS [6] experimental results are also available, is discussed. In the last section the phonon LSDOS at $\overline{\Gamma}$ and $\overline{X}$ of three stepped surfaces (2 1 1), (5 1 1) and (17,1,1) are studied in order to analyze in more details the localization of resonant and surface phonons.

4.1. Atomic relaxation

The determination of the equilibrium atomic structure is obtained by a standard conjugate gradient method, the iteration towards the equilibrium is achieved when the force in less than 10^{-5} eV/Å. Fig. 4 shows a typical displacement field for the (17,1,1) surface. Note that the displacements are not drawn with the same scale as the interatomic distance but have been magnified by the same multiplicative factor in order to get an easy visualization. All terrace atoms, save for the inner edge or corner chain (CC) atom, relax towards the bulk as on low index surfaces, however the direction of the relaxation varies with the atomic position, and one can identify a vortex-like structure, which has also been described in a recent paper by Prévot et al. [23]. The outer edge step atom (SC:Step Chain) shows the largest inward relaxation. The atoms denoted as BNN belong to the $(p+1)$th layer, i.e., the first layer in which atoms have the bulk coordination. Since the SC atom strongly relaxes towards its nearest neighbour BNN, the SC-BNN distance exhibits the largest contraction compared to the equilibrium bulk nearest neighbour distance. As we will see later the shortening of the SC-BNN distance produces a stiffening of the associated force constant. To be

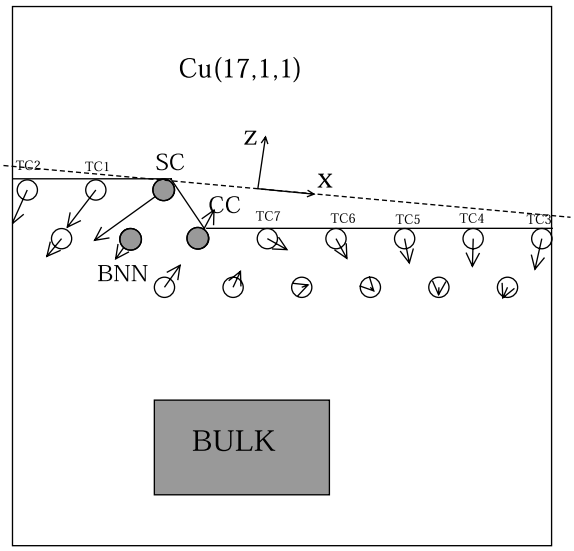

Fig. 4. Side view (perpendicular to the step edges) of the Cu(17,1,1) surface. The relaxation pattern of the atoms is indicated by arrows. All atomic displacements have been magnified compared with the interatomic distance. The labelling of the nine terrace atomic rows is: SC (outer edge), TC_n ($n=1,\ldots,7$) (rows inside the terrace), CC (inner edge). BNN denotes a close-packed atomic row in the first vicinal atomic layer in which atoms have the bulk nearest neighbour coordination.

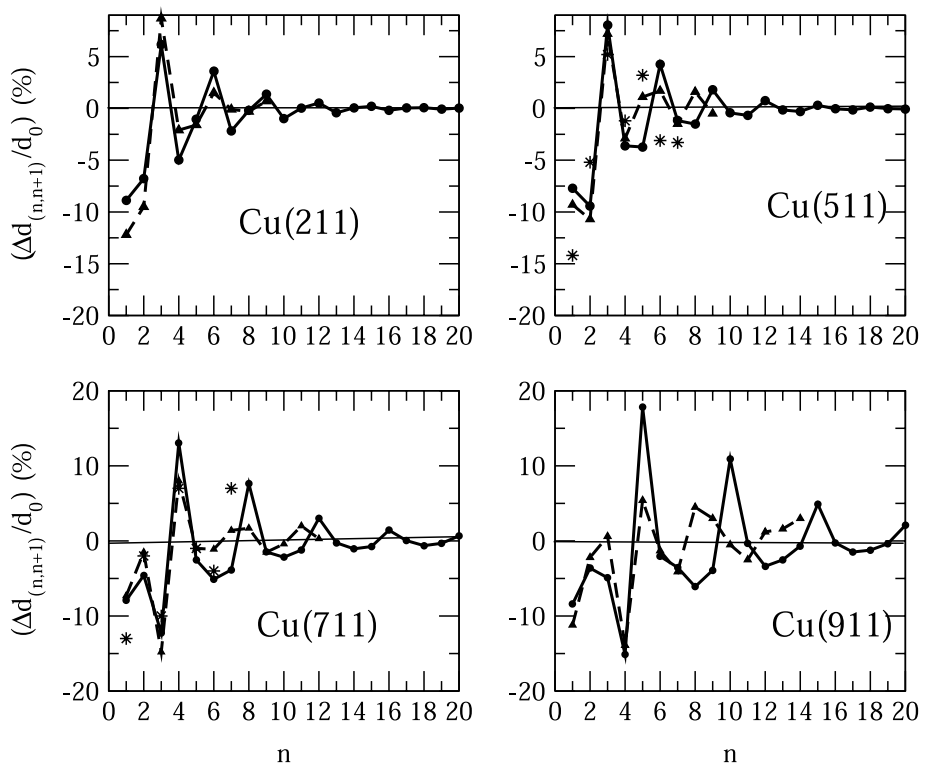

Fig. 5. Multilayer relaxation of (2 1 1), (5 1 1), (7 1 1) and (9 1 1) surfaces in percentage of the bulk interlayer spacing d_0: full dots (our results), full triangles (ab initio results from Ref. [24]. Stars indicate experimental points from Ref. [25].

more quantitative we have calculated the multilayer relaxation of four different vicinal surfaces (2 1 1), (5 1 1), (7 1 1) and (9 1 1), for which ab initio data are available [24]. The results are shown in Fig. 5 and the agreement with these data is striking for the first outmost layers, but is less satisfactory for deeper layers. The difference is more pronounced for surfaces with wide terraces where the shift between the two types of calculations is noticeable. The origin of this discrepancy is clear: ab initio calculations are performed on thin slabs so that the number of layers is not sufficient to reach the bulk behaviour, contrary to empirical potential calculations for which the number of layers can be as large as necessary. Note that our results are in good agreement with EAM calculations [8]. Finally the agreement with experiments [25] is quite reasonable. The equilibrium structure of a vicinal surface with a given terrace width p being known, it is straightforward to calculate the corresponding step energy per step atom $E_{\text{step}}(p)$ using the following equation [26]:

$$E_{\text{step}}(p) = E_{\text{S}}(p) - (p - 1 + f)E_{\text{S}}(\infty) \tag{2}$$

where $E_{\text{S}}(p)$ is the surface energy per surface atom of a vicinal surface with p atomic rows in the terrace (including the inner edge), $E_{\text{S}}(\infty)$ is the surface energy per atom of an infinite surface with the same orientation as the terrace and f is a geometrical factor determined by the projection of the ledge onto the terrace. $E_{\text{step}}(p)$ is varying with p as a result of step–step interactions. The step energy of an isolated step is obtained in the limit $p \to \infty$. In Fig. 6 we have presented the step energy per step atom for the vicinal surfaces $p(1\,0\,0) \times (1\,1\,1)$ and $p(1\,1\,1) \times (1\,0\,0)$ with p ranging from 2 to 9. $E_{\text{step}}(p)$ is strictly decreasing when p increases as expected from a calculation based on a semi-empirical

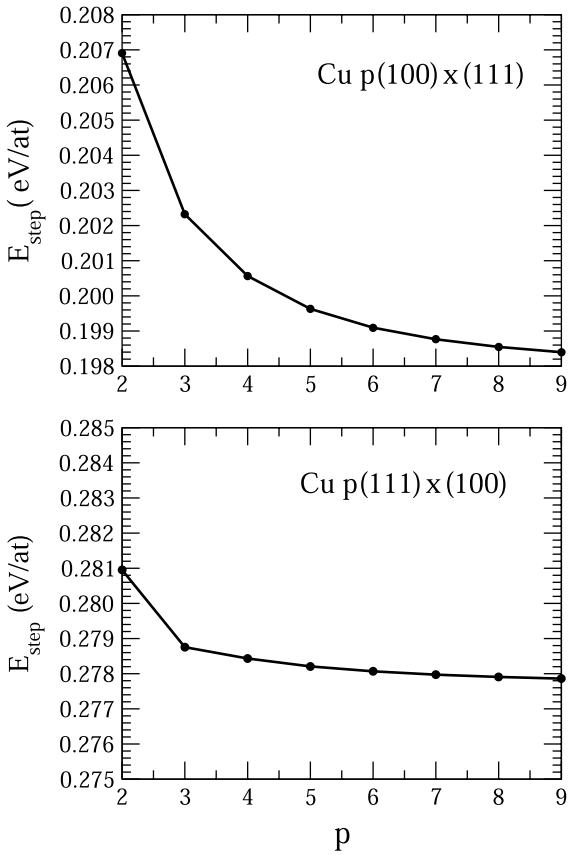

Fig. 6. Variation of the step energy per step atom of the $p(100) \times (111)$ and $p(111) \times (100)$ vicinal surfaces as a function of the terrace width p. The geometry has been fully relaxed.

potential, since no oscillatory electronic effects [1,2] are taken into account, and this variation is due to "purely" elastic step–step interaction which is known to be repulsive. Indeed, with a semi-empirical potential limited to second neighbours on a rigid lattice the step energy is found to be independent of p [3,4].

4.2. Surface projected phonon band structures

In our calculations the number of layers in a slab is $p \times 75$. A mode is considered as being a surface or resonant state if the sum of its weights on the first $p+1$ layers is larger than 6% of the total weight.

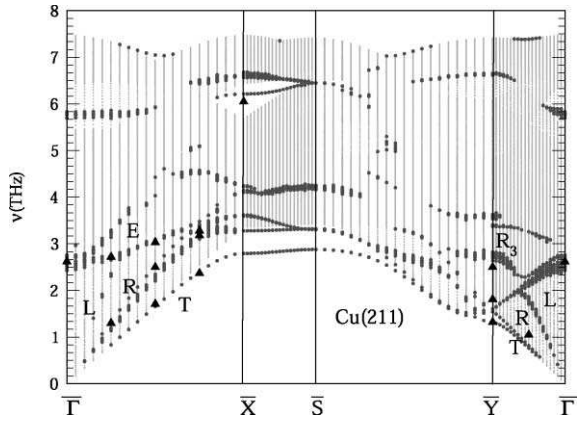

Fig. 7. Same caption as in Fig. 3 for the (2 1 1) surface. The prominent surface features are denoted with the same notations as in Ref. [5] and the localization criterion is 6% on the first four layers. Experimental points are taken from Ref. [5] except for the highest frequency at $\overline{X}$ which corresponds to the EELS data of Ref. [6].

In a previous paper [13] we discussed in details the dispersion curves of the (2 1 1) (or $3(1\,1\,1) \times (1\,0\,0)$) and (5 1 1) (or $3(1\,0\,0) \times (1\,1\,1)$) surfaces for which experiments have been carried out using IHAS [5] and EELS [6]. We will therefore briefly recall their main features (see Figs. 7 and 8b). Let us consider the $\overline{\Gamma}\overline{X}$ and $\overline{\Gamma}\overline{Y}$ directions corresponding to directions of propagation parallel and perpendicular to the step edges, respectively. Along the $\overline{\Gamma}\overline{X}$ direction a transverse mode (T) horizontally polarized, a Rayleigh mode (R) and a longitudinal mode (L), which are purely terrace modes are found on these surfaces. There are also several step modes (E) starting from $\overline{\Gamma}$: two around 2–3 THz and one around 6 THz. For the (5 1 1) surface a longitudinal mode (L) starting at $\overline{\Gamma}$ around 2 THz and ending at $\overline{X}$ around 4.5 THz is also found. Modes propagating perpendicularly to the step (along $\overline{\Gamma}\overline{Y}$) can be qualitatively described as resulting from a "backfolding" [27] of the Rayleigh and transverse modes. However, they have slightly different frequencies due to the confinement of the vibration perpendicular to the steps: a smaller terrace width leads to higher frequencies, similarly to the behaviour of electronic states [2].

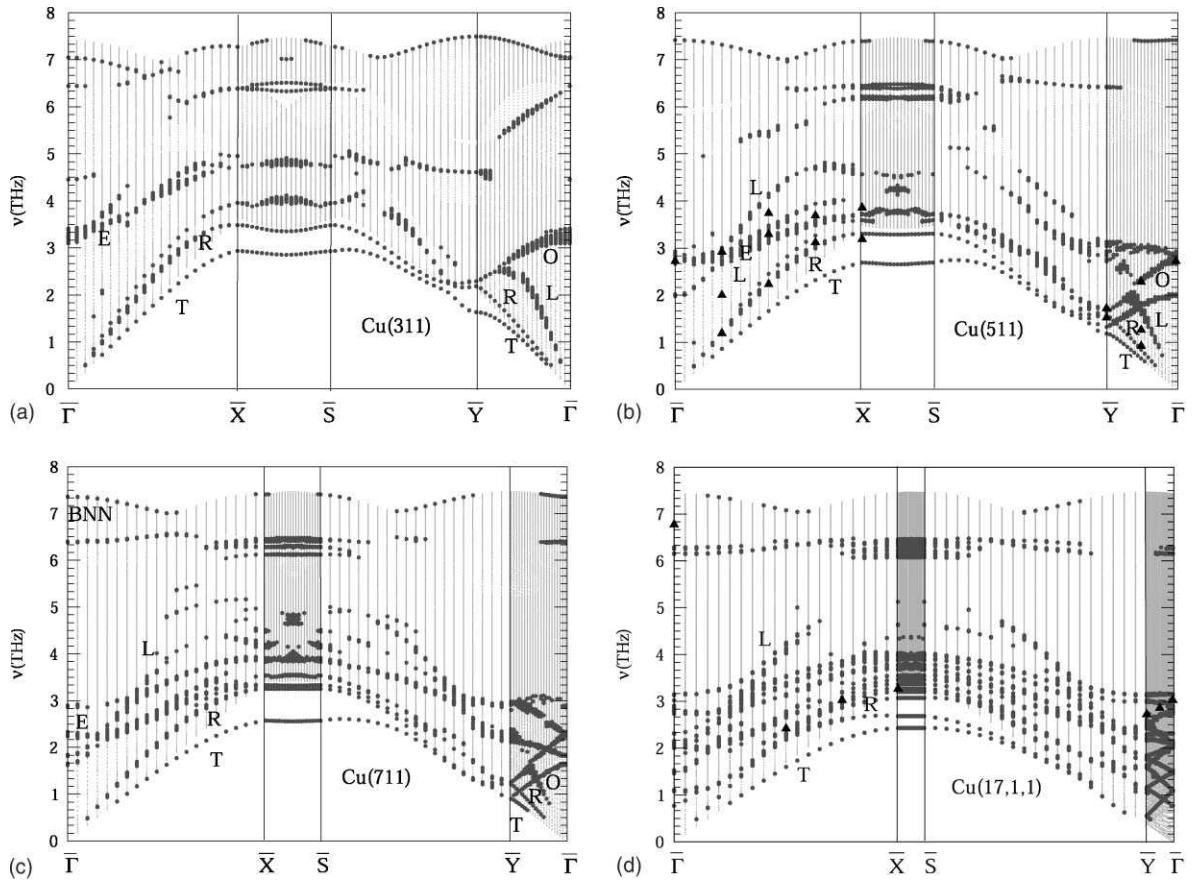

Fig. 8. Same caption as in Fig. 3 for the (3 1 1) (a), (5 1 1) (b), (7 1 1) (c) and (17,1,1) (d) surfaces but the localization criterion is 6% on the first 3, 4, 5 and 10 layers, respectively. Experimental points are available for (5 1 1) taken from Ref. [5] and for (17,1,1) taken from Ref. [6].

Let us now analyze the behaviour of the projected surface band structure as the terrace width increases. For this purpose we have considered the $p(1\,0\,0)\times(1\,1\,1)$ surfaces for $p=2,3,4$ and 9, presented in Fig. 8. First of all a small gap is present for $p=2$ (i.e., the (3 1 1) surface) between $\overline{X}$ and $\overline{S}$ and disappears as soon as p is larger than 2. This can be easily understood since as p increases, the area of the 2D Brillouin zone decreases and the height of the surface adapted bulk Brillouin zone [28], i.e., the sampled domain of k_z for a given $\mathbf{k}_{//}$ increases accordingly. Therefore more and more bulk states corresponding to lines with no symmetry in the 3D Brillouin zone are sampled. This explains the absence of gaps and of true surface states inside the bulk bands when $p>2$. Let us now study in details the $\overline{\Gamma}\overline{X}$ and $\overline{\Gamma}\overline{Y}$ directions.

Along $\overline{\Gamma}\overline{X}$ the dispersion curves of all surfaces show some common features (T,R,E). The main difference is an increasing number of surface resonances with neighbouring frequencies associated with different terrace sites, leading to an overall "blurring" of the surface dispersion curves. However one can still clearly distinguish the transverse mode T which becomes a true surface state separated from the bulk when approaching $\overline{X}$. The Rayleigh mode R is also easily identified for small p since it is slightly separated from the bulk edge at $\overline{X}$ for $p\leqslant 4$ but, when p exceeds 4, the lower

frequency of the bulk band decreases and gets very close to the maximum of the Rayleigh mode (around 3.2 THz) as expected from the (1 0 0) surface dispersion curves in which S_4 at $\overline{X}$ is at the limit of the bulk edge. Moreover for the (17,1,1) surface, true surface states appear around $\overline{X}$ above the transverse mode, but below the Rayleigh mode, so that the Rayleigh mode is more difficult to identify. These surface states should disappear for larger terrace widths since they are not present on the (1 0 0) surface. There is also a clear surface state near $\overline{X}$ (6.4 THz) which progressively extends along $\overline{\Gamma}\overline{X}$ with almost no dispersion as p increases, its weight being more important around $\overline{X}$. This is the signature of the S_6 surface state observed on the (1 0 0) surface. An analysis of the polarization of this surface mode shows that it is purely longitudinal (y polarization, i.e. parallel to the step edge) at the $\overline{X}$ point as the S_6 surface state, but becomes a transverse mode (x polarization, i.e. perpendicular to the step edge) when extending towards the $\overline{\Gamma}$ point. The step edge states (E) starting at $\overline{\Gamma}$ around 3 THz observed experimentally on the (5 1 1) surface also exist at a higher frequency on the (3 1 1) surface, and remain when the width of the terrace increases. However it becomes somewhat blurred. Finally the longitudinal surface mode (L) identified on the (5 1 1) surface is present for all terrace widths, starting at $\overline{\Gamma}$ around 2 THz and ending at $\overline{X}$ around 4.5 THz.

Along $\overline{\Gamma}\overline{Y}$ there is a common backfolded structure of the transverse and Rayleigh modes. This backfolding leads to optical branches (O) separated by gaps, their number increasing with the terrace width. These optical modes have been observed experimentally on the (5 1 1) [5] and also on the (17,1,1) surface [6], in excellent agreement with our calculation.

Let us now consider the case of the $(3\,3\,1) = 3(1\,1\,1) \times (1\,1\,\bar{1})$ and $(5\,5\,1) = 3(1\,1\,0) \times (1\,1\,1)$ surfaces (Fig. 9). At the first glance the two surface projected phonon band structures are very similar since (3 3 1) can also be regarded as the $2(1\,1\,0)\times(1\,1\,1)$ surface. The $\overline{\Gamma}\overline{X}$ direction is interesting to compare with the same direction in the (1 1 0) surface since it is parallel to a closed-packed chain of atoms both in (3 3 1) or (5 5 1) and (1 1 0) surfaces. Indeed one can identify three acoustical surface modes and an optical mode around 6 THz on the vicinal surfaces corresponding to the 5 THz mode on the flat (1 1 0) surface. Let us also note the existence of a small gap between $\overline{X}$ and $\overline{S}$ at high frequencies which shrinks when the terrace width increases.

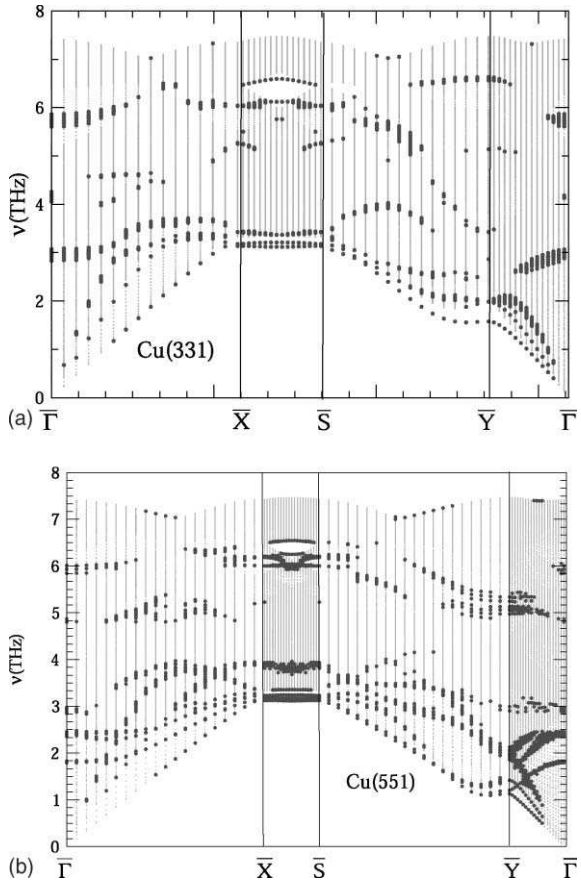

Fig. 9. Same caption as in Fig. 3 for the (3 3 1) (a) and (5 1 1) (b) surfaces but the localization criterion is 6% on the first four layers.

The (5 3 2) surface is a kinked surface with (1 1 1) terrace orientation, (1 0 0) step orientation and (1 1 $\bar{1}$) kink orientation (Fig. 10). The vectors $\mathbf{a}_1$ joining two kink atoms of the same step and $\mathbf{a}_2$ joining two kink atoms of adjacent steps define the (2D) oblique surface lattice. The slab used for the calculation contains 300 layers. The phonon band structure has been computed along the lines $\overline{\Gamma}B_6$

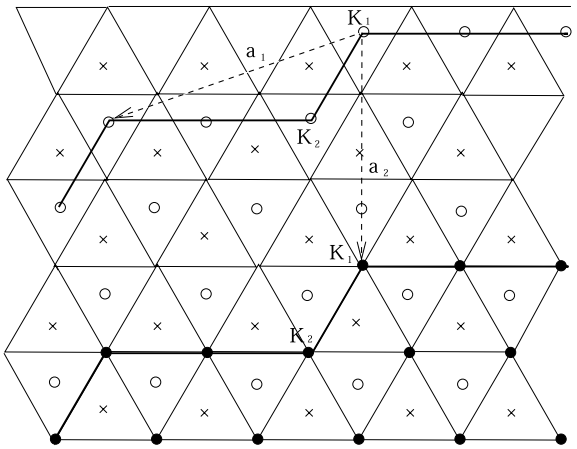

Fig. 10. Schematic top view of the kinked (5 3 2) surface. K_1 and K_2 denote the outer and inner kink sites, respectively.

($\overline{\Gamma}B_n = n\overline{\Gamma}B_1$) parallel to $\mathbf{a}_1$ and $\overline{\Gamma}A_1\overline{\Gamma}A_2\overline{\Gamma} = 4\overline{\Gamma}A_1$ parallel to the step edge drawn in the inset of Fig. 11 since experimental data are available along these lines [6]. Actually the calculation along the second direction exhibits a periodicity, since this line joins the centers $\overline{\Gamma}$ of two adjacent Brillouin zones, and a symmetry with respect to the A points (see the inset of Fig. 11) . In Fig. 11 the surface projected band structure is shown and resonant modes localized on the outer kink site (K_1) along $\overline{\Gamma}B_6$ and on the inner kink site (K_2) along $\overline{\Gamma}A_n$ are singled out. The agreement with experiments is rather good: the flat optical mode found between B_4 and B_6 is clearly visible around 3 THz. The acoustical mode along $\overline{\Gamma}A_n$ is more difficult to follow precisely but the existence of an inner kink mode with a dispersion curve close to the experimental one is obvious, in particular the parabolic shape with a maximum at A_2. The position of the theoretical maximum is slightly larger than the experimental one of about 0.4 THz but the overall agreement is convincing.

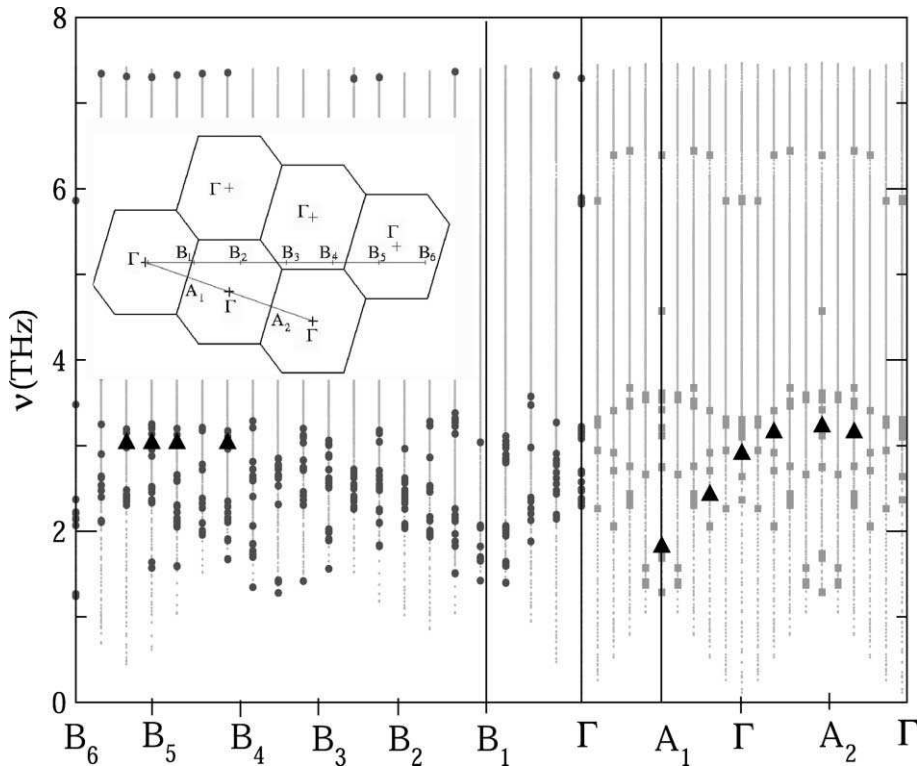

Fig. 11. The surface projected phonon band structure of Cu(5 3 2) calculated along the lines shown in the inset. Bulk states are represented by small dots. The states resonant or localized on the outer(inner) kink site along ΓB_n (ΓA_n) are marked as heavy dots (grey squares). The experimental data (full triangles) are taken from Ref. [6].

Table 3
Calculated change (Δr) of the bond length, of its vertical component (Δz) and of the force constant (Δk_{zz}) in percentage, between the step atom and its BNN, for the two vicinal surfaces, (5 1 1), (17,1,1) and the kinked surface (5 3 2)

Surface	Δr	Δz	Δk_{zz}
(5 1 1)	−2.6%	−3.0%	44%
(17,1,1)	−2.8%	−2.7%	50%
(5 3 2)	−3.7%	−3.9%	66%

Finally there is a very specific mode present on almost all the dispersion curves at the top of the bulk band edge at $\overline{\Gamma}$. This state is purely localized on the BNN atom. EELS experiments [6] have detected a surface phonon either slightly below the top of the bulk edge (17,1,1) surface and above the bulk edge for the (2 1 1) and (5 3 2) surfaces. Our calculations do not reproduce this surface mode at least when it is above the bulk edge, however it is likely associated with a BNN localized mode as will be shown in the next section. Its existence is closely related to the shortening of the BNN-SC bond length, producing a stiffening of the force constant. In Table 3 we give the contraction of the bond length between BNN and SC, and the corresponding stiffening of the force constant. It seems that this stiffening, eventhough as large as 40–66%, is not sufficient to obtain a surface state above the bulk edge. It is however interesting to note that in the case of the (5 3 2) surface the stiffening of the force constant is the largest and it also corresponds to the localized mode of highest frequency observed experimentally.

4.3. Local spectral densities of states

The LSDOS at a given value of $\mathbf{k}_{//}$ is

$$n_i(\nu,\mathbf{k}_{//}) = \sum_{\alpha} n_{i\alpha}(\nu,\mathbf{k}_{//}) = \sum_{\alpha,n} |e_{i\alpha}(\nu_n,\mathbf{k}_{//})|^2 \delta(\nu-\nu_n) \quad (3)$$

where $e_{i\alpha}$ is the α component on atom i of the eigenvector of the reduced dynamical matrix $D(\mathbf{k}_{//})$ corresponding to the wave vector $\mathbf{k}_{//}$ and frequency ν_n. It provides an information complementary to the projected band structure since it allows to determine the localization of each mode on the different atomic sites of the slab and, when decomposed into x, y and z directions, its polarization. In Fig. 12 we present the LSDOS of three stepped surfaces (2 1 1), (5 1 1) and (17,1,1) at $\overline{\Gamma}$ and $\overline{X}$, for three different sites: the step edge site (SC), the BNN site, a terrace site and a bulk site. In the case of (17,1,1) we have averaged the LSDOS over all terrace sites save for the outer and inner edges. The LSDOS of the (2 1 1) and (5 1 1) surfaces show some similarities, in particular the folded Rayleigh mode (FR) around 2.7 THz at $\overline{\Gamma}$, the transverse (T) mode around 2.7 THz and the Rayleigh mode around 3.2 THz at $\overline{X}$. Moreover the (2 1 1) surface exhibits clear step modes (E) (2.4 THz at $\overline{\Gamma}$ and 3.6 THz at $\overline{X}$) which are also found on the (5 1 1) surface. However the (5 1 1) surface shows a longitudinal mode around 2 THz at $\overline{\Gamma}$ which does not exist on the (2 1 1) surface. The case of the (17,1,1) surface is more complex due to the presence of many structures: at $\overline{\Gamma}$ the multiple backfolding of the Rayleigh mode produces several peaks (at least seven) between 0 and 3.2 THz, and at $\overline{X}$ two peaks appear between the transverse mode and the Rayleigh mode, as expected from the phonon dispersion curves of Fig. 8d. In contrast one can more easily identify a step mode with a small dispersion starting at $\overline{\Gamma}$ around 2.8 THz and ending at $\overline{X}$ around 3.8 THz. Let us now consider the structures found at higher frequencies. We note the existence of a pseudo-gap in the bulk SDOS at $\overline{X}$ around 6 THz which is filled with surface resonant modes for the (5 1 1) and (17,1,1) surfaces. In the same domain of frequencies the (2 1 1) surface exhibits an absolute gap in which a surface mode is found. For all surfaces the LSDOS of the BNN site is sharply peaked at the top of the spectrum both at $\overline{\Gamma}$ and $\overline{X}$ as already discussed in the preceding section.

5. Vibrational thermodynamical functions

In this section we present our results on thermodynamical quantities, limiting ourselves to the root mean square displacements and the vibrational free energy of steps. These quantities are obtained from a summation involving special $\mathbf{k}_{//}$

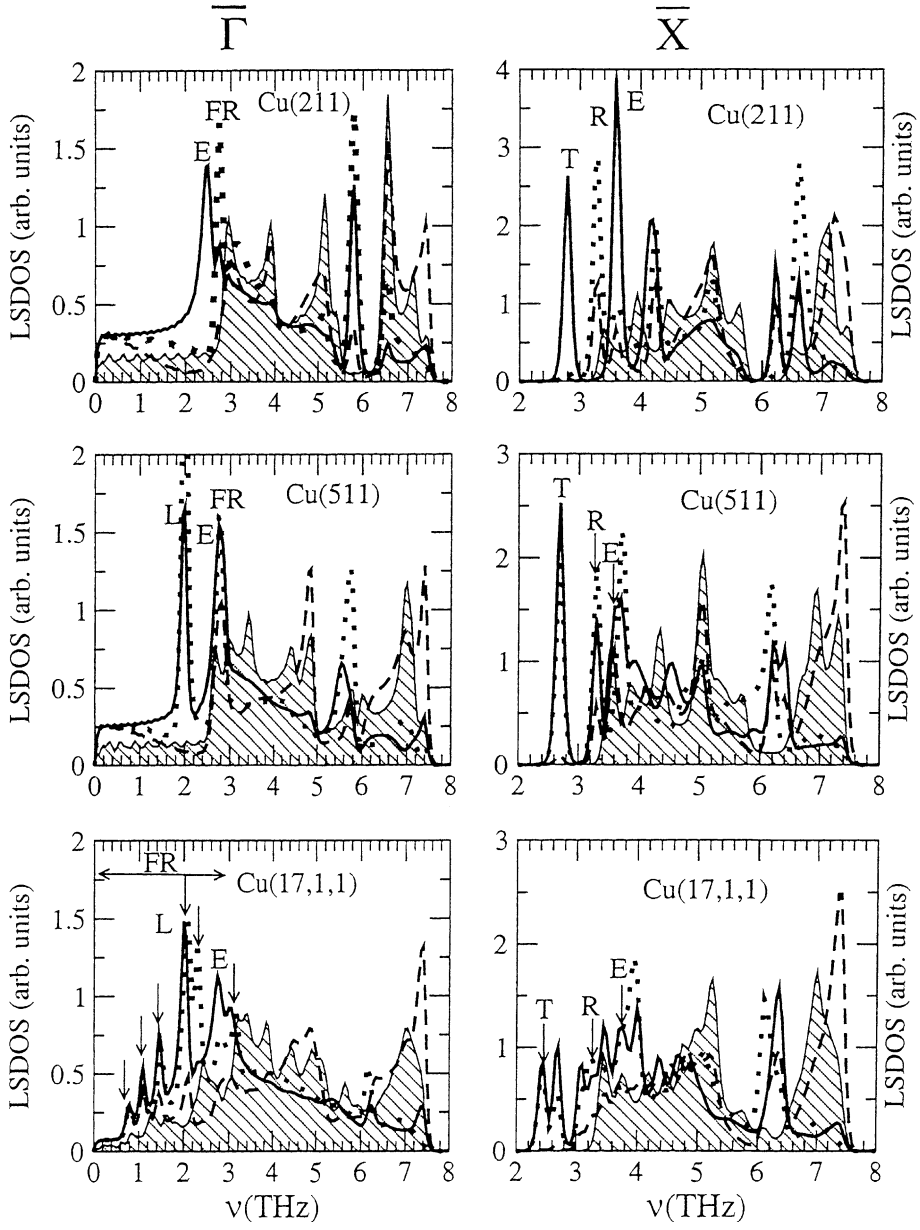

Fig. 12. The LSDOS at $\overline{\Gamma}$ and $\overline{X}$ for the (2 1 1), (5 1 1) and (17,1,1) vicinal surfaces. The hatched area singles out the bulk SDOS. The LSDOS on the outer edge and BNN atoms are drawn as full and dashed lines, respectively. The dotted curves is an average LSDOS over the rows inside the terrace. The main features observed experimentally L: longitudinal, E: edge, T: transverse, FR: backfolded Rayleigh modes are indicated.

points belonging to the irreducible Brillouin zone (see Fig. 2). The convergence with respect to the number of $\mathbf{k}_{//}$ points has been carefully checked.

5.1. Root mean square displacements

Let us call u^i_α the αth Cartesian component of the displacement of atom i relative to its

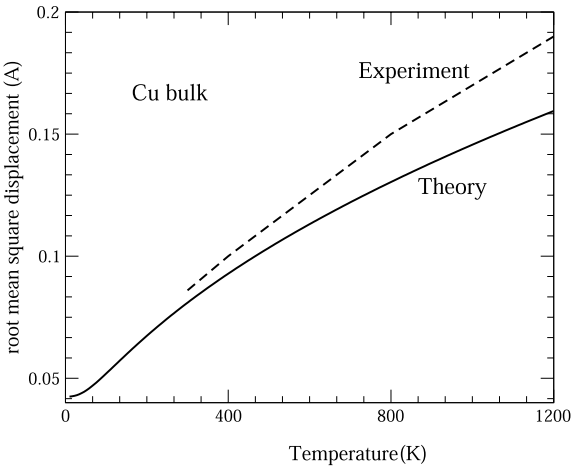

Fig. 13. Variation with temperature of the bulk root mean square displacement of a bulk Cu atom compared to experiments (Ref. [29]).

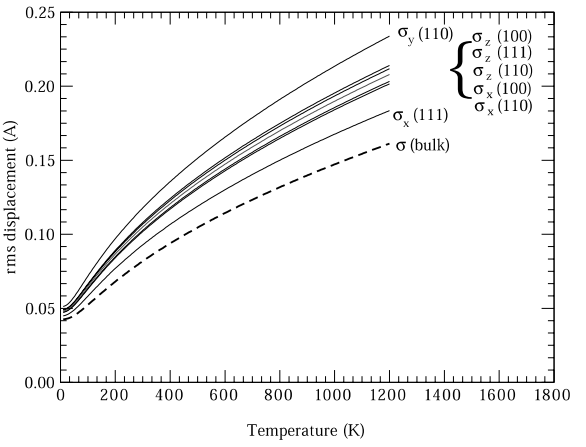

Fig. 14. Variation with temperature of the components of the root mean square displacements of atoms belonging to low index surfaces. The bulk one is given for comparison (dashed line).

equilibrium position. The root mean square value of u_α^i (RMSD) is defined as:

$$\sigma_\alpha^i = \sqrt{\langle (u_\alpha^i)^2 \rangle} = \frac{h}{8\pi^2 M} \int_0^\infty \frac{1}{v} \coth\left(\frac{hv}{2k_B T}\right) n_{i\alpha}(v)\,\mathrm{d}v \qquad (4)$$

where M is the mass of an atom, and $n_{i\alpha}(v)$ is the LSDOS of atom i in direction α, i.e., $n_{i\alpha}(v, \mathbf{k}_{//})$ defined in Eq. (3) and averaged over the 2D Brillouin zone. For bulk atoms, σ_α^i is isotropic: $\sigma_\alpha^i = \sigma^{\mathrm{bulk}}$. In Fig. 13 we show the variation of σ^{bulk} as a function of temperature compared to the experimental data [29] which are available only for $T > 300$ K. Around 300 K experimental data and our theoretical results are very close to each other but for higher temperatures the harmonic approximation starts to break down and, as a consequence, the experimental curve is above the theoretical harmonic RMSD. Let us now consider the RMSD of atoms belonging to the three low index surfaces (1 1 1), (1 0 0) and (1 1 0) (Fig. 14) and denote σ_x and σ_y its components in the surface plane and σ_z its component perpendicular to it. For the (1 0 0) and (1 1 1) surfaces σ_x (or equivalently σ_y) is smaller than σ_z as expected from the high atomic density of the surface, particularly for the (1 1 1) surface. The (1 1 0) surface has a peculiar behaviour since x (along the nearest neighbour direction) and y (along the next nearest neighbour one) are not equivalent. We find that σ_y is the largest component. Finally we have calculated the RMSD along the x, y and z directions for the three atomic sites: outer edge, inner edge and BNN of the (17,1,1) surface. The results are shown in Fig. 15. Along the three directions, the RMSD of the outer edge atom is larger than that of the inner edge, both being larger than for the BNN atom. The same calculations have also been carried out for the (3 1 1) surface with almost identical results, proving that the RMSD depend only on the very local environment.

5.2. Vibrational free energy of steps

The contribution of vibrations to the free energy of a system which has a total phonon frequency density $n(v)$ is given by:

$$F^{\mathrm{vib}}(T) = k_B T \int_0^\infty \ln\left(2\sinh\frac{hv}{2k_B T}\right) n(v)\,\mathrm{d}v \qquad (5)$$

We have calculated the vibrational free energy as a function of temperature of the $p(1\,0\,0) \times (1\,1\,1)$

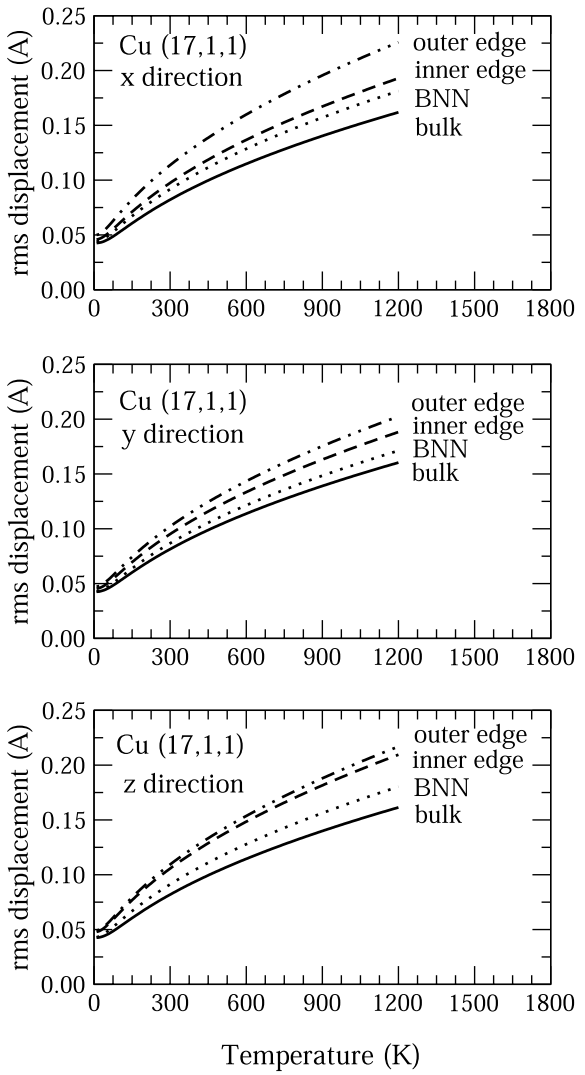

Fig. 15. Variation with temperature of the three components of the root mean square displacements of selected atoms of Cu(17,1,1). The bulk one is given for comparison (full line).

and $p(1\,1\,1) \times (1\,0\,0)$ vicinal surfaces for increasing terrace widths. The influence of this contribution to the total surface free energy on the occurrence of a faceting transition has been studied in details in our preceding papers [3,4]. From the vibrational free energy of vicinal surfaces, low index surfaces and bulk, the vibrational free energy of steps (per step atom) $F^{\mathrm{vib}}_{\mathrm{step}}(T)$ can be derived at any temperature using an equation similar to Eq. (2). In Fig. 16 we show $F^{\mathrm{vib}}_{\mathrm{step}}(T)$ as a function of temperature, for the $p(1\,0\,0) \times (1\,1\,1)$ and $p(1\,1\,1) \times (1\,0\,0)$ vicinal surfaces with $p = 2, \ldots, 7$. The step vibrational free energy is of the order of a few meV and decreases with temperature, reaching its linear regime for T larger than 100 K when the entropy contribution becomes the leading term. More interestingly $F^{\mathrm{vib}}_{\mathrm{step}}(T)$ decreases in absolute value when the terrace width increases, i.e., phonons produce an attractive step–step interaction for these vicinal surfaces. This effect is clearly seen on the right part of Fig. 16, in which we have drawn the vibrational free energy of steps $F^{\mathrm{vib}}_{\mathrm{step}}$ as a function of the terrace width for various temperatures ranging from $T = 0$ to 500 K, since $F^{\mathrm{vib}}_{\mathrm{step}}$ clearly increases with p. Furthermore this attractive step–step interaction increases with temperature. The possibility of interactions between surface defects mediated by phonons has already been investigated by Cunningham et al. [30]. These authors have derived the phonon contribution to the free energy of interaction for an adatom pair on the (1 0 0) face of cubium using the Montroll–Potts model. It is noteworthy that they also found an attractive interaction. From Fig. 16 it appears that at room temperature the variation of the step energy with the terrace width may be of the same order of magnitude (a few meV) as the repulsive elastic one. Fig. 17 shows the variation of the step energy as a function of p including both the elastic and vibrational contributions at 300 K. The correction to the isolated step energy is small but the phonons change the curvature of the step energy and, surprisingly, may even modify its sign. In particular for the $p(1\,1\,1) \times (1\,0\,0)$ surfaces the step energy exhibits a minimum at $p = 3$, i.e., the step–step interactions are attractive. In addition, it must be kept in mind that electronic effects are far from being negligible, at least for small terrace widths (typically less than 10 atomic rows), and usually give rise to oscillatory interactions as shown in our previous works [1,2]. In conclusion the step–step interactions have many physical origins: elastic, phononic, electronic, dipolar present even at 0 K. Moreover at finite temperatures two entropic contributions should be added: the vibrational one and that arising from step fluctuations, the latter being limited by the non-crossing condition. All

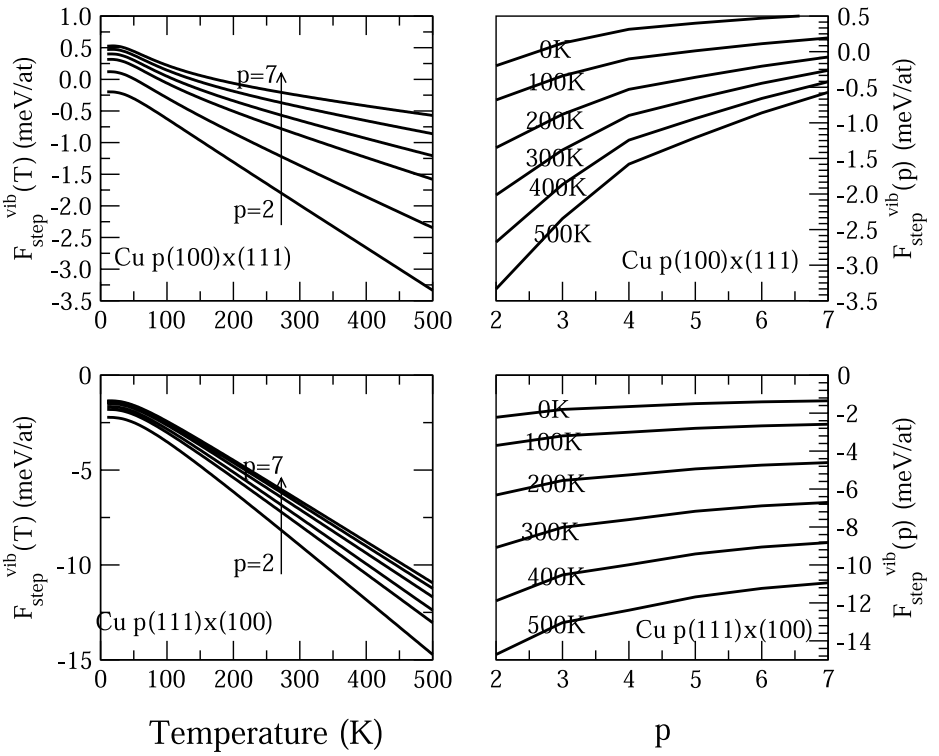

Fig. 16. The contribution of vibrations to the free energy of steps for $p(100) \times (111)$ and $p(111) \times (100)$: as a function of temperature for given values of p (left hand side), as a function of p for given temperatures (right hand side).

these interactions are very weak and thus difficult to calculate. Most of them have the same order of magnitude, at least in the range of medium terrace widths ($p < 10$) and may have different signs. Finally, let us briefly comment on the influence of phonons on the roughening transition temperature. According to Villain et al. [31] the $p(100) \times (111)$ FCC surfaces undergo a roughening transition at a temperature T_R satisfying the following equation:

$$\frac{w_p}{k_B T_R} \exp \frac{W_0}{k_B T_R} = 2 \tag{6}$$

where w_p is the energy necessary to move one step by an interatomic distance and W_0 is the kink energy. The parameter w_p is clearly related to the curvature of the free energy of steps as a function of p. The static calculation including relaxation at 0 K (Fig. 6) shows that w_p is positive and decreases slightly due to phonons (Fig. 16). The contribution of vibrations to the kink free energy is negative due to the lowered coordination of the kink atom. It is then easily shown from Eq. (6) that T_R decreases when vibrational effects are taken into account. The effect is expected to be small and a quantitative determination would need to study kinked (100) vicinal surfaces in order to compute the kink vibrational free energy.

6. Conclusion

In conclusion we have been able to build a many-body empirical potential for Cu which accounts reasonably for the multilayer relaxation of vicinal surfaces and describes accurately the surface projected phonon band structure for low and high index (vicinal) surfaces in the harmonic ap-

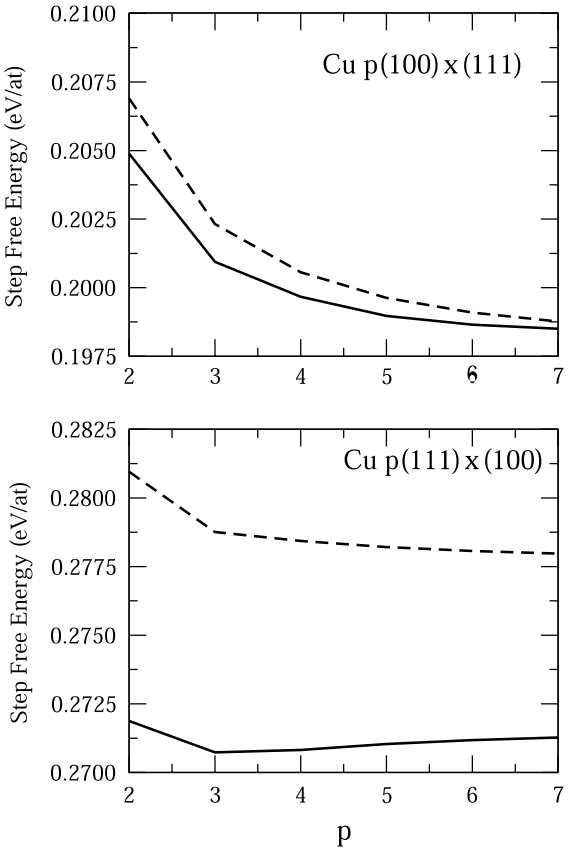

Fig. 17. Variation of the free energy of steps at 300 K as a function of p without (dashed line) and with (full line) the vibrational contribution.

proximation. Indeed, the dispersion curves of the localized or resonant modes due to the surface are in excellent agreement with existing experiments. These spectra have been used to compute vibrational thermodynamical quantities. The results on the root mean square dispacements reveal that anharmonic effects become non negligible above room temperature. In addition we have calculated the contribution of vibrations to the free energy of steps as well as its variation with the step width. We have found that for the $p(100) \times (111)$ and $p(111) \times (100)$ vicinal surfaces the step–step interactions mediated by phonons are attractive, similarly to what has been found for the adatom–adatom interactions. It would be interesting to study other geometries of vicinal surfaces in order to check the generality of this property.

Acknowledgements

We are grateful to F. Lançon and H.J. Ernst for stimulating discussions.

References

[1] F. Raouafi, C. Barreteau, M.C. Desjonquères, D. Spanjaard, Surf. Sci. 482–485 (2001) 1413.
[2] F. Raouafi, C. Barreteau, M.C. Desjonquères, D. Spanjaard, Surf. Sci. 505 (2002) 183.
[3] M.C. Desjonquères, D. Spanjaard, C. Barreteau, F. Raouafi, Phys. Rev. Lett. 88 (2002) 056104.
[4] F. Raouafi, C. Barreteau, D. Spanjaard, M.C. Desjonquères, Phys. Rev. B 66 (2002) 045410.
[5] G. Witte, J. Braun, A. Lock, J.P. Toennies, Phys. Rev. B 52 (1995) 2165.
[6] A. Kara, P. Staikov, T.S. Rahman, J. Radnik, R. Biagi, H.J. Ernst, Phys. Rev. B 61 (2000) 5714.
[7] A. Kara, S. Durukanoglu, T.S. Rahman, Phys. Rev. B 53 (1996) 15489.
[8] I.Yu. Sklyadneva, G.G. Rusina, E.V. Chulkov, Surf. Sci. 416 (1998) 17.
[9] C.Y. Wei, S.P. Lewis, E.J. Mele, A.M. Rappe, Phys. Rev. B 57 (1998) 10062.
[10] J. Guevara, A.M. Llois, M. Weismann, Phys. Rev. B 52 (1995) 11509.
[11] R.M. Nicklow, G. Gilat, H.G. Smith, L.J. Raubenheimer, M.K. Wilkinson, Phys. Rev. 64 (1967) 922.
[12] I. Galanakis, G. Bihlmayer, V. Bellini, N. Papanikolaou, R. Zeller, S. Blügel, P.H. Dederichs, Eur. Phys. Lett. 58 (2002) 751.
[13] F. Raouafi, C. Barreteau, M.C. Desjonquères, D. Spanjaard, Surf. Sci. 507 (2002) 748.
[14] S.L. Cunningham, Phys. Rev. B 10 (1974) 4988.
[15] M. Wuttig, R. Franchy, H. Ibach, Z. Phys. B 65 (1986) 71; M. Wuttig, R. Franchy, H. Ibach, Solid State Commun. 57 (1986) 445.
[16] G. Benedek, J. Ellis, N.S. Luo, A. Reichmuth, P. Ruggerone, J.P. Toennies, Phys. Rev. B 48 (1993) 4917.
[17] F. Hofmann, J.P. Toennies, J.R. Manson, J. Chem. Phys. 101 (1994) 10155.
[18] U. Harten, C. Woll, J.P. Toennies, Phys. Rev. Lett. 55 (1985) 2308.
[19] B.M. Hall, D.L. Mills, M.H. Mohammed, L.L. Kesmodel, Phys. Rev. B 38 (1988) 5856.
[20] C. Kaden, P. Ruggerone, J.P. Toennies, G. Zhang, G. Benedek, Phys. Rev. B 46 (1992) 13509.
[21] P. Zeppenfeld, K. Kern, R. David, K. Kuhnke, G. Comsa, Phys. Rev. B 38 (1988) 12329.
[22] Th. Rodach, K.-P. Bohnen, K.M. Ho, Surf. Sci. 296 (1993) 123.
[23] G. Prévot, C. Cohen, D. Schmaus, P. Hecquet, B. Salanon, Surf. Sci. 506 (2002) 272.
[24] R. Heid, K.P. Bohnen, A. Kara, T. Rahman, Phys. Rev. B 65 (2002) 115405.

[25] S. Walter, H. Baier, M. Weinelt, K. Heinz, Th. Fauster, Phys. Rev. B 63 (2001) 155407, and references therein.
[26] L. Vitos, H.L. Skriver, J. Kollár, Surf. Sci. 425 (1999) 212.
[27] G. Armand, P. Masri, Surf. Sci. 130 (1983) 89.
[28] M.C. Desjonquères, D. Spanjaard, Concepts in Surface Physics, Springer Verlag, Berlin, 1993.
[29] C.J. Martin, D.A. O'Connor, J. Phys. C: Solid State Phys. 10 (1977) 3521.
[30] S.L. Cunningham, L. Dobrzynski, A.A. Maradudin, Phys. Rev. B 7 (1973) 4643.
[31] J. Villain, D.R. Grempel, J. Lapujoulade, J. Phys. F 15 (1985) 809.

ELSEVIER

Surface Science 507–510 (2002) 748–753

SURFACE SCIENCE

www.elsevier.com/locate/susc

The phonon spectra of low and high index surfaces of copper

F. Raouafi [a], C. Barreteau [a], M.C. Desjonquères [a,*], D. Spanjaard [b]

[a] *DSM/DRECAM/SPCSI, Bat 462, CE Saclay, F-91 191 Gif sur Yvette, France*
[b] *Laboratoire de Physique des Solides, Université Paris Sud, F-91 405 Orsay, France*

Abstract

We have built a many-body empirical potential for describing the total energy in Cu crystals. Using this potential we first derive the bulk phonon dispersion curves and the surface projected phonon band structure of the (0 0 1) surface. The agreement with experiments is excellent which proves the very good transferability of the potential. We then investigate the vibrational properties of several vicinal surfaces. The results are presented and discussed in relation with recent experiments. © 2002 Elsevier Science B.V. All rights reserved.

Keywords: Atomistic dynamics; Construction and use of effective interatomic interactions; Copper; Vicinal single crystal surfaces

1. Introduction

Vicinal or more generally stepped surfaces of metals have been the object of numerous theoretical and experimental works due to their importance in many phenomena such as epitaxial growth or heterogeneous catalysis. However the knowledge of their dynamic properties is far from being completely acquired. Indeed the experiments are most often limited to a few peculiar directions of propagation of the vibrations. On the theoretical side, ab initio calculations are restricted to a few high symmetry points due to the large size of the unit cell. Another possibility is to built empirical potentials which should be carefully checked before transferring them to vicinal surfaces. Pair potentials have been used in the early works but, although giving qualitatively good results, discrepancies remain between experiments and theory. In the last 20 years attempts have been done to introduce some many-body character in the potentials but the surface energies are almost always underestimated. Moreover the spatial range of these potentials is somewhat arbitrary and its importance is very often disregarded.

In this work we present an empirical potential for FCC copper which has some similarity with the so-called tight-binding second moment potential [1]. It improves the numerical values of the surface energies and gives the best results when the interactions are cut-off between second and third nearest neighbours. Its transferability is checked on a detailed study of the phonons on Cu(0 0 1). Then it is applied to the determination of the surface phonon dispersion curves of several vicinal surfaces giving excellent agreement with experimental data.

2. The empirical potential

We have developed a new empirical potential to describe the interatomic interactions of a set

* Corresponding author. Tel.: +33-1-69-08-38-56; fax: +33-1-69-08-84-46.
E-mail address: mcdjs@drecam.saclay.cea.fr (M.C. Desjonquères).

PII: S0039-6028(02)01347-X

of atoms located at R_i. Its analytical form is given by:

$$V(R_1,\ldots R_i,\ldots) = A\sum_{i,j,j\neq i}(R_0/R_{ij})^p f_c(R_{ij}) - \xi\sum_i\left(\sum_{j\neq i}\exp(-2q(R_{ij}/R_0-1))f_c(R_{ij})\right)^{\alpha} \quad (1)$$

where R_{ij} is the distance between atoms i and j, R_0 is a reference distance that we take equal to the bulk nearest neighbour spacing and $f_c(R) = 1/(1+\exp[(R-R_c)/\Delta])$ is a smooth cut-off function with a cut-off radius R_c. This potential differs from the conventional second moment potential in which α is fixed ($\alpha = 1/2$) and that is unable to give both the cohesive and the surface energies correctly [1]. Another exponent ($\alpha = 2/3$) has been proposed in the literature [2] to account for higher moments of the density of states and charge neutrality requirements. Even though this exponent $\alpha = 2/3$ is probably not "universal" it is found that for most elements an exponent between 1/2 and 1 (and usually close to 2/3) allows to describe with a reasonable accuracy both bulk and surface properties.

The parameters A, ξ, p and q are fitted to the cohesive energy E_c and the three elastic constants (bulk and shear moduli B, C and C'). The equilibrium equation gives a relation between the four parameters and the first neighbour distance is fixed at the experimental value $R_0 = 2.5526$ Å in the case of copper. We have found that with $\alpha = 0.666$, we are able to obtain an excellent fit (better than 1 meV/atom) of the cohesive energy $E_c = -3.5$ eV/at and of the three elastic constants $B = 10.470$ eV/at, $C = 6.046$ eV/at and $C' = 1.917$ eV/at. Moreover the surface energies of the three low index surfaces (1 1 1), (0 0 1) and (0 1 1), even though not included in the fit, are much more reasonable than with $\alpha = 1/2$.

We have checked several sets of parameters, corresponding to different cut-off radii R_c, by comparing the surface relaxation and the bulk phonon spectra to experiments (see Section 3). It was found that large cut-offs systematically give too small surface relaxations or even outward relaxations when too many neighbours are included in the potential range. We emphasize that surface phonons are extremely dependent on the local modification of force constants and, consequently, the potential must predict surface relaxation correctly. Finally the best set of parameters was obtained for a cut-off radius $R_c = 4.02$ Å between second and third neighbours (with $\Delta = 0.05$ Å) and the corresponding parameters are $A = 0.206$ eV, $\xi = 1.102$ eV, $p = 7.206$, $q = 2.220$. Note that with these parameters the dimer bond-length is very reasonable: 14% bond-length contraction relative to R_0 is found compared to 16% with ab initio DMOL calculations.

In the following we will present the phonon spectra of the bulk and various flat and vicinal surfaces of copper. All structures have been fully relaxed, with a conjugate gradient algorithm. The phonon dispersion relations are then calculated in the harmonic approximation. It is noteworthy that, due to the many-body character of the attractive term, the range of the force constants is twice the range of the potential [3]. Finally let us note that the long range character of the force constants (eighth neighbours in our case) is in perfect agreement with ab initio calculations [4].

3. Bulk phonon spectrum

The calculated dispersion curves for bulk copper are presented in Fig. 1. The agreement with experiments [5] is excellent. Apart from the top of the spectrum at points X and L where the deviation between calculated and experimental frequencies is around 0.2 THz, everywhere else the deviation is less than 0.1 THz. Furthermore there is a rather peculiar feature along the path joining the two equivalent X points $(1, 0, 0)2\pi/a$ and $(1, 1, 0)2\pi/a$ (a: lattice parameter) via the middle point W: the lowest frequency band is showing a shallow minimum at W. It is remarkable that the position and the peculiar shape of this band is perfectly well reproduced only with a second neighbour potential. When including further neighbours, even though the quality of the fit on bulk cohesive energy and elastic constants is often

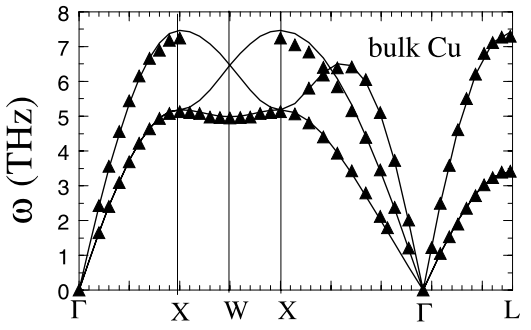

Fig. 1. Phonon dispersion curves of bulk copper. The full lines correspond to the calculated dispersion curves and the triangles to the phonons frequencies measured from neutron inelastic-scattering experiments (Ref. [5]). Each segment along the path $\Gamma(\Delta)X(Z)W(Z)X(\Sigma)\Gamma(\Lambda)L$ is proportional to its length in reciprocal space.

similar, the overall agreement of the phonon dispersion curves is much less satisfactory.

4. An example of a flat surface: Cu(0 0 1)

In order to check the transferability of our potential we have first calculated the projected band structure of phonons for the three low index surfaces (1 1 1), (0 0 1) and (0 1 1). In all cases the agreement with electron energy loss spectroscopy (EELS) and inelastic helium atom scattering (IHAS) experiments is excellent concerning the surface phonon dispersion curves. We will just discuss here our results on the (0 0 1) surface. In good agreement with experiments and other calculations [4] the first interlayer spacing is found to be contracted by $\simeq 2\%$ while the second one is almost unchanged. The projected band structure calculated with a slab of 61 atomic layers is given in Fig. 2.

Let us first discuss the phonons propagating along the $\overline{\Gamma X}$ direction. The surface phonon labelled S_1 is a transverse horizontal mode which is not detected in experiments. Its frequency at the $\overline{X}$ (2.38 THz) compares accurately with the ab initio value (2.3 THz) [4]. The phonon labelled S_4 is the Rayleigh sagittal mode which is seen both in EELS [6] and IHAS [7,8]. We have drawn in Fig. 2 a few typical experimental points [6,7] along the dispersion curve of S_4. Its frequency at $\overline{X}$ is 3.18 THz in excellent agreement with experiments (3.25 THz) and ab initio calculations (3.1 THz). The phonon S_2 (3.46 THz at $\overline{X}$) which is polarized in the sagittal plane is found very close to the bulk band edge and on the higher frequency side while it is found slightly below in ab initio calculations [4]. The gap phonon S_6 which is longitudinal in the first plane and vertically polarized in the second is located at 6.05 THz at $\overline{X}$ compared to the ab initio (6.2 THz) and EELS (6.1 THz) values reported by Chen et al. [4]. Finally a longitudinal resonance (LR) mode of higher frequency is present as a very weak structure in IHAS spectra [7]. With the localization criterion (10% on the first two layers) that has been adopted in Fig. 2 it can be seen at about 1/4 of $\overline{\Gamma X}$ from $\overline{\Gamma}$.

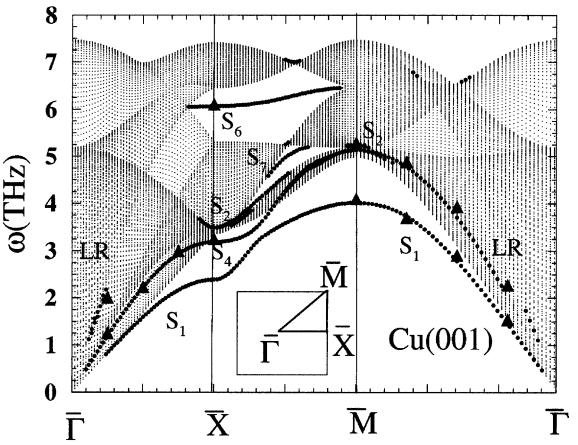

Fig. 2. Frequency spectrum of phonons for the Cu(0 0 1) surface as function of $\mathbf{k}_{\parallel}$ along the path $\overline{\Gamma X M \Gamma}$ in the surface Brillouin zone shown in the inset. Each segment is proportional to its length in the reciprocal space. Bulk states are represented by small dots. Localized and resonant states are denoted by heavy dots and labelled with the usual notations. Only the modes localized more than 10% on the first two layers are shown. Typical experimental points taken from Ref. [6] (S_4, S_1), Ref. [7,8] (LR) and Ref. [4] (S_2, S_6) are denoted by full triangles.

Let us now discuss the phonons propagating along the $\overline{\Gamma M}$ direction. The surface phonon S_1 is the Rayleigh wave, its dispersion is in complete agreement with EELS and IHAS data. In particular its frequency at $\overline{M}$ is 4.01 THz compared with the experimental (4.1 THz) and ab initio (4.3 THz) values [4]. In IHAS experiments [8] a LR with an intensity must larger than along $\overline{\Gamma X}$ is also found

which we reproduce accurately: its frequency at $\overline{M}$ (5.11 THz) is close to the experimental value (5.28 THz). Finally, ab initio calculations reveal the existence of a transverse vertical mode S_2 localized in the second layer at a frequency slightly lower than that of LR. We also find this mode but at a frequency slightly larger than that of LR.

In the direction $\overline{XM}$ no experiments are available. We find the same surface phonons as in an embedded atom model (EAM) [9]. However the experimental dispersion curves of the Rayleigh modes along $\overline{\Gamma X}$ and $\overline{\Gamma M}$ are better reproduced with our potential.

In conclusion, in view of the excellent agreement of our results with experiments, we are confident in the transferability of our potential to study vicinal surfaces.

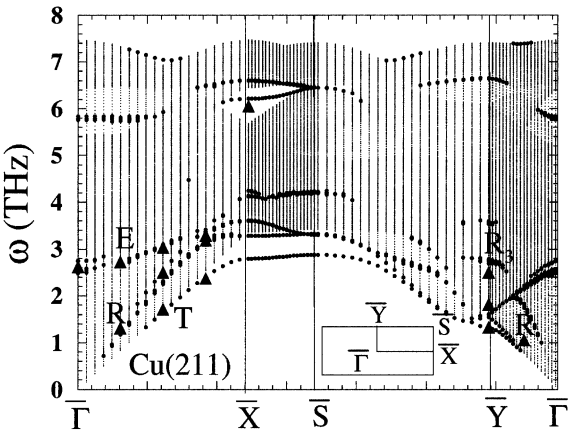

Fig. 3. Same caption as Fig. 2 for the (2 1 1) surface but the prominent surface features are denoted with the same notations as in Ref. [10] and the localization criterion is 10% on the first four layers. Experimental points are taken from Ref. [10] except the highest frequency at $\overline{X}$ which corresponds to the EELS data of Ref. [11].

5. Vicinal surfaces

Let us now present our results on vicinal surfaces. We will limit ourselves here to the (2 1 1) (or $3(1\,1\,1)\times(1\,0\,0)$) and (5 1 1) (or $3(1\,0\,0)\times(1\,1\,1)$) surfaces for which experiments have been carried out using IHAS [10] and EELS [11]. We will also briefly comment on our results for the (3 1 1) (or $2(1\,1\,1)\times(1\,0\,0)$, equivalently $2(1\,0\,0)\times(1\,1\,1)$) surface. A more extensive study including vicinals with wider terraces will be published elsewhere.

The frequency spectrum of phonons of Cu(2 1 1) is shown in Fig. 3 in which we have also drawn experimental points from Refs. [10,11]. It has been calculated using a slab of 225 vicinal layers.

Along the $\overline{\Gamma X}$ direction (i.e., the direction of propagation parallel to the step edges) several induced surface features are clearly identified. The lowest frequency mode T is a transverse mode horizontally polarized. It is clearly seen in IHAS experiments [10] as soon as it peels off the bulk edge. Its frequency at $\overline{X}$ is 2.78 THz in our calculation compared to the experimental (extrapolated) value of 2.72 THz. Above this mode one finds the sagittal Rayleigh (R) mode which is vertically polarized at $\overline{X}$ where its frequency is 3.25 THz. It is localized in the middle row of the terraces. At higher frequency the step localized mode (E) starts at 2.50 THz at $\overline{\Gamma}$ and reaches 3.59 THz at $\overline{X}$. Note that Witte et al. [10] extrapolate the dispersion curves of modes R and E to the same frequency ($\simeq$3.40 THz) whereas in our calculations we predict a separation of $\simeq$0.3 THz. All these results are thus in very good agreement with IHAS and also with EELS [11] experiments. In addition another surface mode at higher frequency (6.1 THz) is observed in EELS at $\overline{X}$ in close agreement with the calculated surface phonon in the gap (6.2 THz). Finally ab initio calculations [12] have been performed at $\overline{\Gamma}$ and revealed three surface induced structures at 2.7, 2.8 and 6.0 THz in good agreement with our calculations in which the corresponding frequencies are 2.5 (mode E), 2.7 and 5.8 THz. However the surface phonon detected by EELS [11] at $\overline{\Gamma}$ above the bulk band edge is found neither with our potential nor in the ab initio method.

Along $\overline{\Gamma Y}$ (i.e., the direction of propagation perpendicular to step edges), the mode with the lowest frequency (T) is a transverse mode that is not detected in experiments. The next mode is the Rayleigh mode (R) with a frequency 1.55 THz at $\overline{Y}$ in our calculations while the observed frequency is 1.33 THz. Resonant states have also been observed near $\overline{Y}$ around 2.5 THz (R_3), a value which is rather close to the resonance around 2.7 THz which is found in our calculations. Other surface features,

in particular the "back-folded" modes, are rather similar to those obtained by Witte et al. [10] using a single force constant model with no relaxation.

Let us now discuss the surface projected band structure of phonons of the (5 1 1) vicinal surface. As for the (2 1 1) surface a slab of 225 vicinal layers has been used. When the same localization criterion as for the (2 1 1) surface is adopted, the most prominent surface structures are very similar in both surfaces, in particular the E and R modes. However, experiments being able to detect weak loss peaks corresponding to longitudinal branches, we have decreased the localization criterion of surface structures to 5% on the first four vicinal planes (instead of 10%) in order to reveal these modes. The corresponding surface projected band structure of phonons is shown in Fig. 4. Along $\overline{\Gamma X}$ the Rayleigh mode is slightly lower in frequency compared to the (2 1 1) surface, this effect being more pronounced half-way between $\overline{\Gamma}$ and $\overline{X}$. The E modes are very similar in both surfaces. Finally the weakly localized longitudinal L mode crosses the E band at about 1/3 of $\overline{\Gamma X}$ from $\overline{\Gamma}$ (actually this L mode also appears on the (2 1 1) surface when decreasing the localization criterion but it is not detected in experiments). Finally the transverse mode T, which is not seen in experiments, has a slightly lower frequency compared with the (2 1 1) surface. Along $\overline{\Gamma Y}$ the Rayleigh mode R is back-folded at $\overline{Y}$ leading to an optical branch O with a gap of 0.1 THz at $\overline{Y}$ and a longitudinal mode L meets the O mode at about 2/3 of $\overline{\Gamma Y}$ from $\overline{\Gamma}$. Finally the transverse T mode is not observed. All these features are in very good agreement with experiments [10,11].

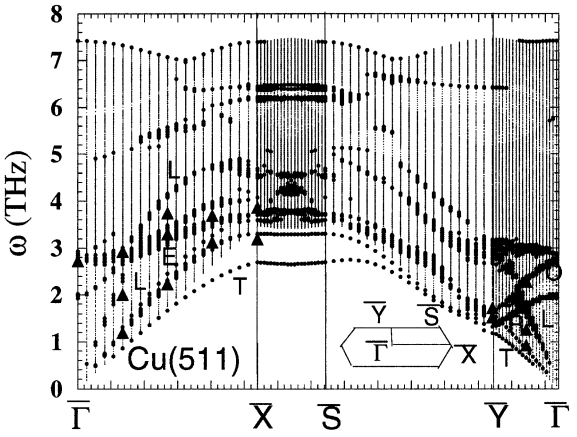

Fig. 4. Same caption as Fig. 3 for the (5 1 1) surface but the localization criterion is 5% on the first four layers. Experimental points are all taken from Ref. [10].

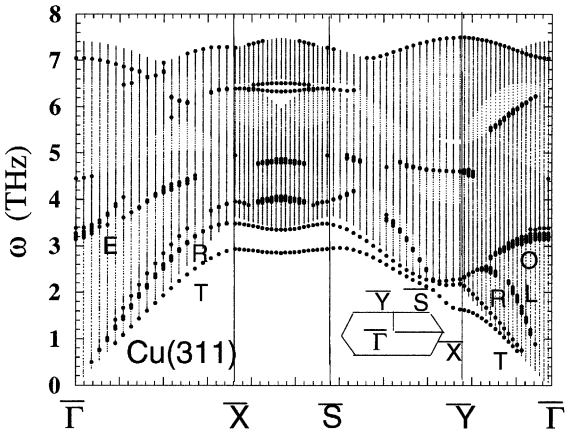

Fig. 5. Same caption as Fig. 3 for the (3 1 1) surface. The localization criterion is 8% on the first three layers.

Let us end this section by presenting our results on the (3 1 1) surface for which no experimental data are available. The phonon spectrum obtained with a slab of 150 vicinal layers is shown in Fig. 5 for which a localization criterion of 8% on the first three vicinal planes has been chosen. There are again strong similarities with the two vicinal surfaces studied above. However along $\overline{\Gamma X}$ the bottom of the bulk band and the modes E, R and T are shifted towards higher frequencies. The same effect is seen along $\overline{\Gamma Y}$ for the bottom of the bulk bands and the modes T, L and O, but the shift is much larger. Note also that the only absolute gap inside the projected bulk band structure, which is found between $\overline{X}$ and $\overline{S}$, has a much larger extension than in the corresponding one in the (5 1 1) surface. Indeed the bulk bands are less back-folded in the (3 1 1) than in the (5 1 1) surface.

6. Conclusion

In summary we have built a simple empirical N-body potential for FCC copper which has been fitted to the bulk cohesive energy and elastic constants. We have shown that this potential is able to

reproduce accurately the phonon spectra of the bulk and flat surfaces. Using this potential we have computed the phonon dispersion curves of Cu(3 1 1), Cu(5 1 1) and Cu(2 1 1) vicinal surfaces. The results are in excellent agreement with existing experimental data. This potential will be useful to understand the thermal properties and stability of vicinal surfaces of copper.

Acknowledgements

We are grateful to F. Lançon and H.J. Ernst for stimulating discussions.

References

[1] V. Rosato, M. Guillopé, B. Legrand, Philos. Mag. A 59 (1989) 321.
[2] J. Guevara, A.M. Llois, M. Weismann, Phys. Rev. B 52 (1995) 11509.
[3] M. Finnis, J.E. Sinclair, Philos. Mag A 50 (1984) 45.
[4] Y. Chen, S.Y. Tong, J.S. Kim, L.S. Kesmodel, T. Rodach, K.P. Bohnen, K.M. Ho, Phys. Rev. B 44 (1991) 11394.
[5] R.M. Nicklow, G. Gilat, H.G. Smith, L.J. Raubenheimer, M.K. Wilkinson, Phys. Rev. 64 (1967) 922.
[6] M. Wuttig, R. Franchy, H. Ibach, Z. Phys. B 65 (1986) 71; M. Wuttig, R. Franchy, H. Ibach, Solid State Commun. 57 (1986) 445.
[7] G. Benedek, J. Ellis, N.S. Luo, A. Reichmuth, P. Ruggerone, J.P. Toennies, Phys. Rev. B 48 (1993) 4917.
[8] F. Hofmann, J.P. Toennies, J.R. Manson, J. Chem. Phys. 101 (1994) 10155.
[9] J.S. Nelson, E.C. Sowa, M.S. Daw, Phys. Rev. Lett. 61 (1988) 1977.
[10] G. Witte, J. Braun, A. Lock, J.P. Toennies, Phys. Rev. B 52 (1995) 2165.
[11] A. Kara, P. Staikov, T.S. Rahman, J. Radnik, R. Biagi, H.J. Ernst, Phys. Rev. B 61 (2000) 5714.
[12] C.Y. Wei, S.P. Lewis, E.J. Mele, A.M. Rappe, Phys. Rev. B 57 (1998) 10062.

Chapitre 4

Etude de la stabilité des surfaces vicinales par rapport à un facettage.

4.1 Introduction

Dans ce chapitre, nous abordons l'étude de la stabilité des surfaces vicinales par rapport à un facettage. On sait que l'énergie $\gamma(\vec{n})$ (par unité de surface) d'une surface varie avec son orientation cristallographique $\vec{n}$. Pour une surface vicinale, γ est élevée et l'énergie correspondant à une aire S est donnée par le produit γS. Il se peut que l'on gagne de l'énergie en modifiant le profil de la surface pour qu'elle présente des facettes dont l'orientation correspond à des faibles valeurs de γ tout en gardant son orientation moyenne, même si dans cette transformation on augmente la surface totale exposée au vide. Ce problème a été résolu dès les années cinquante par Herring [13] qui a proposé une construction à partir de la surface décrite par les extrémités des vecteurs de longueur γ et de direction $\vec{n}$ (γ_{plot}) et qui permet de savoir s'il y a facettage pour un plan de direction donnée. Cependant le calcul de $\gamma(\vec{n})$ pour une direction quelconque nécessite d'atteindre des mailles élémentaires de grande taille. Les progrès numériques récents commencent à permettre de calculer cette énergie avec plus de précision. Le problème du facettage a été repris récemment par Frenken et Stoltze [33] en utilisant un potentiel empirique basé sur la théorie du milieu effectif (EMT) [16,17]. Ces auteurs prédisent que toutes les surfaces vicinales des métaux sont instables à 0K et qu'elles sont stabilisées à température finie par les effets d'entropie vibrationnelle. Nous reprenons d'abord ce problème en utilisant des potentiels empiriques pour calculer la stabilité des surfaces vicinales. Nous montrons en particulier l'importance de la portée du potentiel qui peut changer qualitativement les résultats. Puis reprenant les résultats du chapitre 2, où l'énergie de surface est obtenue par des calculs de structure électro-

nique, nous mettons en évidence que les potentiels empiriques ne peuvent pas décrire la diversité des situations possibles. Enfin, dans le cas du Cu, nous calculons l'effet des vibrations sur l'énergie libre de surface en utilisant les résultats du chapitre 3. Cet effet est très faible, du moins jusqu'à la température ambiante, et peut être stabilisant ou déstabilisant.

4.2 Condition de facettage

Considérons deux surfaces de faibles indices de Miller S_1 et S_2 (avec des normales $\overrightarrow{n_1}$ et $\overrightarrow{n_2}$) qui se coupent le long d'une rangée atomique et appelons θ_2 l'angle $(\overrightarrow{n_1},\overrightarrow{n_2})$. Quand on tourne la surface S_1 autour de la rangée atomique d'intersection vers S_2 en mesurant l'angle de rotation à partir de S_1, on balaye d'abord les surfaces vicinales de terrasses S_1 dont le nombre des rangées atomiques p_1 dans la terrasse décroît de l'infini vers 2 ($\theta = \theta_c$), puis on trouve les surfaces vicinales de terrasses S_2 dont le nombre des rangées atomiques p_2 augmente de 2 vers l'infini . La surface vicinale correspond à $p_1 = p_2 = 2$ ($\theta = \theta_c$) peut donc être considérée à la fois comme une surface vicinale de terrasse S_1 ou bien de terrasse S_2. On montre qu'une surface vicinale d'aire S et de normale $\overrightarrow{n}$ se transforme en facettes de normale $\overrightarrow{n_1}$ (aire S_1) et de normale $\overrightarrow{n_2}$ (aire S_2) en gardant l'orientation moyenne quand :

$$\frac{\gamma(tan(\theta))}{cos(\theta)} > (1 - \frac{tan(\theta)}{tan(\theta_2)})\gamma(0) + (\frac{tan(\theta)}{tan(\theta_2)})\frac{\gamma(\theta_2)}{cos(\theta_2)} \tag{4.1}$$

Cette condition est équivalente à la construction de Herring [13] (voir Appendice de l'article ci-après) et a une interprétation géométrique simple : la surface d'orientation $\overrightarrow{n}$ est instable si son point représentatif dans un diagramme $\frac{\gamma}{cos(\theta)} = f(tan(\theta))$ est au dessus de la droite joignant les points de coordonnées (0,γ_1) et ($tan(\theta_2), \frac{\gamma_2}{cos(\theta_2}$)) et stable dans le cas contraire. Ainsi la déviation $\Delta f(tan(\theta))$ du point $\frac{\gamma}{cos(\theta)} = f(tan(\theta))$ par rapport à la droite précédente détermine aussi la stabilité de la surface vicinale ($\Delta f(tan(\theta)) < 0$) ou l'instabilité ($\Delta f(tan(\theta)) > 0$).

Dans le cas où on néglige les énergies d'interactions entre les marches, la fonction $\frac{\gamma(tan(\theta))}{cos(\theta)} = f(tan(\theta))$ est composée de deux droites avec rupture de pente (Figure 2). Les deux droites se raccordent à $tan(\theta_c)$ puisque la surface correspondant à θ_c peut être considérée comme une surface vicinale de S_1 ou de S_2. La fonction $\Delta f(tan(\theta))$ a donc une forme triangulaire mais qui est perturbée par l'existence d'interactions entre les marches comme nous le verrons par la suite. Nous allons présenter des résultats de

stabilité des surfaces vicinales en utilisant diverses approches : la plus simple est basée sur l'utilisation d'un potentiel de paire, puis de potentiels semi-empiriques obtenus par l'addition d'une contribution à N corps à un potentiel de paire. La troisième est beaucoup plus complexe, elle est basée sur l'utilisation des calculs de structure électronique et, en particulier, des énergies de surface effectués au chapitre 2.

4.3 Résultats

4.3.1 Domaines étudiés

Nous avons analysé la stabilité des surfaces vicinales des éléments de transition Rhodium, Palladium et Cuivre. Nous présentons ci-dessous les deux domaines de surfaces vicinales que nous avons étudiés (Figure 3) :

- le premier domaine est défini par les surfaces vicinales entre les deux faces d'orientations (100) et (111). La surface (100) est considérée comme origine des angles. Le passage continu de la surface (100) à la surface (311) nous permet de balayer les plans cristallographiques (2p-1,1,1) ou p(100)×(111) [25] avec ($\infty > p \geq 2$). Puis de la surface (311) à la surface (111), on balaye les plans (p+1,p-1,p-1) ou p(111)×(100) avec ($2 \leq p < \infty$).

- le deuxième domaine concerne les surfaces vicinales entre les faces ($\overline{1}11$) et (111). Il est symétrique par rapport à la surface (011) qu'on choisit comme origine des angles. Nous ne considérons alors que l'intervalle des surfaces vicinales rencontrées lors du passage continu de (011) à (111). En effet les plans (1,2p-1,2p-1) ou p(011)×(111) [25] correspondent aux surfaces vicinales entre les faces (011) et (133) ($p = 2$). Par contre les plans cristallographiques entre (133) et (111) limitent le domaine des surfaces vicinales p(111)×(011) qui peuvent aussi être considérées comme (p+1)(111)×($\overline{1}11$) et ont pour indices de Miller (p-1,p+1,p+1).

4.3.2 Potentiels semi-empiriques

Nous avons effectué dans un premier temps des calculs analytiques sur un réseau rigide sans prendre en compte les effets de la relaxation atomique. Nous discutons le cas d'un potentiel de paire puis nous étudions l'influence de l'addition d'une contribution à N corps. Ensuite nous calculons numériquement la stabilité des surfaces vicinales de Cu en utilisant le potentiel semi-empirique déterminé au chapitre 3 (Eq.12). Nous déterminons ainsi l'influence de la relaxation et de la portée du potentiel.

a) Potentiel de paire

Nous limitons la portée du potentiel à une distance où les interactions entre marches sont nulles dans le domaine des surfaces vicinales considérées. La fonction $\Delta f(tan(\theta))$ est triangulaire dans les deux domaines. Pour le domaine (100)-(111) les interactions entre marches sont nulles si la portée du potentiel ne s'étend pas au delà des cinquièmes voisins. La fonction $\Delta f(tan(\theta))$ est alors déterminée par les potentiels d'interactions entre troisièmes et cinquièmes voisins V_3 et V_5. En effet $\Delta f(tan(\theta_c))$ est proportionnelle à $-(V_3+V_5)$ et, par conséquent, la surface vicinale est stable par rapport au facettage en facettes (100) et (111) dans le cas où $V_3+V_5<0$. Elle est instable dans le cas contraire. Remarquons que si le potentiel d'interaction n'atteint pas les troisièmes voisins, $\Delta f=0$ et donc les énergies des surfaces vicinales et facettées sont dégénérées.

Dans le deuxième domaine ($\overline{1}11$)-(111), les interactions entre marches sont nulles lorsque la portée du potentiel s'arrête aux quatrièmes voisins. Dans ce cas la stabilité des surfaces vicinales dépend du signe de V_2+2V_3. Elles sont stables par rapport au facettage en facettes ($\overline{1}11$) et (111) dans le cas où $V_2+2V_3>0$ et instables dans le cas contraire. La symétrie de ce domaine nous permet d'étudier le facettage des surfaces vicinales en facettes (011) et (111). Ainsi pour l'intervalle des surfaces vicinales entre les deux faces (011) et (111), les interactions entre marches sont nulles pour une portée du potentiel s'arrêtant aux cinquièmes voisins (En fait, elles deviennent non nulles pour une portée beaucoup plus grande) [28]. La stabilité de ces surfaces vicinales est pilotée par le signe de V_5. Elles sont stables dans le cas où $V_5>0$ et instables dans le cas contraire. Pour des potentiels à plus courte portée $\Delta f=0$.

b) Potentiels semi-empiriques

Il est bien connu que les potentiels de paire ne sont pas adaptés pour décrire l'énergie totale dans les systèmes métalliques. c'est pourquoi depuis une vingtaine d'années un effort a été fait pour introduire une contribution à N-corps dans les potentiels décrivant les métaux [16,17,18,19]. La quasi-totalité des potentiels existant dans la littérature, ne dépendent que des distances interatomiques R_{ij}, et s'écrivent comme un somme de contributions E_i de chaque atome i ($E_i<0$) :

$$E=\sum_i E_i=\sum_i[\sum_{j\neq i}W(R_{ij})+F(\sum_{j\neq i}g(R_{ij}))] \tag{4.2}$$

Le premier terme est un potentiel de paire, le deuxième terme (où g est un fonction positive) a un caractère à N-corps, la fonction F n'étant pas linéaire. On oblige les fonctions W et g à s'annuler au delà d'une distance R_c grâce à une fonction de cou-

pure. Si on pose $\rho_i = \sum_{j \neq i} g(R_{ij})$, on retrouve les potentiels de paire si $F(\rho_i) = 0$, les potentiels de type second moment [20-23] si $F(\rho_i) = \sqrt{\rho_i}$ et celui utilisé au chapitre précédent si $F(\rho_i) = \rho_i^{\frac{2}{3}}$ [12,24]. Les potentiels de type EAM (embedded atom model) [18] et EMT (effective medium theory) [16,17] appartiennent à la même classe.

Dans un premier temps, nous négligeons les relaxations atomiques. Il est alors facile de voir que l'énergie d'un site E_i ne dépend que de ses coordinances successives, jusqu'à la dernière sphère de coordination de rayon inférieur à R_c.

Considérons le domaine (100)-(111). Il est facile de montrer qu'il n'y a pas d'interaction entre marches si le potentiel ne s'étend pas au delà des seconds voisins. Δf a donc une forme triangulaire et son signe est donné par l'expression

$$\Delta E = [F(7+3g_2) - F(9+3g_2)] - [F(8+5g_2) - F(10+5g_2)] \tag{4.3}$$

puisque l'on a vu que dans ce cas la partie de paire ne contribuait pas à Δf (on a posé $g(R_1) = 1$, et $g_2 = g(R_2)$, R_i désignant la distance entre $n^{\text{ièmes}}$ voisins). De même dans le domaine $(\overline{1}11)$-(111), il n'y a pas d'interaction entre marches quand la portée du potentiel ne comprend que les premiers voisins. Dans ces conditions Δf a toujours une forme triangulaire et son signe est donné par :

$$\Delta E = [F(7) - F(9)] - [F(9) - F(11)] \tag{4.4}$$

Pour tous les potentiels existants $\frac{d^2F}{d\rho^2}$ est positive et donc $F(\rho-2) - F(\rho)$ décroît quand ρ augmente. En effet, l'énergie d'un atome n'est pas proportionnelle à sa coordinance mais croît (en valeur absolue) de moins en moins vite lorsque celle-ci augmente [15,29]. Par conséquent, pour les deux domaines de vicinales étudiés, $\Delta E > 0$. Donc quelque soit le potentiel semi-empirique utilisé, et pour un réseau rigide à 0K, les surfaces vicinales appartenant aux domaines (100)-(111) et $(\overline{1}11)$-(111) sont instables respectivement par rapport à un facettage en facettes (100) et (111) si $R_c < R_3$, et $(\overline{1}11)$ et (111) si $R_c < R_2$. De la même façon on peut montrer que, sur un réseau rigide et pour les potentiels semi-empiriques avec $R_c < R_3$, les surfaces vicinales comprises entre (011) et (111) sont instables par rapport à un facettage en facettes (011) et (111).

Pour déterminer l'effet de la portée du potentiel et l'effet de la relaxation sur la stabilité des surfaces vicinales de Cuivre, nous avons effectué un calcul numérique sur les surfaces des deux domaines en utilisant le potentiel semi-empirique (4.2) pour différentes portées en supposant d'abord le réseau rigide. Comme prévu ci dessus les

surfaces vicinales du premier domaine (100)-(111) sont instables par rapport au facettage en facettes (100) et (111) si on limite la portée du potentiel aux seconds voisins. Par contre elles deviennent stables si on l'augmente pour prendre en compte les quatrième voisins (voir Figure 5). De même les surfaces vicinales du deuxième domaine ($\bar{1}11$)-(111) sont instables par rapport au facettage en facettes ($\bar{1}11$) et (111) pour une portée de potentiel limitée aux premiers voisins, alors que l'addition des seconds voisins inverse la stabilité. En effet toutes les surfaces vicinales deviennent stables par rapport aux facettage en facettes ($\bar{1}11$) et (111) mais instables par rapport au facettage en facettes (011) et (111) (voir Figure 6).

Par contre, la relaxation atomique calculée en utilisant ce même potentiel n'a pas de grands effets sur la stabilité des surfaces vicinales et joue en faveur de la stabilisation. Nos résultats permettent de comprendre ceux de Frenken et Stoltze [33]. Ces auteurs ont calculé la fonction $\Delta f(tan(\theta))$ pour le domaine (100)-(111) de l'Ag (et d'autres métaux) avec un potentiel semi-empirique EMT de portée limitée aux troisièmes voisins, mais où la contribution de ces derniers est quasiment négligeable, c'est pourquoi leurs résultats sont très semblables aux nôtres lorsqu'on limite la portée du potentiel aux seconds voisins.

4.3.3 Calculs de structure électronique

Les potentiels semi-empiriques ne dépendent que des distances interatomiques, et ne tiennent donc pas compte des effets dûs aux angles entre les liaisons. De plus les interactions entre marches d'origine électronique que nous avons mises en évidence au chapitre 2 sont complètement négligées. Ces effets ne peuvent être obtenus qu'à partir d'un calcul de structure électronique. Nous avons donc utilisé les énergies de surface calculées au chapitre 2 pour étudier la stabilité de diverses surfaces vicinales de Rhodium, Palladium et Cuivre. Nous avons calculé la fonction $\Delta f(tan(\theta))$ pour les surfaces vicinales des deux domaines (voir Figs. 7-8).

Pour le domaine (100)-(111), toutes les surfaces vicinales de Cu et de Rh sont stables par rapport au facettage en facettes (100) et (111) par contre celles de Pd sont instables. Cependant pour le Rhodium, la courbe $\Delta f(tan(\theta))$ présente deux minima locaux pour les faces (533) et (511) et un maximum local pour la surface (311). Par conséquent, les surfaces vicinales de Rh entre les faces (511) et (533) sont instables et elles ont tendance à se transformer en facettes d'orientation (511) et (533). Ce phénomène est relié aux interactions électroniques entre marches qui sont répulsives pour les surfaces vicinales (311) et (211) mais attractives pour les surfaces vicinales (511)

et (533).

Dans le cas du deuxième domaine, les surfaces vicinales p(111)×($\bar{1}$11) sont stables, pour les trois éléments étudiés, par rapport au facettage en facettes ($\bar{1}$11) et (111). Par contre les surfaces vicinales p(011)×(111) sont instables pour $p \geq 4$ par rapport au facettage en facettes (011) et (177).

4.3.4 Effets de l'énergie libre de vibration

Examinons maintenant l'effet des vibrations. Frenken et Stoltze [33] ont utilisé un modèle simple d'Einstein [33,35,36] pour le domaine (100)-(111) et ont négligé l'énergie interne qui domine aux faibles températures. De plus ils n'ont pris en compte dans l'expression de la contribution des vibrations à l'énergie libre Δf_{vib} que la perturbation des atomes de l'arête saillante de la marche par rapport à la surface (111) et ils ont ignoré celle des atomes de l'arête rentrante par rapport à la surface (100) qui doit également intervenir, comme le montre l'équation (23). Ces deux termes ont un signe opposé et sont de même ordre de grandeur. En conséquence non seulement l'ordre de grandeur de Δf_{vib} dans les calculs de Frenken et Stoltze [33] est trop élevé mais aussi son signe est douteux. Pour calculer correctement Δf_{vib} il est nécessaire d'effectuer un calcul du spectre de phonons aussi bon que possible. Nous avons utilisé donc le potentiel semi-empirique (Eq.12) avec une portée limitée aux seconds voisins qui reproduit correctement les données expérimentales du spectre vibrationnel de volume et celles des surfaces plates et vicinales (chapitre 3) du Cu [12]. Le calcul montre que Δf_{vib} est de l'ordre de quelques dizièmes de meV/A^2. Elle est positive pour le domaine (100)-(111) et tend donc à déstabiliser les surfaces vicinales. Par contre elle est oscillante pour le deuxième domaine ($\bar{1}$11)-(111) puisqu'elle contient des parties positives et d'autres négatives. En conclusion, la température contribue faiblement à la stabilité des surfaces vicinales.

4.4 Conclusion

Dans ce travail, nous avons appliqué diverses approches pour déterminer la stabilité des surfaces vicinales. Nous avons montré que les interactions entre marches apparaissent avec un potentiel semi-empirique pour une plus courte portée de celui-ci qu'avec un potentiel de paire [10,14]. La stabilité peut s'inverser en fonction de la portée du potentiel. La relaxation atomique joue en faveur de la stabilisation des surfaces mais elle ne change pas qualitativement les résultats. Les calculs de struc-

ture électronique montrent la possibilité de facettage des surfaces vicinales en d'autres surfaces vicinales. Ce phénomène est une conséquence des interactions électroniques oscillantes entre les marches. Finalement la température a un effet mineur sur la stabilité des surfaces vicinales.

4.5 Articles :

- **Stability of vicinal metal surfaces : from semi-empirical potentials to electronic structure calculations.**

- **Stability of Metal Vicinal Surfaces Revisited.**

Nous reproduisons tel quels, les articles qui ont été publié dans les revues "Physical Review B" et "Physical Review L".

Stability of vicinal metal surfaces: From semi-empirical potentials to electronic structure calculations

F. Raouafi,[1] C. Barreteau,[1] D. Spanjaard,[2] and M. C. Desjonquères[1]
[1]*DSM/DRECAM/SPCSI, CEA Saclay F-91 191 Gif sur Yvette, France*
[2]*Laboratoire de Physique des Solides, Université Paris Sud, F-91 405 Orsay, France*
(Received 27 March 2002; published 19 July 2002)

The stability of metal vicinal surfaces with respect to faceting is investigated using pair potentials, semi-empirical potentials, and tight-binding electronic structure calculations for several domains of orientations. It is proven that pair potentials are not precise enough to determine the stability of these surfaces. The answer obtained with semi-empirical potentials is shown to be quite sensitive to the cutoff distance chosen for the interactions and may be too schematic. The results derived from electronic structure calculations open up the possibility of a larger diversity of behaviors due to the existence of electronic step-step interactions. Finally it is shown that the effects of temperature are quite small, at least up to room temperature.

DOI: 10.1103/PhysRevB.66.045410 PACS number(s): 68.35.Md, 65.40.Gr, 68.35.Ja, 68.35.Rh

I. INTRODUCTION

A vicinal surface is a surface of high Miller indices and exhibits a periodic succession of terraces and steps of monoatomic height. The study of these surfaces is presently the subject of intensive investigations since they may provide an appropriate substrate for growing nanostructures.[1,2] However, these surfaces are not always stable. Indeed, it might be energetically favorable for the system to increase its total area in order to expose to vacuum facets with low Miller indices with smaller surface energies per unit area. These faceted surfaces may also be interesting to elaborate nanostructures since atoms deposited on these surfaces will preferentially occupy sites in the inner edges in order to maximize their coordination. This may lead to a periodic lattice of nanowires with magnetic and transport properties of high technological interest.

Up to now, in spite of the large number of experiments carried out on these surfaces,[3–7] very few theoretical works based on an atomistic description have been devoted to this problem. The faceting condition implies the calculation of the surface energy for any surface orientation. There exist several ways of computing these energies. The most simple of them use potentials ranging from the crudest empirical pair potentials to semi-empirical ones[8] including an *N*-body contribution. In the latter case the analytical expression of the semi-empirical potentials attempts to mimic the results of more accurate methods based on the calculation of the electronic structure such as the tight-binding approximation or first-principle methods based on the density-functional theory. The latter two methods, in which the electronic structure is explicitly calculated, can also be used. However, in view of the large size of the unit cells of vicinal surfaces with wide terraces, systematic calculations can be carried out only within the tight-binding method.[9,10]

The aim of this paper is to discuss the implications of these different approaches on the stability of vicinal surfaces relative to faceting. Preliminary results of this work have already been presented in Ref. 11 concerning the faceting of the vicinal surfaces found between the (100) and (111) planes into (100)/(111) facets. In the present study we examine the problem in more detail and consider different domains of orientations.

The paper is organized as follows. In Sec. II the faceting condition is established and the geometry of the vicinal surfaces involved in these domains is explained. In Sec. III the stability of these vicinal surfaces is analyzed using different (semi)-empirical potentials. Analytical results are first derived for a rigid lattice and an application to vicinal surfaces of copper, including surface relaxation, is presented using a semi-empirical potential of the tight-binding type[12] with a particular emphasis on the importance of the cutoff radius chosen for atomic interactions. The results of electronic structure calculations based on the tight-binding approximation using a s,p,d orbital basis set on a rigid lattice are then discussed in Sec. IV for rhodium, palladium, and copper. The effects of temperature are studied in Sec. V for copper. Finally conclusions are drawn in Sec. VI.

II. FACETING CONDITION OF AN INFINITE SURFACE

Let us consider two low index surfaces Σ_1 and Σ_2 with normals $\mathbf{n}_1$ and $\mathbf{n}_2$, respectively, which intersect along a given row of atoms and the set of vicinal surfaces with equidistant step edges which is spanned when Σ_1 is rotated around the common atomic row towards Σ_2. Let us take Σ_1 as the origin of angles and denote θ_2 the angle $(\mathbf{n}_1, \mathbf{n}_2)$. During this rotation the surfaces vicinal to Σ_1 are first found and the number of atomic rows p_1 (including the inner edge) on one terrace decreases from ∞ to 2 (angle θ_c). The surface corresponding to θ_c can also be regarded as a vicinal of Σ_2 with $p_2=2$. Then for $\theta_c \leqslant \theta < \theta_2$ the surfaces vicinal to Σ_2 are scanned with increasing terrace widths ($p_2 \geqslant 2$). An area S of any of these high index surfaces will transform into facets of normal $\mathbf{n}_1$ (area S_1) and normal $\mathbf{n}_2$ (area S_2) while keeping its average orientation when (Fig. 1)

$$\gamma S > \gamma_1 S_1 + \gamma_2 S_2 \tag{1}$$

(γ, γ_1 and γ_2 being the surface energies per unit area of the high index, Σ_1 and Σ_2 surfaces, respectively) with the constraints

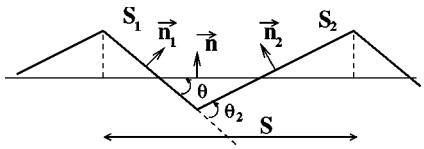

FIG. 1. Faceting.

$$S = S_1 \cos\theta + S_2 \cos(\theta_2 - \theta), \tag{2}$$

$$S_1 \sin\theta = S_2 \sin(\theta_2 - \theta). \tag{3}$$

It is easily shown that the faceting condition can be written

$$f(\eta) > (1-\eta/\eta_2) f(0) + (\eta/\eta_2) f(\eta_2) \tag{4}$$

with $\eta = \tan\theta$ and $f(\eta) = \gamma(\theta)/\cos\theta$. This condition is equivalent to the Herring[13] construction (see Appendix A).

This condition has a simple geometrical interpretation: the point $(\eta, f(\eta))$ must be above the straight line D joining the points $(0, f(0))$ and $(\eta_2, f(\eta_2))$ or, equivalently, the sign of the deviation $\Delta f(\eta)$ from this straight line determines the stability $[\Delta f(\eta) < 0]$ or the instability $[\Delta f(\eta) > 0]$ of the vicinal surface. It can be easily shown (see Appendix B) that

$$\Delta f(\mathbf{n}) = [E_S(\mathbf{n}) - (p_1 - 1) E_S(\mathbf{n}_1) - (p_2 - 1) E_S(\mathbf{n}_2)]/A_0(\mathbf{n}), \tag{5}$$

where $A_0(\mathbf{n})$ is the projected area of the surface unit cell A of the vicinal surface of orientation $\mathbf{n}$ on Σ_1. This formula applies as well in the domain $0 \leqslant \theta \leqslant \theta_c$ with $p_2 = 2$, as when $\theta_c \leqslant \theta \leqslant \theta_2$ with $p_1 = 2$. $E_S(\mathbf{n})$ is the surface energy (per atom) of the surface normal to $\mathbf{n}$. It is interesting to note that the condition of instability of the surface corresponding to η_c (normal $\mathbf{n_c}$) is simply

$$E_S(\mathbf{n}_c) > E_S(\mathbf{n}_1) + E_S(\mathbf{n}_2); \tag{6}$$

we will see below that in many cases the sign of $\Delta f(\eta_c)$ determines the stability for the whole range $[0, \eta_2]$. It is clear that the sign of Δf is independent of the origin of angles, i.e., if Σ_1 is referred by the angle θ_1, since it is given by the sign of the expression between the square brackets in Eq. (5) which will be denoted as $\Delta E(p_1, p_2)$ in the following.

Let us denote A_1 (A_2) the area of the unit cell of Σ_1 (Σ_2). It is straightforward to show that

$$\begin{cases} \Delta f(\eta) = \dfrac{\Delta E(p_1,2)}{A_2 \sin\theta_2}\,\eta, & 0 \leqslant \eta \leqslant \eta_c, \\ \Delta f(\eta) = \dfrac{\Delta E(2,p_2)}{A_1}(1-\eta/\eta_2), & \eta_c \leqslant \eta \leqslant \eta_2. \end{cases} \tag{7}$$

The expression for ΔE can be transformed using the formula given by Vitos *et al.*[14] for the step energy, i.e.,

$$E_{step}(\mathbf{n_i}, p_i) = E_S(\mathbf{n_i}, p_i) - (p_i - 1 + f_i) E_S(\mathbf{n_i}), \tag{8}$$

where $E_{step}(\mathbf{n_i}, p_i)$ is the step energy (per step atom) in the vicinal surface the terraces of which are normal to $\mathbf{n_i}$ and have p_i atomic rows. $E_S(\mathbf{n_i}, p_i)$ is the surface energy per atom of this vicinal surface which was equivalently denoted as $E_S(\mathbf{n})$ in Eq. (5). Finally f_i is a geometrical factor which is equal to the ratio of the area, projected on the terrace, of the unit cell of the ledge to the area of the unit cell of the terrace $[f_1 = A_2\cos(\theta_2)/A_1,\ f_2 = A_1\cos(\theta_2)/A_2]$. Substituting for $E_S(\mathbf{n_i}, p_i)$ from Eq. (8) into $\Delta E(p_1, 2)$, for instance, yields

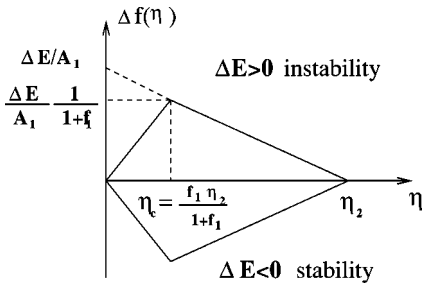

FIG. 2. Behavior of $\Delta f(\eta)$ when there are no interactions between steps. η_c corresponds to $p_1 = p_2 = 2$.

$$\Delta E(p_1, 2) = E_{step}(\mathbf{n}_1, p_1) - E_S(\mathbf{n}_2) + f_1 E_S(\mathbf{n}_1); \tag{9}$$

a similar equation can be written for $\Delta E(2, p_2)$ by interchanging the indices 1 and 2 in the right-hand side of Eq. (9). Note that, due to the continuity of $\Delta f(\eta)$ at η_c ($p_1 = p_2 = 2$), the following relation holds:

$$E_{step}(\mathbf{n}_1, 2) - E_{step}(\mathbf{n}_2, 2) = (1+f_2) E_S(\mathbf{n}_2) - (1+f_1) E_S(\mathbf{n}_1). \tag{10}$$

If we note that when, in a first approach, we assume that the contribution of the ledge to the surface energy of the vicinal surface can be approximated by the corresponding macroscopic surface energy, then ΔE vanishes. Thus ΔE is a measure of the deviation to this approximation. Rigorously, ΔE does not vanish and is a function of η since $E_{step}(\mathbf{n_i}, p_i)$ depends on p_i due to step-step interactions.

When these interactions are neglected $\Delta E(p_1, 2)$ and $\Delta E(2, p_2)$ are equal to the same constant ΔE since they must be equal for $\eta = \eta_c$. When ΔE is not vanishing $\Delta f(\eta)$ has a triangular shape [see Eq. (7)] and both quantities have the same sign (see Fig. 2). In the particular case $\Delta E = 0$, any vicinal surface between Σ_1 and Σ_2 has the same energy as the corresponding faceted surface.

Actually, this simple picture is modified by the interactions between steps even at 0 K. When neglecting relaxation, steps start to interact when the range of the potential is large enough. Then the two straight lines of Fig. 2 transform into as many segments (with discontinuities of slope) as there are different step energies when p increases. In addition, in calculations based on the determination of the electronic structure, long-range oscillatory interactions are present.[9,10] Finally, atomic relaxation introduces step-step repulsive interactions which tends to lower $\Delta f(\eta)$ and to give it a positive curvature in both domains ($0 \leqslant \eta \leqslant \eta_c$, $\eta_c \leqslant \eta \leqslant \eta_2$). In the next sections the stability of vicinal surfaces is analyzed using different methods giving the total energy

ranging from pair potentials, semi-empirical potentials including an *N*-body contribution, and, finally, electronic structure calculations. Then we will study the effects of temperature.

Let us finally remark that the curvature of $f(\eta)$ has the same sign as $\gamma(\theta)+d^2\gamma/d\theta^2$ since

$$\frac{d^2f}{d\eta^2}=\frac{d^2[\gamma(\theta)/\cos\theta]}{(d\tan\theta)^2}=\cos^3\theta[\gamma(\theta)+d^2\gamma/d\theta^2] \quad (11)$$

with $0\leqslant\theta<\pi/2$. It is well known that when $\gamma(\theta)+d^2\gamma/d\theta^2\leqslant 0$, the surface orientation θ is unstable and will minimize its energy by developing facets. Therefore in the domain of η where $d^2f/d\eta^2$ is negative, the corresponding surfaces are unstable. Otherwise they are stable or metastable.[15]

III. STABILITY OF VICINAL SURFACES AT 0 K FROM SEMI-EMPIRICAL POTENTIALS

Empirical potentials belonging to a very large class can be written as a sum of contributions E_i of each atom i (the origin of energy being the energy of a free atom so that $E_i<0$) depending on its environment of neighbors j at the interatomic distance R_{ij}, i.e.,

$$E=\sum_i E_i=\sum_i\left[\sum_{j\neq i}V(R_{ij})+F\left(\sum_{j\neq i}g(R_{ij})\right)\right]. \quad (12)$$

E is the total energy of the system at 0 K neglecting the zero-point vibrational energy. In the following we set $\rho_i=\Sigma_{j\neq i}g(R_{ij})$. The first term of Eq. (12) is thus pairwise while the second one (in which g is a positive function) has an *N*-body character. The functions V and g are usually cutoff smoothly around a given radius R_c. This class of potentials includes pair potentials [$F(\rho_i)=0$], potentials based on effective medium theory (EMT),[16,17] embedded atom model (EAM),[18] and glue model,[19] and potentials derived from the tight-binding approximation in the second moment approach [$F(\rho_i)\propto\sqrt{\rho_i}$],[20–23] or fitted to calculations including higher-order moments [$F(\rho_i)\propto\rho_i^{2/3}$].[12,24] Note that in potentials of the tight-binding type, the *N*-body part is strictly attractive while the pairwise part is strictly repulsive.

We first fix the interatomic distances to their bulk equilibrium values, i.e., atomic relaxation effects are ignored. With this assumption $\Sigma_{j\neq i}V(R_{ij})$ and $\Sigma_{j\neq i}g(R_{ij})$ are linear combinations of the number of neighbors Z_N^i of atom i in the Nth coordination sphere of radius R_N ($R_N<R_c$) and $E_i=E(Z_1^i\cdots Z_N^i\cdots)$. It is usual to take R_1 as the reference distance and set $g(R_1)=1$.

To proceed further we must specify the set of vicinal surfaces we want to study. We limit ourselves to fcc crystals and consider here two domains (Fig. 3). The first domain is defined by $\mathbf{n}_1=(1,0,0)$ and $\mathbf{n}_2=(1,1,1)$. In this domain, when $0<\eta\leqslant\eta_c(\eta_c=\sqrt{2}/3)$ the crystallographic planes $(2p-1,1,1)$ are spanned and correspond to the $p(100)\times(111)$ surfaces in Somorjai notations[25] and when $\eta_c\leqslant\eta<\eta_2$ ($\eta_2=\sqrt{2}$) the crystallographic planes are $(p+1,p-1,p-1)$ and

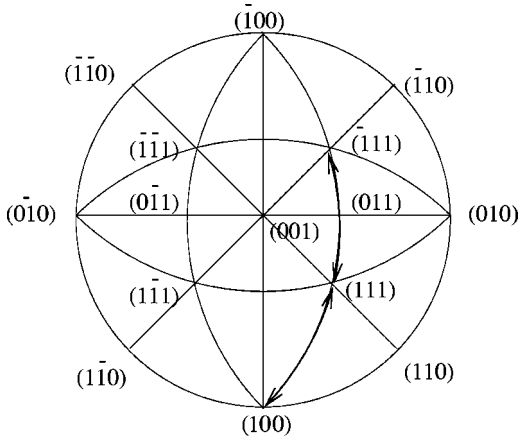

FIG. 3. Stereographic projection of the two ranges of orientations studied (heavy lines).

the corresponding vicinal surfaces are $p(111)\times(100)$. Note that for $\eta=\eta_c$ the Miller indices of the surface are (311).

The second domain that we will study is the domain of vicinals between $(1\bar{1}1)$ and (111), i.e., $p(1\bar{1}1)\times(111)$ [with Miller indices $(2-p,p,p)$] and $p(111)\times(1\bar{1}1)$ [with Miller indices $(p-2,p,p)$]. The surface corresponding to η_c ($p=2$) is (011). This domain being symmetrical with respect to the (011) surface we take the origin of angles at this surface, i.e., $\eta_c=0$, thus $\eta\in[-\eta_2,\eta_2]$ with $\eta_2=\sqrt{2}/2$. This range is interesting since, in particular, it will give information on the possibility of faceting of the (011) surface into $(1\bar{1}1)$ and (111) facets. Indeed the missing row reconstruction which is observed at the (011) surface of some fcc transition metals[26] can be viewed as a ''microscopic'' faceting of this type. Let us consider in more detail the interval $[0,\eta_2]$: the surfaces that are first spanned are the $p(011)\times(111)$ vicinal surfaces [with Miller indices $(1,2p-1,2p-1)$] until $p=2$, i.e., the (133) surface [$\eta_c=\sqrt{2}/6$]. Then the surfaces between (133) and (111) are $p(111)\times(011)$ or $(p-1,p+1,p+1)$ which have the same geometry as the $(p+1)(111)\times(1\bar{1}1)$ surface since the choice of the ledge is somewhat arbitrary (note that the number of rows being increased by 1 in the last case, the corresponding geometrical factor f should be decreased by 1). Thus the study of $\Delta f(\eta)$ between 0 and η_2 will give the stability of these vicinal surfaces with respect to faceting into (011) and (111) facets.

The geometry of the studied surfaces being now defined, it is easy to determine the coordination numbers $Z_1^i,Z_2^i,\cdots Z_N^i\cdots$ for the successive atomic layers i of any surface. The values of f and these coordination numbers are given in Tables I –Vfor each surface up to $N=5$ since interactions are very rapidly screened in metals. The last atomic layer of each surface refers to the first layer which has the same first five coordination numbers as a bulk atom. In the next two subsections we first discuss the case of pair potentials and then the influence of the contribution of an *N*-body term. In all cases, assuming a rigid lattice, we will determine the largest range R_{max} of the potential for which the step energies remain a constant for $p\geqslant 2$ for both types of steps involved in the considered domain. Then we limit ourselves to ranges

TABLE I. Coordination numbers Z_N in the Nth coordination sphere of atoms belonging to successive atomic layers for the (111), (100), and (011) fcc surfaces up to the first layer in which atoms have the same first five coordination numbers as a bulk atom. $n^N(\infty)$ is the total number of Nth neighbors (per surface atom) suppressed by the surface.

(111) surface					
Layer	Z_1	Z_2	Z_3	Z_4	Z_5
1	9	3	15	9	12
2	12	6	21	9	18
3	12	6	24	12	24
$n^N(\infty)$	3	3	12	6	18
(100) surface					
Layer	Z_1	Z_2	Z_3	Z_4	Z_5
1	8	5	12	8	16
2	12	5	20	8	20
3	12	6	24	12	20
4	12	6	24	12	24
$n^N(\infty)$	4	2	16	8	16
(011) surface					
Layer	Z_1	Z_2	Z_3	Z_4	Z_5
1	7	4	14	7	12
2	11	4	18	7	16
3	12	6	20	11	18
4	12	6	24	11	22
5	12	6	24	12	24
$n^N(\infty)$	6	4	20	12	28

$R_c \leqslant R_{max}$ in which case $\Delta f(\eta)$ has a triangular shape and examine its sign given by ΔE (Fig. 2). We will end by a numerical study of Cu vicinal surfaces using a potential of the tight-binding type, discussing the influence of relaxation and of the position of the cutoff R_c.

A. Pair potentials

These potentials are the simplest ones which have been used in the past. We will limit ourselves to the study of unrelaxed surfaces since it is well known that they most often lead to an outward relaxation instead of the inward one generally observed at metal surfaces. However, such pair interactions V_N between an atom and one of its neighbors in the Nth coordination shell have been used on a rigid lattice by Vitos *et al.*[14] in order to estimate step energies in transition and noble metals and study the stability of the fcc(011) surfaces.[27] From Eq. (8) it is seen that

$$E_{step}(p) = \sum_{R_N < R_c} n^N_{step}(p) V_N \tag{13}$$

with

$$n^N_{step}(p) = n^N_{vici}(p) - (p - 1 + f) n^N(\infty), \tag{14}$$

where $n^N_{vici}(p)$ and $n^N(\infty)$ are, respectively, the total number of neighbors in the Nth coordination shell suppressed by the vicinal surface with p atomic rows on the terraces and by the flat surface parallel to the terrace. In Eq. (13) the sign of V_N is defined in such a way that the energy of a bulk atom is written $E_{bulk} = -\Sigma_{R_N < R_c} Z^b_N V_N$ where Z^b_N is the number of Nth neighbors for a bulk atom and the surface energy is $E_S = \Sigma_{R_N < R_c} n^N_S V_N$ where n^N_S is the total number of Nth neighbors (per surface atom) suppressed by the surface.

There are no interactions between steps as long as $n^N_{step}(p)$ does not depend on $p (p \geqslant 2)$. We will see in the following that this condition is fulfilled only when R_c is

TABLE II. Same caption as Table I for the $p(100)\times(111)$ or $(2p-1,1,1)$ vicinal surfaces ($f = 1/2$). n^N_{vici} is the total number of Nth neighbors (per surface atom) suppressed by the surface. The values of n^N_{step} which determine the step energies in the pair potential model of Vitos *et al.* (Ref. 14) are also given.

$p=2$, (311) surface					
Layer	Z_1	Z_2	Z_3	Z_4	Z_5
1	7	3	14	7	14
2	10	5	16	7	16
3	12	5	19	10	18
4	12	6	23	10	20
5	12	6	24	12	22
6	12	6	24	12	24
n^N_{vici}	7	5	24	14	30
n^N_{step}	1	2	0	2	6
$p=3$, (511) surface					
Layer	Z_1	Z_2	Z_3	Z_4	Z_5
1	7	3	12	7	12
2	8	5	14	7	16
3	10	5	16	8	18
4	12	5	18	8	18
5	12	5	21	10	20
6	12	6	23	10	20
7	12	6	24	12	20
8	12	6	24	12	22
9	12	6	24	12	24
n^N_{vici}	11	7	40	22	46
n^N_{step}	1	2	0	2	6
$p=4$, (711) surface					
Layer	Z_1	Z_2	Z_3	Z_4	Z_5
1	7	3	12	7	12
2	8	5	12	7	14
3	8	5	14	8	18
4	10	5	16	8	18
5	12	5	18	8	18
6	12	5	20	8	20
7	12	5	21	10	20
8	12	6	23	10	20
9	12	6	24	12	20
10	12	6	24	12	20
11	12	6	24	12	22
12	12	6	24	12	24
n^N_{vici}	15	9	56	30	62
n^N_{step}	1	2	0	2	6

TABLE III. Same caption as Table II for the $p(111)\times(100)$ or $(p+1,p-1,p-1)$ vicinal surfaces ($f=2/3$). For $p=2$, see the (311) surface in Table II but n^N_{step} should be replaced by (2, 0, 4, 4, 0).

			$p=3$, (211) surface		
Layer	Z_1	Z_2	Z_3	Z_4	Z_5
1	7	3	12	7	12
2	9	3	16	7	14
3	10	5	17	9	16
4	12	5	19	9	16
5	12	6	21	10	18
6	12	6	23	10	22
7	12	6	24	12	22
8	12	6	24	12	24
n^N_{vici}	10	8	36	20	48
n^N_{step}	2	0	4	4	0
			$p=4$, (533) surface		
Layer	Z_1	Z_2	Z_3	Z_4	Z_5
1	7	3	12	7	12
2	9	3	14	7	12
3	9	3	17	9	14
4	10	5	17	9	16
5	12	5	19	9	16
6	12	6	21	9	16
7	12	6	21	10	20
8	12	6	23	10	22
9	12	6	24	12	22
10	12	6	24	12	24
n^N_{vici}	13	11	48	26	66
n^N_{step}	2	0	4	4	0

small enough. Then, $\Delta f(\eta)$ is linear in both domains $[0,\eta_c]$ and $[\eta_c,\eta_2]$. However, depending on the range of the potential, either these two straight lines join at η_c with a discontinuity of slope, or $\Delta f(\eta)=0$ when $\eta\in[0,\eta_2]$. In the former case, the sign of $\Delta f(\eta_c)$ is sufficient to know whether the vicinal surfaces are stable or not.

1. $p(100)\times(111)$-$p(111)\times(100)$ domain

From Tables II and III it is seen that $E^{p(100)\times(111)}_{step}$ and $E^{p(111)\times(100)}_{step}$ are independent of p when the pair interactions do not reach the sixth neighbors (actually they begin to depend on p when the pair interactions reach the seventh and sixth neighbors, respectively). Let us thus assume that the pair interactions are cut beyond the fifth neighbors and determine the sign of ΔE from Eq. (5) and Tables I and II. We find

$$\Delta E=E_S(311)-E_S(100)-E_S(111)=-4(V_3+V_5). \tag{15}$$

As a conclusion, if the range of the pair potential is limited to the first and second neighbors $\Delta E=0$, so that the energy of any vicinal surface is equal to the energy of the faceted (100)/(111) surface. If the range is extended to fifth

TABLE IV. Same caption as Table II for the $p(111)\times(\bar{1}11)$ or $(p-2,p,p)$ vicinal surfaces ($f=1/3$). The same table can be used for $(p-1)(111)\times(011)$ ($f=4/3$) (see the main text).

			$p=2$, (011) surface		
Layer	Z_1	Z_2	Z_3	Z_4	Z_5
1	7	4	14	7	12
2	11	4	18	7	16
3	12	6	20	11	18
4	12	6	24	11	22
5	12	6	24	12	24
n^N_{vici}	6	4	20	12	28
n^N_{step}	2	0	4	4	4
			$p=3$, (133) surface		
Layer	Z_1	Z_2	Z_3	Z_4	Z_5
1	7	3	12	7	14
2	9	4	16	7	14
3	11	4	19	9	14
4	12	6	19	9	18
5	12	6	22	11	20
6	12	6	24	11	22
7	12	6	24	12	24
n^N_{vici}	9	7	32	18	42
n^N_{step}	2	0	4	4	0
			$p=4$, (122) surface		
Layer	Z_1	Z_2	Z_3	Z_4	Z_5
1	7	3	12	7	12
2	9	3	14	7	14
3	9	4	17	9	14
4	11	4	19	9	14
5	12	6	19	9	16
6	12	6	21	9	20
7	12	6	22	11	20
8	12	6	24	11	22
9	12	6	24	12	24
n^N_{vici}	12	10	44	24	60
n^N_{step}	2	0	4	4	0
			$p=5$, (355) surface		
Layer	Z_1	Z_2	Z_3	Z_4	Z_5
1	7	3	12	7	12
2	9	3	14	7	12
3	9	3	15	9	14
4	9	4	17	9	14
5	11	4	19	9	14
6	12	6	19	9	16
7	12	6	21	9	18
8	12	6	21	9	20
9	12	6	22	11	20
10	12	6	24	11	22
11	12	6	24	12	24
n^N_{vici}	15	13	56	30	78
n^N_{step}	2	0	4	4	0

TABLE V. Same caption as Table II for the $p(011)\times(111)$ or $(1,2p-1,2p-1)$ vicinal surfaces ($f=1/2$). For $p=2$, see Table IV for the (133) surface, but n^N_{step} should be replaced by (0,1,2,0,0).

$p=3$, (155) surface					
Layer	Z_1	Z_2	Z_3	Z_4	Z_5
1	7	3	12	7	12
2	7	4	14	7	14
3	9	4	16	7	14
4	11	4	18	7	14
5	11	4	19	9	16
6	12	6	19	9	18
7	12	6	20	11	18
8	12	6	22	11	20
9	12	6	24	11	22
10	12	6	24	11	22
11	12	6	24	12	24
n^N_{vici}	15	11	52	30	70
n^N_{step}	0	1	2	0	0
$p=4$, (177) surface					
Layer	Z_1	Z_2	Z_3	Z_4	Z_5
1	7	3	12	7	12
2	7	4	14	7	12
3	7	4	14	7	14
4	9	4	16	7	14
5	11	4	18	7	14
6	11	4	18	7	16
7	11	4	19	9	16
8	12	6	19	9	18
9	12	6	20	11	18
10	12	6	20	11	18
11	12	6	22	11	20
12	12	6	24	11	22
13	12	6	24	11	22
14	12	6	24	11	22
15	12	6	24	12	24
n^N_{vici}	21	15	72	42	98
n^N_{step}	0	1	2	0	0

neighbors the surface is stable if $V_3+V_5<0$ and unstable otherwise. Then $\Delta f(\eta)$ behaves as shown in Fig. 2. If we look at the numerical values of V_3 given by Vitos *et al.*[14] when $R_3<R_c<R_4$, the only element for which V_3 is negative is Au, but it is well known that Au(100) and Au(111) reconstruct and thus the present analysis, which assumes unreconstructed flat surfaces, cannot be applied.

2. $p(\bar{1}\bar{1}\bar{1})\times(111)$-$p(111)\times(\bar{1}\bar{1}\bar{1})$ *domain*

In this domain, as already stated, we choose θ_c as the origin of angles ($\eta_c=0$) and $\eta\in[-\eta_2,\eta_2]$ with $\eta_2=\sqrt{2}/2$. In these conditions D is the horizontal line at ordinate $f(\eta_2)=\gamma(111)/\cos\theta_2$. The corresponding steps do not interact as long as $R_c<R_5$ (see Table IV). Then $\Delta f(\eta)$ has a triangular shape and the position of its apex relative to the η axis determines the stability of the vicinal surfaces. From Eq. (6) they are unstable when

$$\Delta E=E_S(011)-2E_S(111)>0, \tag{16}$$

i.e., when $V_2+2V_3<0$ and stable otherwise. Note that in the former case, the step energy (V_2+2V_3) of the $p(011)\times(111)$ is negative and the (011) surface is less stable than the missing row reconstructed $(011)(2\times1)$ surface.[10,14] All these findings are consistent with an instability of the (011) surface when $V_2+2V_3<0$. The latter condition is not fulfilled for the fcc elements of the $3d$ and $4d$ transition-metal series when using the pair interactions given by Vitos *et al.*, in accordance with the stability of the (011) surface of these elements. For Pt and Au, V_2+2V_3 is negative and this would be consistent with the missing row reconstruction occurring for both elements. However, we must note that the condition (16) is not really applicable for Au(111) since this surface is reconstructed. The case of Ir(011) is still under debate since V_2+2V_3 is positive according to Ref. 14 and very close to 0 from Ref. 27.

3. $p(011)\times(111)$-$p(111)\times(011)$ *domain*

This domain is defined by $\eta\in[0,\sqrt{2}/2]$. The surface $p=2$ corresponding to $\eta_c=\sqrt{2}/6$ is the (133) crystallographic plane. From Tables IV and V we see that, when $R_c<R_6$ at least, the step energies $E^{p(011)\times(111)}_{step}$ and $E^{p(111)\times(011)}_{step}$ are independent of p (actually, steps begin to interact when $R_c>R_{12}$ for the first ones, and $R_c>R_8$ for the second ones![28]). From Eq. (6) these vicinal surfaces are unstable with respect to faceting into (011)-(111) facets when

$$E_S(133)>E_S(011)+E_S(111). \tag{17}$$

This inequality is fulfilled when $V_5<0$ if $R_c<R_6$. As a consequence when $R_c<R_5$, all vicinal surfaces in this domain are degenerate with the faceted ones. If $R_c<R_6$ and $V_5\neq0$, $\Delta f(\eta)$ has the triangular shapes shown in Fig. 2 with $\Delta E>0$ ($V_5<0$) and $\Delta E<0$ ($V_5>0$).

Let us now summarize our results. We have found that the faceted surface is nondegenerate with the vicinal one when the pair potential includes third neighbors for the (100)-(111) domain, second neighbors for the $(\bar{1}\bar{1}1)$-(111) domain, and fifth neighbors for the (011)-(111) domain. However, we have shown in a recent work[10] that pair potentials derived from *ab initio* calculations of surface energies are very dependent of the used data base, in particular even the sign of V_2 is uncertain. Thus the use of pair potentials to study the faceting of metal surfaces is questionable.

B. *N*-body semi-empirical potentials

Let us now examine the case of semi-empirical potentials including an *N*-body contribution. We will first neglect atomic relaxation and derive general trends for potentials of type (12). Then we will present examples of the use of such a semi-empirical potential in the case of Cu vicinal surfaces without and with relaxation.

1. Case of rigid lattices

Here the interatomic distances are fixed to their bulk equilibrium values and, as stated above, the energy of an atom i

is completely determined by its coordination numbers up to the cutoff radius, i.e., $E_i = E(Z_1^i, \cdots Z_N^i)$.

(a) $p(100)\times(111)$-$p(111)\times(100)$ domain. We limit ourselves to values of R_c such that $R_c < R_4$ since, as we will see below, $\Delta f(\eta)$ deviates from the triangular shape as soon as R_c reaches the third neighbors. Let us first examine when $E_{step}^{p(100)\times(111)}$ is independent of p. Using Tables I, II, and III and Eq. (8) we find

$$E_{step}^{2(100)\times(111)} = E(7,3,14) - 3E(8,5,12)/2 + E(10,5,16) + E(12,5,19) - 3E(12,5,20)/2 + E(12,6,23) - E(12,6,24) \quad (18)$$

and

$$E_{step}^{3(100)\times(111)} = E(7,3,12) - 5E(8,5,12)/2 + E(8,5,14) + E(10,5,16) + E(12,5,18) - 5E(12,5,20)/2 + E(12,5,21) + E(12,6,23) - E(12,6,24). \quad (19)$$

It is easily seen that, when $R_3 < R_c < R_4$ these two steps energies are different but become equal when $R_2 < R_c < R_3$ in which case

$$E_{step}^{2(100)\times(111)} = E_{step}^{3(100)\times(111)} = E(7,3) + E(10,5) - 3E(8,5)/2 - E(12,5)/2. \quad (20)$$

For the $p(111)\times(100)$ vicinal surfaces a similar calculation shows also that the two step energies are different when $R_3 < R_c < R_4$ but are equal when $R_2 < R_c < R_3$:

$$E_{step}^{2(111)\times(100)} = E_{step}^{3(111)\times(100)} = E(7,3) - 5E(9,3)/3 + E(10,5) + E(12,5) - 4E(12,6)/3. \quad (21)$$

Using Tables II and III the reader can verify that, when $R_2 < R_c < R_3$, the step energies of both $p(100)\times(111)$ and $p(111)\times(100)$ surfaces are not changed for $p > 3$.

Consequently for any semi-empirical potential of the form (12) including first and second nearest neighbors only, $\Delta f(\eta)$ has the triangular shape (Fig. 2) when relaxation is neglected and its sign is given by

$$\Delta E = E_S(311) - E_S(100) - E_S(111) \quad (22)$$

or

$$\Delta E = [E(7,3) + E(10,5)] - [E(8,5) + E(9,3)]. \quad (23)$$

This expression has an obvious physical meaning: ΔE arises from the difference of the sum of energies of, on the one hand, atoms belonging to the outer and inner step edges, and, on the other hand, of (100) and (111) surface atoms. From the previous subsection we know that the pair potential, when limited to second-nearest neighbors, does not contribute to ΔE which can be written as a function of the N-body part of the potential only. Noting that, since $g(R_1) = 1$, $\rho_i = \Sigma_{j\neq i} g(R_{ij}) = Z_1^i + Z_2^i g_2$ with $g_2 = g(R_2)$, ΔE is finally given by

$$\Delta E = [F(7 + 3g_2) - F(9 + 3g_2)] - [F(8 + 5g_2) - F(10 + 5g_2)]. \quad (24)$$

For all the existing potentials of the form (12) $F''(\rho) = d^2F/d\rho^2$ is positive. As a consequence $F(\rho - 2) - F(\rho)$ is a decreasing function of ρ, therefore ΔE [and thus $\Delta f(\eta)$] is always positive in the whole domain. This common property of this class of potentials has a clear physical origin: the energy E_i of an atom i should decrease more and more slowly when its coordination increases towards the bulk coordination.[15,29] This clearly implies that $F''(\rho)$ must be positive. We have then proved that for *any* empirical potential of the general form (12) on a rigid lattice at 0 K and a cutoff radius $R_c < R_3$, *any* vicinal surface from (100) to (111) is *unstable* with respect to faceting.

(b) $p(\bar{1}11)\times(111)$-$p(111)\times(\bar{1}11)$ domain. We will limit ourselves to the values of R_c such that $R_c < R_3$ since the step energies cease to be a constant when $R_c > R_1$. Indeed for $p = 2$ and 3 they are not equal:

$$E_{step}^{2(111)\times(\bar{1}11)} = E(7,4) - 4E(9,3)/3 + E(11,4) - 2E(12,6)/3 \quad (25)$$

and

$$E_{step}^{3(111)\times(\bar{1}11)} = E(7,4) - 7E(9,3)/3 + E(9,4) + E(11,4) - 2E(12,6)/3. \quad (26)$$

It is easily shown that $E_{step}^{p(111)\times(\bar{1}11)}$ remains constant for $p \geqslant 3$ when first- and second-nearest neighbors are included and for $p \geqslant 2$ when interactions are limited to first-nearest neighbors.

As a consequence $\Delta f(\eta)$ has a triangular shape when $R_c < R_2$ and the vicinal surfaces between $(\bar{1}11)$ and (111) are unstable when Eq. (16) is fulfilled, i.e.,

$$[F(7) - F(9)] - [F(9) - F(11)] > 0 \quad (27)$$

since the pair potential V does not contribute to this condition. This inequality is always obeyed since, as explained above, $F(\rho - 2) - F(\rho)$ is a decreasing function of ρ. In such a model, at least when atomic relaxation is neglected, the (011) surface is unstable relative to faceting into $(\bar{1}11)$ and (111) facets. Note that due to the very short range of the potential, the condition (27) gives also the instability relative to the missing row (1×2) reconstruction which has indeed $(\bar{1}11)$ and (111) microfacets.

When $R_c < R_3$, $\Delta f(\eta)$ is no more a simple triangle. However, it remains linear in the domain $(\bar{1}11)$-$(\bar{1}33)$, i.e., $\eta \in [-\sqrt{2}/2, -\sqrt{2}/6]$ and in the domain symmetrical with respect to $\eta = 0$. In these domains, the sign of $\Delta f(\sqrt{2}/6)$ [or $\Delta f(\eta)$] is given by

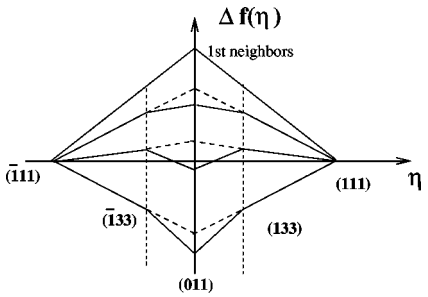

FIG. 4. Expected evolution of $\Delta f(\eta)$ (full lines) obtained with a semi-empirical potential including first- and second-nearest neighbors as a function of the energy contribution of the latter. $\Delta f(\eta)$ is lowered and may change sign depending on this contribution.

$$E_S(133)-3E_S(111)=E(7,3)+E(9,4)+E(11,4)-3E(9,3) \tag{28}$$

and it is expected to depend on the relative contributions of the first- and second-nearest neighbors to the energy. In addition the point $\Delta f(0)$ is not at the intersection of these two lines since the step energies are not the same for $p=2$ (011) and $p=3$ (133) [see Eqs. (25) and (26)]. It can be easily shown that $\Delta f(0)$ is below this intersection when

$$E_S(011)<E_S(133)-E_S(111) \tag{29}$$

or

$$[E(7,4)-E(9,4)]-[E(7,3)-E(9,3)]<0. \tag{30}$$

The pair part of the potential does not play any role in this condition which can be rewritten

$$[F(7+3g_2)-F(9+3g_2)] -[F(7+4g_2)-F(9+4g_2)]<0. \tag{31}$$

This inequality is always fulfilled since $F(\rho-2)-F(\rho)$ is a decreasing function of ρ.

As a conclusion, when $\Delta f(\eta)>0$ for $\eta\in[\pm\sqrt{2}/6, \pm\sqrt{2}/2]$ the (011) surface is stable relative to faceting into (111)/(111) facets if $\Delta f(0)$ is negative, i.e.,

$$E_S(011)-2E_S(111)=E(7,4)+E(11,4)-2E(9,3)<0. \tag{32}$$

This last condition may or may not not be fulfilled depending on the importance of second-nearest neighbors. When $\Delta f(\eta)<0$, $\Delta f(011)$ is below $\Delta f(133)$ (Fig. 4). Thus the semi-empirical potential (12) with $R_c<R_3$ cannot explain the faceting of the (011) surface into (133)/(133) facets observed for Ir,[30] at least when relaxation is neglected.

(c) $p(011)\times(111)$-$p(111)\times(011)$ domain. Limiting ourselves to $R_c<R_5$, we find that the step energies $E_{step}^{p(011)\times(111)}$ are independent of p in the whole range ($p\geqslant 2$) and equal to

$$\begin{aligned}E_{step}^{p(011)\times(111)}=&E(7,3,12,7)-3E(7,4,14,7)/2+E(9,4,16,7)\\&-3E(11,4,18,7)/2+E(11,4,19,9)\\&+E(12,6,19,9)-3E(12,6,20,11)/2\\&+E(12,6,22,11)-E(12,6,24,11)/2.\end{aligned} \tag{33}$$

Consequently, when $R_c<R_5$, $\Delta f(\eta)$ is linear between $\eta=0$ [(011) surface] and $\eta_c=\sqrt{2}/6$ [(133) surface].[31] It is easily seen from Tables IV and V that steps start to interact if the fifth neighbors are taken into account. We have seen above that $E_{step}^{(p+1)(111)\times(\bar{1}11)}$ (i.e., $E_{step}^{p(111)\times(011)}$) is a constant when $p\geqslant 2$ if $R_c<R_3$ but not when $R_c>R_3$. As a conclusion, in this domain, $\Delta f(\eta)$ has a triangular shape only when $R_c<R_3$ and, as shown above [Eqs. (29)–(32)], its sign is positive (see Fig. 3) which means that the corresponding vicinal surfaces are all unstable with respect to faceting into (011)/(111) facets.

Finally, if we compare the results obtained with a pair potential to those derived from usual potentials including an *N*-body part, we note that step interactions appear at a shorter cutoff distance in the latter case than in the former.

2. Application to vicinal surfaces of Cu

So far we have demonstrated general results on the stability of vicinal surfaces based on a rigid lattice description, both from pair potentials and *N*-body semi-empirical potentials. Most results were demonstrated under the assumption that the range of the potential is restricted to the first shells of neighbors, and it was often difficult to predict the exact behavior when the range of the potential is extended to further neighbors. Moreover, the effect of atomic relaxation was neglected. We will now consider a "real" case with a potential of the form given by Eq. (12) (see Ref. 10):

$$\begin{aligned}&E(R_1,\cdots R_i,\cdots)\\&\quad=A\sum_{i,j,j\neq i}(R_0/R_{ij})^p f_c(R_{ij})\\&\qquad-\xi\sum_i\left(\sum_{j\neq i}\exp[-2q(R_{ij}/R_0-1)]f_c(R_{ij})\right)^{\alpha},\end{aligned} \tag{34}$$

where R_{ij} is the distance between atoms i and j, R_0 is a reference distance that we take equal to the bulk nearest-neighbor spacing and $f_c(R)=1/\{1+\exp[(R-R_c)/\Delta]\}$ is a smooth cutoff function with a cutoff radius R_c and a characteristic length Δ that we set equal to 0.05 Å.

The parameters A, ξ, p, and q are fitted to the cohesive energy E_c and the three elastic constants (bulk and shear moduli B, C, and C'). The equilibrium equation gives a relation between the four parameters and the first-neighbor distance is fixed at the experimental value R_0. In the case of copper ($R_0=2.5526$ Å) we have found that with $\alpha=0.666$ we obtain an excellent fit (of the order of meV per atom) of the cohesive energy $E_c=-3.5$ eV/atom and of the bulk modulus, $B=10.470$ eV/atom, but the quality of the fit for

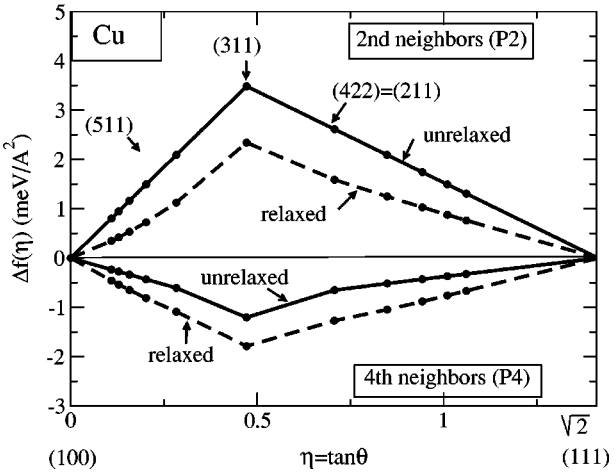

FIG. 5. $\Delta f(\eta)$ for Cu derived from the semi-empirical potential given in the text for two cutoff radii with and without relaxation for the (100)-(111) domain.

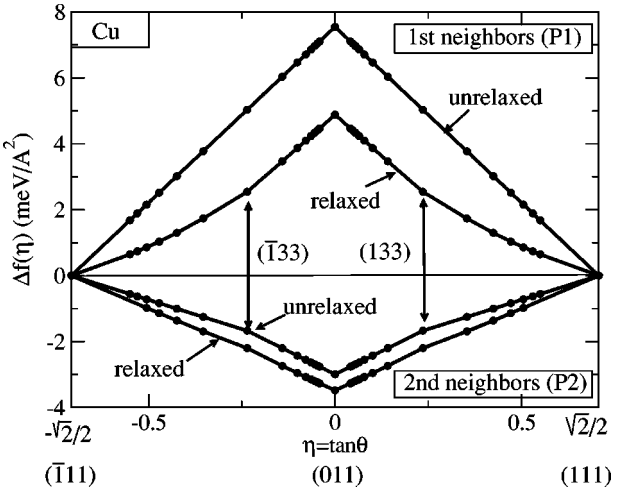

FIG. 6. Same as Fig. 5 for the $(\bar{1}11)$-(111) domain.

the two other elastic constants $C=6.046$ eV/atom and $C'=1.917$ eV/atom is strongly dependent on the cutoff radius. Moreover, the surface energies of the three low index surfaces (111), (001), and (011), even though not included in the fit, are better with $\alpha=0.666$ than with $\alpha=1/2$.

We have checked several sets of parameters, corresponding to different cutoff radii R_c, by comparing to experiment the result of the fit (in particular the two elastic constants C and C') and also the surface relaxation and the bulk phonon spectra.[12] It was found that the best set of parameters (called P_2) was obtained for a cutoff radius $R_c=4.02$ Å between second and third neighbors, the corresponding numerical values being $A=0.206$ eV, $\xi=1.102$ eV, $p=7.206$, $q=2.220$. However, to test the influence of R_c on the stability of vicinal surfaces we have also considered two other sets of parameters one, denoted as P_1, with a cutoff radius $R_c=3.08$ Å between first and second neighbors leading to $A=0.339$ eV, $\xi=1.447$ eV, $p=6.069$, $q=2.449$, and another one (P_4) with a cutoff radius $R_c=5.4$ Å between fourth and fifth neighbors, the corresponding parameters being $A=0.195$ eV, $\xi=1.021$ eV, $p=7.357$, $q=2.100$. In all cases the atomic structure of each surface has been fully relaxed using a conjugate gradient algorithm.

We will now examine the cases of the (100)-(111) domain. In Fig. 5 we have represented $\Delta f(\eta)$ with and without atomic relaxation for the two potentials P_2 and P_4. As expected from our previous analysis all vicinal surfaces between (100) and (111) are unstable for the P_2 potential the range of which is restricted to second neighbors (the potential P_1 leads qualitatively to the same results). However, we can see that the effect of farther neighbors is crucial since, with potential P_4, all vicinal surfaces between (100) and (111) become stable.

The case of the $(\bar{1}11)$-(111) domain is presented in Fig. 6 where we have shown $\Delta f(\eta)$ with and without atomic relaxation for the two potentials P_1 and P_2. Here again the range of the potential is crucial: as expected potential P_1 leads to an upward triangle and therefore an instability of all the vicinal surfaces [in particular the (011) surface is unstable with respect to faceting into (111) and $(\bar{1}11]$ facets], the inclusion of further neighbors totally modifies this picture since with potential P_2, $\Delta f(\eta)$ is negative and the (011) surface is stable. Moreover, as expected from analytical results (see Sec. II B 1 b) $\Delta f(0)$ is below the straight line defined by the (111) and (133) points and therefore all vicinals surfaces between (011) and (111) are unstable with respect to faceting into (011) and (111) orientations.

Finally one can see that atomic relaxation always acts in favor of a stabilization since the relaxation is larger on a vicinal surface that on a flat one. Typically the displacement of an atom relative to its lattice position is 0.035 and 0.037 Å inwards for a (100) and (111) surface atom, respectively, while it is also inwards but about 0.13 Å for an atom of the step edge using the potential P_2. A detailed study of this relaxation will be presented in a forthcoming paper.[32]. Nevertheless, this effect is rather small and in most cases it will not be large enough to modify the stability (or instability) of a surface. The only case where it could influence the stability is when $\Delta f(\eta)$ is positive but very small, the inclusion of atomic relaxation could then make $\Delta f(\eta)$ negative in some regions and positive in others leading to a more complex behavior. However, this situation is very unlikely and the inclusion of new effects (like that of vibrational energy) would also modify the picture in that specific case.

Let us discuss and summarize our results. From our analytical study and Figs. 5 and 6 it appears that the range of the potential plays an important role but it is difficult to draw general conclusions. In all cases considered here the effect of farther neighbors is to stabilize vicinal surfaces, however, including them will not automatically make vicinal surfaces stable, this crucially depends on their relative importance and therefore on the dependence of the functions $V(r)$ and $g(r)$ with distance [Eq. (12)]. The stability also depends on the relative importance of V with respect to $F(\rho)$ since when farther neighbors are included both terms are present in the energy balance. Moreover, in EAM and EMT potentials the embedding and pair parts are not necessarily purely attractive or purely repulsive, therefore even the sign of these terms is not known. Let us finally compare our results with those of

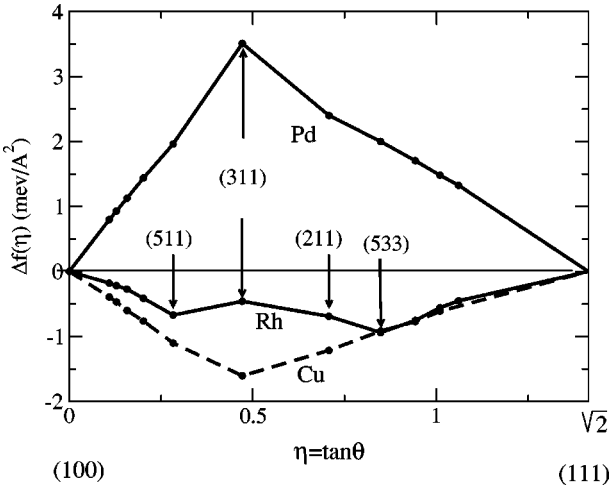

FIG. 7. $\Delta f(\eta)$ for Rh, Pd, and Cu from tight-binding calculations for the (100)-(111) domain.

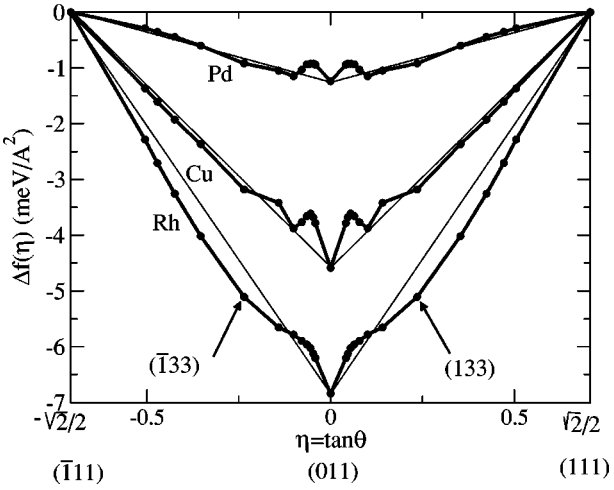

FIG. 8. Same as Fig. 7 for the $(\bar{1}11)$-(111) domain.

of Frenken and Stoltze.[33] These authors have calculated $\Delta f(\eta)$ for the fully relaxed (100) and (111) vicinal surfaces of Ag (and other metals) using an EMT potential with $R_3 < R_c < R_4$. However, the role played by the third neighbors is very small compared to that of first and second neighbors (to fix ideas, $g_1=1$, $g_2 \simeq 3\times10^{-2}$, $g_3 \simeq 3\times10^{-3}$). Our analysis shows that all the $\Delta f(\eta)$ curves calculated with a potential of type (12) and a cutoff radius $R_c < R_3$ will behave identically. In the case of their potential, even though third neighbors are included, their role is too small to have a significant influence. This explains the strong similarity between our results on relaxed Cu (Fig. 5) with potential P_2 and those of Frenken and Stoltze for Ag.

IV. STABILITY OF VICINAL SURFACES AT 0 K FROM TIGHT-BINDING CALCULATIONS

The potentials considered above have a common drawback: the energy of an atom i (on a rigid lattice) is completely fixed by its coordination numbers Z_N^i whereas it should also depend on the angular arrangement of its neighbors. This effect is accounted for in electronic structure calculations which, moreover, include long-range interactions (often oscillatory). These interactions, although small, may play a role in the very delicate energy balance which determines the stability of vicinal surfaces. In a recent paper[10] we calculated the step energies of various vicinal surfaces from a realistic tight-binding model for Rh, Pd, and Cu. The functions $\Delta f(\eta)$ derived from the results of this paper are plotted in Figs. 7 and 8 for the (100)-(111) vicinal surfaces and $(\bar{1}11)$-(111) vicinal surfaces, respectively.

As can be seen there is a great variety of shapes and the (100)-(111) domain is very different from the (111)-(111) domain. On the (100)-(111) domain we find that for Cu all vicinal surfaces are stable at 0 K while for Pd they are unstable. For Rh the situation is more complex: all vicinal surfaces are stable with respect to faceting into (100) and (111) surfaces, however, the curve presents two local minima at $\eta=\sqrt{2}/5$ [(511) surface] and $\eta=3\sqrt{2}/5$ [(533) surface] with a local maximum at $\eta=\sqrt{2}/3$ [(311) surface]. This means that the vicinal surfaces of orientation such that $\sqrt{2}/5 < \eta < 3\sqrt{2}/5$ are unstable relative to faceting into (511) and (533) orientations. This peculiar behavior is related to electronic step-step interactions which are repulsive for the (311) and (211) surfaces and attractive for (511) and (533) surfaces.[10] In the $(\bar{1}11)$-(111) domain the situation is rather different but some general features can, however, be drawn from Fig. 8: for the three considered elements the $(01\bar{1})$ surface is stable with respect to faceting into (111) and $(\bar{1}11)$ facets in agreement with experiment but it appears that vicinal surfaces $p(011)\times(111)$ are unstable for $p \geqslant 4$ since there is an inversion of curvature for $p \geqslant 4$. For copper and palladium there is a range of instability between $2(011)\times(111)$ or (133) and $4(011)\times(111)$ or (177) meaning that vicinal surfaces in this range are expected to facet into (133) and (177) orientations. For rhodium this instability is not present. Concerning the vicinal surfaces $p(111)\times(\bar{1}11)$ for $p>2$, Fig. 8 shows that they are stable for copper and rhodium but unstable for palladium. Unfortunately there are very few experimental data for this range of orientations, the only experimental result we are aware of is a study of Cu(133),[34] which is found to be stable in agreement with our findings. It would therefore be very interesting to have experimental studies of (011) vicinal surfaces with higher index ($p \geqslant 4$) to check the validity of our calculations.

V. FINITE TEMPERATURE EFFECTS ON THE STABILITY OF VICINAL SURFACES

So far all calculations were carried out at 0 K; we will now consider the influence of finite temperatures. There are two sources of variation of $f(\eta)$ with temperature: a purely statistical term $f_{stat}(T)$ due to the entropy S_{stat} gained by the meandering of steps regulated by the kink formation energy (ε_{kink}), therefore decreasing the free energy for step formation, and the vibrational free energy f_{vib} due to the vibrational motion of atoms. We then have

$$f(\eta,T) = f_0(\eta) + f_{stat}(\eta,T) + f_{vib}(\eta,T), \qquad (35)$$

where $f_0(\eta)$ is the static term independent of temperature. Actually f_{stat} is very difficult to calculate, it can, however, be evaluated analytically in a simple first-nearest neighbor Ising model for a free step on a (100) fcc surface[15] leading to

$$f_{stat}^{free}(\eta,T) = -\frac{k_B T}{A_0(\mathbf{n})} \ln\left[\coth\frac{\varepsilon_{kink}}{2k_B T}\right], \tag{36}$$

this expression being only valid when steps fluctuate independently of each other. Indeed, when the meandering of steps is large enough compared to the terrace width one must take into account the fact that steps cannot cross. This restriction decreases the configurational entropy and leads to an effective repulsion of the steps. One can formally write f_{stat} as the sum of two terms: f_{stat}^{free} and $f_{stat}^{nocross}$ which is the positive contribution due to the noncrossing condition.

For f_{stat} the low index surfaces do not contribute since the only allowed events that we consider are kink creation, therefore $\Delta f_{stat} = f_{stat}$. If we neglect the term due to the noncrossing condition Δf_{stat} has a simple downward triangular shape and the minimum is obtained for the intermediate vicinal surface corresponding to $\eta = \eta_c$ (or equivalently $p=2$) and is equal to

$$\Delta f_{stat}(\eta_c) = -k_B T \ln[\coth(\varepsilon_{kink}/2k_B T)]/[S_1(1+f_1)]. \tag{37}$$

This statistical contribution f_{stat} is obviously stabilizing vicinal surfaces and it varies rapidly with temperature. To fix ideas let us take the (100)-(311) domain [which corresponds to vicinal surfaces with (100) terraces] and a kink energy typically of 0.12 eV/atom for copper. One finds that $\Delta f_{stat}(\eta_c)$ is of the order of 10^{-9} eV/Å^2 at 100 K, 10^{-6} eV/Å^2 at 200 K, 0.05 meV/Å^2 at 300 K, and 0.5 meV/Å^2 at 500 K. Therefore at room temperature this statistical energetic contribution will be at most a few hundredths of meV for Cu and completely negligible in the case of elements with higher kink energies like rhodium and palladium. In any case f_{stat} has a negligible influence on the stability of vicinal surfaces.

The excess vibrational free energy has two contributions: the internal energy which dominates at low temperature and vanishes at high temperature and the entropy part which has the inverse behavior. This excess free energy has been evaluated in recent publications using a simple model of the Einstein type,[33,35,36] but in view of the rather delicate energy balance involved here it is more advisable to use a complete description of the phonon spectrum and include both the internal energy and the entropy part. Therefore we have calculated the vibrational free energy from precise phonon spectra based on the empirical potential P_2 which is known to reproduce very accurately the experimental data for the vibration spectra of bulk Cu and its low- and high-index surfaces.[12] Contrary to the statistical term the vibrational energy is obviously not zero on the flat surface and there is an important cancellation when calculating the difference of energy giving Δf_{vib}. On Figs. 9 and 10 we have represented Δf_{vib} for the two domains (100)-(111) and $(\bar{1}11)$-(111) at different temperatures from 0 to 500 K.

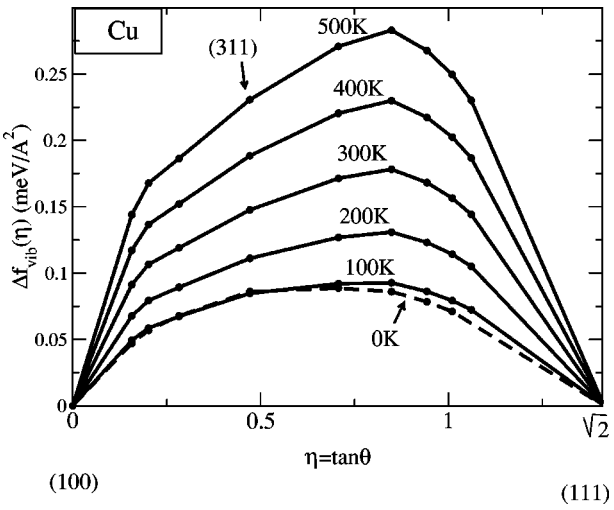

FIG. 9. $\Delta f_{vib}(\eta)$ for Cu in the (100)-(111) domain from potential P_2 as a function of temperature.

The main conclusion is that the order of magnitude of Δf_{vib} is approximately some tenths of meV/Å^2 and therefore in most cases it will have a negligible role on the stability. However, Δf_{stat} may become of the same order of magnitude as Δf_{vib} for temperatures above 300 K. One should also note that the shape of Δf_{vib} is very different for the two domains: it is positive for the (100)-(111) domain and consequently tends to destabilize vicinal surfaces, it is oscillatory with some positive and negative parts for the $(\bar{1}11)$-(111) domain.

Finally, let us note that our results concerning the influence of the vibrational energy are in contradiction with those of Frenken and Stoltze,[33] since these authors claimed that phonons stabilize vicinal surfaces in the (100)-(111) domain. In their work they evaluated the role of phonons using a simplified Einstein model and neglected the internal energy, which is quite questionable at low temperatures. Moreover, in their evaluation of Δf_{vib} they used a formula similar to Eq. (23) but in which they only included the difference be-

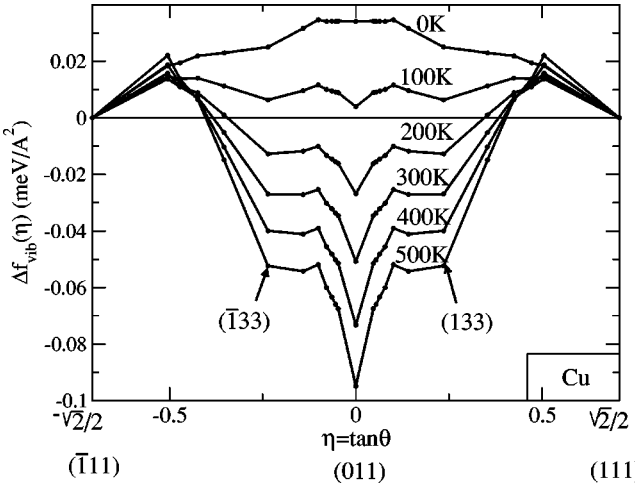

FIG. 10. $\Delta f_{vib}(\eta)$ for Cu in the $(\bar{1}11)$-(111) domain from potential P_2 as a function of temperature.

tween the outer edge and a (111) surface atom, i.e., $E(7,3)-E(9,3)$. Our analytical calculations [Eq. (23)] show that at least another term should imperatively be considered, namely $E(10,5)-E(8,5)$ arising from the difference between the inner edge and a (100) surface atom. These two terms have opposite signs and are expected to be of the same order of magnitude. This explains why not only the order of magnitude of Frenken and Stoltze estimation is too large (meV instead of tenths of meV) but even the sign is wrong since we find that phonons tend to destabilize vicinal surfaces, at least for Cu, in the (100)-(111) domain whereas the influence of phonons can be stabilizing in some regions and destabilizing in some others in the $(1\bar{1}1)$-(111) domain.

VI. CONCLUSION

In this paper we have investigated the implications of different approaches for calculating the surface energies on the stability of vicinal surfaces with respect to faceting. We have shown that, although effective pair potentials are useful to estimate step energies,[10,14] this method is not precise enough to determine the stability of vicinal surfaces. First, in this model, the stability would be governed by pair potentials beyond first-nearest neighbors, at least. As emphasized in Ref. 10 the sign of these terms is not known with certainty since it depends on the surface energy data base used to determine them. When surface energies are calculated from semi-empirical potentials, we have seen that the results depend on the cutoff distance chosen for the interatomic interactions and of the importance of farther neighbors compared with first-nearest neighbors. Moreover, the shape of $\Delta f(\eta)$ remains schematic, even when atomic relaxation is included. In addition, pair potentials, as well as *N*-body semi-empirical ones, have a common drawback: they only depend on the interatomic distances and not on the angular arrangement of atoms. This latter effect is small in metals. However, it cannot be neglected in view of the delicate energy balance which governs the stability of vicinal surfaces with respect to faceting. On the contrary, electronic structure calculations take this effect into account and open up the possibility of a large variety of behaviors, including a possible faceting of a vicinal surface into two different vicinal surfaces. Such a phenomenon is a consequence of electronic oscillatory step-step interactions. Finally temperature effects are found to be most often negligible, at least up to room temperature.

APPENDIX A: FACETING CONDITION AND HERRING GEOMETRICAL CONSTRUCTION

In this appendix we show the equivalence between the geometrical construction of Herring and the simpler faceting criterion derived in Sec. II. Let us recall the Herring construction.[13] One starts from the γ plot in polar coordinates. An example of a γ plot, obtained for copper from our tight-binding calculations, is given in Fig. 11. Its most striking feature is the existence of well defined cusps in some directions, namely (111), (100), and (011). The more close packed the surface, the deeper the cusp. This appears clearly in Fig. 11 where the direction corresponding to the (111)

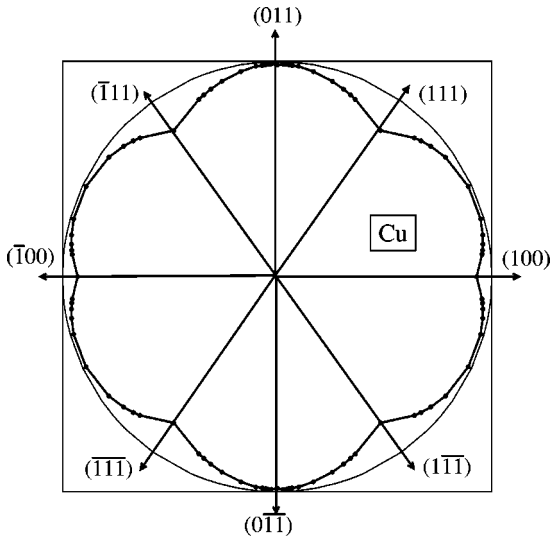

FIG. 11. γ plot of Cu for the orientations studied in the main text.

surface has a more pronounced cusp than the (100) direction, while that of the (011) direction is hardly visible. We consider a schematic case with a strong anisotropy, for the sake of clarity, as shown in Fig. 12. First we construct the plane π, perpendicular to the radius vector of the γ plot and tangent to the Wulff equilibrium shape at point *I*. Let us call *H* the projection of the center of the γ plot *O*, on π, and set $\gamma_f = OH$. When the radius vector scans all the γ plot the point *H* scans a surface that we will call Γ. From Herring criterion, the surface is unstable with respect to faceting if the surface Γ is inside the γ plot.

We will now recast this geometrical construction into the more straightforward one derived in Sec. II. Let us first calculate $\gamma_f(\theta)$:

$$\gamma_f(\theta) = OH = OI\cos(\theta_\perp - \theta) \tag{A1}$$

with $OI = \gamma(\mathbf{n}_1)/\cos(\theta_\perp)$, therefore we have

$$\gamma_f(\theta) = \frac{\cos(\theta_\perp - \theta)}{\cos(\theta_\perp)}\gamma(\mathbf{n}_1). \tag{A2}$$

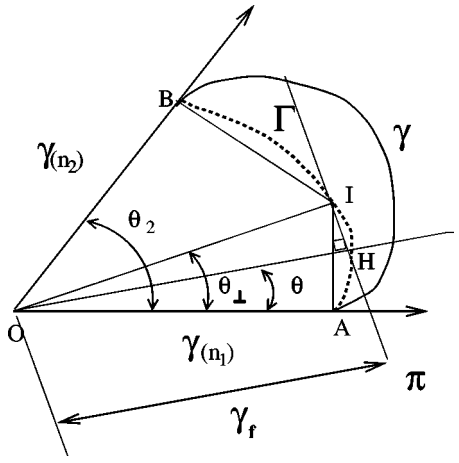

FIG. 12. The Herring construction.

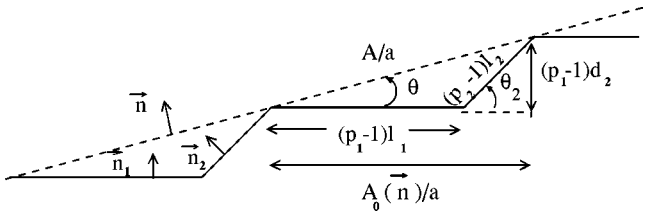

FIG. 13. Cut of a vicinal surface with terraces of orientations $\mathbf{n}_1$ when $p_2=2$ and $\mathbf{n}_2$ when $p_1=2$.

As seen from Sec. II, the relevant function is $\gamma(\theta)/\cos(\theta)$. Let us then calculate

$$\frac{\gamma_f(\theta)}{\cos(\theta)}=\gamma(\mathbf{n}_1)+[\gamma(\mathbf{n}_1)\tan\theta_\perp]\tan\theta. \tag{A3}$$

Actually OI has two equivalent expressions whether the origin of the angles are the directions $\mathbf{n}_1$ or $\mathbf{n}_2$, one gets

$$OI=\frac{\gamma(\mathbf{n}_1)}{\cos(\theta_\perp)}=\frac{\gamma(\mathbf{n}_2)}{\cos(\theta_2-\theta_\perp)} \tag{A4}$$

which allows one to derive an expression for $\tan\theta_\perp$:

$$\tan\theta_\perp=\frac{\gamma(\mathbf{n}_2)}{\gamma(\mathbf{n}_1)\sin\theta_2}-\frac{1}{\tan\theta_2}. \tag{A5}$$

Substituting Eq. (A5) for $\tan\theta_\perp$ into Eq. (A3) yields

$$\frac{\gamma_f(\theta)}{\cos(\theta)}=\left(1-\frac{\tan\theta}{\tan\theta_2}\right)\gamma(\mathbf{n}_1)+\left(\frac{\tan\theta}{\tan\theta_2}\right)\frac{\gamma(\mathbf{n}_2)}{\cos\theta_2}. \tag{A6}$$

Comparing Eq. (A6) with the inequality (4) the faceting condition can be written

$$\gamma(\theta)>\gamma_f(\theta). \tag{A7}$$

Thus the faceting condition given by Herring construction is equivalent to the inequality (4).

APPENDIX B:

Let us consider the stepped surface of orientation $\mathbf{n}$ shown in Fig. 13. The planes of normal $\mathbf{n}_1$ are taken as the origin of angles, i.e., $\theta=(\mathbf{n}_1,\mathbf{n})$, $\theta_2=(\mathbf{n}_1,\mathbf{n}_2)$. The spacing of atomic rows parallel to the step edges is denoted as l_1 (l_2) in the face of normal $\mathbf{n}_1$ ($\mathbf{n}_2$), d_1 is the interplanar spacing along direction $\mathbf{n}_1$, and a the interatomic spacing along the rows. p_1 and p_2 denote the numbers of atomic rows in each facet including the inner edge. All vicinal surfaces with monoatomic steps encountered in the domain $[0,\theta_2]$ are of this type with

$$\infty>p_1\geqslant 2;\quad p_2=2\quad \text{when}\quad 0<\theta\leqslant\theta_c,$$

$$p_1=2;\quad 2\leqslant p_2<\infty\quad \text{when}\quad \theta_c<\theta\leqslant\theta_2.$$

We want to prove Eq. (5) starting from [see Eq. (4)]

$$\Delta f(\mathbf{n})=\frac{\gamma(\mathbf{n})}{\cos\theta}-\left(1-\frac{\tan\theta}{\tan\theta_2}\right)\gamma(\mathbf{n}_1)-\left(\frac{\tan\theta}{\tan\theta_2}\right)\frac{\gamma(\mathbf{n}_2)}{\cos\theta_2}, \tag{B1}$$

where $\gamma(\mathbf{n})$ is the surface energy per unit area of a surface of orientation $\mathbf{n}$. Let us denote as A, A_1, and A_2 the areas of the unit cells of the planes with normals $\mathbf{n}$, $\mathbf{n}_1$, and $\mathbf{n}_2$, respectively, and $A_0(\mathbf{n})=A\cos\theta$ the projection of A on the plane of orientation $\mathbf{n}_1$. The following relations hold:

$$A_1=al_1, \tag{B2}$$

$$A_2=al_2=\frac{ad_1}{\sin\theta_2}, \tag{B3}$$

$$\tan\theta=\frac{(p_2-1)d_1\tan\theta_2}{(p_2-1)d_1+(p_1-1)l_1\tan\theta_2}. \tag{B4}$$

Introducing the surface energies per surface atom $E_s(\mathbf{n})$ into Eq. (B1) gives

$$\Delta f(\mathbf{n})=\frac{E_s(\mathbf{n})}{A\cos\theta}-\left(1-\frac{\tan\theta}{\tan\theta_2}\right)\frac{E_S(\mathbf{n}_1)}{A_1}-\left(\frac{\tan\theta}{\tan\theta_2}\right)\frac{E_S(\mathbf{n}_2)}{A_2\cos\theta_2}. \tag{B5}$$

Substituting Eqs. (B2), (B3), and (B4) for A_1, A_2, and $\tan\theta$ into Eq. (B5) yields

$$\Delta f(\mathbf{n})=[E_S(\mathbf{n})-(p_1-1)E_S(\mathbf{n}_1)-(p_2-1)E_S(\mathbf{n}_2)]/A_0(\mathbf{n}). \tag{B6}$$

[1] P. Gambardella, M. Blanc, K. Kuhnke, K. Kern, F. Picaud, C. Ramseyer, C. Girardet, C. Barreteau, D. Spanjaard, and M.C. Desjonquères, Phys. Rev. B **64**, 045404 (2001).

[2] S. Rousset, F. Pourmir, J.M. Berroir, J. Klein, J. Lecoeur, P. Hecquet, and B. Salanon, Surf. Sci. **422**, 33 (1999).

[3] J. Frohn, M. Giesen, M. Poensgen, J.F. Wolf, and H. Ibach, Phys. Rev. Lett. **67**, 3543 (1991).

[4] W.W. Pai, J.S. Ozcomert, N.C. Bartelt, T.L. Einstein, and J.E. Reutt-Robey, Surf. Sci. **307-309**, 747 (1994).

[5] M. Giesen and G. Schulze Icking-Konert, Surf. Rev. Lett. **6**, 25 (1999).

[6] M. Giesen, Prog. Surf. Sci. **68**, 1 (2001), and references therein.

[7] L. Masson, L. Barbier, and J. Cousty, Surf. Sci. **317**, L1115 (1994).

[8] A.E. Carlsson, Solid State Phys. **43**, 1 (1990), and references therein.

[9] S. Papadia, M.C. Desjonquères, and D. Spanjaard, Phys. Rev. B **53**, 4083 (1996).

[10] F. Raouafi, C. Barreteau, M.C. Desjonquères, and D. Spanjaard, Surf. Sci. **482-485**, 1413 (2001); **505**, 183 (2002).

[11] M.C. Desjonquères, D. Spanjaard, C. Barreteau, and F. Raouafi, Phys. Rev. Lett. **88**, 056104 (2002).

[12] F. Raouafi, C. Barreteau, M.C. Desjonquères, and D. Spanjaard, Surf. Sci. **507-510,** 748 (2002).

[13] C. Herring, Phys. Rev. **82**, 87 (1951)

[14] L. Vitos, H.L. Skriver, and J. Kollár, Surf. Sci. **425**, 212 (1999).

[15] M.C. Desjonquères and D. Spanjaard, *Concepts in Surface*

Physics, 2nd edition (Springer-Verlag, Berlin, 1996).
[16] P. Stoltze, J. Phys.: Condens. Matter **6**, 9495 (1994).
[17] K.W. Jacobsen, P. Stoltze, and J.K. Norskov, Surf. Sci. **366**, 394 (1996).
[18] M.S. Daw, S.M. Foiles, and M.I. Baskes, Mater. Sci. Rep. **9**, 251 (1993), and references therein.
[19] F. Ercolessi, M. Parrinello, and E. Tosatti, Philos. Mag. A **58**, 213 (1988).
[20] F. Ducastelle, J. Phys. (France) **31**, 1055 (1970).
[21] M.W. Finnis and J.E. Sinclair, Philos. Mag. A **50**, 45 (1984).
[22] V. Rosato, M. Guillopé, and B. Legrand, Philos. Mag. A **59**, 321 (1989).
[23] A.P. Sutton and J. Chen, Philos. Mag. Lett. **61**, 139 (1990).
[24] J. Guevara, A.M. Llois, and M. Weissmann, Phys. Rev. B **52**, 11 509 (1995).
[25] B. Lang, R.W. Joyner, and G.A. Somorjai, Surf. Sci. **30**, 440 (1972).
[26] A. Gaussmann and N. Kruse, Surf. Sci. **266**, 46 (1992).
[27] L. Vitos, B. Johansson, H.L. Skriver, and J. Kollár, Comput. Mater. Sci. **17**, 156 (2000).
[28] It is worth noticing that, in the pair potential model, steps start to interact when R_c is equal or larger than the smallest bond joining two atoms belonging to two consecutive outer (or inner) step edges for $p=3$.
[29] I.J. Robertson, M.C. Payne, and V. Heine, Europhys. Lett. **15**, 301 (1991).
[30] J. Kuntze, S. Speller, and W. Heiland, Surf. Sci. **402-404**, 764 (1998).
[31] This means also that in the study of the $(\bar{1}11)$-(111) domain with $R_c<R_3$, the point (011) and (133) [and (011) and $(1\bar{3}3)$] are connected by a straight line.
[32] C. Barreteau, F. Raouafi, M.C. Desjonquères, and D. Spanjaard, Surf. Sci. (to be published).
[33] J.W.M. Frenken and P. Stoltze, Phys. Rev. Lett. **82**, 3500 (1999).
[34] B. Loisel, Ph.D. thesis, University of Paris 7 (1989).
[35] H.P. Bonzel and A. Emundts, Phys. Rev. Lett. **84**, 5804 (2000).
[36] H.J.W. Zandvliet, O. Gurlu, and B. Poelsema, Phys. Rev. B **64**, 073402 (2001).

Stability of Metal Vicinal Surfaces Revisited

M. C. Desjonquères, D. Spanjaard, C. Barreteau, and F. Raouafi
DSM/DRECAM/SPCSI, CEA Saclay, F-91191 Gif sur Yvette, France
Laboratoire de Physique des Solides, Université Paris Sud, F-91405 Orsay, France
(Received 11 October 2001; published 22 January 2002)

The stability of metal vicinal surfaces with respect to faceting is investigated using empirical potentials as well as electronic structure calculations. It is proven that for a wide class of empirical potentials all vicinal surfaces between (100) and (111) are unstable at 0 K when the role of third and farther nearest neighbors is negligible. However, electronic structure calculations reveal that the answer concerning the stability of vicinal surfaces is not so clear-cut. Finally, it is shown that surface vibrations at finite temperatures have little effect on the stability of vicinal surfaces.

DOI: 10.1103/PhysRevLett.88.056104 PACS numbers: 68.35.Md, 65.40.Gr, 68.35.Ja, 68.35.Rh

The study of energetics of vicinal surfaces is of prime interest for the understanding of various surface processes such as crystal growth, surface morphology, or roughening transition. Recently Frenken and Stoltze [1] raised the important question of the stability of vicinal surfaces in metals. Using a potential based on the effective medium theory (EMT), they predicted that most vicinal surfaces are unstable relative to faceting at 0 K and claimed that the observed stability at room temperature arises from the entropic contribution due to thermal vibrations. In this Letter, we show that the first prediction results entirely from the analytical form and range of interactions of the potential used and that the same conclusion holds for a wide class of empirical potentials. This is in contradiction with calculations based on an explicit determination of the electronic structure which reveals a variety of other behaviors for vicinal surfaces at 0 K. Finally, we show that the vibrational free energy contribution has, most often, a negligible role when calculated correctly.

Let us consider two (low-index) surfaces and denote **n** and **n** their normal vector and surface energy (per unit area), respectively, and the angle **n** **n** . Let us also consider a (high-index) surface of surface energy and normal **n** belonging to the plane defined by **n** , **n** and making an angle with **n** .

An area of this high-index surface will transform into facets of normal **n** (area) and normal **n** (area) while keeping its average orientation (Fig. 1) when [2]

(1)

with the constraints = cos cos and sin = sin . It is easy to show that the faceting condition (1) is

(2)

with = tan and = cos . This simply means that the point [ ] must be above the straight line joining the points [ ] and [ ].

We study here in detail the case of the or and or vicinal surfaces and their stability with respect to faceting. These surfaces have close-packed step edges, atomic rows parallel to the step edge (including the inner edge) in each terrace, and make an angle with the (100) surface. The domain = $\sqrt{}$ corresponds to (100) vicinal surfaces with decreasing from infinity to 2 [(311) surface]. The domain = $\sqrt{}$ is that of (111) vicinal surfaces with increasing from 2 [(311) surface] to infinity [(111) surface)]. Thus the (311) surface can be regarded either as a (111) or a (100) vicinal surface with the highest step density.

As already stated in Ref. [1], falls almost exactly on the straight line joining the points and $\sqrt{}$ $\sqrt{}$. However, there is a small, yet significant, deviation from this linear behavior and, from Eq. (2), its sign for any intermediate surface determines the stability of this surface with respect to faceting into (100) and (111) facets: If the vicinal surface is unstable (stable). As noted above, for the (311) surface plays a special role and is given by

= (3)

where is the surface energy per surface atom of the surface, and is the area of the projection of the unit cell of the (311) surface on the (100) plane.

In order to distinguish between different energetic contributions, we will first consider a rigid lattice (i.e., without atomic relaxation) at 0 K and calculate the energy with

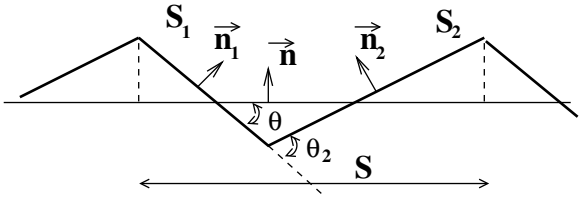

FIG. 1. Faceting.

usual empirical potentials analyzing the effects of the range of interactions and of relaxation. We will also present results from a realistic tight-binding model showing the influence of electronic effects. Finally, the temperature dependence of will be included with a particular focus on the phonon free energy contribution.

Empirical potentials belonging to a large class can be written as a sum of contributions of each atom , i.e.,

$$= \sum \quad = \sum \left\{ \sum \qquad \left[\sum \qquad \right] \right\} \tag{4}$$

In the following we set $= \sum$. The first term of Eq. (4) is pairwise while the second one (in which is a positive function) has an -body character. The functions and of the interatomic distance are usually cut off smoothly after a given radius . Pair potentials [=], second moment potentials [$\sqrt{\ }$] [3], as well as embedded atom model [4] and EMT potentials [5] belong to this class.

We first fix the interatomic distances to their bulk equilibrium values; i.e., atomic relaxation effects are ignored. With this assumption $\sum$ and $\sum$ are linear combinations of the number of neighbors of atom in the th coordination sphere of radius and = . It is usual to take as the reference distance and set = .

When the range of the potential is restricted to the first and second neighbors only, it can be shown [6] that the step energies (per step atom) and do not depend on ; i.e., there is no interaction between steps even when = . Then it can be proven that the curve is made of two straight lines, the slopes of which are a function of the corresponding step energy and of and . These two lines meet at the intermediate point $\sqrt{\ }$ and the sign of determines the stability of the vicinal surfaces. A counting of coordination numbers leads to

$$= \tag{5}$$

in which the first two terms refer to the outer and the inner step edges, respectively, and the last two terms to a (100) and (111) surface atom. is the projected area of the surface unit cell on the (100) surface. In the case of a pair potential is strictly equal to 0 so that the energy of any vicinal surface is equal to the energy of the faceted (100)–(111) surface. Thus, when the potential includes an -body contribution, can be written

$$= \tag{6}$$

with = . For all the existing potentials of the form (4) $''$ = is positive. As a consequence, is a decreasing function of and therefore is always positive and in particular . This common property of this class of potentials has a clear physical origin: The energy of an atom should decrease more and more slowly when its coordination increases towards the bulk coordination [7]. It clearly implies that $''$ must be positive. We have then proven that for *any* empirical potential of the general form (4) on a rigid lattice at 0 K and a cutoff radius , *any* vicinal surface from (100) to (111) is *unstable* with respect to faceting. As an example, we show in Fig. 2 the result of a calculation for Cu with a potential denoted in which = , = , and = exp .

When the range of the potential is extended to further neighbors this result is no longer valid. First, for a general potential, steps with narrow terraces start to interact and the curve is no longer made of two straight lines. The pair potential does not contribute to this interaction at least when but it gives a contribution to which tends to destabilize (stabilize) the vicinal surfaces when is negative (positive). Moreover, additional terms due to other sites appear in Eqs. (5) and (6), and therefore the sign of the contribution of the -body function to cannot be inferred since it depends on the magnitude of . This is shown in Fig. 2 in which , obtained with a potential of the same functional form as but with , is drawn. In this potential the role played by third and fourth neighbors is sufficient to reverse the

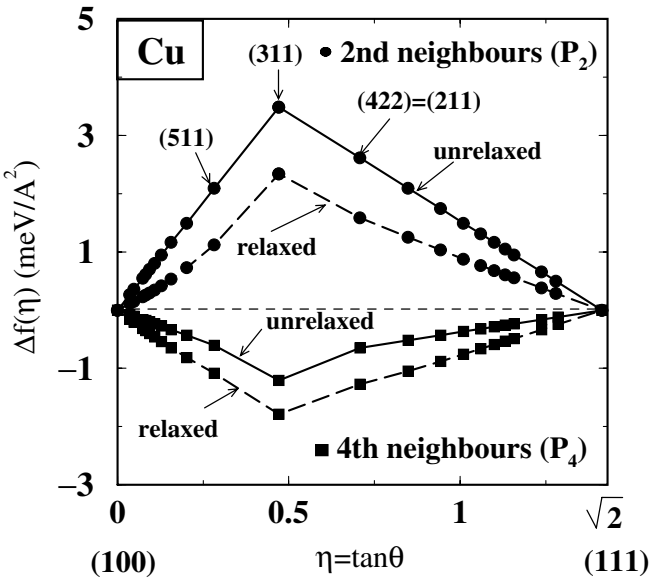

FIG. 2. for Cu from empirical potential calculations up to second and fourth neighbors, with and without relaxations.

sign of . Thus, the range of the potential may play a crucial role on the stability of vicinal surfaces.

Furthermore, the potentials discussed above have a common drawback: The energy of an atom is completely fixed by its coordination numbers whereas it should also depend on the angular disposition of its neighbors. This effect is accounted for in electronic structure calculations which, moreover, include long range interactions (often oscillatory). These interactions, although small, may play a role in the very delicate energy balance which determines the stability of vicinal surfaces. In a recent paper [8], we calculated the step energies of various vicinal surfaces from a realistic tight-binding model for Rh, Pd, and Cu. The functions derived from the results of this paper are plotted in Fig. 3 for the (100) and (111) vicinal surfaces.

As can be seen there is a great variety of shapes. For Cu the curve is below the straight line and the vicinal surfaces are stable at 0 K while for Pd they are unstable. For Rh all vicinal surfaces are stable with respect to faceting into (100) and (111) surfaces. However, the curve presents two local minima at $= \sqrt{}$ [(511) surface] and $= \sqrt{}$ [(533) surface] with a local maximum at $= \sqrt{}$ [(311) surface]. This means that the vicinal surfaces of orientation such that $\sqrt{}$ $\sqrt{}$ are unstable relative to faceting into (511) and (533) orientations. This peculiar behavior is related to electronic step-step interactions which are repulsive for the (311) and (211) surfaces and attractive for (511) and (533) surfaces [8]. We have also plotted points deduced from Eq. (3) using the *ab initio* calculations of Galanakis *et al.* [9] on the three surfaces (111), (100), and (311) of Cu, Pd, and Rh. For Rh and Pd the *ab initio* calculations are in qualitative agreement with our results but for Cu they predict at least an unstable range of orientations.

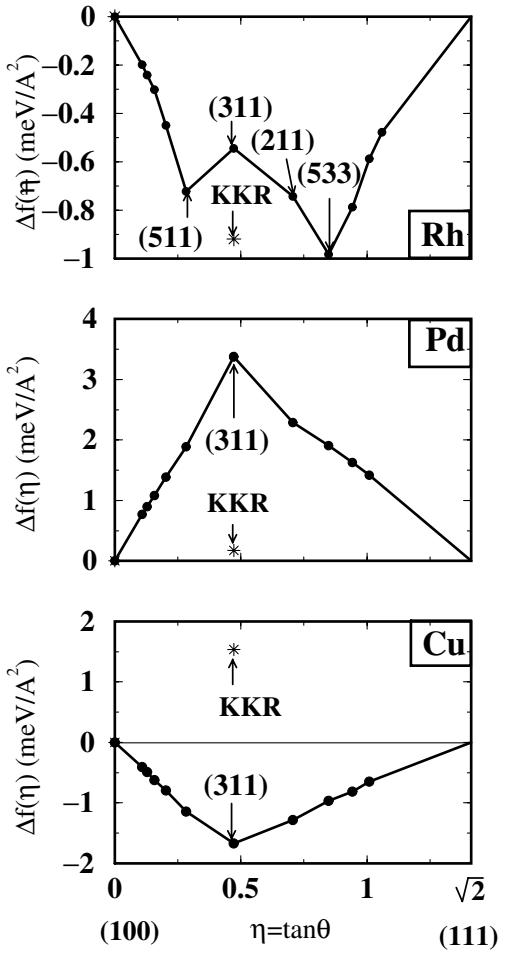

FIG. 3. for Rh, Pd, and Cu from tight-binding [8] and Korringa, Kohn, and Rostoker (KKR) [9] calculations.

Until now we have neglected the effect of atomic relaxations. Relaxation leads to a decrease of the surface energies by a few percents (up to 10%) and one could wonder if, in view of the small value of , it could change the results obtained on the rigid lattice. However, it must be kept in mind that the stability depends on energy differences [Eq. (3)]. Thus, some kind of cancellation is expected. Actually, we have performed a full energy minimization using the potentials and and, in both cases (Fig. 2) it acts in favor of the stabilization since the relaxation is larger on a vicinal surface than on a flat one. Nevertheless, this effect is not large enough to modify the stability (or instability) of a surface, and the results obtained on the rigid lattice remain qualitatively valid except when is positive but very small. Besides the lowering of , relaxation effects modify its shape. In particular, when using the potential , the curves joining, on the one hand, the (100) and (311) points and, on the other hand, the (311) and (111) points are no longer straight lines but get a positive curvature due to the repulsive elastic step-step interactions.

The above study sheds light on the results of Frenken and Stoltze [1] at 0 K. These authors have calculated for the fully relaxed (100) and (111) vicinal surfaces of Ag using an EMT potential with [10] but in which the role played by third neighbors is very small compared to that of first and second neighbors as well in the pair as in the -body part of the potential (to fix ideas, =). Our analysis shows that all the curves calculated with a potential of type (4) and a cutoff radius will behave identically: This explains the strong similarity between our results on relaxed Cu with potential and those of Frenken and Stoltze for Ag. Therefore the instability of vicinal surfaces at 0 K is an unavoidable consequence of the type of potentials and range of interactions used in Ref. [1]. However, these potentials may be not accurate enough. Indeed, electronic structure calculations predict other possible behaviors at 0 K. Vicinal surfaces can be stable or unstable relative to faceting into (100) and (111) facets or they can also present a faceting into other high index surfaces.

Let us now consider the influence of a finite temperature. varies with temperature due to the excess

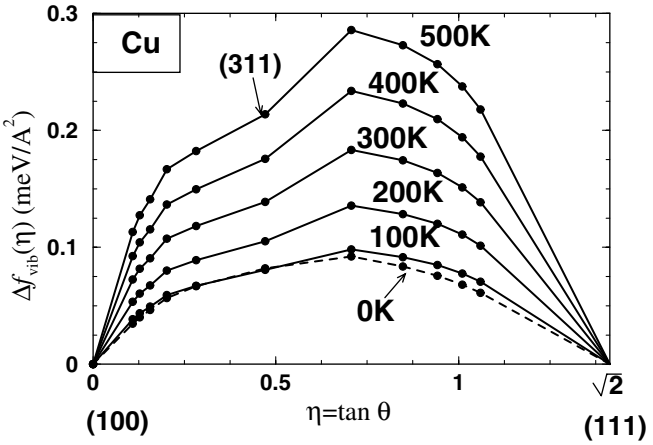

FIG. 4. for Cu from potential .

vibrational free energy and to the entropy gained by the meandering of steps. As stated in Ref. [1], the meandering entropy has a stabilizing effect but it is negligible at room temperature for Cu and Ag. This is *a fortiori* true for Rh and Pd in which the formation energy of a kink is much larger than in noble metals. The excess vibrational free energy has two contributions: the internal energy which dominates at low temperature and vanishes at high temperature, and the entropy part which has the inverse behavior. Indeed Eq. (5) applies to any energy, and, in particular, to the vibrational free energy provided that the contribution of an atom is completely determined by its numbers of neighbors inside the first two coordination spheres, at most. It is seen that besides the vibrational entropic energy estimated by Frenken and Stoltze in an isotropic Einstein model as coming from the difference between the outer edge and a (111) surface atom, i.e., , another term *should* be considered, namely, arising from the difference between the inner edge and a (100) surface atom. These two terms have opposite signs and are expected to be of the same order of magnitude. Thus, the calculation of the contribution of vibrational free energy to needs a precise knowledge of the vibration spectra of the bulk metal as well as of the flat and vicinal surfaces and should include the internal energy part (omitted in Ref. [1]), at least at low temperatures. We have recently shown that a potential of type is able to reproduce very accurately the experimental data for the vibration spectra of the bulk Cu and of its low- and high-index surfaces [11]. We have used these vibration spectra to calculate as a function of temperature (Fig. 4).

Two main conclusions can be drawn from the results: First, the order of magnitude is approximately some tenths of meV Å ; secondly, is positive. Consequently, not only phonons have a very small effect on the stability of vicinal surfaces but their contribution to the energy balance tends to destabilize the vicinal surface, at least for Cu, contrary to what is claimed in Ref. [1]. This does not mean that the vibrational free energy is always negligible. For instance, it will play a role in the temperature dependence of the step-free energy [12] and, thus, on the thermal roughening.

In summary, we have shown that the energy balance which drives the stability of vicinal surfaces at 0 K is very delicate and that the result may depend on the method used to calculate the total energy. This means that many behaviors can occur, namely, stability or instability relative to faceting into low-index as well as high-index orientations. Furthermore, the contribution of thermal vibrations is small, and it is unlikely that it stabilizes vicinal surfaces that are unstable at 0 K.

We thank I. Galanakis for sending us his results prior to publication. We are also indebted to H. Ness, H. J. Ernst, and E. Søndergård for a critical reading of the manuscript.

[1] J. W. M. Frenken and P. Stoltze, Phys. Rev. Lett. **82**, 3500 (1999).
[2] E. D. Williams and N. C. Bartelt, *Physical Structure,* Handbook of Surface Science Vol. 1, edited by W. N. Unertl (North-Holland, Amsterdam, 1996).
[3] F. Ducastelle, J. Phys. (Paris) **31**, 1055 (1970); M. W. Finnis and J. M. Sinclair, Philos Mag. A **50**, 45 (1984); A. P. Sutton and J. Chen, Philos Mag. Lett. **61**, 139 (1984).
[4] M. S. Daw and M. I. Baskes, Phys. Rev. B **29**, 6443 (1984); Z.-J. Tian and T. S. Rahman, Phys. Rev. B **47**, 9751 (1993).
[5] K. W. Jacobsen, P. Stoltze, and J. K. Norskov, Surf. Sci. **366**, 394 (1996).
[6] Details will be given in a forthcoming publication.
[7] M. C. Desjonquères and D. Spanjaard, *Concepts in Surface Physics* (Springer-Verlag, Berlin, 1996); I. J. Robertson, V. Heine, and M. C. Payne, Phys. Rev. Lett. **70**, 1944 (1993); P. Stoltze, J. Phys. Condens. Matter **6**, 9495 (1994).
[8] F. Raouafi, C. Barreteau, M. C. Desjonquères, and D. Spanjaard, Surf. Sci. **482–485**, 1413 (2001); Surf. Sci. (to be published).
[9] I. Galanakis *et al.* (to be published); (private communication).
[10] P. Stoltze (private communication).
[11] F. Raouafi, C. Barreteau, M. C. Desjonquères, and D. Spanjaard, Surf. Sci. (to be published).
[12] H. P. Bonzel and A. Emundts, Phys. Rev. Lett. **84**, 5804 (2000); H. J. W. Zandvliet, O. Gurlu, and B. Poelsema, Phys. Rev. B **64**, 73402 (2001).

Conclusion générale.

Résumons les résultats obtenus dans cette thèse. Nous nous sommes d'abord intéressés au calcul de la structure électronique des surfaces vicinales des métaux de transition par la méthode des liaisons fortes en base *spd*. Ceci nous a permis d'obtenir leurs énergies de surface. Nous en avons déduit les énergies de marche sur les surfaces de terrasses denses (111), (100) et (110) du Rhodium, du Palladium et du Cuivre en fonction de la largeur des terrasses. L'écart entre ces énergies de marche et leur valeur asymptotique, c'est à dire l'énergie de la marche isolée, révèle l'existence d'interactions entre marches présentant un profil oscillant qui met en évidence que les interactions peuvent être attractives pour certaines distances et répulsives pour d'autres. Leur comportement est très différent selon les types de marche et de surface. L'énergie de formation d'une marche isolée nous a permis d'étudier la forme des îlots en homoépitaxie sur les surfaces (111) et (100). De plus, nous avons obtenu les énergies de cran à l'aide d'une méthode de supercellules. Les résultats sont en bon accord avec les données expérimentales existantes sur le Cuivre.

Nous avons comparé nos résultats à ceux obtenus par Vitos et al. à l'aide d'un modèle d'interactions de paires effectives s'étendant jusqu'au troisième voisins. Les énergies de surfaces denses calculées avec le modèle de liaisons fortes *spd*, nous ont permis de déterminer ces potentiels d'interaction. Les valeurs des énergies de marches correspondantes sont en bon accord avec le calcul complet utilisant le modèle des liaisons fortes *spd*. Ceci justifie l'approche de Vitos et al.. Par contre ce modèle ne permet pas de déterminer les interactions entre marches. De plus il ne fait aucune distinction ni entre les marches de types A et B sur la surface plate (111), ni entre les énergies de crans sur les marches. Il faut noter que les énergies de marche et de cran dans l'approche de Vitos et al. sont sensibles aux valeurs des énergies des surfaces denses (111), (100) et (110) qui varient notablement selon le code de calcul utilisé. Enfin l'étude de

la structure électronique et en particulier des densités d'états locales montre la possibilité d'existence d'un moment magnétique le long des bords de certaines marches pour le Rhodium.

Dans la deuxième partie de cette thèse nous avons effectué une étude de la structure vibrationnelle des surfaces vicinales de Cuivre. Le calcul a été réalisé à l'aide d'un potentiel semi-empirique à N-corps dans l'approximation harmonique. Ce potentiel donne les meilleurs résultats lorsque les interactions sont coupées entre les deuxièmes et troisièmes voisins et rend bien compte de la relaxation des surfaces de bas indices et des surfaces vicinales. Les résultats obtenus pour le spectre des phonons de volume et la structure de bande projetée, aussi bien pour les surfaces plates que les surfaces vicinales, sont en bon accord avec les données expérimentales existantes qui donnent accès aux courbes de dispersion de certains modes localisés ou résonants. Nous avons aussi calculé des grandeurs thermodynamiques vibrationnelles. Nous avons montré que le déplacement carré moyen dépend essentiellement de l'environnement local et que les effets anharmoniques commencent à jouer un rôle dès la température ambiante. La contribution vibrationnelle à l'énergie libre de marche varie en fonction de la largeur des terrasses. Cette variation révèle l'existence d'interactions attractives entre marches dues aux phonons pour les surfaces vicinales $p(100)\times(111)$ et $p(111)\times(100)$.

Finalement nous avons discuté dans la troisième partie de cette thèse diverses approches pour étudier la stabilité des surfaces vicinales par rapport à un facettage. En raisonnant sur un réseau rigide nous avons pu obtenir analytiquement, pour toute une classe de potentiels semi-empiriques, un ensemble de résultats très utiles dans la suite pour la compréhension qualitative de ceux dérivés de calculs plus complets basés sur ces mêmes potentiels. En utilisant le potentiel semi-empirique déterminé dans la deuxième partie pour le Cuivre, nous avons montré que la stabilité peut s'inverser en fonction de la portée du potentiel et que si la relaxation atomique joue en faveur de la stabilisation des surfaces, elle ne change pas qualitativement les résultats. Les calculs de structure électronique montre des comportements plus variés par exemple la possibilité de facettage des surfaces vicinales en d'autres surfaces vicinales. Ce phénomène est une conséquence des interactions électroniques oscillantes entre les marches. Enfin nous avons montré que la température a un effet mineur sur la stabilité des surfaces vicinales.

En conclusion le bilan énergétique déterminant la stabilité des surfaces vicinales par rapport à un facettage est très délicat et nécessite un calcul très précis des énergies de surface à 0K. Ce bilan peut être modifié soit si l'une des facettes présente une reconstruction, soit par l'adsorption d'impuretés. Il s'agit là d'un domaine de recherches

très vaste qui reste à explorer sur lequel il existe des données expérimentales mais très peu de travaux théoriques.

bibliographie de l’introduction et du Chapitre 1 :

voir page 63-64

Bibliographie

[1] F. Fabre, D. Gorse, B. Salanon et J. Lapujoulade. *J. Physique*, **48** :1017, (1987).

[2] B. Salanon, F. Fabre, J. Lapujoulade et W. Selke. *Phys. Rev. B*, **38** :7385, (1988).

[3] H. J. Ernst, R. Folkerts et L. Schwenger. *Phys. Rev. B*, **52** :8461, (1995).

[4] M. Giesen, J. Frohn, M. Poensgen, J. F. Wolf et H.Ibach. *J. Vac. Sci. Technol.*, **A10 (4)** :2597, (1992).

[5] S. Rousset, S. Gauthier, O. Siboulet, J.C. Girard, S. de Cheveigné, M. Huerta-Garnica, W. Sacks, M. Belin et J. Klein. *Ultramicroscopy*, **42-44** :515, (1992).

[6] L. Masson, L. Barbier et J. Cousty. *Surf. Sci.*, **317** :L1115, (1994).

[7] L. Masson, L. Barbier, J. Cousty et B. Salanon. *Surf. Sci.*, **324** :L378, (1994).

[8] K.W. Jacobsen, J.K. Norskov et M.J. Puska. *Phys. Rev. B*, **35** :7423, (1987).

[9] M. S. Daw et M. I. Baskes. *Phys. Rev. B*, **29** :6443, (1984).

[10] F. Ducastelle. *J. Phys. (Paris)*, **31** :1055, (1970).

[11] F. Willaime et C. Massobrio. *Phys. cond. Matt.*, **3** :6225, (1991).

[12] W. Kohn et L. J. Sham. *Phys. Rev.*, **140** :A1133–A1138, (1965).

[13] P. Hohenberg et W. Kohn. *Phys. Rev.*, **136** :B864, (1964).

[14] C. Barreteau, D. Spanjaard et M. C. Desjonquères . *Phys. Rev. B*, **58** :9721, (1998).

[15] M. J. Mehl et D. A. Papaconstantopoulos. *Phys. Rev. B*, **54** :4519, (1996).

[16] W. Rosenhain. *Proc.Roy.Soc.*, **A70** :252, (1902).

[17] C. Herring. *Phys. Rev.*, **82** :87, (1951).

[18] F. Ducastelle. Contribution à l'étude de la structure électronique des métaux de transition et de leurs alliages. Thèse de doctorat d'état (Orsay), (1972).

[19] M. C. Desjonquères et D. Spanjaard. *Concepts in Surface Physics*. *Springer-Verlag, Berlin*, (1996).

[20] J. C. Slater et G. F. Koster. *Physical Review*, **94** :285, (1954).

[21] R. E. Cohen, M. J. Mehl et D. A. Papaconstantopoulos. *Phys. Rev. B*, **50** :14694, (1994).

[22] F. Ducastelle. *North-Holland, Elsevier Science Publishers*, **3**, (1991).

[23] S. L. Cunningham. *Phys. Rev. B*, **10** :4988, (1974).

[24] M. C. Desjonquères. Contribution à l'étude de la structure électronique des métaux et alliages de transition. *Thèse de doctorat d'état (Grenoble).*, , (1976).

[25] N. Bernstein, M. J. Mehl, D. A. Papaconstantopoulos, N. I. Papanicolaou Martin, Z. Bazant et Efthimios Kaxiras. *Phys. Rev. B*, **62** :4477, (2000).

[26] P. O. Lowdin. *J. Chem. Phys.*, **18** :365, (1950).

[27] D. J. Chadi et Marvin L. Cohen. *Phys. Rev. B*, **8** :5747, (1973).

[28] M. Weinert et J. W. Davenport. *Phys. Rev. B*, **45** :13709, (1992).

Etude de la stabilité des surfaces vicinales des métaux de transition à partir de leurs structures électronique et vibrationnelle.

Ce travail théorique concerne l'étude des surfaces vicinales de Rh, Pd et Cu et, en particulier, de leur stabilité par rapport à un facettage. L'étude comporte trois parties. Elle commence par le calcul de leurs énergies de surface, effectué sur réseau fixe à 0K, à l'aide de la méthode de liaisons fortes dans une base d'orbitales atomiques de valence *s*, *p* et *d*. Ces énergies permettent d'extraire les énergies de marches isolées, dont on déduit la forme des îlots en homoépitaxie sur les surfaces de bas indices, et les interactions entre marches qui présentent un profil oscillant. Leur comportement est très différent selon les types de marches et de surfaces. Les énergies de cran sont déterminées par la même méthode. La structure électronique est brièvement décrite. Puis les propriétés vibrationnelles des surfaces vicinales de Cuivre sont étudiées en utilisant un potentiel semi-empirique qui donne de bons résultats pour la relaxation des surfaces et décrit correctement, dans l'approximation harmonique, leur structure de bande projetée de phonons. Il est ainsi possible de déterminer des quantités thermodynamiques vibrationnelles, telles que le déplacement carré moyen et l'énergie libre. Enfin, la stabilité des surfaces vicinales est discutée à l'aide de potentiels semi-empiriques et de calculs de structure électronique. Il est montré que la stabilité peut s'inverser en fonction de la portée du potentiel et que la relaxation atomique joue en faveur de la stabilisation des surfaces mais ne change pas qualitativement les résultats. Contrairement aux potentiels semi-empiriques, les calculs de structure électronique montrent une grande diversité de comportements incluant la possibilité de facettage des surfaces vicinales en d'autres surfaces vicinales. Ce phénomène est dû aux interactions électroniques oscillantes entre marches. Enfin, il est prouvé que, jusqu'à l'ambiante, la température a un effet mineur sur la stabilité des surfaces vicinales.

Study of the stability of vicinal surfaces in transition metals from their electronic and vibrational structures.

This theoretical work is dedicated to the study of vicinal surfaces of Rh, Pd and Cu and, in particular, of their stability with respect to faceting. The manuscript includes three parts. It starts with the calculation of their surface energies, on a rigid lattice at 0K, using a tight-binding method with a basis set including *s*, *p* and *d* atomic valence orbitals. The energies of isolated steps are deduced from this calculation. They allow to determine the shape of adislands built by homoepitaxy on low-index surfaces, as well as step-step interactions which exhibit an oscillatory behavior. This behavior is strongly depending on the types of steps and surfaces. Kink energies are also computed by the same method. The electronic structure is briefly described. Then the vibrational properties of vicinal surfaces of Copper are studied using a semi-empirical potential which leads to good results for the relaxation of surfaces and describes correctly, in the harmonic approximation, their projected phonon band structure. It is thus possible to determine vibrational thermodynamical quantities, such as the root mean square displacement and the free energy. Finally, the stability of vicinal surfaces is discussed with semi-empirical potentials and with the calculation of electronic structure. It is shown that the stability can be inverted as a function of the potential range and that the atomic relaxation plays in favor of the stabilization of the surface but does not change qualitatively the results. Contrary to the semi-empirical potentials, electronic structure calculations open up the possibility of a large variety of behaviors, including a possible faceting of a vicinal surface into other vicinal surfaces. This phenomenon is due to electronic oscillatory step-step interactions. Finally, it is proven that the temperature has a minor effect on the stability of vicinal surfaces, at least up to room temperature.